

**MECHANISMS OF SENESENCE BYPASS
IN CELLS DERIVED FROM
THE SYRIAN HAMSTER EMBRYO CELL TRANSFORMATION ASSAY**

A thesis submitted for the degree of Doctor of
Philosophy

by

Jessica Chiara Pickles

Department of Life Sciences, Biological Sciences

Brunel University

November 2014

Abstract

Recent European legislation has enforced a reduction in the use of animal models for safety assessment purposes and carcinogenicity testing. The Syrian hamster embryo cell transformation assay (SHE CTA) has been proposed as a suitable animal alternative, but its implementation into test batteries has been delayed. This is due to concerns regarding the assay's endpoint subjectivity and, moreover, the model's relevance to carcinogenicity remains mostly unexplored.

Senescence is an essential barrier against uncontrolled cell proliferation and its evasion is necessary for clonal evolution and tumour development. Carcinogenesis can be modelled by reproducing underlying mechanisms leading to senescence bypass. In this project, the SHE CTA was performed using the known mutagen and human carcinogen, benzo(a)pyrene, and the resulting SHE colonies were analysed. It was found that morphological transformation (MT) does not guarantee senescence bypass and cell immortalisation, but increases the likelihood of MT-derived cells subsequently acquiring unlimited growth potential. A limited number (between 10 and 20 %) of MT colonies produced cell clones capable of sustained proliferation and in most cases secondary events were necessary for the evasion of senescence barriers.

With regard to mechanisms, *p53* point mutations were present in 30 % of immortal B(a)P-induced MT colony-derived cells and located within the protein's DNA binding domain. No *p16* mutations were identified. Expression of *p16* mRNA was commonly silenced or markedly reduced by a combination of mechanisms including monoallelic deletion, promoter methylation and *BMI-1* overexpression. Taking advantage of the recently available Syrian hamster genomic sequence information generated by the Broad Institute, the coding regions of the Syrian hamster *CDKN2A/B* locus were shown to have good homology to human nucleotide sequences and confirmed the exonic structures of SH *p16*, *ARF* and *p15*. The findings further implicate the importance of *p16* in regulating senescence while providing a molecular evaluation of SHE CTA-derived MT clones.

Table of Contents

| | | |
|-------|--|----|
| 1 | General Introduction | 13 |
| 1.1 | Cancer – The Problem | 14 |
| 1.1.1 | Somatic mutation theory of cancer | 14 |
| 1.2 | Toxicology and <i>in vitro</i> safety testing..... | 16 |
| 1.3 | Cell transformation..... | 18 |
| 1.3.1 | Cell transformation assays (CTAs)..... | 19 |
| 1.3.2 | SHD CTA assay | 21 |
| 1.4 | The SHE CTA..... | 21 |
| 1.4.1 | Improving the SHE CTA | 23 |
| 1.4.2 | Current molecular understanding of MT | 25 |
| 1.5 | Cellular senescence, an inbuilt safeguard | 27 |
| 1.5.1 | Markers of senescence | 27 |
| 1.5.2 | Replicative senescence | 28 |
| 1.5.3 | DNA Damage response | 29 |
| 1.5.4 | Stress-induced senescence (SIPS) | 30 |
| 1.5.5 | Oncogene-induced senescence (OIS)..... | 30 |
| 1.5.6 | Species differences..... | 32 |
| 1.6 | The tumour suppressor gene <i>p53</i> | 33 |
| 1.6.1 | Post-translational modifications | 34 |
| 1.6.2 | <i>p53</i> mutations | 35 |
| 1.6.3 | <i>p53</i> splice variants..... | 37 |
| 1.7 | The tumour suppressor gene <i>p16</i> | 38 |
| 1.7.1 | The <i>CDKN2A/B</i> locus | 39 |
| 1.7.2 | Epigenetic regulation | 41 |
| 1.8 | The Syrian hamster as a model | 44 |

| | | |
|-------|---|----|
| 1.8.1 | SH carcinogen-induced immortalisation..... | 45 |
| 2 | General Materials and Methods..... | 48 |
| 2.1 | Cell culture..... | 49 |
| 2.1.1 | Cell culture medium and supplements | 49 |
| 2.1.2 | Tissue culture plastics | 49 |
| 2.1.3 | Routine subculture of cells..... | 49 |
| 2.1.4 | Cryostorage and recovery of cells..... | 49 |
| 2.2 | Senescence-associated beta-galactosidase staining..... | 50 |
| 2.3 | RNA extraction..... | 51 |
| 2.3.1 | Nucleotide quantification | 51 |
| 2.3.2 | RNA purification | 51 |
| 2.4 | First strand synthesis (cDNA) | 52 |
| 2.5 | Quantitative real-time PCR (qPCR) using SYBR chemistry | 52 |
| 2.6 | DNA extraction | 53 |
| 2.7 | Polymerase chain reaction (PCR) | 53 |
| 2.8 | Gel extraction | 54 |
| 2.9 | Sequencing analysis..... | 54 |
| 3 | Characteristics of SHE Cell Transformation Assay-Derived Cells..... | 55 |
| 3.1 | Introduction..... | 56 |
| 3.2 | Materials and Methods | 59 |
| 3.2.1 | Syrian Hamster Embryo Cell Transformation Assay (SHE-MT) | 59 |
| 3.2.2 | Establishing colony-derived SHE cell cultures..... | 62 |
| 3.2.3 | Establishing cultures derived from SHE-MT colonies generated at BioReliance | 63 |
| 3.2.4 | Basic cell growth characteristics of colony-derived SHE cells..... | 63 |
| 3.2.5 | Growth curves | 64 |

| | | |
|-------|--|-----|
| 3.3 | Results | 64 |
| 3.3.1 | The SHE-MT assay | 64 |
| 3.3.2 | Cells derived from the SHE-MT assay | 68 |
| 3.3.3 | Morphological transformation does not guarantee senescence bypass | 72 |
| 3.3.4 | Determining growth characteristics and cell lifespan of SHE-MT clones obtained from BioReliance | 75 |
| 3.4 | Discussion | 92 |
| 4 | The Syrian Hamster <i>CDKN2A/B</i> Locus | 96 |
| 4.1 | Introduction..... | 97 |
| 4.2 | Materials and methods | 98 |
| 4.2.1 | Annotated <i>CDKN2A/B</i> sequences available via NCBI..... | 98 |
| 4.2.2 | WGS sequences available via NCBI | 98 |
| 4.2.3 | Sequence alignments | 99 |
| 4.2.4 | Sequencing of ~1.6 Kb upstream of the <i>p16</i> transcriptional start site (TSS) | 99 |
| 4.2.5 | Investigating the <i>p16</i> gene promoter | 100 |
| 4.3 | Results | 100 |
| 4.3.1 | Conservation of <i>CDKN2A-CDKN2B</i> coding regions | 100 |
| 4.3.2 | Identification of genomic <i>CDKN2A</i> sequences in Syrian hamster | 105 |
| 4.4 | Discussion | 110 |
| 5 | Molecular Characteristics of SHE-MT Colony-Derived Cells..... | 114 |
| 5.1 | Introduction..... | 115 |
| 5.2 | Materials and methods | 117 |
| 5.2.1 | Mutation screening of <i>p53</i> and <i>p16</i> | 117 |
| 5.2.2 | Gene expression analysis | 118 |
| 5.2.3 | Gene copy number variation (CNV) analysis | 120 |
| 5.3 | Results | 123 |

| | | |
|-------|---|-----|
| 5.3.1 | Mutation screening of <i>p53</i> and <i>p16/ARF</i> in immortalised transformed SHE cells | 123 |
| 5.3.2 | Gene expression analysis of immortal colony derived cells | 133 |
| 5.3.3 | Copy number variation (CNV) in immortal colony-derived SHE cells | 143 |
| 5.4 | Discussion | 148 |
| 6 | The Role of DNA Methylation in Regulating <i>p16</i> | 161 |
| 6.1 | Introduction | 162 |
| 6.2 | Materials and methods | 164 |
| 6.2.1 | DNA methylation analysis of <i>p16</i> | 164 |
| 6.2.2 | Demethylation Analysis | 169 |
| 6.3 | Results | 172 |
| 6.3.1 | Silencing of <i>p16</i> by DNA methylation | 172 |
| 6.4 | Discussion | 191 |
| 7 | General Discussion | 197 |
| 7.1 | Discussion | 198 |
| 7.2 | Conclusion and future perspectives | 208 |
| 8 | Appendix | 210 |
| 9 | References | 212 |

Table of figures

| | |
|--|-----|
| Figure 1 - Non-transformed versus morphologically transformed SHE CTA colonies | 23 |
| Figure 2 – The p16-pRb and p53 pathways promote cellular senescence | 32 |
| Figure 3 – p53 functional domains and mutation hotspots..... | 36 |
| Figure 4 – The <i>CDKN2A/B</i> locus | 40 |
| Figure 5 – SHE cell transformation assay time scale..... | 59 |
| Figure 6 – Example test plates from the Syrian hamster cell transformation assay (SHE CTA) | 66 |
| Figure 7 – SHE MT assay colony examples..... | 68 |
| Figure 8 – Picked morphologically transformed colonies that immortalised..... | 70 |
| Figure 9 – Picked morphologically transformed colonies that senesced | 71 |
| Figure 10 – Immortal B(a)P-MT colony-derived SHE cells proliferate beyond 35 population doublings..... | 75 |
| Figure 11 - Non-transformed cells, derived from the SHE-MT cell transformation assay (CTA) group that were treated with DMSO enter terminal senescence | 78 |
| Figure 12 –DMSO MT colony-derived cells show signs of poor growth before widespread senescence. | 83 |
| Figure 13 – One transformed colony from the DMSO-treated group (SHE 14) spontaneously immortalised..... | 84 |
| Figure 14 – Cell growth of B(a)P-treated morphologically transformed (MT) colony-derived SHE cells from BioReliance..... | 85 |
| Figure 15 – MT colony-derived cells require one or more additional events to acquire immortality..... | 87 |
| Figure 16- Most colony-derived SHE cells senesced by 35 population doublings..... | 88 |
| Figure 17 – Morphologically transformed (MT) characteristics are lost in two immortal BP MT colony-derived SHE cells obtained following crisis..... | 89 |
| Figure 18 –MT characteristics are retained in clones derived from MT colonies that were immortal from the outset | 90 |
| Figure 19 – Alignment of Syrian hamster <i>p16</i> coding regions..... | 102 |
| Figure 20 – Alignment of Syrian hamster <i>ARF</i> coding regions..... | 103 |
| Figure 21 – Alignment of Syrian hamster <i>p15</i> coding regions..... | 104 |

| | |
|---|-----|
| Figure 22 – <i>p16</i> nucleotide sequence alignments with unannotated <i>Mesocricetus auratus</i> WGS sequences..... | 106 |
| Figure 23 – Suggested genomic structure of the <i>CDKN2A-CDKN2B</i> locus in <i>Mesocricetus auratus</i> | 108 |
| Figure 24 – Regulatory motifs and GC content of sequences upstream of <i>p16</i> in the Syrian hamster | 110 |
| Figure 25 – A good quality Sanger sequencing profile example..... | 124 |
| Figure 26 – Sanger sequencing of <i>p16</i> mRNA identified a strain variation in SHE colony-derived cells compared to the published NCBI sequence. | 126 |
| Figure 27 – Sanger sequencing of <i>p53</i> mRNA identified non-synonymous point mutations in 30 % of immortal MT colony-derived SHE cells and a common strain variation in all samples compared to the published NCBI sequence. | 129 |
| Figure 28 – Sanger sequencing profile sections containing non-synonymous <i>p53</i> mutations..... | 132 |
| Figure 29 – Synonymous base change <i>p53</i> c195 bp is selected for in SHE MT BP9 over time in B(a)P-induced immortalised colony-derived SHE cells | 133 |
| Figure 30 – Gene expression in proliferating DMSO-treated non-transformed SHE colony-derived SHE cells | 134 |
| Figure 31 - Heat map of gene expression patterns in all B(a)P-treated MT immortalised SHE cells | 135 |
| Figure 32 – mRNA transcripts in SHE colony-colony derived cells (cont. on next page)... | 138 |
| Figure 33 – Rb1 gene expression in B(a)P-induced immortal SHE colony-derived cells ... | 142 |
| Figure 34 – Mdm2 and Rb1 gene expression is positively correlated | 142 |
| Figure 35 - Copy numbers for SHE and SHD calibrator samples used for CNV analysis | 144 |
| Figure 36 - Copy number variation of <i>p53</i> in immortalised colony-derived SHE-MT cells | 146 |
| Figure 37 – Copy number variation at the <i>CDKN2A/B</i> locus in immortalised colony-derived SHE-MT cells..... | 147 |
| Figure 38 – Copy number variation (CNV) and point mutations in <i>p53</i> and <i>CDKN2A/B</i> genes in SHE colony-derived cells..... | 150 |
| Figure 39 - Transcriptional changes potentially leading to immortalisation and senescence bypass..... | 155 |
| Figure 40 – The pJET1.2 blunt cloning vector | 167 |

| | |
|--|-----|
| Figure 41 – Diagram of the <i>p16</i> promoter in the Syrian hamster | 173 |
| Figure 42 – Analysis of DNA methylation in <i>p16</i> 5' promoter and exon 1 α using methyl specific PCR (MSP)..... | 175 |
| Figure 43 – Excision of bisulphite-converted <i>p16</i> promoter PCR products..... | 176 |
| Figure 44 – Bacterial colony PCR to confirm the correct <i>p16</i> promoter insert into pJET1.2 vector | 176 |
| Figure 45– DNA methylation status of CpG sites in -457 bp upstream region of the SH <i>p16</i> transcriptional start site (TSS)..... | 178 |
| Figure 46 – Growth curves for SHE cells treated with the demethylating agent 5-aza-dC | 180 |
| Figure 47 - SHE cells treated with the demethylating agent 5-aza-dC are visibly altered. | 182 |
| Figure 48 – Cell recovery occurs after 10 to 17 days following methyltransferase inhibition | 183 |
| Figure 49 – Senescence associated beta-galactosidase (SA- β gal) staining increases following treatment with 5-aza-dC..... | 185 |
| Figure 50– Demethylated SHE cells stain positive for SA- β gal | 186 |
| Figure 51 – <i>p16</i> transcript levels following treatment with 5-aza-dC | 188 |
| Figure 52 – Following exposure to 5-aza-dC there is a reduction of DNA methylation in the <i>p16</i> promoter after 4 and 8 days | 190 |

Acknowledgements

I would firstly like to thank my supervisor Professor Robert Newbold for his expertise and continuous advice, and second supervisor Amanda Harvey for her guidance and opinion.

Thank you to my industrial supervisor Andrew Scott for his input in the project and Claire Moore for her help in setting up the lab while on placement. Thank you to the funding bodies, the BBSRC and Unilever for making this project possible.

I would also like to acknowledge Hemad Yasaei and Terry Roberts for showing me the ropes in the lab and sharing their knowledge with me. I greatly appreciated advice on plasmid preparation from Evgeny Makerov and special thanks to Alison Marriott for her tissue culture expertise and encouragement in those tricky times.

I have to thank my friends who have all helped in their own way: Hannah for our countless qPCR discussions, my housemates and Dan for believing in me and their patience, Paola and the Derhill 2 lot for keeping me sane, plus all my fellow PhDs for the coffees and giggles.

Lastly, I would like to say a big thank you to my family for their endless support, even if it did mean constant questioning over 'the cells'.

Author's declaration

All the work presented in this thesis is my own unless stated. Any work of others is appropriately referenced.

Jessica Chiara Pickles, November 2014.

Abbreviations

| | |
|-----------------|--|
| ARF | Alternative reading frame |
| B2M | beta-2-microglobulin |
| B(a)P | Benzo(a)pyrene |
| BSA | Bovine serum albumin |
| BMI-1 | BMI1 polycomb ring finger oncogene |
| cDNA | Complementary DNA |
| CDK | Cyclin dependent kinase |
| CDKI | Cycling dependent kinase inhibitor |
| CNV | Copy number variation |
| CMF-HBSS | Ca ²⁺ and Mg ²⁺ free Hank's Balanced Salt Solution |
| CTA | Cell transformation assay |
| DMBA | 7,12-dimethylbenz[α]anthracene |
| DMEM | Dulbecco's Modified Eagle Medium |
| DMEM-L | LeBoeuf's Dulbecco's Modified Eagle Medium |
| DMSO | Dimethyl sulfoxide |
| EDTA | Ethylenediaminetetraacetic acid |
| EZH2 | Enhancer of zeste homolog 2 |
| FBS | Fetal bovine solution |
| GAPDH | Glyceraldehyde 3-phosphate dehydrogenase |
| HMEC | Human mammary epithelial cells |
| IARC | International Agency for Research on Cancer |
| LB | Luria-Bertani |
| LN ₂ | Liquid nitrogen |
| MDM2 | Mouse double minute 2 homolog |
| MEF | Mouse embryonic fibroblast cells |
| MNU | N-Nitroso-N-methylurea |
| MT | Morphologically transformed |
| MTF | Morphological transformation frequency |
| mRNA | Messenger RNA |
| NCBI | National Centre for Biotechnology Information |
| NTC | Non template control |

| | |
|-----------------|--|
| P15 | Cyclin-dependent kinase inhibitor 2B |
| P16 | Cyclin-dependent kinase inhibitor 2A |
| p53 | Tumour protein p53 |
| PBS | Phosphate buffered saline |
| PBST | Phosphate buffered saline with Tween-20 |
| PcG | Polycomb group |
| PCR | Polymerase chain reaction |
| PD | Population doubling |
| PDL | Population doubling level |
| PE | Plating efficiency |
| PTM | Post-translational modifications |
| PRC | Polycomb repressor complex |
| Rb | Retinoblastoma |
| RD | Regulatory domain |
| RPE | Relative plating efficiency |
| RT | Reverse transcriptase |
| rRNA | Ribosomal RNA |
| RQ | Relative quantity |
| SA- β gal | Senescence-associated beta-galactosidase |
| SH | Syrian hamster |
| SHD | Syrian hamster dermal |
| SDHA | Succinate dehydrogenase complex, subunit A |
| SHE | Syrian hamster embryo |
| SHE-MT | Syrian hamster embryo cell morphological transformation |
| SNP | Single-nucleotide polymorphism |
| TBE | Tris-Borate-EDTA |
| TBP | TATA-binding protein |
| WGS | Whole genome shotgun |
| X-gal | 5-bromo-4-chloro-3-indolyl- β -D-galactopyranoside (BCIG) |
| YWHAZ | tyrosine 3-monooxygenase/tryptophan 5-monooxygenase activation protein, zeta |

CHAPTER 1

1 General Introduction

1.1 Cancer – The Problem

In 2012 it was estimated that there were 14.1 million new cases of cancer world-wide and 8.2 million cancer-related deaths (Ferlay et al., 2014). Of the 3.4 million patients diagnosed with cancer in Europe alone, around 50 % of malignancies were identified in breast, prostate, colorectal and lung tissues, with the latter being the highest cause of mortality (Ferlay et al., 2013). Cancer is defined by abnormal and uncontrolled cell growth which expands beyond its usual organised tissue setting, eventually spreading or metastasising to other organs. Risk factors include an unhealthy diet, smoking, alcohol consumption and a lack of exercise, but susceptibility to cancer can be genetically inherited, and chronic viral infections can also lead to its development. The incidence of cancer is increasing annually worldwide (Ferlay et al., 2014). In the UK one in three people will develop some form of cancer, but the prognosis for patients is improving through early diagnosis and preventative approaches, such as routine screening in higher risk groups. The onset of cancer is also age related. As global healthcare, sanitation and wellbeing continue to improve, life expectancy is rising but so therefore are the numbers of those affected with cancer. Sixty percent of individuals newly diagnosed with cancer live in developing countries, although this is in part due to better survey response rates (Ferlay et al., 2014), the increase is also related to ageing populations. Unlike in westernised countries, these individuals do not necessarily have access to high quality medical care and routine screens may be unavailable, contributing to higher mortality rates. Cardiovascular diseases and strokes remain the main causes of death world-wide (13.2 % and 11.9 % of total deaths respectively in 2012 - WHO). However, the burden of cancer is continuously rising, which is for the most part caused by increased life-expectancy, lifestyle choices and the environment.

1.1.1 Somatic mutation theory of cancer

The progression of cancer is dependent on the continual selection of cellular subpopulations containing acquired genetic variations that confer growth advantages (Bell, 2010); this process is known as 'clonal evolution'. Accumulation of sufficient sporadic mutations impacting a cell's normal function may ultimately lead to the evasion of inbuilt safeguard mechanisms and uncontrolled malignant growth. The somatic

mutation theory describes a multistep progression of tumourigenesis which can be conceptualised in several key stages and biological outcomes (Hanahan and Weinberg, 2000). In becoming autonomous, cancerous cells must acquire the ability to proliferate independently of normal mitogenic signalling and growth-inhibitory signalling. In order to sustain continued growth they must then evade and bypass inbuilt safeguards, such as apoptosis and senescence, thus also acquiring immortality. Finally, tumourigenic cells lack contact inhibition thus conferring invasive growth and metastasis and can promote angiogenesis to further sustain autonomous tumour growth (Hanahan and Weinberg, 2011).

The emerging complexity of cancer genomes has highlighted the heterogeneity of tumours across patients and tumour types, even within the same metastasis (Vogelstein et al., 2013). Cancer encompasses over a hundred disease subtypes originating from different cell types and organs, and is caused by a multitude of genetic and epigenetic alterations, including gene mutations, chromosomal amplifications, deletions, translocations, and changes in gene and protein expression often accompanied by chromatin remodelling (Hanahan and Weinberg, 2011). Genomic sequencing of tumours has highlighted their vast array of aberrations, many of which are passenger mutations believed not to have any selective growth advantage but that have silently accumulated (Copeland and Jenkins, 2009, Vogelstein et al., 2013) in clonally evolving populations. Relatively few genes (138 according to Vogelstein) are considered to be key somatic drivers of cancer and less than 5 % of these may be commonly altered within the same tumour type (Copeland and Jenkins, 2009). The genetic landscapes and mutations observed between individuals affected by equivalent cancer types are unlikely to be identical, even within the same targeted gene. Estimates predict that two to eight somatic mutations in genes conferring growth advantages are sufficient for tumourigenesis (Vogelstein et al., 2013) but the extent of their cumulative effects will be additionally influenced by non-genetic factors, specific to the cell's micro-environment and determining cell-type (Hanahan and Weinberg, 2011).

1.2 Toxicology and *in vitro* safety testing

The assessment of carcinogenic risk is essential in ensuring product safety, whether it be a novel consumer product, a medicine or an agricultural chemical. Safety testing is of the utmost importance to prevent additional and unnecessary incidences of cancer. Genetic toxicology aims to determine potential adverse effects, following exposure of cells or organisms to test chemicals and compounds under controlled laboratory conditions. In order to reliably predict carcinogenicity, the appropriate assays must be performed to effectively detect any hazardous consequences.

Rodent bioassays have been considered the 'gold standard' for use in toxicology as they provide *in vivo* data while addressing long-term effects in a complex organism. In the context of chemical screening, animal testing is impractical given its expense both in terms of experimental and labour costs. They can take over two years to complete, not to mention the increased requirement to focus on ethical issues concerning animal use (Vanparys et al., 2011, Creton et al., 2012). More recently, European legislation has constrained the use of animals for chemical and agrochemical testing (EC, 2007b), but still requires information on chemical carcinogenicity, and has placed a complete animal testing ban on the cosmetics industry since 2013 (EC, 2003b). This has fuelled the need for alternative methods to conform to REACH requirements and the application of the '3Rs' principles that encourage the reduction of animal usage, their replacement with *in vitro* test systems and protocol refinement.

Based on the long-standing acceptance that a major driver of carcinogenesis is genetic damage, assays have been developed to detect chemical genotoxicity and mutagenic properties. Genotoxic agents are those that are capable of causing direct damage to the DNA leading to cancer initiation events. The Ames test assesses mutagenicity using a bacterial strain of *Salmonella* that is deficient for the synthesis of the amino acid histidine. After incubation with a metabolised test compound, the number of resulting bacterial colonies that acquire the ability to grow in histidine-deficient medium is proportional to the mutagenic potency of the chemical. Chromosomal instability can be measured by the micronucleus (MN) assay that detects fragmented chromosomes as markers of chromosome breaks or losses, apoptosis and misrepaired DNA (Fenech, 2007). Another

biological assay that gauges DNA damage is the Comet assay in which carcinogen-exposed cells are embedded in agarose; single-strand DNA breaks are determined by gel electrophoresis and the extent of damaged DNA is identified in the comet 'tail' (Azqueta and Collins, 2013).

The problem with genotoxicity assays is that they cannot accurately identify non-genotoxic carcinogens that do not directly alter an organism's genetic makeup but act epigenetically by, for example, influencing signal transduction pathways via the aberrant regulation of gene transcription (Creton et al., 2012). Carcinogenesis in these instances can be promoted by changes in growth factor receptor expression, forced cell proliferation, inhibition of intracellular communication and DNA hypermethylation (Hernandez et al., 2009). For a test battery to be fully comprehensive, it is necessary to include assays with sufficient predictive power for both genotoxic and non-genotoxic carcinogens to avoid false negatives (OECD, 2007); this is of course complicated by the non-availability of rodent bioassays. Other caveats are: (i) that bacterial assays such as the Ames test may not pick up mammalian carcinogens and, (ii) that there can be non-concordance between rodent-based assays and human toxicity, additionally leading to false positive results (Benigni and Bossa, 2011). By combining test batteries, a weight of evidence approach is useful to gauge the potential of an unknown chemical to cause cancer and possibly to understand its mode of action (Balls et al., 2006, Hernandez et al., 2009). Lastly *in silico* modelling to predict toxicity based on carefully selected existing *in vitro* and *in vivo* datasets is starting to be implemented (Modi et al., 2012) and is likely to aid risk assessments and help evaluate induced adverse outcomes (Adeleye et al., 2014).

The carcinogenic potential of a given chemical or test article must be thoroughly investigated before it can be classed as safe to the consumer and the environment. Initial toxicological tests must have the capability to detect accurately DNA damage, chromosome aberrations and epigenetic (non-genotoxic) changes directly resulting from carcinogen exposure. Cell transformation assays (CTAs) have long been proposed as potential representatives of *in vivo* models to complement genotoxicity screening and have been shown to produce good correlations with rodent bioassay data (Colacci et al.,

2011, LeBoeuf et al., 1999), although this does not always predict human carcinogenicity (Mauthe et al., 2001). Importantly, CTAs have predictive power for detecting non-genotoxic carcinogens and are relatively quick and cost effective (Benigni and Bossa, 2011, Hernandez et al., 2009, Vanparys et al., 2012). As suitable animal alternatives, they are concordant with REACH requirements and should, at least in theory, also provide a quality of data in line with EU legislation (Corvi et al., 2012, Vanparys et al., 2011).

1.3 Cell transformation

Early *in vitro* and *in vivo* studies demonstrating the progressive nature of cell transformation were largely based the observation of cellular characteristics and growth properties (Barrett et al., 1979, LeBoeuf et al., 1990). The step-wise process of transformation is thought to recapitulate clonal evolution events leading to neoplasia and is characterised by the acquisition of a number of traits that can be identified in tumourigenic cells (Isfort and LeBoeuf, 1996). The first is described as a block in cell differentiation and clonal expansion (Isfort and LeBoeuf, 1996). Berwald and Sachs (1963) first observed this phenomena when they exposed Syrian hamster embryo-derived cells (SHE cells) to known carcinogens and observed cellular changes in phenotype, such as random patterns of growth, spindle-shaped cells and increased fibrinolytic activity (Berwald and Sachs, 1963). Initial results identified morphological transformation (MT) as an early indicator of neoplastic potential but in itself, MT was not sufficient for tumour formation (Barrett and Ts'o, 1978). Barrett suggested that early morphological alterations could represent the initiation of transformation but could not accurately predict the frequency of neoplasia. It was only after multiple population doublings that transformed cells formed colonies in semi-solid agar, indicating that the acquisition of additional mutagenic events took time and were necessary for anchorage-independent growth (Barrett and Ts'o, 1978, LeBoeuf et al., 1990, Newbold, 1985b). Fully transformed cells were capable of developing into tumours at the site of injection when explanted *in vivo* into hamsters or athymic mice (DiPaolo et al., 1969). The following characteristics are thus commonly used to describe fully transformed cells: (1) a block in cell differentiation leading to clonal expansion of transformed cells, (2) cell immortalisation and genetic

instability, permitting an extended lifespan (3) anchorage-independent growth and loss of contact inhibition and (4) if explanted have the capacity to form tumours at sites of injection (OECD, 2007, Newbold, 1985a, Schechtman, 2012). The apparent similarity between induced cell transformation and cancer was deemed to support its proposed use as an *in vitro* model of tumourigenicity.

1.3.1 Cell transformation assays (CTAs)

By exposing the transforming potential of known chemical carcinogens, cell transformation assays (CTAs) were subsequently developed as *in vitro* systems capable of predicting chemical carcinogenicity and were proposed for the testing of unknown compounds. Depending on the assay employed, transforming properties are measured differently and assessed by changes to morphological characteristics, growth patterns and anchorage-independent proliferation. To date there are several well established rodent CTAs which employ different cell types assessing the various endpoints (Creton et al., 2012). The Syrian hamster embryo derived assay (SHE) uses normal, diploid and metabolically competent primary cells whereas the mouse BALB/c 3T3, C3H 10T1/2 and Bhas 42 focus assays are aneuploid, pre-immortalised rodent cell lines which are contact-inhibited (Schechtman, 2012). The Bhas 42 assay was derived from the BALB/c 3T3 (by stable transfection with v-Ha-Ras); both can be used as a two-step model to predict tumour-initiators or tumour promoters, depending on stage of target cells used. Typically, focus assays have a defined subculture regime whereby the cells are re-seeded after a set number of days to avoid contact-inhibition and to maintain the treated cells at subconfluent levels. Chemically-induced transformation in these instances is identified by disorganised, multilayered discrete cell foci growing over a background of contact inhibited cells (Combes et al., 1999, Sasaki et al., 2012). On the other hand, the SHE CTA assay measures the frequency of induced morphological transformation (MT) and is discussed later in this Chapter in more detail. Events leading to cellular transformation, as detected by CTAs, are not fully understood but are believed to result from the deregulation of cell-signalling pathways either by direct genetic disruption (eg. mutations or chromosomal damage) or by epigenetic mechanisms (Hernandez et al., 2009, Waters et al., 2010) that are representative of an *in vivo* biological response.

Typically, transformation assays have been shown to have good concordance with rodent bioassay data and were therefore postulated as potential *in vitro* animal alternatives. In addition, CTAs are metabolically competent systems believed to be capable of picking up non-genotoxic carcinogens that remain undetected by most test systems that rely on genetic damage as their endpoint. As an attractive and cost effective model, CTAs were considered as potential candidates for carcinogenic screening (Isfort and LeBoeuf, 1996, Kerckaert et al., 1996a, LeBoeuf et al., 1996). However, following several workshops, concerns were raised due to the lack of molecular and mechanistic data confirming the link between transformation and carcinogenesis, along with difficulty in assay reproducibility and missing protocol standardisation (Combes et al., 1999, Farmer, 2002). In response to these criticisms, a number of recommendations were made by ECVAM (the European Centre for the Validation of Alternative Methods) to address the limitations of CTAs (Combes et al., 1999, Schechtman, 2012). Since then, European legislative changes have further driven the need for appropriate animal replacements for chemical risk assessments by implementing a complete ban on animal testing for cosmetics from 2013 (EC, 2003b, EC, 2007b). Stimulated by REACH regulations and the cosmetic directive, pre-validation work was carried out for CTAs in the context of assessing their suitability for *in vitro* predictive toxicology, according to OECD guidelines. At the same time, data originating from previously tested chemicals using CTAs were pooled together by the OECD so as to have a comprehensive wealth of accessible data (OECD, 2007, Vasseur and Lasne, 2012). These studies highlighted the high concordance of the CTAs to rodent bioassay data plus good carcinogen sensitivity and specificity. Publications detailing refined methodologies for the SHE MT assay at both pHs (pH 6.7 and pH 7.3, discussed later) have been produced (Maire et al., 2012a) and ECVAM pre-validation studies have ensured that the assay could be reproducibly followed according to recommended guidelines in different laboratory settings (Maire et al., 2012b, Pant et al., 2012, Vanparys et al., 2011). Similar pre-validation work has also been carried out with the murine BALB/c 3T3 assay (Vanparys et al., 2011, Mascolo et al., 2010, Sasaki et al., 2012, Tanaka et al., 2012).

1.3.2 SHD CTA assay

A variation of the SHE-MT assay has been developed using Syrian hamster dermal (SHD) cells. SHD cells are normal, diploid, and metabolically active, plate with high frequencies (30-40%) and grow in monolayers. Unlike SHE cells, SH dermal cells are homogeneous and on average untreated mass cultures begin to enter senescence following 15-20 population doublings, which is much earlier than their embryo derived counterparts (Newbold et al., 1982). After incubation with the test article, the cells are serially subcultured until transformed rare immortalised variants emerge from the cell population. Similarly to human fibroblast lines, no spontaneous immortalisation has so far been reported (Yasaei et al., 2013). This is in contrast to mouse fibroblasts which show higher relative frequencies of immortalisation (Pant et al., 2008). Compared to the vast amount of historical data available for SHE CTA and BALB/c 3T3 there is limited data supporting the use of the SHD assay for toxicology screening which explains why it has not yet been implemented for this purpose (Creton et al., 2012).

1.4 The SHE CTA

The Syrian hamster embryo cell transformation assay (SHE CTA) is a clonogenic *in vitro* assay based on primary SHE cells derived from disaggregated hamster embryos. With this assay a chemical's transforming potential is based on scoring morphological change in the resulting colonies. The SHE CTA is unique in that pre-immortalization events are identified in a normal, diploid and finite-lifespan cell model (Trott et al., 1995). Unlike established cell lines such as BALB/c 3T3 or C3H 10T1/2, the SHE system offers a heterogeneous cell population derived from early embryos, meaning that multiple cell types can be simultaneously tested and targeted (Isfort and LeBoeuf, 1996). Typically in a single test plate a variety of colony morphologies will be visible, such as epithelial, fibroblast and myocardial-like cells which is advantageous for screening applications (Custer et al., 2000). The heterogeneity of the target cells eliminates the cell-type bias encountered in systems employing established sub-clones of cells (as with the focus assays) which can influence transformation frequencies or spontaneous rates of immortalisation.

Although a small number of live animals must be used to generate the SHE embryo-derived cells for the SHE CTA, primary cell stocks are cryopreserved in virtually identical assay-ready batches. Typically 3-4 animals may be used to obtain 30-35 embryos that are sufficient for the cell isolation procedure, generating enough SHE cells for hundreds of CTAs. For the assay itself, SHE cells are plated at very low seeding densities on a supportive feeder-layer of X-irradiated SHE cells that cannot replicate and, following chemical dosing, the cells are allowed to grow undisturbed in the test article for a total of 7 days, at which point the resulting colonies are individually examined and scored for morphologically transformed (MT) characteristics (Mauthe et al., 2001, Maire et al., 2012a). MT colonies are characterised by highly disorganised cell growth (see Figure 1): MT cells are elongated with limited cytoplasm and they extensively overlap each other in a criss-crossed fashion; whereas normal or non-transformed SHE colonies form organised and flowing cell monolayers at high cell confluency (Bohnenberger et al., 2012, Maire et al., 2012c). Scoring is aided by the staining of colonies with Giemsa, a dibasic stain which typically stains MT colonies dark blue (more basophilic) in contrast to normal colonies which stain more lightly and are purple (Kerckaert et al., 1996b, LeBoeuf et al., 1996). A large number of plates must be assayed for a single SHE CTA experiment due to the relatively low frequencies of MT (MTF) observed following chemical treatment (LeBoeuf et al., 1996, Pienta et al., 1977); the MTF for a given compound is determined relative to the appropriate controls and is the assay's endpoint (Kerckaert et al., 1996b).

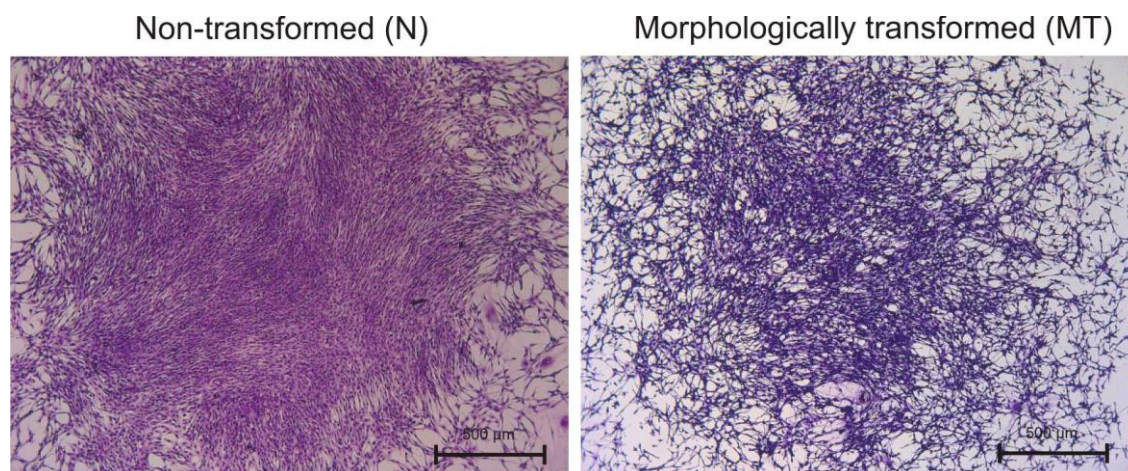


Figure 1 - Non-transformed versus morphologically transformed SHE CTA colonies

Non-transformed or normal colonies contain organised monolayers of cells that have a flowing pattern of cell growth; in Giemsa they stain purple. Morphologically transformed colonies are more basophilic and stain blue, MT colonies contain disorganised cells that stack on top of each other and are more spindle shaped with high nuclear to cytoplasm ratios. (Images were taken using a 5X objective on a Zeiss Axioskop microscope).

1.4.1 Improving the SHE CTA

Over 500 carcinogenic agents have been tested using the SHE-MT assay (OECD, 2007). Like other CTAs, the SHE assay is believed to have the predictive power to identify non-genotoxic carcinogens in addition to genetic damage either at a DNA or chromosomal level. Although deemed to have predictive value and, despite extensive efforts by the validation bodies such as ECVAM and the OECD to standardise the assay (Corvi et al., 2012), the underlying mechanistic underpinnings confirming the link between MT, immortality and tumourigenesis remain mostly unaddressed (Combes et al., 1999, Combes, 2012). The model's questionable relevance to carcinogenesis has hindered the incorporation of the SHE CTA into routine testing strategies and remains a topic of debate (Creton et al., 2012, Vanparys et al., 2011). This section highlights some of the technical improvements specific to the SHE CTA that have been implemented and discusses more recent protocol amendments.

The major criticism of the SHE assay is focused on the subjective nature of scoring and selecting morphologically transformed colonies, despite numerous papers detailing methodology and the scoring process (Kerckaert et al., 1996b, LeBoeuf et al., 1996, Custer et al., 2000). Following optimisation and refinement, the overall evaluation of the assay

reported 87.7 % inter-laboratory consistency and an overall concordance of 85 % with rodent bioassays (Vasseur and Lasne, 2012). Previous to ECVAM, the issue of reproducibility was initially addressed by decreasing the pH of the culture media from pH 7.3 to 6.7 in LeBoeuf's modified Dulbecco's modified Eagle's medium (DMEM-L). This change retains optimal SHE cell clonal proliferation (Isfort et al., 1996b, LeBoeuf et al., 1996). Although the mechanisms are not fully understood, the acidification of the culture medium evidently improves the predictive power of the assay, solves problems of low frequencies of MT and increased cell proliferation, and results in a higher colony density (Pienta et al., 1977, LeBoeuf and Kerckaert, 1987, LeBoeuf et al., 1996). No effect on plating efficiency was detected compared to cells grown in pH 7.3 medium, but a 4-fold increase in replicative lifespan was noted prior to senescence when growing untreated SHE cells at pH 6.7 (Isfort et al., 1996b, Kerckaert et al., 1996c). The reduced pH assay also improved inter-laboratory reproducibility, as the SHE cells acquire a more elongated, spindle-shaped appearance which in principle facilitates the discrimination between normal and MT cells by making the typical MT criss-crossed pattern readily identifiable. Despite this, a detailed review paper (DRP) from the OECD states that the choice of pH at which the assay is conducted can be considered immaterial in terms of performance (Vasseur and Lasne, 2012). However, questions have been raised concerning which pH is most physiologically relevant (DRP in progress – personal communication from Nathalie Delrue and Laurence Musset to RFN). Further, in a bid to assist the scoring of MT SHE colonies, photo catalogues have been made available, that act as valuable visual aids for the identification of various types of colonies obtained at the SHE CTA assay's endpoint (Bohnenberger et al., 2012, Maire et al., 2012c). From these images, SHE colony heterogeneity is immediately apparent which raises the importance of appropriate expert training prior to conducting the assay, in order to alleviate concerns over the subjective nature of scoring.

Computational image analysis of SHE CTA colonies has been attempted to eliminate manual scoring bias and this achieved correct identification of colony phenotypes in up to 93 % of instances analysed (Ridder et al., 1997). However, sparse colonies were not included in the analysis, dramatically reducing the sample size from which the MTF value was calculated; such automated analysis may thus reduce the sensitivity of the assay

(Ahmadzai et al., 2012a). Another approach to assess transforming properties of chemical carcinogens has been developed using Fourier-transform infrared (FTIR) spectroscopy in a bid to obtain a more objective evaluation of MT (Walsh et al., 2009). Infrared (IR) wavelengths are absorbed differently by bio-molecules such as DNA, RNA and protein so that, depending on their relative content, the reflected IR spectra might be used to quantitatively and objectively distinguish between the biochemical properties of MT and non-transformed cells (Ahmadzai et al., 2012ba). This method was effectively able to discriminate between SHE colonies treated with different carcinogens, but spectra obtained from MT and non-transformed cells treated with the same carcinogen were more difficult to analyse (Ahmadzai et al., 2012bb), suggesting that further work is needed to find an appropriate objective scoring process.

An additional minor protocol amendment has also been developed which is worth noting. The SHE CTA is traditionally carried out using a supportive feeder-layer of X-ray irradiated cells. During scoring, the toxicologist must be able to distinguish between MT and non-transformed colonies that grow over a background of non-dividing cells. This protocol has now been modified and validated using conditioned medium as a feeder-layer replacement to aid the scoring process (Pant et al., 2008, Pant et al., 2010). This is clearly advantageous as the discrimination between SHE cell growth on feeder cells and actual MT stacking does not need to be made, eliminating such background interference. No substantial differences in the morphological transformation rates were described (Pant et al., 2008), although the spontaneous rate was marginally higher than experiments using feeder cells.

1.4.2 Current molecular understanding of MT

The second major concern of the SHE CTA is the lack of information supporting morphological transformation in the Syrian hamster as a mechanistically valid (i.e. cancer related) endpoint and whether the model in general is suitable for modelling, at least in part, human carcinogenesis. Acquisition of transformed phenotypes has been correlated with an increased probability of immortality and bypass of senescence (LeBoeuf et al., 1990, Watanabe and Suzuki, 1991) but limited studies have analysed SHE cells derived from MT colonies at a molecular level. Studies addressing MT have analysed SHE cells treated with known transforming agents, but independently of actual morphological (MT)

scoring, and have used mass cultures instead of cells derived from MT colonies. This is useful for understanding the general mechanisms of carcinogenesis but perhaps less informative of MT-specific molecular changes. For example, zinc is a known inhibitor of apoptosis (programmed cell death) and has been found to induce MT at 100-150 μ M concentrations (Alexandre et al., 2003, Truong-Tran et al., 2001). Zinc chloride-treated SHE cells (not derived from the SHE CTA) had altered ratios of the *Bcl-2/Bax* favouring inhibition of apoptosis but no changes in the oncogene *c-myc* were noted (Maire et al., 2005a). Induction of mitogenic *c-myc* was identified in SHE cells exposed to transforming concentrations of the herbicide 2,4-dichlorophenoxyacetic acid (2,4-D) but *c-myc* expression was also unchanged following exposure to benzo(a)pyrene (Maire et al., 2007). Unlike zinc, treatment with 2,4-D did not affect expression of *Bcl-2* or *Bax* (Maire et al., 2007). It has been suggested that early events leading to MT may involve the inhibition of apoptotic pathways via upregulation of *Bcl-2*, although the result may also be specific to the biological effects of zinc chloride rather than to the MT phenotype itself (Truong-Tran et al., 2001, Sztalmachova et al., 2012). That said, the carcinogen di-(2-ethylhexyl)-phthalate (DEHP) was also found to increase *Bcl-2* and negatively regulate *c-myc* in SHE cells (Maire et al., 2005b). In another study DEHP exposure caused transcriptional changes in cytoskeletal genes and reduced cell-cell adhesion and cell adhesion to the extracellular matrix (Landkocz et al., 2011), possibly consistent with a non-genotoxic carcinogenic mode of action. Although these studies do not specifically address mechanisms of morphological transformation, they do strongly point towards the applicability of using SHE cells as biologically relevant models for studying carcinogenesis.

In summary, due to EU legislation requiring the reduction of animal use in toxicology there has been renewed interest in *in vitro* cell transformation assays (CTAs). Concerns regarding their reproducibility have been partly addressed by protocol standardisation, and validation studies have confirmed their suitability for incorporation into OECD Test Guidelines. In the case of the SHE CTA, efforts have been made to reduce the assay's subjectivity and develop novel, unbiased, scoring methods. Reservations still remain with regards to CTAs, since the mechanisms underpinning cellular transformation have not been fully explained. Beyond the propensity of morphologically transformed (MT) cells to

immortalise and acquire anchorage-independent growth, little is still known about the relationship between MT and carcinogenesis.

1.5 Cellular senescence, an inbuilt safeguard

Cellular senescence is an irreversible state whereby progression through the cell cycle is impeded despite an adequate supply of nutrients and appropriate growth conditions, while cell viability and metabolic activity are fully maintained (Kuilman et al., 2010). To this day the 'Hayflick limit' describes the point at which cells irreversibly lose their ability to proliferate and enter replicative senescence after a finite number of divisions (Hayflick, 1965, Ogrunc and Fagagna, 2011). Initially this phenomenon was thought to be caused by inadequate culture conditions but senescence has been proved to be a physiological event taking place *in vitro* and *in vivo*. Senescent cells have been identified in benign skin lesions such as naevi (moles) and increased numbers of senescent cells have been identified in aged mice and humans, suggesting an accumulation of growth-arrested cells with age (Gray-Schopfer et al., 2006). Senescence can also be triggered prematurely in response to oncogene activation and hyper-proliferation, acting as an essential barrier against uncontrolled proliferation and thus as an early tumour suppressor mechanism (Campisi and d'Adda di Fagagna, 2007).

1.5.1 Markers of senescence

Progression to cellular senescence can be visually identified *in vitro* by striking morphological alterations. Changes include low saturation density, a general flattening and enlargement of cells, which is accompanied by increased cytoplasmic area (Campisi and d'Adda di Fagagna, 2007, Kuilman et al., 2010). The nucleolus of senescent cells can become highly condensed forming senescence-associated heterochromatic foci (SAHF), which are thought to contain silenced proliferation-associated genes (Zhao *et al.*, 2010). However, *in vivo* SAHF have not yet been observed. Besides a lack of DNA replication which is common to quiescent as well as senescent cells; senescence-associated beta-galactosidase (SA- β gal) staining is the most widely used marker of cellular senescence (Dimri et al., 1995, Debacq-Chainiaux et al., 2009). Histochemical staining for SA- β gal at pH 6.0 is related to increased lysosomal content that accumulates in senescent cells (Kurz

et al., 2000), although its function in senescence is unclear. As an alternative, immunohistochemical staining of Ki-67 or incorporation of BrdU can be used to estimate cellular proliferation (Schluter et al., 1993) but these methods cannot discriminate between quiescent and senescent cells. No single marker of senescence has been universally identified relevant to all cell types (Collado and Serrano, 2006, Buajeeb et al., 2009) but senescent cells accumulate senescence-associated molecules with ageing and tend to overexpress negative regulators of the cell-cycle, such as *p16* and *p21*, which can also be used as markers (Campisi and d'Adda di Fagagna, 2007, Kurz et al., 2000).

1.5.2 Replicative senescence

Telomere shortening provided the first molecular explanation for senescence, linking aging with increased growth arrest and is essentially what Hayflick observed (Campisi and d'Adda di Fagagna, 2007). Telomeric tandem repeats (5'-TTAGGG-3') protect and 'cap' eukaryotic chromosome ends; each time a cell divides the linear ends of telomeres gradually become shortened. This is due to the requirements of the DNA polymerase enzyme during replication that requires an existing strand from which to initiate elongation; this is known as the 'end-replication problem' (Zhao et al., 2014). As a consequence the lagging strand is incompletely replicated by DNA polymerase. Eventually, and after multiple rounds of replication, the telomeric repeat sequences reach a critical length due to attrition (Harley et al., 1990). A protective protein complex, known as Shelterin, helps to form a telomeric loop structure (t-loop) to hide the chromosomal ends (Stewart et al., 2012). When these proteins fall away due to telomere erosion, the unprotected telomeres are interpreted as DNA double strand breaks by the cell. This initiates a DNA damage response (DDR), halting progression through the cell-cycle and promoting replicative senescence via p53 activation, and phosphorylation by ATM and ATR kinases that sense DNA strand breaks (Parkinson, 2010, Ogrunc and Fagagna, 2011). Thus, telomeres act as a molecular clock limiting cellular lifespan (Harley et al., 1990, Zhao et al., 2014).

Telomerase is the ribonucleoprotein responsible for the maintenance of telomeres (Blackburn and Collins, 2011) and can extend them by reverse transcription from the chromosomal ends' tandem repeats. In humans, the catalytic component of telomerase (hTERT) is switched off except for in germ-line cells at around 20 weeks of development

meaning that, in most mammalian cells, their proliferative lifespan is finite due to telomere shortening. In human fibroblast cells, replicative senescence takes place after around 60 population doublings (Hayflick and Moorhead, 1961). Over 80 % of human tumour tissue samples re-express *hTERT* whereas normal tissues minimally express it. The reintroduction of *TERT* rescues cells from senescence as well as immortalising human primary cell lines (Bodnar et al., 1998, Collins and Mitchell, 2002, Finkel et al., 2007).

Replicative senescence is thought to have evolved as a protective anticancer mechanism to avoid the unlimited proliferation of unregulated cells. In smaller rodents such as mice and hamsters, telomerase is constitutively switched on (Prowse and Greider, 1995, Russo et al., 1998) maintaining telomeres and removing the replicative senescence barrier. Mice have exceptionally long telomeres (over 40 kb compared to 10-15 kb in humans) and *TERT*-deficient mice can produce viable and fertile offspring without defects for up to four generations, at which point telomere dysfunction starts to take its toll on proliferation and tissue renewal (Chang, 2005). Interestingly, telomerase activity is switched off in the largest rodents, e.g. the capybara and beaver, indicating that telomerase repression could be linked to body mass and longevity (Seluanov et al., 2007). Yet, both *in vivo* and in culture, wild-type cells from small rodents have limited life-spans and enter senescence under normal conditions after 20-30 population doublings (Russo et al., 1998). This is indicative of other intrinsic barriers to cellular immortality that must be bypassed for continuous cell growth.

1.5.3 DNA Damage response

The DNA damage response (DDR) senses DNA strand breaks caused by dysfunctional telomeres but also by other DNA damage that can place anywhere in the genome, for example in response to ionising radiation. The resulting cell-cycle arrest serves to impede replication of damaged genetic information that would otherwise lead to genomic instability. If repairable, cycling will continue upon the reinstatement of cellular homeostasis, but extensive or continuous DDR signalling may induce a permanent escape from the cell cycle; either initiating apoptosis or activating entry into cellular senescence. Like telomere-initiated senescence, DNA damage-initiated growth arrest is dependent on p53 activation which mediates DDR signalling. Double strand breaks are the most severe type of DNA damage and they activate p53 via ATM kinase phosphorylation while ATR

senses single-strand breaks. p53 acts as a transcription factor to promote the transcription of p21, a Cdk-inhibitor (CDKI) which inactivates the cyclin dependent kinases CDK2 and CDK4 that are necessary for progression into S phase of the cell cycle (see Figure 2) (Campisi and d'Adda di Fagagna, 2007, d'Adda di Fagagna, 2008). Senescent cells that undergo growth arrest due to persistent DDR signalling can contain nuclear foci that co-localise with DNA repair complexes, suggesting that their DNA remains permanently damaged (d'Adda di Fagagna et al., 2003, Larsson, 2011).

1.5.4 Stress-induced senescence (SIPS)

Inadequate culture conditions can be a cause of premature cellular senescence. When a cell line is initially established from a living tissue or organ the cell population needs to adapt to an artificial and non-physiological environment. This imposes varying degrees of stress which may drive the cells into senescence if the appropriate growth factors and oxygen levels are not provided (Kuilman et al., 2010, Sherr and DePinho, 2000). Multiple sub-lethal doses of hypoxia have been shown to induce premature senescence (Toussaint et al., 2000) whereas physiological oxygen levels can extend cellular lifespan (Parrinello et al., 2003). *In vivo* stress-induced premature senescence (SIPS) may occur when cells are removed from their normal surroundings, for example when a cell escapes its niche and finds itself in a new microenvironment.

1.5.5 Oncogene-induced senescence (OIS)

Premature senescence takes place when cells are exposed to oncogenic stimuli which initiate uncontrolled growth. This can be shown *in vitro* by transfecting human and rodent primary fibroblasts with genes encoding members of the RAS pathway family, which under normal settings relay extracellular mitogenic signals stimulating cell division. Instead of increasing proliferation, introduction of oncogenic forms of Ras and Raf leads to premature growth arrest (Newbold and Overell, 1983, Serrano et al., 1997, Zhu et al., 1998) and increases expression of the tumour suppressor genes (TSG) p16 and p53. When either of these two key TSG genes were disrupted, cells overexpressing RAS members bypassed senescence and continued to proliferate (Serrano et al., 1997). Oncogene-induced senescence (OIS) is therefore thought to have a protective role against tumour development and counteracts hyper-proliferation stimulated by excessive mitogenic signalling (Sharpless and DePinho, 2004).

Activation of senescence barriers is dependent on the p53 and p16-pRB pathways (Figure 2) which induce and maintain growth arrest (usually in the G1 phase of the cell cycle). Depending on the required response, one or both pathways may be activated to counteract DNA damage, such as telomere erosion, oncogene activation and stress. Both p53 and p16 pathways can converge on the retinoblastoma pocket protein (pRb) which functions to block the cell cycle, but each pathway modulates pRb via different cyclin dependent kinase (Cdk) activity (see Figure 2). Once bound together Cdks and cyclins (Cyclin E to CDK2 and 4 or Cyclin D to CDK4 and 6) target pRb and inactivate it by phosphorylation. Cdk-inhibitors (CDKI) p16 and p21 inhibit Cdk activity and maintain pRb in an active and unphosphorylated state. Active pRb binds directly to repress the E2F family of transcription factors which promote expression of genes involved in DNA synthesis and cell division. The tight control of the transition of G1 to S phase via pRb phosphorylation is therefore important to inhibit cell division until the cell is ready to replicate.

For entry into senescence, Cdk activity must be fully inactivated to ensure complete withdrawal from the cell cycle and maintenance of pRb activity. Repression of E2F transcription factors during senescence is maintained by pRb that, on binding the DNA, recruits remodelling proteins to condense the local chromatin by histone deacetylation and methylation (Talluri and Dick, 2012). For example, trimethylation of lysine 9 at histone 3 (H3K9me3) is catalysed by SUV39H1 and recognised by histone binding protein HP1 which appears to be specific to senescent cells and not quiescent cells. These repressive marks are thought to aid the formation of senescence-associated heterochromatin foci (SAHFs) which can accumulate in senescence cells (Narita et al., 2003).

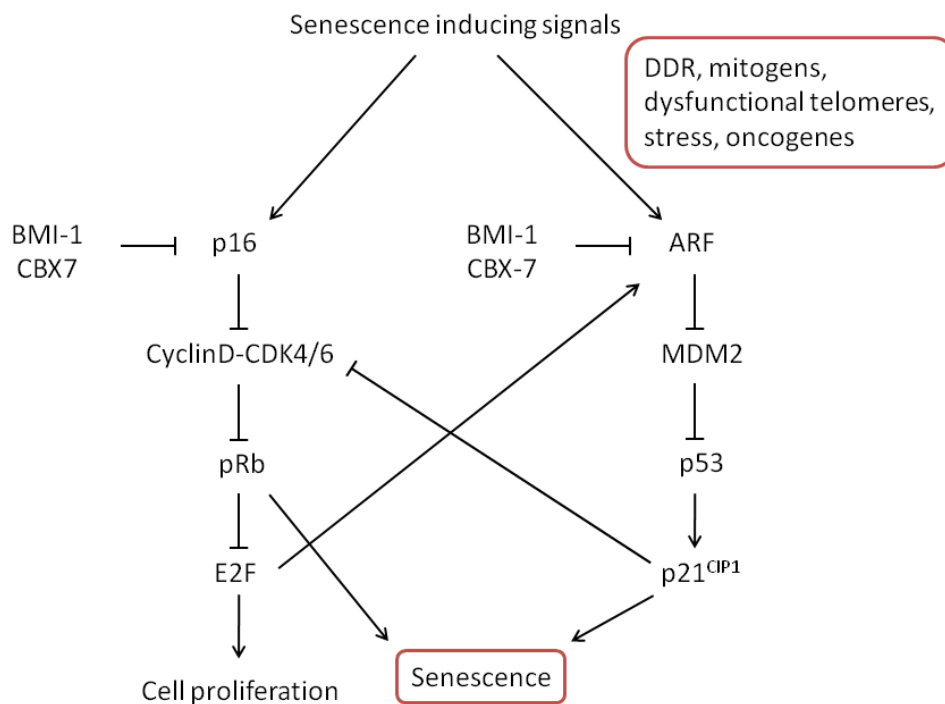


Figure 2 – The p16-pRb and p53 pathways promote cellular senescence

Senescence induction can be promoted by a number of stimuli which are relayed by intracellular signalling via the p16-pRb pathway and/or the p53 pathway; the latter is also involved in the DNA damage response pathway. In mice, ARF has an important role in sensing mitogens and oncogenic stress whereas, in humans, p16 seems to have the dominant role in inhibiting progression through the cell cycle. The p16-pathway inactivates Cyclin dependent kinases CDK4/6 to maintain pRb activation whereas p21 inactivates CDK2/4. Adapted from: (Campisi and d'Adda di Fagagna, 2007)

1.5.6 Species differences

The extent to which either senescence promoting pathway is engaged can be influenced by the cell-type and species. In mice, p53 inactivation is sufficient to bypass Ras-induced senescence, and abrogation of its upstream activator ARF has the same outcome (Kamijo et al., 1997). ARF is believed to have a more dominant role in murine models than p16 at promoting senescence (Sharpless et al., 2004), and has a stabilising role on p53 by sequestering its negative regulator Mdm2. Despite activation of both ARF and p16 in response to mitogenic signalling, MEFs lacking ARF spontaneously immortalise, whereas p16-null MEFs can still engage oncogene-induced senescence (Sharpless et al., 2001, Gil and Peters, 2006). Knockout of ARF in mice leads to early evasion of senescence and development of tumours *in vivo* (Kamijo et al., 1997, Zindy et al., 2003) with a broad

spectrum of tumour types (Kamijo et al., 1999). In humans, *p16* is predominantly activated in response to oncogenic signalling, and is believed to play a more important role in the commitment to cellular senescence. *In vivo* benign nevi (skin lesions) contain senescent cells that overexpress *p16* (Gray-Schopfer et al., 2006) while melanomas frequently lack functional *p16*. *ARF* specific mutations are rare, even though *ARF* and *p16* are found in the same genomic region and share exonic sequences (discussed later), whereas *p16* mutations have been described in many cancers (Kim and Sharpless, 2006, Forbes et al., 2010).

Escape from cellular senescence leads to immortalisation and it is thus considered the first barrier against malignancy. Infinite proliferative potential in itself is not harmful, but may permit successive mutational events to take place (Newbold et al., 1982, Newbold, 1985b). On average, 20-30 population doublings are required for a single cell to produce a daughter population large enough for a second mutation to occur. It is through such repeated rounds of mutation and selection (clonal evolution) that increased autonomy is acquired and, in rare cases, spontaneous immortalisation may take place, frequencies of which are species dependent (Newbold, 1985a, Trott et al., 1995). In humans, replicative senescence is activated by telomere shortening, but premature senescence can be triggered when the cell encounters oncogene activation, stress or sufficient DNA damage. Disruption of tumour suppressor genes and their regulatory networks can alter a cell's response to mitogenic signals and deregulate the control of the cell cycle. The bypass of senescence barriers by the disruption of the *p16*-*pRb* and *ARF*-*p53* pathways can be attained as a result of cooperating molecular events, leading to cellular immortalisation.

1.6 The tumour suppressor gene *p53*

Almost half of all tumours carry defective copies of the tumour suppressor gene *p53* and its deregulation is an established hallmark of cancer. Its main function is to preserve genomic stability and, in its wild type conformation, *p53* is capable of responding to many cellular stressors such as telomere shortening, DNA damage, oncogene activation and

hypoxia (Rufini et al., 2013). p53 signalling can induce a temporary cell cycle arrest to re-establish homeostasis and promote DNA repair or if necessary stimulate a permanent exit either by initiating apoptosis and cell death or promoting senescence pathways. *p53* knockout mice are known to be susceptible to spontaneous tumourigenesis from a young age (Donehower et al., 1992) and models carrying point mutations are also prone to cancer. Reintroduction of *p53* into deficient mouse lymphomas inhibits tumour growth and causes tumour regression following reactivation of senescence (Martins et al., 2006, Xue et al., 2007).

The activity of *p53* is highly regulated to permit rapid cellular responses to the range of stimuli that it is responsible for integrating. Post-transcription, p53 is assembled as a protein tetramer that acts as a transcription factor, binding to a large variety of downstream targets via p53-responsive elements. It has been estimated that murine p53 has over 3600 direct gene targets in mouse embryonic stem cells (Li et al., 2012). Its protein turnover is mediated by the E3 ubiquitin ligase Hdm2 (or Mdm2 in mice) which marks p53 for proteosomal degradation via poly-ubiquitination activity (Honda et al., 1997). In a negative-feedback loop, activated p53 acts as a transcription factor of *Mdm2* to promote its own degradation; quickly re-establishing homeostasis. Upstream of p53 is ARF that responds to oncogenic signalling by binding and sequestering Mdm2, inhibiting degradation of p53, indicating that p53 is available to interact with the Cdk-inhibitor p21 promoter (refer to Figure 2). The CDKI *p21* promotes cell-cycle arrest via inactivation of Cyclin E-CDK2/4 complexes. Induction of *p21* is elevated in senescing cells but only in those with functional p53 while *p21* knockout mice cannot arrest in G1 following DDR activation (Brugarolas et al., 1995). In a negative feedback loop, ARF is repressed by pRb-E2F complexes that form from p21 signalling (Sherr, 2006). ARF protein turnover is also regulated through ubiquitination from the E3 ubiquitin ligase ULF which when inhibited stabilises ARF, leading to p53-dependent growth arrest (Chen et al., 2010).

1.6.1 Post-translational modifications

p53 activity is tightly controlled at the post-translational level especially within its N-terminal transactivation and C-terminal regulatory domains. Post-translational modifications (PTMs) modulate p53, broadly speaking either by increasing protein stability (activating) or by promoting protein degradation (inactivating), like ubiquitination

(Marouco et al., 2013). Following DNA damage and exposure to carcinogens, multiple serine and threonine residues can be phosphorylated to stabilise p53. ATM and ATR kinases target Ser15 phosphorylation to promote Mdm2 release and transcriptional target transactivation (Saito et al., 2003, Loughery et al., 2014). A number of different PTMs have been identified with interdependent roles which may take place in a cell-type specific manner, regulating p53 and ultimately promoting growth arrest or increased cell proliferation (Marouco et al., 2013). Phosphorylation of Ser46 in mice is associated with p53-dependent senescence and reduced cellular immortalisation in MEF cells following oncogenic stress by Ras-induction (Feng et al., 2006), while Ser15 was phosphorylated by p38 MAPK activation following ionising radiation in HMEC cells (Wang et al., 2013). Acetylation is also an important PTM and its complete abolishment prevents p53 transactivation of *p21* leading to excessive cell proliferation (Tang et al., 2008), although removal of individual acetyl-sites can be compensated for by acetylation at other sites (Carter and Vousden, 2009). On sensing DNA damage, six lysine (K) residues that are targeted by Mdm2 for ubiquitination in the C-terminal domain, are instead acetylated to stabilise p53 by the histone acetyltransferase CBP/p300 (Kruse and Gu, 2008, Dai and Gu, 2010). In response to oncogenic *myc*, acetylation of K120 takes place due to ARF signalling which promotes OIS (Mellert et al., 2007). Finally, methylation at site-specific lysines can also influence p53 activity by either stimulating growth arrest via increased promoter binding affinity or by repressing gene target activation (Scoumanne and Chen, 2008).

1.6.2 *p53* mutations

In a recent study by The Cancer Genome Atlas (TCGA) 42 % of all tumours tested carried a *p53* mutation (Kandoth et al., 2013) and, although substitutions are frequently located in six mutational hotspots within its DNA binding domain (see Figure 3), point mutations have been identified across the whole gene locus (Leroy et al., 2013). Missense mutations leading to amino acid substitutions are most commonly associated with the disruption of *p53* function, and the resulting mutant p53 proteins can often act independently and in a dominant-negative way to wild-type *p53* (Muller and Vousden, 2014).

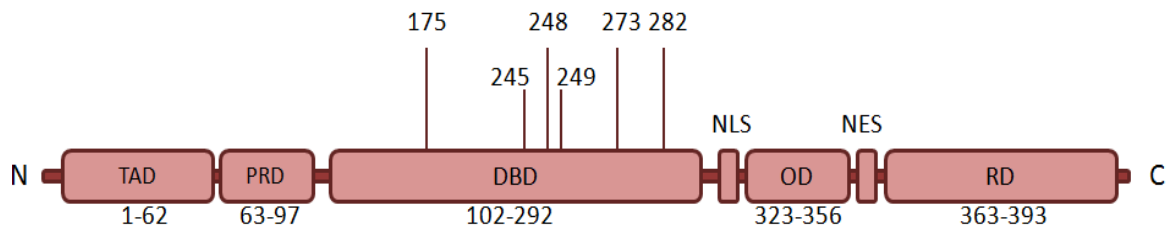


Figure 3 – p53 functional domains and mutation hotspots

A diagram of the human p53 protein and its six mutational hotspots that are often identified in cancers. Over 90 % of mutations are found within the DBD and are mostly missense point mutations. TAD: transactivation domain, PRD: proline rich domain, DBD: DNA binding domain, OD: oligomerisation domain, RD: regulatory domain, NLS: nuclear localisation signal, NES: nuclear export signal. The amino acid numbers are below. Adapted from: (Vousden and Lu, 2002, Marouco et al., 2013).

A single substitution in the p53 DNA binding domain can affect the protein's affinity to its targets, thus modulating downstream transcriptional activation, and may even confer recognition of alternative binding sites. *p53* mutations can also influence protein folding and stability (i.e. structural mutants) which may disrupt normal protein function, alter a PTM site and potentially also uncover new protein interaction sites (Muller and Vousden, 2013). Consistent with a dominant-negative function, mice with one mutated *p53* allele are prone to more types of malignant lesions than those that are *p53* null or have a single mutated gene copy (Doyle et al., 2010, Kenzelmann Broz and Attardi, 2010). Li-Fraumeni syndrome patients with germline *p53* missense mutations are more susceptible to the onset of early cancers than those with reduced p53 protein expression (Zerdoumi et al., 2013). These findings are suggestive of a dominant role of a dysfunctional p53 protein which has tumour promoting functions (gain-of-function) and thus contributes to oncogenesis (Muller and Vousden, 2013). As an example, mutated forms of p53 can bind and inhibit TAp63 (Strano et al., 2002), which if deleted leads to promotion of cell invasion and metastasis (Su et al., 2010) also indicating important co-operative roles of p53 family members in suppressing oncogenesis (Qian and Chen, 2013).

1.6.3 *p53* splice variants

Canonical *p53* contains seven different functional domains (shown in Figure 3) and the full length human protein (*p53* α) is 393 amino acids long. The locus found on chromosome 17p13 encodes ten or more *p53* isoforms via alternative splicing of its 11 exonic regions, contains two transcriptional promoter sites (P1 and P2) (Bourdon et al., 2005) and two translational initiation sites. Its multiple isoforms are expressed in normal cells and their relative abundance is cell- and tissue-type dependent, implying subtle functional differences (Khoury and Bourdon, 2011). Following DNA damage, *p53* can self-activate its internal promoter situated in intron 4 and thus upregulate its $\Delta 133p53\alpha$ isoform (Aoubala et al., 2011). $\Delta 133p53\alpha$ has been shown to reduce G1 arrest and apoptosis but has no effect on G2 arrest; in human fibroblasts it can induce cellular proliferation by *p21* transcriptional inhibition and thus also act in repressing senescence (Aoubala et al., 2011). In the cell's resting state, *p53* β (which has an alternative C-terminal domain) preferentially binds and activates promoter regions of the cell-cycle regulator *p21*, unlike *p53* α which preferentially binds to Mdm2 (Bourdon et al., 2005). The isoform *p53* β can also induce expression of the microRNA miR-34a to upregulate replicative senescence while $\Delta 133p53\alpha$ is believed to repress miR-34a expression (Fujita et al., 2009). It is unsurprising then that in cancer, malignant cells can also differentially express *p53* isoforms; for example, in melanoma *p53* β and $\Delta 40p53$ isoforms have been identified whereas they are not found in normal melanocytes and fibroblasts. Clinical studies suggest that isoform expression profiles may be linked to tumour stage and be predictive of prognosis (Surget et al., 2013).

p53 is a highly regulated transcription factor that controls and responds to many pathways. Alternative splicing and post translational modifications help fine-tune its expression and modulate its cellular activities. The deregulation of *p53* by point mutations is commonly associated with cancer and the disruption of its signalling pathway can have detrimental effects on its ability to induce senescence.

1.7 The tumour suppressor gene *p16*

In the context of replicative senescence, activation of the p16/pRb pathway seems to play a secondary, albeit critical role in finalising induced growth arrest. In response to telomere erosion and DNA damage, human cells activate both p16 and p53 pathways which work together in promoting senescence (Jacobs and de Lange, 2004). Mouse *p53*^{-/-} knockouts failed to enter senescence when provoked with telomeric disruption, indicating that the p16 pathway alone may be insufficient to trigger growth arrest in response to DNA damage (Smogorzewska and de Lange, 2002). However, following premature senescence induced by *p16* expression, inactivation of key regulators p53, pRb as well as p16 had no effect on senescence reversal and replicative rescue (Beausejour et al., 2003) indicating that once the p16-pathway is fully engaged it is irreversible. This is in contrast to p53-induced senescence where inactivation of the p53-pathway can reinitiate cell growth (Gire et al., 2004, d'Adda di Fagagna et al., 2003). Serial passaging of cultured cells has also been correlated with increasing transcript levels of *p16* in many human primary cell lines and thus implicating its role in cellular ageing (Collado et al., 2007, Krishnamurthy et al., 2004, Kim and Sharpless, 2006). Its upregulation in response to carcinogenic exposure, oxidative stress and DNA damage, and chromatin alterations demonstrates the importance of p16 signalling in OIS (Campisi and d'Adda di Fagagna, 2007).

Like p21, p16 is a cyclin dependent kinase (Cdk) inhibitor that functions by blocking progression from the G1 to S phase. It maintains Retinoblastoma protein (pRb) activity by inactivating CDK4 and CDK6 so that they cannot complex with cyclin D, thus locking pRb into its hypophosphorylated and active form. In turn, active pRb sequesters the E2F transcription factors responsible for transactivating genes that are required for proliferation and cell-cycle progression leading to senescence entry. There are two phosphorylation sites at either end of the p16 protein which can confer stability and are known to modulate CDK4 association (Gump et al., 2003, Guo et al., 2010). Double knockout of Cdk-inhibitors p21 and p16 rendered mice highly susceptible to tumour formation when painted with DMBA/TPA, and senescence barriers were rapidly bypassed in MEF-derived cells following introduction of ectopic Ras signalling, despite strong upregulation of *p15* (Takeuchi et al., 2010). The study suggests a compensatory role

between p21 and p16 in oncogene-induced senescence; in the absence of one the other CDKI is upregulated, although *p16*^{-/-} mice suffered from aggressive lesions while benign lesions were found in *p21*^{-/-} mice (Takeuchi et al., 2010).

Compared to *p53* the tumour suppressor gene *p16* (also known as CDKN2A or Ink4a) is less frequently mutated, but many tumours are prone to homozygous or heterozygous gene deletion and silencing of *p16* to such an extent that 50% of all human cancers display *p16* inactivation (Gonzalez and Serrano, 2006). Deregulation of *p16* has been described as a necessary early event in the progression of tumourigenesis in Barrett's oesophageal cancer (Chao et al., 2008, Paulson et al., 2008), and its inactivation has been associated with carcinogenesis (Li et al., 2008, Yasaei et al., 2013). *p16* overexpression has also been identified in several late-stage tumours, which initially contradicts its accepted tumour suppressor role (Romagosa et al., 2011). High levels of *p16* are found in benign lesions which retain functional p16-Rb pathways capable of inducing senescence (Gray-Schopfer et al., 2006) but, if evaded by further downstream mutations, then p16 signalling is ineffective. In this scenario, high-grade malignant tumours overexpress *p16* as a result of positive feedback due to non-functional pRb permitting uncontrolled proliferation (Romagosa et al., 2011).

1.7.1 The *CDKN2A/B* locus

Located on chromosome 9p21 in humans, the *CDKN2A/B* locus (also known as *INK4-ARF*) encodes three known tumour suppressor genes (Gil and Peters, 2006, Simboeck et al., 2011). Extending over 35 Kb, this region is situated in a gene desert and is prone to deletions that contribute to melanoma, carcinomas and leukaemias, while knockout mice are susceptible to spontaneous lesions (Gu et al., 2013). The region encodes *p16*, *p15*, *ARF*, *p16γ* and *p12*; the latter two are splice variants of *p16* and are mostly uncharacterised, although *p12* expression is restricted to the pancreas. *ARF* and *p16* are under the control of separate autonomous promoters and are located 20 Kb from each other, but share a second exon which is read in an alternative reading frame (hence ARF). The resulting translated proteins are completely distinct from one another and both promote senescence by independent pathways; p16 acting via pRb and ARF via p53. Located upstream of both *ARF* and *p16*, *p15* is thought to have arisen by gene duplication of *p16* and also targets CDK4/6 for cell cycle regulation (Krimpenfort et al., 2007).

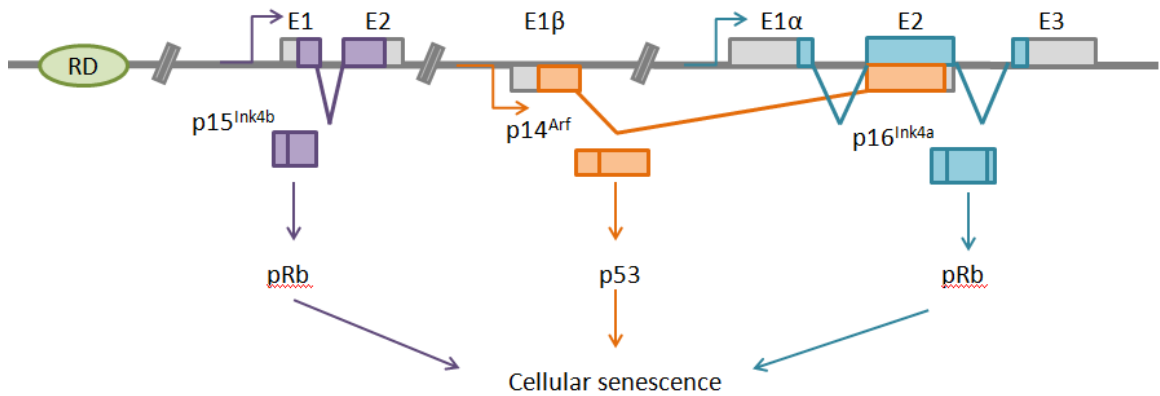


Figure 4 – The *CDKN2A/B* locus

Located on chromosome 9p21 in humans and chromosome 4 in mouse, the *CDKN2A/B* locus encodes three tumour suppressor genes which act to promote cellular senescence: encoded proteins p16 and p15 inhibit CDK4/6 to keep the Retinoblastoma protein (pRb) hypophosphorylated and active, while ARF (p14 in humans, p19 in mice, p13 in rat and hamster) which is read in alternative reading frame to p16, sequesters Mdm2 to stabilise and promote p53 activity. Upstream of the locus is a regulatory domain (RD) that is bound by Polycomb group proteins (PcG) that can repress transcription by influencing local histone modifications and may also function to coordinate *CDKN2A/B* gene expression. Adapted from (Peters, 2008)

The *CDKN2A/B* locus has been identified in tumours as a site of mutation, or more commonly deletion, suggesting its anti-tumourigenic role (Gil and Peters, 2006, Li et al., 2014). In most cases, mutations are contained within the *p16* portion of the locus and rarely solely target *ARF*, while *p15* mutations are equally uncommon. The majority of mutations are missense which can take place across the whole protein length and tend to influence p16’s ability to interact with its cyclin kinase targets CDK4/6, but mutations may also influence cellular localisation (McKenzie et al., 2010). Around 40 % of melanoma patients inherit germline *p16/ARF* gene mutations that predispose them to developing lesions (Goldstein et al., 2007). The *CDKN2A/B* locus is also frequently targeted in urinary bladder cancers (>50 %), but its inactivation is predominantly due to homozygous deletion (HD) and loss of heterozygosity (LOH) of *p16* and *ARF* (Williamson et al., 1995, Berggren et al., 2003). Mouse knockout studies for each of the three encoded genes

correlated with increased tumour formation and a triple knockout developed a wide range of lesions within seven months (Krimpenfort et al., 2007).

1.7.2 Epigenetic regulation

Multiple epigenetic mechanisms are being unveiled in the regulation of the *CDKN2A/B* locus, adding layers of complexity for the coordinated expression of *p16*, *ARF* and *p15* during development, and later when promoting senescence. During embryogenesis and early developmental stages the expression of the *CDKN2A/B* locus is minimal, presumably to permit rapid cellular division (Li et al., 2009). Although not fully understood, disruption of epigenetic molecular components can lead to deregulation and senescence bypass (Gil and Peters, 2006, Popov and Gil, 2010).

DNA methylation is mostly associated with transcriptional repression of genes, occurring in the promoter regions enriched for CG dinucleotides known as CpG islands. Covalent binding of methyl groups to CpG sites can alter the binding affinity of transcription factors, or recruit repressive methyl binding and histone modifying proteins to further enhance gene silencing (Sharma et al., 2010). Cancers are generally associated with a deregulation of methyl marks, leading to genome-wide hypomethylation, but with site-specific hypermethylation at CpG islands that would normally be unmethylated (Jones and Baylin, 2002). The tumour suppressor gene *p16* is commonly silenced in cancer by promoter hypermethylation and has been suggested as a predictive marker of *p16* status (Wang et al., 2012), in some cases promoter methylation is thought to be an early event predisposing cells to evasion of senescence barriers (Al-Kaabi et al., 2014). Similarly, *ARF* and *p15* gene promoters have also been found to be methylated in cervical cancers, glioblastomas and oral carcinomas; thus the identification of methylation at *CDKN2A/B* gene promoters has prognostic potential (Robertson and Jones, 1998, Wemmert et al., 2009, Jha et al., 2012).

The *CDKN2A/B* locus is regulated epigenetically by local chromatin remodelling which coordinately influences gene transcription of three crucial regulators of senescence (Simboeck et al., 2011). In proliferating cells, the Polycomb group (PcG) of proteins is known to target the *CDKN2A/B* locus and associates with the DNA as two complexes. The PRC2 contains the histone methyltransferase EZH2 that trimethylates histone 3 lysine 27

(H3K27me3), which then serves as a recruiting mark for PRC1 members (such as RING1B, BMI-1 and CBX proteins). Once bound, PRC1 proteins maintain the repressive state by mono-ubiquitinating histone H2A which, together with PRC2 complexes, locally compact the DNA and hinder transcriptional initiation (Henikoff et al., 2004). During senescence and following cellular stress, *EZH2* is downregulated (Agherbi et al., 2009), leading to a loss of repressive histone trimethylation at the *CDKN2A/B* locus and a progressive release of bound PcG proteins spanning *p16/ARF*; this is correlated with an increase in expression of *p16* and *ARF* (Bracken et al., 2007). Additional histone modifiers have been found to associate with the *CDKN2A/B* locus to further activate it; JMJD3 (a lysine specific demethylase) removes repressive methyl marks and replaces them with ones associated with transcription, thereby promoting senescence (Agherbi et al., 2009). The deregulation of histone modifications and chromatin binding protein-complexes leading to the perturbation of transcriptional regulation is thus implicated in tumorigenesis (Mills, 2010, Fullgrabe et al., 2011, Varier and Timmers, 2011). Indeed, overexpression of PRC1 and PRC2 components have been identified in cancers that cooperate with oncogene activation to bypass senescence and promote sustained cell division (Dietrich et al., 2007, Velichutina et al., 2010, Larsson, 2011, Jia et al., 2014).

Displacement of PcG proteins from the *CDKN2A/B* locus during senescence also includes BMI-1 which does not seem to undergo changes in gene expression during ageing (Agherbi et al., 2009). However, if overexpressed BMI-1 can act oncogenically by repressing SIPS/OIS and binding to the *p16* promoter along with CBX8 (Bracken et al., 2007). In MEFs lacking *BMI-1* premature senescence takes place, while its overexpression induces immortalisation (Jacobs et al., 1999). Upregulation of *BMI-1* has been shown to extend human cellular lifespan and was dependent on functional pRb but not p53 activity, implicating its suppressive role on the p16 pathway (Itahana et al., 2003). Finally, the *p16* promoter contains a BMI-1 binding element (BRE) that negatively regulates transcription, suggesting that the PRC1 member BMI-1 can also act directly as a transcription factor to repress *p16* expression (Meng et al., 2010).

A regulatory domain (RD) has been identified in a conserved non-coding region 1.5 Kb upstream of *p15*'s transcriptional start site, which contains a potential replication origin which might confer synchronized regulation of the *CDKN2A/B* locus (Gonzalez and

Serrano, 2006, Li et al., 2011). Additionally, the 150 bp RD element is recognised by Cdc6, a protein that is strongly overexpressed in cancers and that recruits histone deacetylases (Gonzalez et al., 2006, Gonzalez and Serrano, 2006). Polycomb proteins including BMI-1 and EZH2 have also been identified to localise at the RD in young proliferating MEFs, indicating a regulatory role on local chromatin (Agherbi et al., 2009). The RD upstream of *CDKN2A/B* has been found to be deleted in tumour samples and malignant human cell lines, further implicating the domain in carcinogenesis (Li et al., 2014).

MicroRNAs (miRNAs) have also been associated in promoting senescence (Abdelmohsen et al., 2012). Only 21-23 bp in length, they are processed non-coding mRNAs that target gene transcripts by sequence specific binding inhibiting protein translation or promoting mRNA degradation. A recent screen suggests 16 putative miRNAs could significantly upregulate *p16* expression following oncogene-induced senescence from Braf activation, and a further seven miRNAs could potentially downregulate *p16* (Kooistra et al., 2014). Suppression of BMI-1, promoting *p16* expression, has been found to be controlled by miR-141 which was upregulated during cellular senescence, (Dimri et al., 2013, Itahana et al., 2013) while miR-378a-5p represses *p16* protein expression and attenuates oncogene-induced senescence following Braf activation, although the specific miR-378a-5p target is unknown (Kooistra et al., 2014). In HMECs and in human fibroblasts, a further four miRNAs were shown to be progressively upregulated during cellular senescence, (miRNA 26b, 181a, 210 and 424) and their overexpression led to increased *p16* levels and decreased cell growth rates (Overhoff et al., 2014). Moreover these miRNAs targeted members of the Polycomb repressor complexes such as EZH2 and CBX7; the authors suggest a regulatory feedback loop between miRNAs to stimulate PRC2/PRC1 release from the *CDKN2A/B* locus while the PcG proteins repress miRNA expression to keep the locus silenced (Overhoff et al., 2014). Other silencing mechanisms include long non-coding RNAs like *ANRIL* (antisense non-coding RNA in the *INK4* locus), which is transcribed in the opposite direction to the *CDKN2A/B* locus, overlaps with *p15* and its promoter is in close proximity to *ARF*'s transcriptional start site (Popov and Gil, 2010). It is thought that *ANRIL* can suppress *p15* and *p16* transcription and may further coordinate recruitment of PRC proteins to the locus (Aguilo et al., 2011).

The *CDKN2A/B* locus contains three important tumour suppressor genes that act via the p53 and pRb-pathways to promote growth arrest. Together p16, p15 and ARF restrain cell proliferation in response to oncogenic signals. Their expression can be co-ordinately controlled by protein complexes and epigenetic modifications influencing local chromatin structure at chromosome 9p21, but *CDKN2A/B* gene products can also be independently regulated. Inactivation of p16 is frequent in human cancers, and has an important role in inducing senescence, although in mice ARF seems to be more influential in promoting growth arrest.

1.8 The Syrian hamster as a model

In contrast to rodents, human cells have two major barriers safeguarding unlimited proliferative potential; premature senescence (OIS/SIPS) and replicative senescence (RS). Their combined role in protecting the cell from malignant growth explains the observed low frequency of immortalisation and cell transformation in human cells (Trott et al., 1995, Russo et al., 1998). It has been postulated that large mammals evolved a second senescence-inducing mechanism to minimise accumulative damage resulting from a longer lifespan and a larger soma. Small rodents must rely on oncogene-induced senescence as their only failsafe senescence barrier, but this also implies that the bypass of OIS/SIPS can be thus analysed in isolation in mice and hamsters, without needing to reactivate TERT (Russo et al., 1998). Since the 1960s the Syrian or Golden hamster (*mesocricetus auratus*) has been used as a model to study chemical cell transformation and carcinogenesis (Berwald and Sachs, 1963). Compared to classically implemented mouse models which are genetically better characterised, the Syrian hamster has a lower rate of spontaneous immortalisation, and a higher innate resistance to genetic aberrations (Trott et al., 1995). Human cells very rarely immortalise even when exposed to carcinogens, so as a model the Syrian hamster is a good compromise; transformation can be readily induced by chemical exposure but, unlike mouse cells, hamster cells have a relatively low rate of spontaneous immortalisation (frequency of $<10^{-9}$ per primary SH cell compared to $>10^{-5}$ in mice) (Newbold, 1985b, Trott et al., 1995).

1.8.1 SH carcinogen-induced immortalisation

To aid the study of senescence bypass and the mechanisms regulating immortalisation, cells can be exposed to known carcinogens and mutagenic agents. Using SH dermal cells (SHD cells) mechanisms underlying OIS/SIPS and its bypass in the Syrian hamster have been studied following exposure to a number of chemical and physical carcinogens (Yasaei et al., 2013). SHD clones were generated using the SHD mass culture CTA and senescence bypass was induced by treatment with benzo(a)pyrene, nickel chloride and ionizing radiation (IR). Components of the p53 and p16/Rb-pathway were differentially affected, suggesting specific mutagenic fingerprints. Complete physical loss of the *CDKN2A/B* locus was identified in SHD clones immortalised by IR. However, karyotyping did not reveal gross chromosome aberrations, indicating locus-specific losses. No gene expression was detected for *p16*, *p15* or *ARF* in these clones. SHD cells exposed to the known point mutagen benzo(a)pyrene produced immortalised clones with missense mutations (mainly G to T transversions) in the DNA binding domain of *p53* and single allele losses of *p16* was commonly observed, possibly indicating haploinsufficiency. *p53* mutations were not identified in IR- or nickel-treated SHD cell lines and, in *p16*, gene substitutions were rare. However, in the majority of immortalised B(a)P-treated lines, *p16* expression was upregulated together with *ARF* but *p15* was transcriptionally repressed, raising the possibility that *p15* downregulation may have cooperated with *p53* point mutations to bypass oncogene-induced senescence. Finally, all nickel clones had downregulated *p16* expression but expressed *ARF* and *p15*. Extensive DNA methylation in the 5' promoter region of *p16* accounted for epigenetic gene silencing due to nickel exposure; nickel is a known non-genotoxic carcinogen. Finally, one B(a)P treated line was also methylated and had low levels of *p16* expression. The data indicates a critical role for p16 in establishing OIS/SIPS, possibly more akin to that in human senescence rather than in mice (Sherr and DePinho, 2000). Bypass of senescence in SHD was described as either a one-step hit (termed Type I immortalization) whereby *p16* and the whole *CDKN2A/B* locus was deleted leading to sustained uncontrolled proliferation, or as a two-step process (Type 2 immortalization) involving *p53* mutations and suppression of *p16* or *p15* (Yasaei et al., 2013).

Deletion and inactivation of the *CDKN2A/B* locus containing *p16* is commonly observed in tumours (Goldstein et al., 2007, Williamson et al., 1995, Berggren et al., 2003, Gu et al., 2013). Several studies have also identified *p16* alterations in chemically-induced tumours derived from the Syrian hamster. Tumourigenic hamster cell lines derived from pancreatic and oral SH tumours were lacking both *p16* and *p15* due to homozygous deletions (*ARF* was not analysed) (Muscarella et al., 2001). Others have identified downregulation of *p16* expression due to heterozygous deletion and/or DNA methylation at the *p16* promoter in pancreatic cancers (Li et al., 2004, Hanaoka et al., 2005). Although these studies did not involve analysis of ARF-p53 pathways, they further confirm the protective role of *p16* against tumourigenesis. p53 on the other hand has been studied in SH cheek-pouch lesions that model squamous cell carcinomas (SCC), and accumulates in pre-malignant and malignant tissues, most likely to due to the induced point mutations observed in the p53 DNA binding domain (Gimenez-Conti et al., 1996, Chang et al., 2000).

The Syrian hamster can be considered a suitable model for studying carcinogenesis and senescence-bypass in isolation from telomere erosion. Molecular mechanisms that inactivate the p16 and p53 tumour suppressor pathways have shown similarities between human and hamster senescence bypass and tumourigenesis. Characterisation of oncogene-induced senescence and carcinogen-induced immortalization has been performed in primary SHD cells, but has not yet been undertaken in SHE cells derived from the SHE CTA. In order to validate the SHE CTA the molecular analysis of cellular transformation events needs to be addressed and that constituted a major aim of this project.

PROJECT OVERVIEW AND AIMS

Current legislative and ethical pressures require a substantial reduction in the number of animals used in carcinogenicity testing for safety purposes. Pre-validation studies conducted on behalf of ECVAM have concluded that the Syrian hamster embryo cell transformation assay (SHE CTA) could be a promising assay for predicting carcinogenicity. However, the underlying mechanisms of carcinogen-induced morphological transformation are unknown and the relevance of the SHE CTA as a representative model of carcinogenesis has not been confirmed. It has been shown that the rate-limiting immortalisation step in the Syrian hamster (SH) requires only the bypass of the oncogene/stress-induced senescence barrier (SHE cells have constitutive telomerase activity) meaning that OIS can be studied in isolation and spontaneous progression towards immortalization is a rare event. Therefore, SHE cells should be further exploitable as a useful *in vitro* cell transformation model for carcinogen screening.

The objective of this project was to evaluate the SHE CTA and demonstrate that the assay has a sound mechanistic basis. The results of an extensive body of work to characterise early-events leading to senescence bypass and cellular immortalisation are described, and these provide a more detailed molecular understanding of the SH morphologically transformed (MT) phenotype, following induction by the known mutagen and potent human carcinogen, benzo(a)pyrene. The findings address some of the current concerns regarding the SH CTA while, at the same time highlighting work that still needs to be done to improve the assay's objectivity and reproducibility.

CHAPTER 2

2 General Materials and Methods

Details of specific experimental procedures are located
at the beginning of each results chapter

2.1 Cell culture

2.1.1 Cell culture medium and supplements

Syrian hamster embryo-derived (SHE) cell lines were grown in Dulbecco's modified Eagle's medium, LeBoeuf's modification without L-Glutamine (DMEM-L) (Quality Biological) supplemented with 20 % (v/v) fetal bovine solution (FBS) (Invitrogen Gibco®), 4 mM GlutaMAX™ supplement (Invitrogen Gibco®), 100 units/mL penicillin and 100 µg/mL streptomycin (Gibco®) and incubated in a humidified HERAcell (Heraeus) incubator at 37°C ± 1°C with 10 % CO₂ ± 1 %. Medium was used within 2 weeks and discarded if its pH was visibly altered.

2.1.2 Tissue culture plastics

Cells were grown in disposable plastic petri dishes (60, 100 or 150 mm) or flasks (75 or 175 cm²) (Sarstedt). Centrifugation took place in 15 mL disposable centrifuge tubes (Sarstedt).

2.1.3 Routine subculture of cells

All cellular manipulations were performed in a HERASafe (Heraeus) safety cabinet. Media was changed in cultures every 2-3 days by aspirating the existing culture medium and replacing it with 5 mL fresh medium per 60 mm dish or 10 mL medium per 100 mm dish.

On reaching 60-80 % confluence, SHE cells were subcultured at a seeding density of 5 x10⁴ to 6 x10⁵ cells per 100 mm dish depending on the individual cell line. Cells were detached by washing in 4 mL Ca²⁺ and Mg²⁺ free Hank's Balanced Salt Solution without phenol red (CMF-HBSS) (Gibco®) before incubating cells in 4 mL 0.05 % Trypsin-EDTA (Gibco®) for 3-5 min at 37 °C. After gentle tapping, the effects of trypsin were neutralised by adding equal volumes of media to dislodge cells and any clumps were removed by retropipetting. Cells were then centrifuged to remove traces of trypsin-EDTA at 1000 x g for 5 min and fully resuspended in fresh media. Appropriate volumes of cell suspension were then seeded into equilibrated fresh media and returned to the incubator.

2.1.4 Cryostorage and recovery of cells

Exponentially growing cells were trypsinised and centrifuged before being resuspended drop-wise in cryostorage medium made from FBS with 10 % DMSO (v/v) (Sigma-Aldrich®)

to limit the extent of freeze-thaw damage. Resuspended cells were aliquoted into 1 mL screw-cap cryovials (Sarstedt) at a freezing density of 10^6 - 10^7 cells/mL. Vials were placed in freezer heads and frozen overnight at a rate of approximately -1 °C/min in the gaseous phase of liquid nitrogen (LN₂). Cells were then stored at temperatures below -170 °C in liquid nitrogen until needed. To recover cryostored cells, each vial of frozen cells was rapidly thawed in a 37 °C water bath. The cells were then aseptically transferred to fresh equilibrated media and allowed to attach. The next day, medium was changed to remove DMSO and from then on media was changed every 2-3 days while in culture.

2.2 Senescence-associated beta-galactosidase staining

Cells were considered terminally senescent when no signs of cell growth were visible after once month of seeding without further sub-culture. An increase in cellular beta-galactosidase activity is a marker of cellular senescence and this can be detected by staining fixed cells with X-gal which, in senescent cells, forms a blue precipitate.

Cells were seeded in 60 mm or 100 mm dishes and allowed to attach. Proliferating cells were included as negative controls. Medium was aspirated and cells washed in phosphate buffered saline (PBS) twice for 30 sec before being permeabilised and fixed for 5 min in 2 % formaldehyde (v/v) and 0.2 % glutaraldehyde (v/v) made in PBS buffer. The fixation solution was aspirated and cells washed twice in PBS again for 30 sec. Cells were then incubated overnight at 37 °C in the dark with SA-βgal staining solution. The staining solution was prepared on the day in ultra-pure water (Debacq-Chainiaux et al., 2009): 40 mM Citric acid/Sodium phosphate buffer (adjusted to pH 6.0), 5 mM Potassium hexacyano-ferrate (II) trihydrate { $K_4[Fe(CN)_6]3H_2O$ }, 5 mM Potassium hexacyano-ferrate (III) { $K_3[Fe(CN)_6]$ }, 150 mM sodium chloride, 2 mM magnesium chloride and 1 mg/ml X-gal in N,N-dimethylformamide (pre-warmed at 37 °C for 1 hour to avoid aggregates). (All reagents were from Sigma-Aldrich®). The following day, the staining solution was removed and cells washed twice in PBS before air drying through the use of 1-2 mL methanol. Plates were stored at RT in the dark. Fixed and stained cells were then imaged using an Olympus CK40 microscope with a Dino-Eye digital eyepiece (Dino-Lite) and DinoCapture v2.0 Software. Stained cells were counted for intense blue staining corresponding to SA-βgal activity.

2.3 RNA extraction

RNA was obtained via phenol-based extractions of cultured SHE cells using peqGOLD TriFast (PeqLab Ltd). At 75-85 % cell confluence, media was removed from 100 mm dishes and cell monolayers were washed twice using ice cold CMF-HBSS. 1 ml TriFast reagent (10 X) was added per dish and incubated at room temperature for 2 minutes to lyse cells. The resulting lysate was retro-pipetted and transferred into a chilled 1.5 ml microfuge tube with the aid of a cell scraper. Sample preparations were then either stored at -80 °C or used directly for RNA extraction.

At room temperature, 200 µl chloroform was added to each tube for every 1 ml TriFast reagent used, before vigorously shaking for 15 sec; this was followed by a 5 min incubation at room temperature to allow phase separation to take place. Samples were then centrifuged at 12,000 x g for 5 min at 4 °C. The resulting clear supernatant containing RNA was carefully transferred into appropriately labelled clean 1.5 ml microfuge tubes containing 500 µl isopropanol (Sigma-Aldrich®) before inverting the tube several times to precipitate the RNA. Samples were incubated on ice for 5 min and then centrifuged at 12,000 x g for 10 min to pellet the RNA. At this point the supernatant was decanted and 500 µl 75 % ethanol was added to wash the RNA pellet twice before vortexing and further centrifuging for 10 min. Finally, remaining ethanol was removed and the RNA pellet allowed to air dry before resuspending in 20-40 µl chilled DNase, RNase-free H₂O depending on pellet size. Samples were quantified and then stored at -80 °C.

2.3.1 Nucleotide quantification

RNA concentrations were quantified using a NanoDrop 2000 (Thermo Scientific™) which uses a 1 µl sample for quantification (in ng/µl) and also assesses RNA quality by determining the $A_{260/280}$ and $A_{260/230}$ ratio. Quality of RNA was also assessed by running representative samples on an agarose gel to check 18S and 24S ribosomal RNA (rRNA) subunit integrity as well as messenger RNA (mRNA) integrity.

2.3.2 RNA purification

RNA extractions performed using phenol-based methods need to be cleaned up for residual genomic DNA by DNase treatment. For every 1 µg of RNA, 1 µl 10 X DNase buffer

and 1 μ l DNaseI enzyme (Invitrogen™) were added to a final volume of 10 μ l in RNase/DNase-free dH₂O. Treated RNA was then incubated at RT for 15 min before adding 1 μ l of 25 mM EDTA solution to stop the reaction, along with 10 min incubation at 65° C to inactivate the enzyme. Samples were either stored at -80 °C or used directly for reverse transcription.

2.4 First strand synthesis (cDNA)

A high-capacity cDNA reverse transcription kit (Applied Biosystems®) was used to reverse transcribe single-stranded cDNA from extracted RNA samples. For a final cDNA volume equal to 20 μ l the following was added per RT reaction: 2 μ l 10X RT buffer, 0.8 μ l 25X dNTP mix (100 mM), 2 μ l 10X RT random primers, 1 μ l multiScribe reverse transcriptase, 1 μ l RNase OUT (Invitrogen™) and 2.2 μ l nuclease-free water. The reaction was gently mixed together with 1 μ g total RNA treated with DNase I as described above in section 2.3.2. For reverse transcription, samples were incubated on a thermal cycler, DNA Engine Tetrad2 (MJ Research): 25 °C for 10 min, 37 °C for 120 min, 85 °C for 5 min and held at 4 °C until stored at -20 °C.

2.5 Quantitative real-time PCR (qPCR) using SYBR chemistry

Real-time PCR was performed using 7900HT fast real-time PCR system with SDS v2.4 software (Applied Biosystems®) in 10 μ l reactions in a clear MicroAmp fast optical 96-well reaction plate (Applied Biosystems®). Typical working reactions were made from 5 μ l fast SYBR green (Applied Biosystems®) or iTaq universal SYBR green supermix (BioRad), 1 μ l 5 μ M primer mix (forward and reverse primers), 2 μ l cDNA and 2 μ l DNase/RNase free H₂O. Typical cycling parameters (see appendix for gene specific annealing temperatures): initial denaturation at 95 °C for 20 sec, 45 cycles of 95 °C for 1 sec and annealing and extension at 60 °C for 20 sec. Fluorogenic data was collected through the SYBR green channel during the annealing phase. After spinning down the plate, a dissociation protocol was carried out to confirm primer binding specificity and expected amplicon. Dissociation cycling was as follows: 95 °C for 15 sec, 60 °C for 15 sec and 95 °C for 15 sec; data was collected during the second 95 °C incubation to identify the amplicon's melting temperature.

Genes analysed were *p16*, *p15*, *ARF*, *p53*, *Rb1*, *Mdm2* and *Bmi-1*. *GAPDH* and β -*Act* were selected as endogenous controls and expression levels were compared to appropriate controls. Ct values were analysed using the delta delta Ct method, all samples were calibrated to the relative expression of the average of the two reference genes and then the target gene's expression was compared to the expression of the control samples. Expression suite software v1.0.3 (Applied Biosystems®), RQ manager v1.2.1 (Applied Biosystems®) and qBASE^{PLUS} (Primerdesign Ltd) were all used to analyse qPCR data. PCR replicates were run in triplicate and outliers were excluded from the analysis. Where possible two or more separate qPCR runs were performed using cDNA prepared at different times.

2.6 DNA extraction

DNA was extracted from adherent SHE cells by using the DNA Purification Kit (Promega) and following the protocol provided. Briefly, harvested cells were spun down and the pellet washed twice using CMF-HBSS before removing the supernatant. Cell pellets were resuspended in 600 μ l nuclei lysis solution and transferred to a 1.5 mL centrifuge tube. RNA was removed from the lysate by adding 3 μ l RNase solution and incubating for 15 min at 37 °C in a water bath. After cooling at room temperature for 5 min, 200 μ l of protein precipitation solution was added and samples vortexed at high speed before chilling on ice for a further 5 min. Protein was removed by centrifuging samples for 15 min at 16,000 x g and 4 °C and the resulting supernatant added into 600 μ l isopropanol to precipitate the DNA strands followed by further centrifuging to form a pellet. The DNA pellet was then washed in 75 % ethanol and air dried before resuspending in DNA rehydration solution overnight at 4 °C, before quantification and storage at -20 °C.

2.7 Polymerase chain reaction (PCR)

cDNA or DNA was amplified on a thermal cycler, DNA engine tetrad2 (MJ Research) using the appropriate polymerase enzyme in a final reaction volume of 20 μ l or 50 μ l. Please refer to appendix (section 8) for primer lists and their specific annealing temperatures. Cycling conditions were enzyme specific but generally consisted of an initial denaturation step followed by 30-40 cycles of denaturation, annealing and extension before a final extension step. Reactions were prepared in 0.2 mL PCR tubes and thoroughly mixed

before loading onto the thermal cycler. The resulting PCR products were electrophoresed and resolved on 1-2 % agarose gels made in 1 X TBE buffer diluted in distilled water. Appropriate DNA ladders were loaded alongside PCR products to estimate amplicon size. Gel electrophoresis was carried out in a gel tank with 1X TBE buffer at 70-90 V for around 1.5 hours before imaging.

2.8 Gel extraction

After gel imaging using UV, expected bands of interest were excised using a sterile scalpel and UV box. The correct amplicon was extracted and purified using PureLink quick gel extraction and PCR purification combo kit (Invitrogen™) as per the manufacturer's instructions. Briefly, according to weight, the gel slice was solubilised in three gel slice volumes of gel solubilisation buffer and incubated at 50 °C before adding one gel slice volume of isopropanol. Using spin columns provided with the kit, the band was bound to the column, washed twice and then the purified DNA amplicon eluted with 40 µl pre-warmed elution buffer. The resulting DNA was quantified and stored at – 20 °C until needed for further analysis.

2.9 Sequencing analysis

Purified PCR fragments were outsourced for Sanger sequencing at Beckman Coulter Genomics using ABI3730XL (Beckman Coulter Genomics) at room temperature, according to shipment guidelines. Sequencing primers diluted to 5 µM were also sent where necessary. Nucleotide reads (.abl or .seq files) were analysed using CLC main workbench software v5.5 (CLCbio, Aarhus, Denmark). Sequence profiles were checked for their quality, individual peaks and minimum background fluorescence. Nucleotide sequences generated were then aligned to corresponding wild type reference sequences and checked for any differences.

CHAPTER 3

3 Characteristics of SHE Cell Transformation Assay- Derived Cells

3.1 Introduction

The application of the Syrian hamster embryo cell transformation assay (SHE-CTA) towards the prediction of the carcinogenic potential of chemicals is becoming of increasing interest to toxicologists seeking alternative *in vitro* assays for safety testing and screening (Creton et al., 2012). However, the origins of the assay date from the 1960's and its endpoint relies on the identification of morphologically transformed (MT) colony characteristics, and is therefore based on an individual's visual assessment of every colony obtained. Concerns over the reproducibility and subjective nature of this CTA have recently been addressed by pre-validation studies coordinated by ECVAM (Pant et al., 2012) and the formulation of OECD test guidelines is underway. Photo catalogues have been published to provide the scientific community with a range of examples of normal and morphologically transformed (MT) SHE colonies (Bohnenberger et al., 2012).

The process of cellular transformation was originally observed in rodent (including SHE) cells and is believed to recapitulate the stages of tumourigenesis. Carcinogen-induced alterations of cellular morphology are thought to be followed by unlimited proliferative potential (immortalisation) and subsequently the acquisition of anchorage-independent growth. However, the actual relevance of morphological transformation as an end point in relation to subsequent events leading to uncontrolled growth and senescence bypass has not been properly investigated, and a significant gap therefore remains in our knowledge. Although exposure of SHE cells to a chemical compound may lead to significant increases in the frequency of MT, which would imply a carcinogenic potential, we do not fully understand the relationship between MT and the immortalisation process. Therefore this project set out to evaluate the SHE-MT assay, initially by establishing if morphological transformation is directly associated with senescence bypass, leading to immortality in colony-derived SHE cells.

Benzo(a)pyrene is a polycyclic aromatic hydrocarbon (PAH) which is naturally formed by the incomplete combustion of organic materials and can be found in coal tar, cigarette smoke and in cooked foods from fat burning. The IARC recognises B(a)P as a Group I carcinogen and its metabolism produces highly reactive oxygenated species that are responsible for its mutagenic properties and DNA adduct formation. Cytochrome P450

proteins are responsible for B(a)P oxidation to B(a)P-7,8-epoxides, which are further metabolised by epoxide hydrolases to B(a)P-7,8-diols which are re-oxidised to form B(a)P-diol-epoxides (BPDE) again by the CYP enzymes (Jarvis et al., 2014). PAHs act as ligands to the aryl hydrocarbon receptor (AhR) which when activated can lead to increased expression of the CYP enzymes and thus increased breakdown of B(a)P (Nebert et al., 2004).

Syrian hamster embryo cells are considered to be metabolically active and capable of oxidising B(a)P in culture. Metabolic profiles of benzo(a)pyrene in SH embryonic cell cultures indicate a preference towards a left-side oxidation, giving rise to increased B(a)P derivatives oxidised at the 7,8 and 9,10 carbon positions compared with generation of 4,5-diols and 3-hydroxybenzo(a)pyrene typically identified in liver fractions (Selkirk et al., 1976). Increased concentrations of B(a)P lead to increases in the presence of metabolised oxygenated products (Nemoto et al., 1979) and the activity of the aryl hydrocarbon hydrolase enzyme was noted to be highest in tertiary SHE cells, decreasing over subsequent passages (Hirakawa et al., 1979).

In collaboration with our industrial sponsors Unilever, SHE MT assays were performed at BioReliance, Rockville (MD) USA by expert toxicologists familiar with the CTA. SHE cells were exposed to either the vehicle control DMSO or to the known mutagen and potent human carcinogen benzo(a)pyrene (normally the assay's positive control). At the end of the one week incubation period required for colony formation, unstained SHE colonies that had been treated either with DMSO or benzo(a)pyrene were isolated. Cultures were established from these clones which were then transported to our laboratories at Brunel University. Four groups of colony-derived SHE cells were obtained: those scored as non-transformed and those which had been scored as morphologically transformed (MT) from the two groups initially treated with either B(a)P or DMSO.

In order to further understand the SHE-CTA it was important to gain experience in conducting the assay in-house at Brunel, which also generated an increased number of colony-derived SHE cells for subsequent molecular analysis. A short visit to the BioReliance laboratories helped me become familiar with colony scoring, although the subjective nature of the assay was apparent. For the purposes of this project and, unlike

in the ECVAM studies, both BioReliance and in-house SHE-CTAs were performed using conditioned media (Pant et al., 2008) as a replacement for x-irradiated feeder layers in order to facilitate colony picking. A comprehensive protocol is detailed in the Materials and Methods section to this Chapter, 3.2.1.

3.2 Materials and Methods

3.2.1 Syrian Hamster Embryo Cell Transformation Assay (SHE-MT)

The SHE-MT assay was performed independently at BioReliance, Rockville (MD) USA (Kamala Pant) and at Brunel University. The assay was carried out by following ECVAM recommended protocol guidelines (Maire et al., 2012a) but with the use of conditioned medium instead of a supportive feeder layer of irradiated SHE cells as supported by (Pant et al., 2008). SHE cells were treated with the same concentrations of vehicle control (DMSO at a final concentration of 0.2 %) and the known carcinogen benzo(a)pyrene. A summary diagram of the assay is shown in Figure 5.

It should be noted that the primary cultures used in each of the two laboratories were obtained from different batches of Syrian hamster embryos. Stocks of embryo-derived cells cryopreserved at Brunel had been prepared as part of research by a previous PhD student (Dafou, 2003) and the resulting SHE primary cells (passage 1) stored in liquid nitrogen until required. All colony-derived SHE cell cultures from SHE-MT experiments were analysed at Brunel: those prepared at BioReliance were shipped to our laboratory under cryostorage in a liquid nitrogen Dewar.

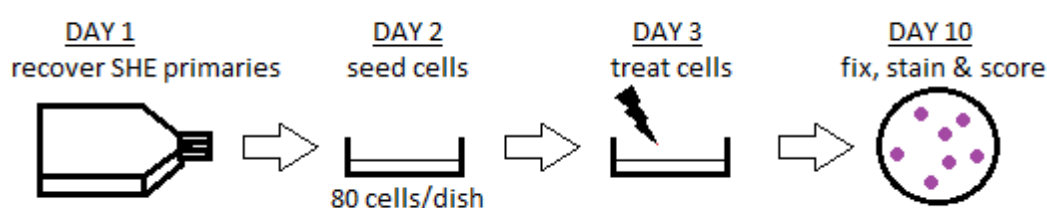


Figure 5 – SHE cell transformation assay time scale

SHE primary cells were seeded at low densities in conditioned medium so that individual cells receiving chemical treatments would form individual colonies. Over an incubation period of 7 days, attached viable cells proliferated to form colonies which were then visually assessed for morphological transformation (MT) and the frequency of MT compared with cells treated with the vehicle control (DMSO) was then calculated.

Isolation of Primary SHE Cells

SHE cells were grown in LeBoeuf's modified DMEM (DMEM-L, Quality Biologicals) at reduced pH 6.7 as described in the General Material and Methods (section 2.1). Primary SHE cells previously isolated from disaggregated embryos were frozen at a cell density of 2.5×10^6 cells/ml in 10 % DMSO (by Dr Dimitra Dafou 2003 at Brunel University).

Preparation of Conditioned Medium

Conditioned medium was prepared, as a replacement to feeder cells, by seeding secondary-tertiary SHE cells in 175 cm² flasks containing 45 mL DMEM-L medium. When 70-80 % confluent (2-4 days after seeding) the conditioned media was decanted, pooled together and filtered using 0.22 µm low protein binding filters (Merk-Millipore). Storage was at 4 °C for a maximum of 2 weeks. Secondary SHE cells were subsequently subcultured as a reserve stock for the preparation of additional stocks of conditioned medium.

Target Cell Preparation

A single vial of primary SHE cells was recovered in a 75 cm² flask in 35 mL of complete medium and incubated for 24 h. The next day cells were detached and, after staining in 0.4 % (v/v) Trypan Blue, counted using a Countess Automated Cell Counter (Invitrogen™). Cells were diluted in fresh medium to a density of 40 cells/ mL and 2 mL of cell suspension was then seeded in 60 mm dishes already containing 2 mL equilibrated conditioned medium, giving a total volume per dish of 4 mL. Cells were incubated for 24 h to allow the secondary SHE cells to adhere. Target cells were seeded in conditioned medium prepared from the same batch of SHE cells for consistency. Seeding of ~80 cells per dish routinely yielded 25–45 SHE colonies as recommended by the assay guidelines (Maire et al., 2012a).

Target Cell Treatment

SHE target cells were treated with a final concentration of 5 µg/mL benzo(a)pyrene [B(a)P]. A 600 X stock solution of the test compound was prepared in DMSO and stored at -20 °C until required. On the day of treatment the B(a)P stock solutions was diluted in complete fresh DMEM-L medium to achieve a 3 X solution. To each plate, 2 mL of fresh medium containing the compound were added to achieve a final 1 X solution with no

more than 0.2 % (v/v) DMSO (as suggested (Maire et al., 2012a) and as previously performed at Brunel by Dafou (2003). Dishes were returned to the incubator at 37°C and 10 % CO₂ for 7 days before scoring.

Controls

Vehicle control test plates were included and prepared as above in conditioned media and treated with 0.2 % (v/v) DMSO. A minimum of 20 dishes per treatment (B(a)P and DMSO) were seeded. Untreated plates seeded with 80 cells/dish were also included as further controls as well as dishes containing only conditioned media (i.e. with no cells seeded) to check there was no cell growth caused by the conditioned media.

SHE colony staining

After 7 days of incubation the culture medium was removed, the cells washed in 3 mL CMF-HBSS and then fixed in 2-3 mL methanol for a minimum of 10 min. The methanol was then removed and the plates allowed to air dry before staining the SHE colonies in 3 mL 10 % (v/v) Giemsa in pure water for a minimum of 20 min. Plates were then rinsed well in tap water to remove excess stain and air dried upside-down overnight.

Colony scoring

Individual SHE colonies were visually assessed under a light microscope for their morphological characteristics before being scored as normal (N) or morphologically transformed (MT). This evaluation was based on a combination of cell size, colony density, cell orientation, pattern of growth across the whole colony and the nuclear to cytoplasmic ratio of the cells. The detection of all of these features is enhanced by addition of the Giemsa stain. 'Altered' and 'washed' colonies were not included in the MTF calculation but were taken into account for the plating efficiency calculations. This is according to previous work (Bohnenberger et al., 2012) and ECVAM pre-validation studies (Pant et al., 2012) which describe altered colonies as those which are not fully developed and cannot be accurately scored. Washed colonies are those that fail to take up the Giemsa stain (and are usually found at the plate edges).

Typically normal SHE colonies stain light purple in Giemsa, their cell growth patterns are organised and flowing, especially in the centre of the colony and the cells are contact inhibited. In contrast, morphologically transformed SHE colonies tend to be highly

basophilic staining dark purple or blue with Giemsa, their cells are more spindle-shaped and disorganised with noticeable cell stacking or criss-crossed growth across the whole colony.

Assay assessment

Plating efficiencies and transformation frequencies were calculated and compared with published data for B(a)P. Because we were not performing an ECVAM study it was not necessary to adhere rigidly to the assay acceptance guidelines.

Plating efficiency (PE) was calculated as follows:

$$\text{PE (\%)} = (\text{total No. colonies} / \text{total No. target cells seeded}) \times 100 \quad (1)$$

Relative plating efficiency (RPE) was calculated as follows:

$$\text{RPE (\%)} = (\text{PE of treated cells} / \text{PE of control cells}) \times 100 \quad (2)$$

Morphological transformation frequency (MTF) was calculated for treatment and control plates as follows:

$$\text{MTF (\%)} = (\text{No. transformed colonies} / \text{total number of colonies}) \times 100 \quad (3)$$

3.2.2 Establishing colony-derived SHE cell cultures

In this project, a major objective was to characterise, at a cellular and molecular level, colony-derived SHE cells generated from the SHE-MT cell transformation assay (CTA). Therefore it was necessary to score unstained SHE colonies for normal or transformed characteristics *before* the assay's normal end point; that is to say before fixing and staining, in order to be able to pick living cells for further analysis.

SHE colony picking

After incubation for a week at 37 °C in 10 % CO₂, SHE colonies were observed under an Olympus CK40 light microscope for MT characteristics. Unstained colonies from treated [B(a)P] and vehicle control (DMSO) plates with clear transformed morphologies were circled and labelled before returning to the incubator, typical non-transformed control colonies were also marked. One plate at a time, the medium was removed from each

plate and the cells washed in CMF-HBSS. Plates were allowed to drain after removing the wash buffer. Half of each colony of interest was lifted off using a blunted Pasteur pipette and then disaggregated by repeated gentle pipetting into 0.5 mL DMEM-L conditioned medium (diluted 1:1 with fresh complete DMEM-L) in a 24-well plate. The remaining colonies were fixed and stained in the same way as described above using 10 % (v/v) Giemsa. Brightfield colour images were taken of the remaining picked colonies when still intact using a Zeiss Axioskop microscope.

Establishing SHE-MT colony derived cultures

On the day after picking colonies, a further 0.5 mL fresh DMEM-L media was added per well and the cultures were observed for the presence of proliferating cells. On reaching 80-90 % confluence, 200 μ l Tryple-Express (Gibco®) was added to detach the disaggregated clone and the resulting cell suspension was then transferred to a 6-well plate with 1 mL 50 % conditioned media until the cells could be transferred to a 60 mm dish. From this point onwards the SHE cells were detached with Trypsin-EDTA 0.05 % as described earlier and counted with a haemocytometer.

3.2.3 Establishing cultures derived from SHE-MT colonies generated at BioReliance (Prepared by Kamala Pant)

Frozen vials containing cells derived from picked SHE colonies were also provided by BioReliance, Rockville (MD) USA. However, these cells were taken from *whole* colonies, isolated by using cloning cylinders and a few drops of trypsin-EDTA to detach the cells. This differed from the approach described above (paragraph 3.2.2) where half the colony was scraped using a glass pipette. The BioReliance-derived cells were cultured until there were enough for freezing and shipment to the Brunel laboratories. On arrival at Brunel, SHE cells prepared at BioReliance were recovered into 60 mm dishes with 5 mL fresh DMEM-L media and analysed in the same way as those prepared at Brunel.

3.2.4 Basic cell growth characteristics of colony-derived SHE cells

SHE cultures obtained from the SHE-MT assay were serially sub-cultured (ie. trypsinised and split) to determine their growth characteristics and cellular lifespan. Cells were considered terminally senescent after over one month in culture with no signs of cellular division or proliferation. Previous research by Dafou (2003) noted that untreated SHE

primary cells continued to divide for up to 55 population doublings in reduced pH medium before entering irreversible growth arrest and terminal senescence. Cells that continued to proliferate beyond this were considered immortal once they reached over 60 to 70 population doublings which, depending on the rate of proliferation of each colony-derived SHE culture, roughly equalled 20-30 sub-cultures.

3.2.5 Growth curves

Following trypsinisation and pelleting, colony-derived SHE cells were resuspended in 2-4 mL of fresh complete DMEM-L and counted using a haemocytometer. The total number of cells and growth incubation time was used to calculate population doublings and these figures were used to plot growth curves.

Cumulative population doubling level (PDL) was calculated as follows:

$$\text{PDL} = 3.32 \times (\log N_2 - \log N_1) + X \quad (4)$$

Where: N_2 is the total number of cells at a given time point

N_1 is the number of cells initially seeded

X is the previously calculated PDL of the cell culture used

3.3 Results

3.3.1 The SHE-MT assay

The SHE-MT assay was performed at BioReliance and at Brunel using the vehicle control DMSO and the known mutagen and potent human carcinogen benzo(a)pyrene (normally the assay's positive control). Cells were seeded at a low density (80 cells per dish) so as to obtain between 25 and 45 colonies per plate, with each colony presumed to originate from a single cell. Figure 6 contains example test plates from the assay and each colony was individually assessed for its growth characteristics and appearance in order to be scored either as 'non-transformed' (N) or 'morphologically transformed' (MT). The assay therefore generated four groups of colony-derived SHE cell cultures these are shown in Table 1.

Normal SHE colonies contain cells that are contact-inhibited and display organised flowing patterns of growth. Morphologically transformed SHE colonies differ as the cells overlap each other in a random orientation and cell nuclei will also stack on top of each other. Generally MT cells are basophilic and stain dark purple or blue in Giemsa compared with normal cells which stain light purple (Bohnenberger et al., 2012). Examples of normal and transformed colonies from my SHE-MT CTA experiments are shown in Figure 7.

The plating efficiencies (PE) and morphological transformation frequencies (MTF) for SHE cells treated with DMSO and B(a)P are listed in Table 2 and were calculated according to the assay's pre-validation studies (Maire et al., 2012a, Pant et al., 2012). The average number of colonies obtained routinely per plate was above 25, the PE of the vehicle control was above 20%, and no colonies or cells grew in dishes containing only conditioned media, which is in line with ECVAM's assay guideline acceptance criteria (Maire et al., 2012a). The relative PE (RPE) of the positive control compared with the vehicle control (DMSO) was 117.19 %. The MTF for DMSO was 1.39% and for B(a)P was 6.20 %. The statistical significance between observed MT frequencies following DMSO or B(a)P treatment was calculated using a one-sided Fisher's exact test. Altered colonies which contain low density cells, still undergoing colony formation or process stacking; were not scored and were only included in the plating efficiency calculations.

Table 1 – Types of SHE-CTA colony from which SHE cultures were obtained

| | Treatment | Scoring |
|----------------|------------------|-----------------------------|
| DMSO N | 0.2% DMSO | Non-transformed |
| DMSO MT | 0.2% DMSO | Morphologically transformed |
| BP N | 5 µg/mL B(a)P | Non-transformed |
| BP MT | 5 µg/mL B(a)P | Morphologically transformed |

Primary SHE cells were treated with either the vehicle control, DMSO (0.2%) or B(a)P (5 µg/mL). After a one-week incubation period, the resulting colonies were then scored according to their morphological characteristics. The cells isolated from the selected colonies were then used for further analysis.

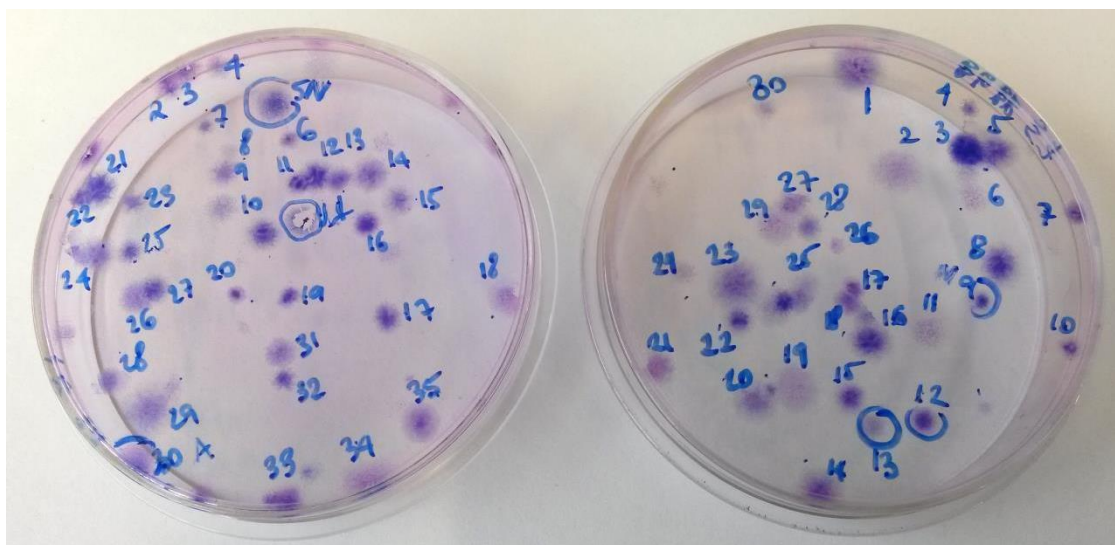


Figure 6 – Example test plates from the Syrian hamster cell transformation assay (SHE CTA)

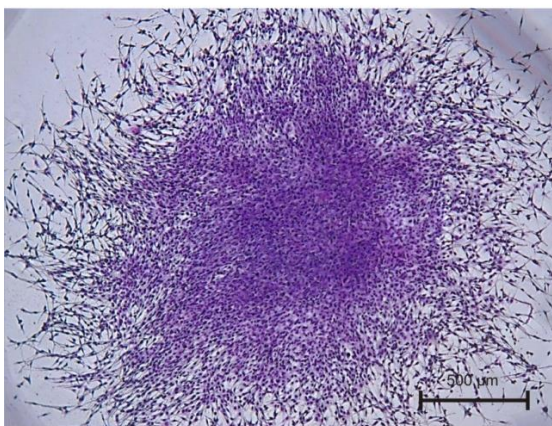
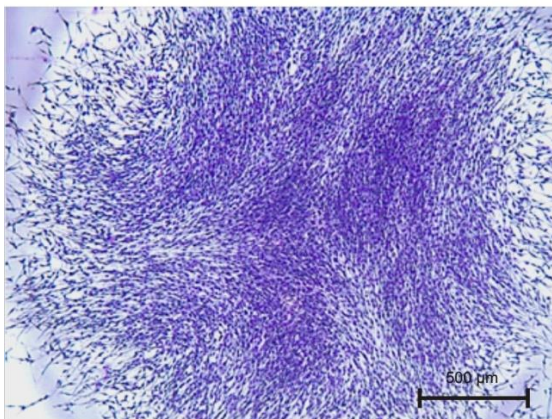
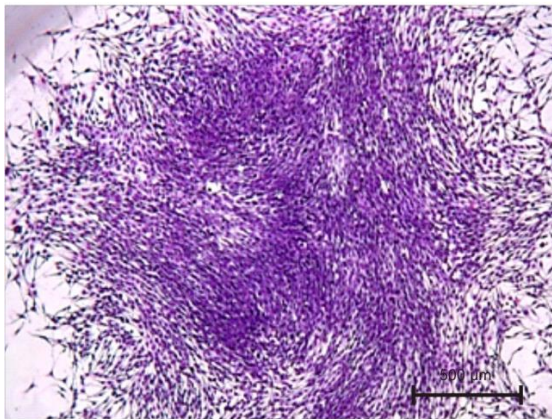
Secondary SHE cells were seeded at 80 cells/dish (60 mm) in conditioned media. After a 7-day incubation period with test article, a minimum of 20 test plates per treatment were scored per SHE CTA experiment. The total number of colonies was used to calculate the plating efficiency (PE) and scoring of each colony was recorded to work out the frequency of morphological transformation (MTF).

Table 2 – SHE cell transformation assay summary (performed by me at Brunel, 7 day treatment)

| Treatment | Total colonies scored | Average colonies per dish | PE (%) | RPE (%) | MTF (%) | MTF <i>p</i> value |
|--------------|-----------------------|---------------------------|--------|---------|---------|--------------------|
| 0.2% DMSO | 509 | 25.45 | 31.81 | n/a | 1.39 | n/a |
| 5µg/mL B(a)P | 1879 | 29.83 | 37.28 | 117.19 | 6.20 | <0.01 |

A total of 80 cells per dish were seeded to obtain 25 or more colonies per dish after treatment. Twenty dishes were treated with DMSO and 63 dishes with B(a)P (experiment BP B6). Colonies were scored according to established criteria for morphological transformation (Bohnenberger et al., 2012, Maire et al., 2012a); those that were altered and undergoing process stacking were not included in the MTF calculation. MTF p values were calculated using the one-sided Fisher's exact test. As expected, no cells or colonies grew in the control plates containing only conditioned media.

Non-transformed (N)



Morphologically transformed (MT)

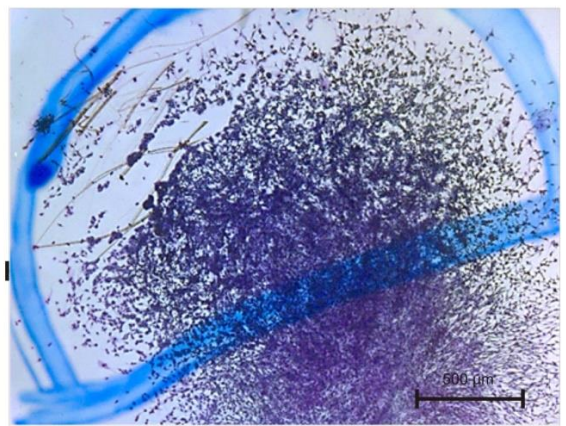
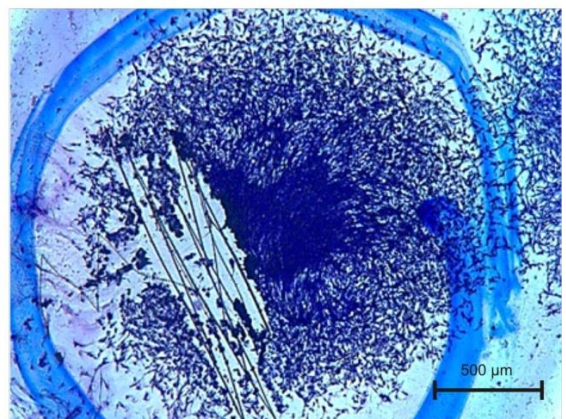
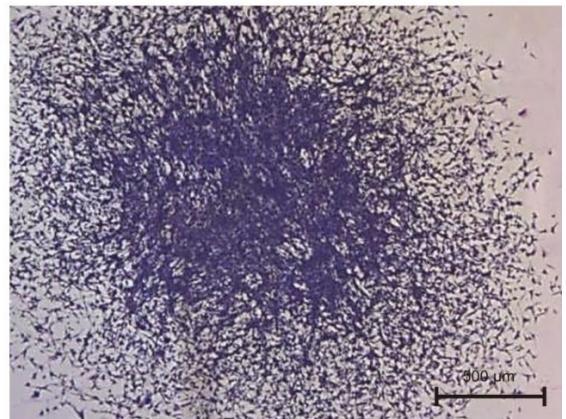


Figure 7 – SHE MT assay colony examples

Colonies were fixed in 100% methanol and stained in 10 % (v/v) Giemsa. Colonies shown in the left panel typify those scored as normal or non-transformed: the cells form organised flowing monolayers and they stain light purple. Colonies in the right panel are representative of those scored as morphologically transformed (MT): cell growth is disorganised and criss-crossed across the whole colony; typically these cells are spindly and elongated with increased nuclear to cytoplasmic ratios. Nuclear overlapping is visible and the colonies stain dark blue due to their basophilic nature. (Images were taken using a 5X objective on a Zeiss Axioskop microscope).

3.3.2 Cells derived from the SHE-MT assay

Live unstained colonies were scored and picked to understand the relationship between morphological characteristics, cellular lifespan and molecular analysis. SHE cells derived from colonies scored at Brunel were lifted using a Pasteur pipette, from unstained colonies, and transferred to 24-well plates containing conditioned media so that they could be expanded. Only half of each colony was picked so as to leave the remaining cells behind for staining in Giemsa, in order to confirm the preliminary scoring performed on unstained colonies. Areas lacking cells in the photographs in Figure 7, Figure 8 and Figure 9 are where the cells have been scraped off in the picking process. In some instances the process of picking damaged the colony so that there were no cells left to image. In these instances, the initial scoring on unstained colonies was relied upon.

Figure 8 and Figure 9 show examples of B(a)P-treated SHE CTA colonies that were picked at Brunel. From one SHE CTA experiment, cells derived from 4 out of a total 48 B(a)P-treated colonies scored morphologically transformed (MT), imaged in Figure 8, continued to proliferate and established immortal cell lines. In contrast, the remaining 44 BP MT colonies (examples of which are shown in Figure 9) did not immortalise and ceased to proliferate (i.e. they senesced). A further two BP MT clones were isolated from other SHE CTA experiments. Despite these colonies not being intact on imaging due to sections having been removed for culture, both images clearly show typical MT characteristics. With the exception of D37 #1, (Figure 8D) and D51 #2, (Figure 9D) MT colonies stained dark blue in Giemsa. Under the microscope the cells appeared highly mitotic with large numbers of rounded telophase pairs visible. Cells were small in size with limited cytoplasm compared with normal and non-transformed SHE cells. There were significant

areas of cell aggregation and cell stacking visible typical of MT characteristics, in colony D37#1 (Figure 8D). Areas of nuclear stacking and clustering are also identifiable in MT colony D51 #2 (Figure 9D). By established criteria (Bohnenberger et al., 2012, Maire et al., 2012c, Maire et al., 2012a), these colonies should be scored as MT. In all morphologically transformed colonies, the cells were disorganised, nuclear stacking was observed and their random cell orientation was visible across the remaining colony areas at both the colony periphery and the centre. MT cells even grew on top of senescent looking cells (Figure 8E, arrow).

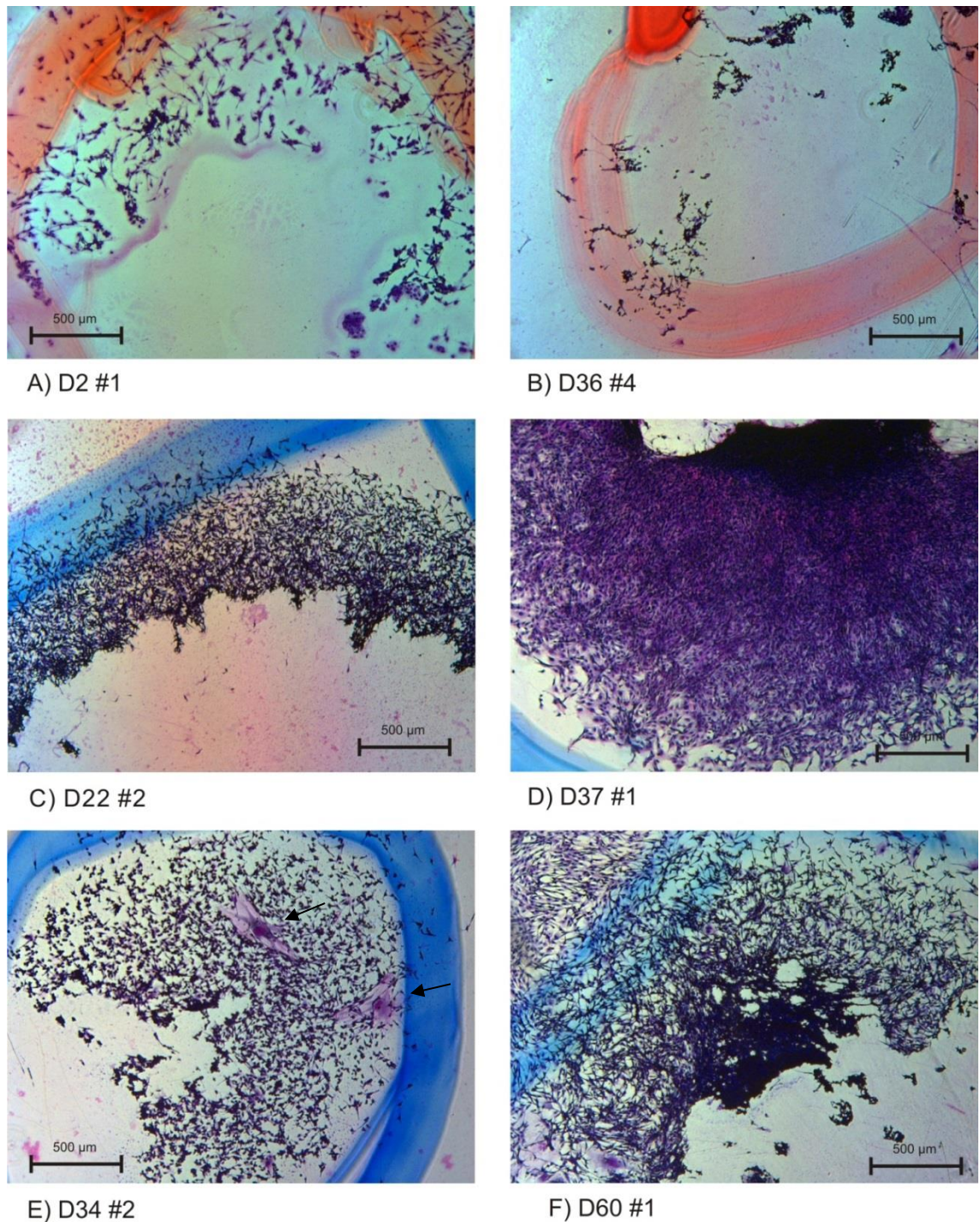
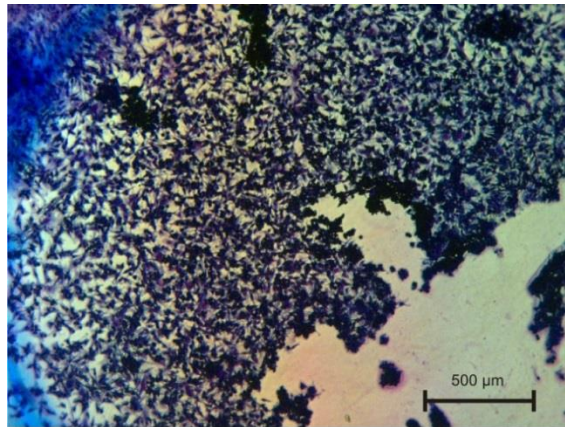
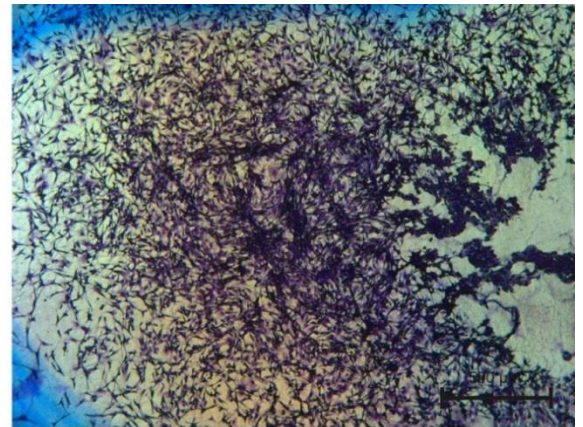


Figure 8 – Picked morphologically transformed colonies that immortalised

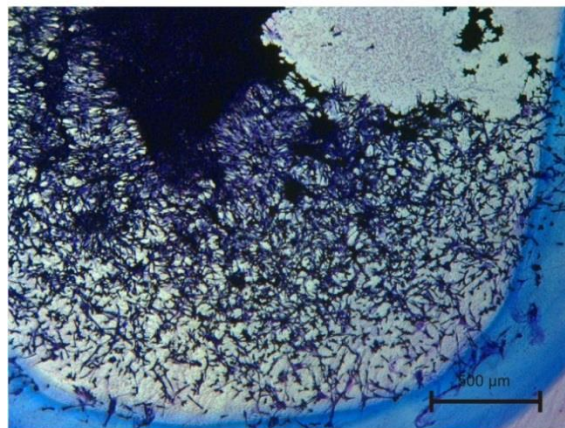
SHE cells were picked from unstained colonies which were then stained in Giemsa to confirm their MT phenotypes. From 2 separate SHE-CTAs, only 2 (A-B) and 4 (C-F) BP MT colonies progressed to immortality. To confirm senescence bypass, over 70 population-doublings had to take place which, depending on culture procedures, equated to around 30 sub-cultures; this process took over 3 months to complete. Images were taken using a 5X objective on a Zeiss Axioskop microscope.



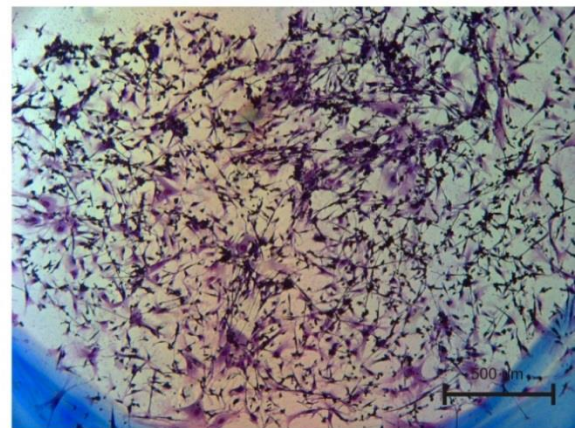
A) D27 #2



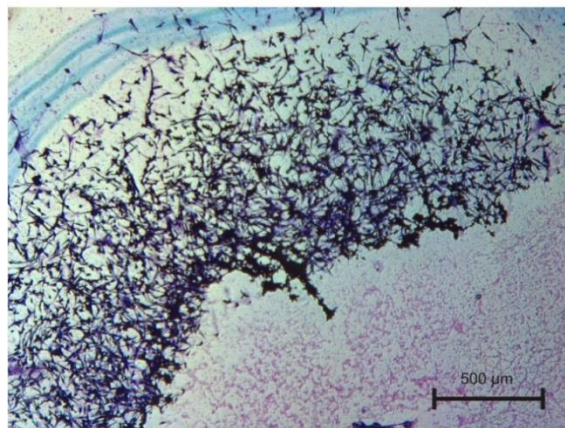
B) D9 #2



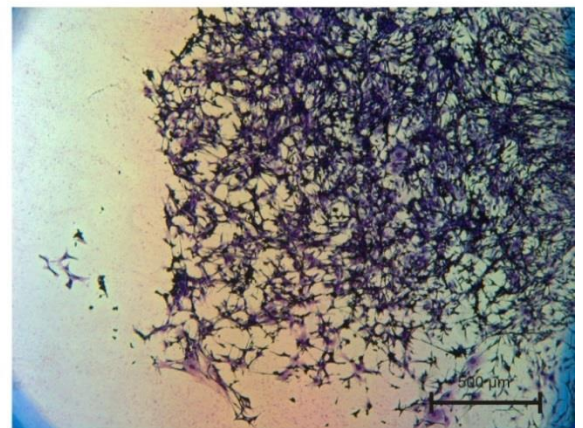
C) D16 #3



D) D51 #2



E) D17 #1



F) D52 #2

Figure 9 – Picked morphologically transformed colonies that senesced

SHE cells were picked from the unstained colonies which were subsequently stained in Geimsa to confirm their MT phenotypes. 68% of cell populations (33 out of 48) derived from B(a)P-treated MT colonies, such as those imaged above, senesced by ~PD18 and did not immortalise despite overt MT characteristics. Images were taken using a 5X objective on a Zeiss Axioskop microscope.

3.3.3 Morphological transformation does not guarantee senescence bypass

SHE colony sizes after the 7 day incubation varied in density and size: between 5×10^3 - 2×10^4 cells were counted using a graticule. The average colony contained 8×10^3 cells, which assuming these originated from a single cell indicates ~13 population doublings at the point of colony picking and assay end point (passage 2). Picked colonies were transferred to a 24-well plate and expanded to a 60 mm and later 100 mm dish (passage 5); 80 % of all colonies picked, that established, senesced before they had undergone a total of 18 population doublings (i.e. stopped dividing once transferred to a 100 mm dish) and could not be studied further. Table 3 shows how the population doublings observed were estimated when the picked colonies were transferred and expanded from a 24-well plate to a 60 mm dish and later to 100 mm dish.

Table 3 – Estimation of SHE cell population doublings undergone by colony-derived SHE cells

| | Number of cells | Population doublings | Passage No. |
|------------------------------|--------------------|----------------------|-------------|
| Single cells seeded | 1 | 0 | P2 |
| Colony size (average) | 8×10^3 | 13 | P2 |
| Seed in 100 mm dish | $5-30 \times 10^4$ | 18 | P5 |

Primary cells were recovered from liquid nitrogen and replated at 80 cells per dish 24 hours prior to treatment (passage 2). Several assumptions were made. First, each colony was generated from a single cell and second that, after 7 days incubation, an average colony contained around 8×10^3 cells, i.e. approximately 13 or more population doublings had taken place. Picked cells were initially expanded in a 24-well plate. An average taken from counting confluent SHE cells in a 60 mm dish, (passage 4) indicated that 18 or more population doublings had taken place. These cells were then expanded in a 100 mm dish (passage 5).

All picked DMSO-treated colonies senesced as did all non-transformed B(a)P treated colonies. As highlighted in Table 4, the remaining 20 % of dividing clones continued to divide until a maximum of 35 population doublings (PD) before senescing (by passage 10) except for 4 out of 48 B(a)P-treated MT colony-derived cells that immortalised (a frequency in this experiment of <10 %) and continued to proliferate for over 60 PD; the original colonies from which these clones originated are imaged in Figure 8. Out of a total

of 142 SHE colonies picked from one SHE-MT assay (experiment BP B6), only 4 colony-derived cultures immortalised (BP MT colonies C-F Figure 8). A further 2 B(a)P MT immortal clones were generated during other SHE MT assays. At the time of writing two BP MT colonies had undergone over 100 PD.

Table 4 – Low frequency of immortalization of cells isolated from SHE-MT colonies

| Treatment | Scoring | No. colonies picked | Division at P5 (~18PD) | No. Immortal |
|----------------------------|----------------------------------|---------------------|------------------------|--------------|
| DMSO | Normal (N) | 6 | 2/6 | none |
| DMSO | Morphologically transformed (MT) | 5 | 2/5 | none |
| DMSO | Unscorable | 2 | 0/2 | none |
| B(a)P | Normal (N) | 47 | 4/47 | none |
| B(a)P | Morphologically transformed (MT) | 48 | 15/48 | 4 |
| B(a)P | Unscorable | 34 | 6/34 | none |
| Expt. 'BP B6' total | | 142 | 29 | 4 |

The table gives examples of colonies picked from a SHE MT assay at Brunel, SHE cells were either treated with DMSO or B(a)P. Most colony-derived cell cultures either stopped dividing before 18 population doublings from the point of CTA seeding (passage 5- transferred to 100 mm dish) and could not be further studied, or continued to divide for a maximum of 35 population doublings before senescing (by passage 10). From the cells generated in this representative assay 4 B(a)P treated MT colony-derived cells continued to proliferate beyond 60 population doublings and thus could be considered immortal. Unscorable colonies included: 22 altered, 9 washed and 3 extensively damaged colonies.

Serial sub-culturing of colony-derived cells demonstrated that, with the exception of a total of 6 B(a)P-induced MT colonies, all DMSO and B(a)P-exposed non-transformed and transformed colonies stopped dividing without signs of growth by 35 population doublings (~passage 10). Growth curves for the 6 immortalised B(a)P MT lines prepared at Brunel and a representative non-immortal BP MT culture (D14 #1) are shown in Figure 10. When kept in culture, immortal lines continued to proliferate beyond 100 population doublings (Table 5A). Immortal clones divided exponentially once established as shown in Figure 10, for example BP MT D37 #1 and D36 #4 with mean doubling times of 23 hours

and 33 hours respectively. BP MT D60 #1 had mean population doubling of around 38 hours but had an initial cell growth 'lag' period following colony picking and establishment at around 18-20 PD (see Figure 10). Doublings times increased to over 80 hours for about 20 days before exponential growth was observed. Similarly, following 20 population doublings in BP MT D2 #1 there was a period of around 25 days without any cell division followed by an estimated 5 PDs in the following 21 days; cells were replated and doubling times stabilised to around 85 hours (Figure 10). A list of immortal lines generated in-house during this project is presented in Table 5A. In addition, two B(a)P-treated colony-derived SHE MT immortal lines were sourced from stocks prepared by a previous PhD student (Dafou, 2003), these are listed in Table 5B.

Table 5– Frequencies of senescence-bypass of SHE-MT colonies scored as morphologically transformed (MT)

A) BP treated, immortalised scored at Brunel by JCP

| Clone Name | Senescence Bypass | Crisis | Passaged to |
|--------------|-------------------|--------|----------------------|
| B4 BP D36 #4 | 2/2 | N | P45 (approx. 120 PD) |
| B4 BP D2 #1 | 2/2 | Y | P39 (approx. 75 PD) |
| B6 BP D22 #2 | 2/2 | N | P34 (approx. 70 PD) |
| B6 BP D37 #1 | 2/2 | N | P47 (approx. 135 PD) |
| B6 BP D34#2 | 2/2 | N | P22 (approx. 80 PD) |
| B6 BP D60#1 | 2/2 | Y | P23 (approx. 65 PD) |

B) BP treated, scored at Brunel by a previous PhD student Dimitra Dafou (DD)

| Sample Name | Senescence Bypass | Crisis | Passaged to |
|-------------|-------------------|---------|-------------|
| DD 8B-BP1 | 2/2 | Unknown | P19 |
| DD 8B-BP2 | 2/2 | Unknown | P21 |

A total of 6 immortal SHE lines derived from B(a)P treated MT colonies were generated and the population doublings at the time of writing are stated (A). An additional 2 MT immortal SHE lines derived from previous SHE CTA and induced by B(a)P (B) were sourced from frozen stocks previously prepared at Brunel University by Dafou (2003).

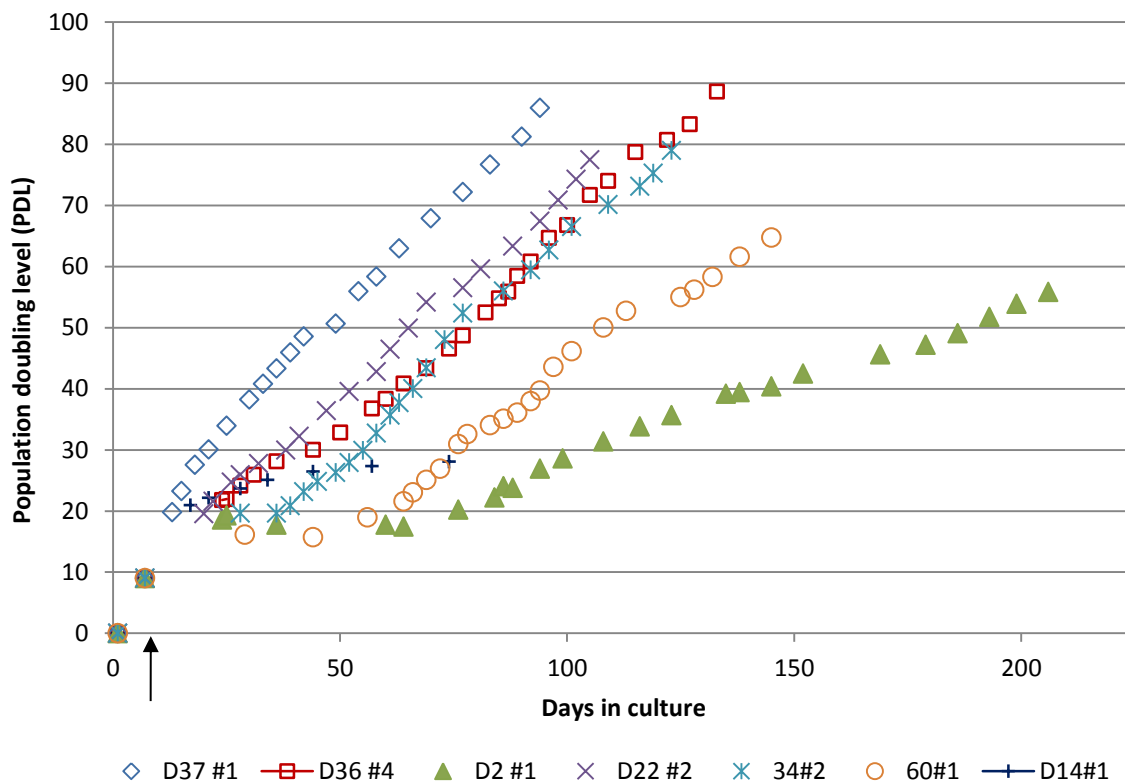


Figure 10 – Immortal B(a)P-MT colony-derived SHE cells proliferate beyond 35 population doublings

Secondary (passage 2) SHE cells were seeded on day zero and the colonies picked after 7 days exposure (black arrow). Cells taken from B(a)P-treated MT colonies were serially sub-cultured and their characteristics studied. Finite-lifespan SHE cells senesced before 35 population doublings and are represented by D14 #1. BP MT cultures that continued to expand were kept in culture for over 60 population doublings from the point of seeding for the assay. Cells were counted using a haemocytometer and calculated PDL values were plotted. BP MT D2#1 and D60#1 have distinct growth curves from the remaining BP MT clones that divided exponentially once established (e.g. by D37 #1).

3.3.4 Determining growth characteristics and cell lifespan of SHE-MT clones obtained from BioReliance

In addition to SHE clones from the SHE-MT assay performed by me at Brunel, representative colonies were also picked by the BioReliance (USA) team and grown there before shipping to the Brunel laboratories. The SHE CTA was performed at BioReliance by expert toxicologists who are familiar with the assay and their laboratory took part in previous CTA ECVAM validation studies (Pant et al., 2012). BioReliance-derived MT clones

scored as normal (non-transformed) are listed in Table 6 and Table 7. SHE cells derived from unstained colonies scored at BioReliance had been picked using cloning cylinders; in these instances the whole colony was picked and no reference image of the colony is available. On arrival at Brunel, cells were recovered from frozen ampoules and assigned passage number of P+1. Given that these cells were independent clones, and that cultures would have needed to have been expanded sufficiently to freeze these cells prior to shipping, it can be confidently assumed that they had undergone a minimum of 13 population doublings on arrival (estimated from average Brunel SHE colony size) at P+1. These colony-derived cells from BioReliance were also studied for their general cellular morphologies and any unifying or distinguishing characteristics.

Non-transformed SHE colony-derived cells senesce

SHE-derived clones that had been treated with DMSO and scored as non-transformed (DMSO N), see Table 6A and representative images in Figure 11, displayed uniform organised growth as observed in the SHE colony based assay. As cells reached a high cell density they appeared as a flowing single monolayer of cells. Colonies scored as non-transformed and treated with benzo(a)pyrene (BP N - see Table 6B) on recovery showed growth patterns similar to DMSO non-transformed cells and displayed characteristics typical of normal SHE cells.

After 3-4 rounds of subculture there were increasingly visible signs of cellular senescence in cells derived from non-transformed colonies. SHE cells had enlarged cytoplasm, fewer mitotic cells and the non-transformed SHE colonies treated with DMSO and B(a)P stained positive for SA- β gal activity. All cells derived from DMSO N- and B(a)P N colonies entered cellular senescence by P+8. Terminally senescent cells were maintained in culture for at least one month to confirm lack of proliferation. It should be noted that, in six cases, non-MT (DMSO exposed) colony-derived SHE cells obtained from BioReliance senesced immediately after recovery (P+1) and therefore could not be analysed further.

Table 6 – Senescence-bypass frequencies in non-transformed or normal SHE clones obtained from the SHE-CTA (provided by BioReliance)

A) DMSO N: DMSO treated, scored non-transformed by BioReliance

| Abbreviation | Sample Name | Senescence Bypass | Passaged to |
|---------------------|--------------------|--------------------------|---------------------|
| SHE 1 | #4 DMSO 36 4N | 0/2 | P+5 (approx. 25 PD) |
| SHE 2 | #1 DMSO 38 1N | 0/3 | P+6 (approx. 30 PD) |
| SHE 3 | #2 DMSO 36 1N | 0/6 | P+6 (approx. 30 PD) |
| SHE 4 | #8 DMSO 40 2N | 0/2 | P+8 (approx. 30 PD) |
| SHE 5 | #9 DMSO 40 4N* | 0/1* | P+1 (approx. 13 PD) |
| SHE 6 | #3 DMSO 36 3N* | 0/1* | P+1 (approx. 13 PD) |
| DMSO N1 | DMSO AD29ZG 1N | 0/2 | P+7 (approx. 16 PD) |
| DMSO N2 | DMSO AD29ZH 1N | 0/3 | P+5 (approx. 16 PD) |
| DMSO N3 | DMSO AD29ZH 5N | 0/5 | P+6 (approx. 30 PD) |
| DMSO_N1 | DMSO N1 | 0/1* | P+2 (approx. 13 PD) |
| DMSO_N2 | DMSO N2 | 0/1* | P+2 (approx. 13 PD) |
| DMSO_N3 | DMSO N3 | 0/1* | P+1 (approx. 13 PD) |
| DMSO_N4 | DMSO N4* | 0/1* | P+1 (approx. 13 PD) |

B) BP N: B(a)P treated, but scored as non-transformed by BioReliance

| Abbreviation | Sample Name | Senescence Bypass | Passaged to |
|---------------------|--------------------|--------------------------|---------------------|
| SHE 7 | #2 BP 27 1N | Unknown | Infection |
| SHE 8 | #8 BP 1 1N | 0/2 | P+4 (approx. 16 PD) |
| SHE 9 | #11 BP 34 1N | 0/2 | P+5 (approx. 25 PD) |
| SHE 10 | #12 BP 34 3N | unknown | Infection |
| SHE 11 | #13 BP 35 4N | 0/2 | P+4 (approx. 16 PD) |
| SHE 12 | #10 BP 22 2N | 0/2 | P+6 (approx. 30 PD) |
| BP 4N | BP AD29ZJ 4N | 0/2 | P+4 (approx. 16 PD) |
| BP 1N | BP 1N (Batch 3) | 0/1* | P+2 (approx. 13 PD) |
| BP N1 | BP N1 | 0/1* | P+1 (approx. 13 PD) |
| BP N2 | BP N2 | 0/1* | P+5 (approx. 18 PD) |
| BP N3 | BP N3 | 0/1* | P+1 (approx. 13 PD) |
| BP N4 | BP N4 | 0/1* | P+4 (approx. 18 PD) |

*cells were senescent on recovery, unable to freeze cell stocks.

A total of 13 vials containing cells derived from DMSO-treated non-transformed colonies (A) and 12 vials containing cells derived from B(a)P-treated non-transformed colonies (B) were obtained from BioReliance (via Unilever, the industrial partner in my BBSRC CASE studentship).

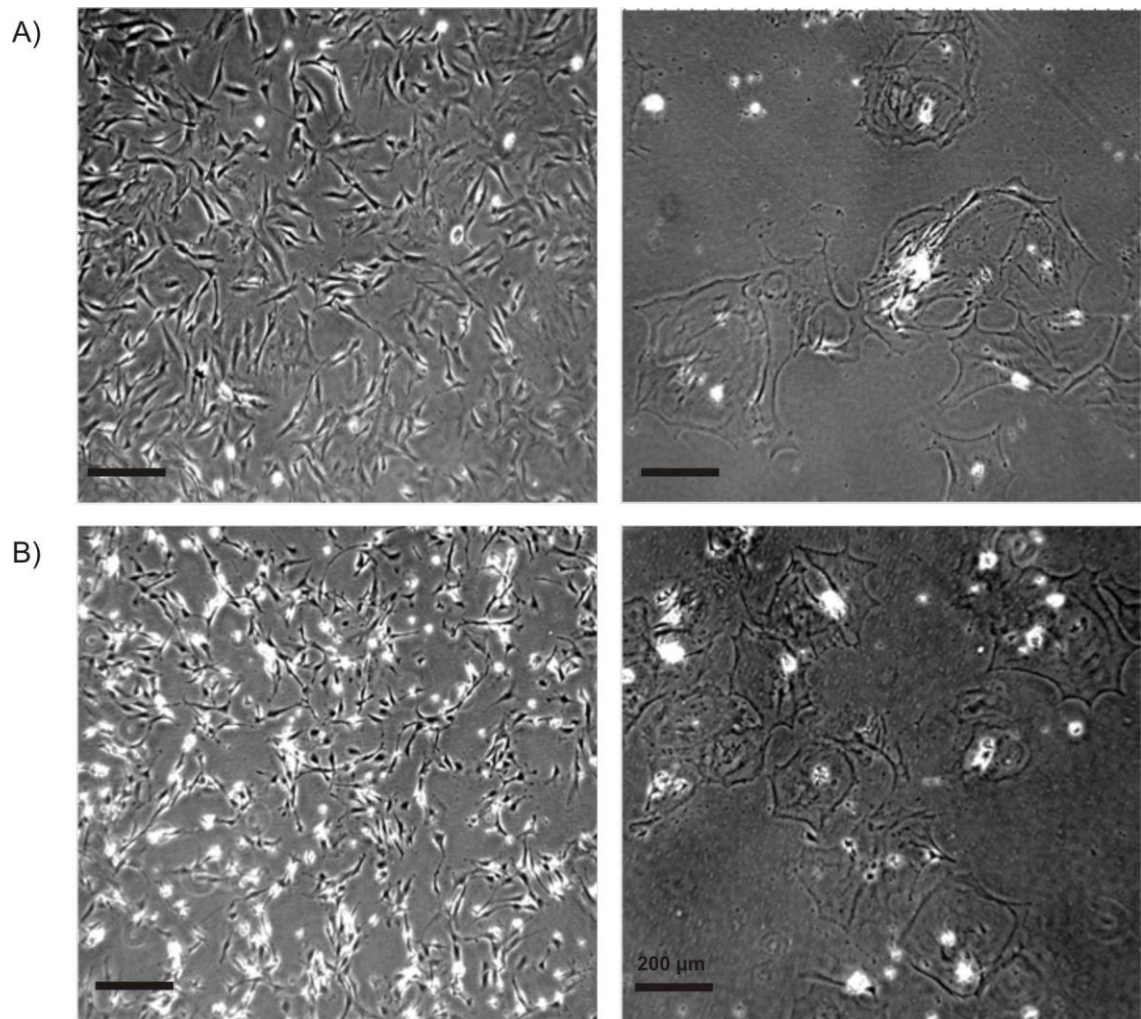


Figure 11 - Non-transformed cells, derived from the SHE-MT cell transformation assay (CTA) group that were treated with DMSO enter terminal senescence

On recovery (P+1) cells were healthy and at high density formed flowing cell monolayers. Entry into terminal senescence took place within 2-4 subcultures. Cells shown in the Figure are derived a Syrian hamster embryo CTA performed at BioReliance. For the CTA, plates were treated with the vehicle control DMSO and clones isolated as described earlier from normal or non-transformed clones. (A) Top row; SHE#2 DMSO36 1N P+1 and P+5 (B) bottom row; SHE #1 DMSO38 1N P+1 and P+6. Images taken on a Carl Zeiss Axioshop microscope with a 4X objective.

Table 7 - Senescence-bypass frequencies in cells derived from SHE-MT colonies scored as morphologically transformed (MT)(provided by BioReliance) – cont. on next page

A) DMSO MT: DMSO treated, scored morphologically transformed by BioReliance

| Abbreviation | Sample Name | Senescence Bypass | Crisis | Passaged to |
|---------------|----------------------|-------------------|----------|-----------------------------|
| SHE 13 | #10 DMSO 35 1T | 0/2 | | P+6 (approx. 25 PD) |
| SHE 14 | #4 DMSO 10 1T | 1/3 | Y | P+42 (approx. 95 PD) |
| SHE 15 | #9 DMSO 33 2T | 0/2 | | P+4 (approx. 18 PD) |
| SHE 16 | #5 DMSO 23 1T | 0/1* | | P+4 (approx. 18 PD) |
| SHE 17 | #4 DMSO 4 2T | 0/1* | | P+2(approx. 13 PD) |
| SHE 18 | #15 DMSO 37 1T | 0/2 | | P+15 (approx. 35 PD) |
| DMSO T1 | DMSO T1 | 0/2 | | P+3 (approx. 16 PD) |
| DMSO T2 | DMSO T2 | 0/1* | | P+1 (approx. 13 PD) |
| DMSO T3 | DMSO T3 | 0/1* | | P+3 (approx. 16 PD) |
| DMSO T4 | DMSO T4 | 0/1* | | P+1 (approx. 13 PD) |

*cells were senescent on recovery, unable to freeze cell stocks.

Table 7–Senescence-bypass frequencies in cells derived from SHE-MT colonies scored as morphologically transformed (MT)(provided by BioReliance)

B) **BP MT**: BP treated, scored morphologically transformed by BioReliance

| Abbreviation | Sample Name | Senescence Bypass | Crisis | Passaged to |
|--------------|--------------|-------------------|--------|---|
| 19 | #19 BP 10 1T | 0/8 | | P+8 (approx. 20PD) |
| 20 | #18 BP 37 1T | unknown | | infection |
| 21 | #17 BP 37 2T | 2/7 | Y | P+7 (approx. 25 PD) P+39 (approx. 80 PD) |
| 22 | #22 BP 17 1T | 0/7 | | P+5 (approx. 20 PD) |
| 23 | #16 BP 7 1T | 5/5 | N | P+42 (approx. 140 PD) |
| 24 | #3 BP 10 1T | 1**/10 | Y | P+6 (approx. 20 PD) |
| BP T4 | BP AD29ZJ 4T | 2/3 | Y | P+27 (approx. 70 PD) |
| BP T1 | BP T1 | 0/3 | | P+5 (approx. 20 PD) |
| BP T5 | BP T5 | 0/1* | | P+5 (approx. 20 PD) |
| BP T8 | BP T8 | 0/1* | | P+3 (approx. 16 PD) |
| BP T9 | BP T9 | 2/2 | Y | P+25 (approx. 65 PD) |
| BP T10 | BP T10 | 0/1* | | P+2 (approx 13 PD) |
| BP T11 | BP T11 | 0/1* | | P+3 (approx. 16 PD) |
| BP T13 | BP T13 | 0/1* | | P+1 (approx. 13 PD) |
| BP T15 | BP T15 | 0/1* | | P+4 (approx. 18 PD) |
| BP T17 | BP T17 | 0/1* | | P+1 (approx. 18 PD) |
| BP T19 | BP T19 | 0/2 | | P+7 (approx. 20 PD) |
| BP T21 | BP T21 | 0/1* | | P+1 (approx. 13 PD) |

*cells were senescent on recovery, unable to freeze cell stocks.

**SHE 24 cells post crisis lost due to infection

A total of 10 vials containing cells derived from DMSO-treated MT colonies (A) and 18 vials containing cells derived from B(a)P treated transformed colonies (B) were obtained via Unilever from BioReliance. On arrival at our laboratories these cells were recovered and grown to study their growth characteristics and cellular lifespan. In red typeface are those colony derived cells that immortalised (5 out of 28 MT colonies, 4 of which were derived from BP-treated CTA groups). In 4 out of 5 cases a cell crisis had to be overcome to bypass senescence barriers.

Morphological transformation does not (as in 3.3.3) guarantee senescence bypass in SHE-MT clones generated by BioReliance

DMSO MT

Areas of criss-crossed cell growth were not initially identified in cells derived from DMSO MT colonies inconsistent with their scored MT characteristics (Figure 12). Eight out of 10 DMSO MT colony-derived cells from BioReliance entered senescence and stopped dividing by P+6 (Table 7A). A further clone continued to proliferate for around 35 population doublings (SHE 18) but then ceased to proliferate and also senesced. In one out of ten cases, cells from a DMSO-treated MT colony (SHE 14) continued to grow and divide, overcoming a cell crisis in which most of its population ceased to proliferate (Figure 13). Expansion of SHE 14 was repeated from early passages but events leading to spontaneous immortalisation only occurred in one out of three expansion attempts, implying the occurrence of a further stochastic immortalization event. The frequency of immortalisation in cells derived from DMSO-exposed MT colonies was 1 in 10; although, given the known low rate of spontaneous immortalisation in SHE cells (Trott et al., 1995) this is believed to be a very rare event.

B(a)P MT

SHE populations obtained from benzo(a)pyrene-treated transformed colonies (BP MT) initially retained their MT characteristics; cell growth was disorganised and random with many cells overlapping each other. Fourteen out of eighteen (78 %) BP-treated MT colony-derived SHE cells prepared by BioReliance subsequently flattened, enlarged and entered senescence, see Table 7B. Eight of these BP MT colony-derived cells were

senescent on recovery from cryostorage (P+1) and could not be further analysed. The typical appearances of senescent cells from the BP MT colony, SHE 19 are shown in Figure 14A. SHE 19 was slow growing at P+1 after recovery and, although signs of overlapping MT growth were initially noted, cell proliferation then slowed such that by passage +5 cultures were dominated by enlarged overlapping cells that looked granular with irregular cells membranes. Dishes containing SHE 19 cells at passage +8 (around 20 population doublings) were maintained for over 2 months without any subculture or signs of cell growth. The frequency of immortalisation of morphologically transformed SHE cells that had initially been treated with B(a)P from BioReliance was 22 % (4 out of 18). These clones bypassed senescence and continued to divide and proliferate beyond 70 population doublings; when kept in culture immortalised MT cells reached beyond 100 population doublings. Those cultures that went on to bypass senescence barriers are identified in Table 7 and shown in bold, red typeface.

The growth kinetics of MT-derived SHE cells from both BioReliance and those prepared at Brunel confirm that immortality is not a direct consequence of morphological transformation following the SHE-MT colony CTA. They also indicate that events subsequent to MT are necessary for senescence barriers to be successfully overcome.

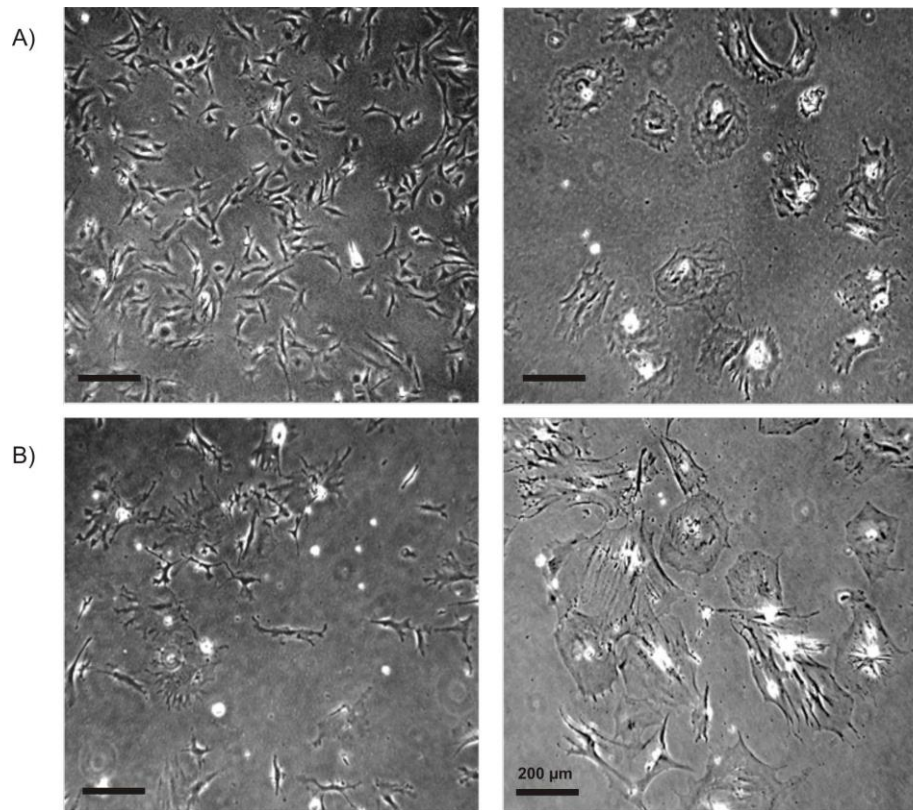


Figure 12 –DMSO MT colony-derived cells show signs of poor growth before widespread senescence.

On subculture, DMSO-treated morphologically transformed SHE clones (DMSO MT) for the most part enter terminal senescence and stop dividing, except in one instance shown in Figure 9. Cells shown are representative of cells derived from SHE DMSO T colonies. (A) SHE 13 P+2 and P+5; (B) SHE 18 P+2 and P+3.

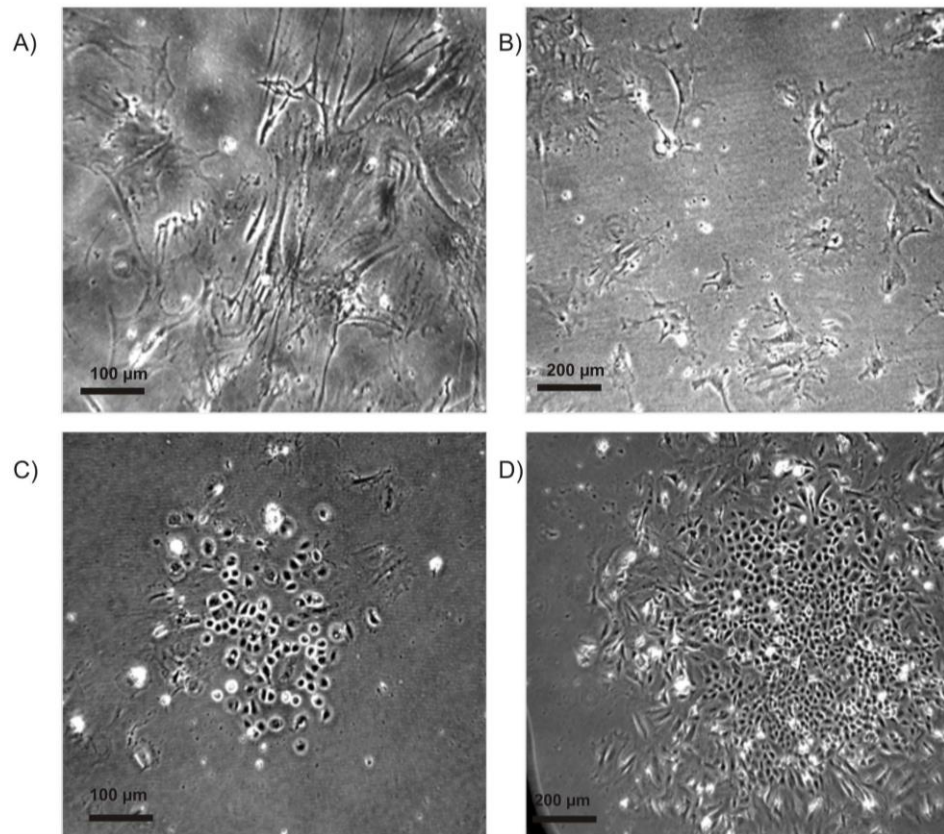
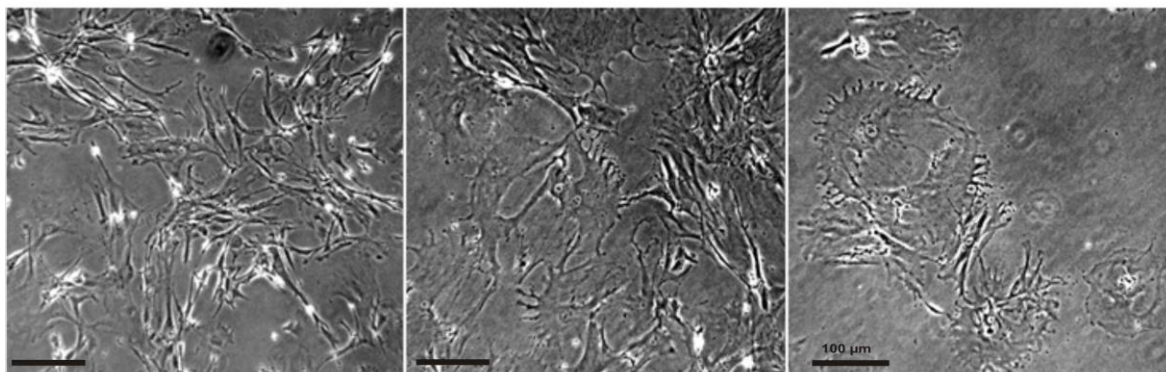


Figure 13 – One transformed colony from the DMSO-treated group (SHE 14) spontaneously immortalised

Time course of DMSO-treated MT SHE 14 cell growth. On recovery, SHE 14 was phenotypically similar to other DMSO MT colony-derived cells and most of its cell population terminally senesced by passage +4 (A and B). A rare clonal event spontaneously took place at P+5 (C) these cells continued to proliferate (D) and on replating expanded to bypass senescence barriers and spontaneously immortalised.

A) SHE 19



B) SHE 23

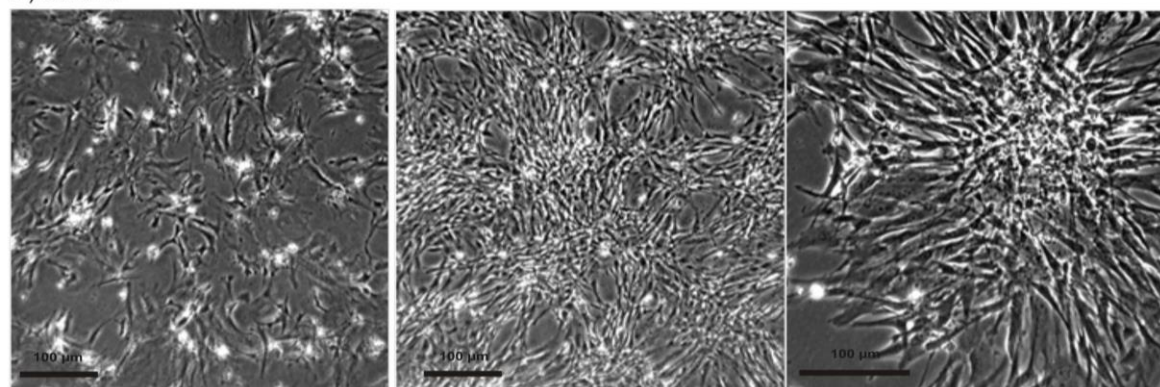


Figure 14 – Cell growth of B(a)P-treated morphologically transformed (MT) colony-derived SHE cells from BioReliance

(A) 77% of B(a)P treated MT clones senesce and do not immortalise. Phase contrast images were taken of cells derived from a representative SHE B(a)P-treated MT colony that senesced (SHE 19). On recovery, cell organisation of these cells was disorganised but following 3-6 subcultures cells entered senescence, had enlarged cytoplasm and ceased to proliferate. This indicated that MT does not guarantee cellular immortality. From left to right images were taken at passages +4, +5 and +6.

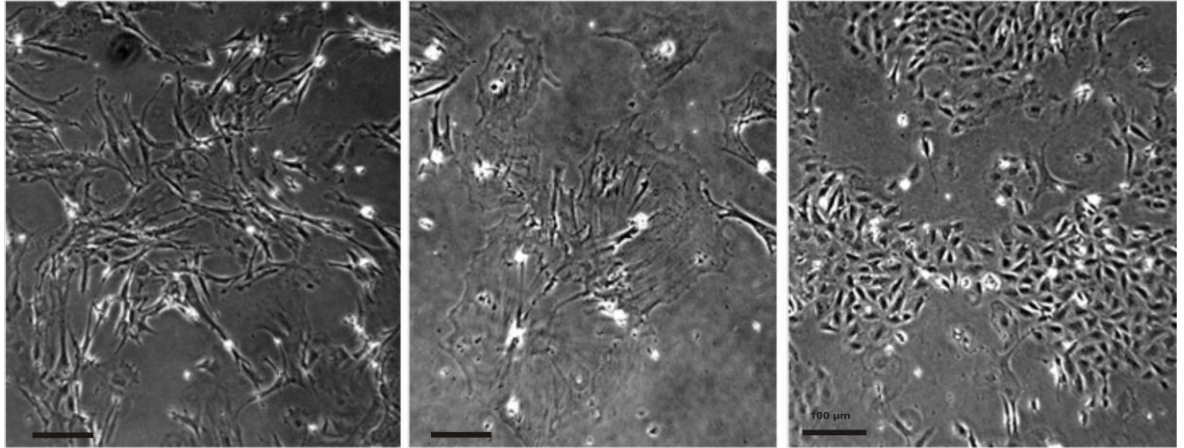
(B) Only 1 out of 18 B(a)P-treated MT clones showed no signs of senescence and was found to be immortal from the outset. On recovery, SHE 23 cells displayed MT phenotypes and had a high rate of population doubling. MT cells continued to proliferate for over 100 population doublings; no signs of senescence were observed and cells were negative for SA- β gal (not shown). From left to right images were taken at passages +2, +5 and +6 using a Carl Zeiss Axioshop inverted microscope.

Secondary immortalising events following MT

A single BP MT culture (SHE 23) from BioReliance continued to proliferate with no signs of senescence (cultured to passage P+42, over 140 population doublings). SHE 23 cells were highly spindle-shaped, retained MT characteristics (Figure 14B) and had short population doubling times of ~30 hours (Figure 16). Stocks of early passage SHE 23 were recovered on 5 separate occasions (Table 7B) and cells were cultured for over 140 population doublings with no signs of senescence indicating that these cells were immortal from the outset.

On the other hand, three BP-treated MT cultures needed to overcome a cell crisis visually similar to cellular senescence and from then continued to proliferate. Cell population doubling times increased (as shown in Figure 16) for a period of around 20 days with no growth as similarly observed in the clones generated at Brunel (see Figure 10). Following this incubation time, rare pockets of clonal growth were readily identifiable in the case of BP MT SHE 21 that emerged from a background of senescent cells (Figure 15A) and also in BP MT SHE 24 (Figure 15B). In SHE 21, once the clonal growth was replated and distributed across the cell plate, population doubling times decreased to 58 hours and from then on cells continued to divide without signs of senescence (Figure 16). SHE cells from MT colonies BP T4 and BP T9 also progressed to immortality with similar lag times. However, unlike SHE 21, pockets of clonal cell growth were not observed in these instances but BP MT cells still overcame what phenotypically looked like a cell crisis with enlarged cytoplasm and a distinct lack of telophase cells. Gradually, the cell population bypassed senescence between 10 and 20 population doublings and, after around 80 days in culture (from CTA seeding), began to proliferate with decreased doubling times (Figure 16). This suggests that rare immortalising events are not necessarily phenotypically obvious in contrast to those observed in Figure 15. Unfortunately SHE 24 was lost due to a bacterial infection; while stocks previous to the (likely) immortalising event were frozen it was not observed again, indicating a stochastic nature of secondary events leading to senescence bypass.

A) SHE 21 (BP MT)



B) SHE 24 (BP MT)

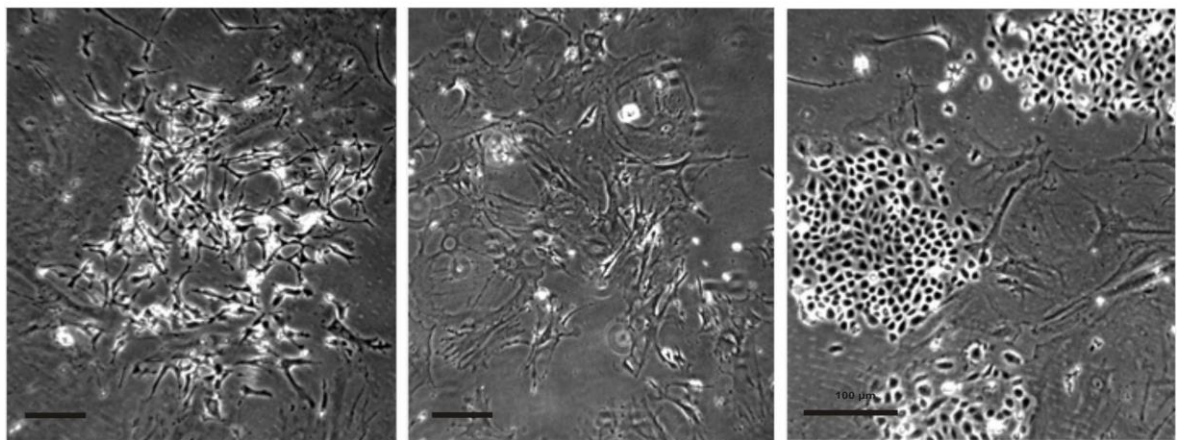


Figure 15 – MT colony-derived cells require one or more additional events to acquire immortality

B(a)P-treated MT-derived cells underwent a prolonged crisis identified by high senescent backgrounds and increasingly slow growth rates which lasted up to a month in culture. In SHE 21 (A) and SHE 24 (B) rare events eventually took place, initiating clonal division after around 20-25 population doublings. These proliferating cells through subsequent rounds of replating and subculture took over the cell population. (A) SHE 21, images taken (from left to right) at P+2, P+5, P+16. (B) SHE 24 images taken at P+2, P+4 and P+4 (different fields of vision from the same plate). Note the dish containing SHE 24 with clonal growth was lost to infection. Images were taken using a Carl Zeiss Axioshop inverted microscope.

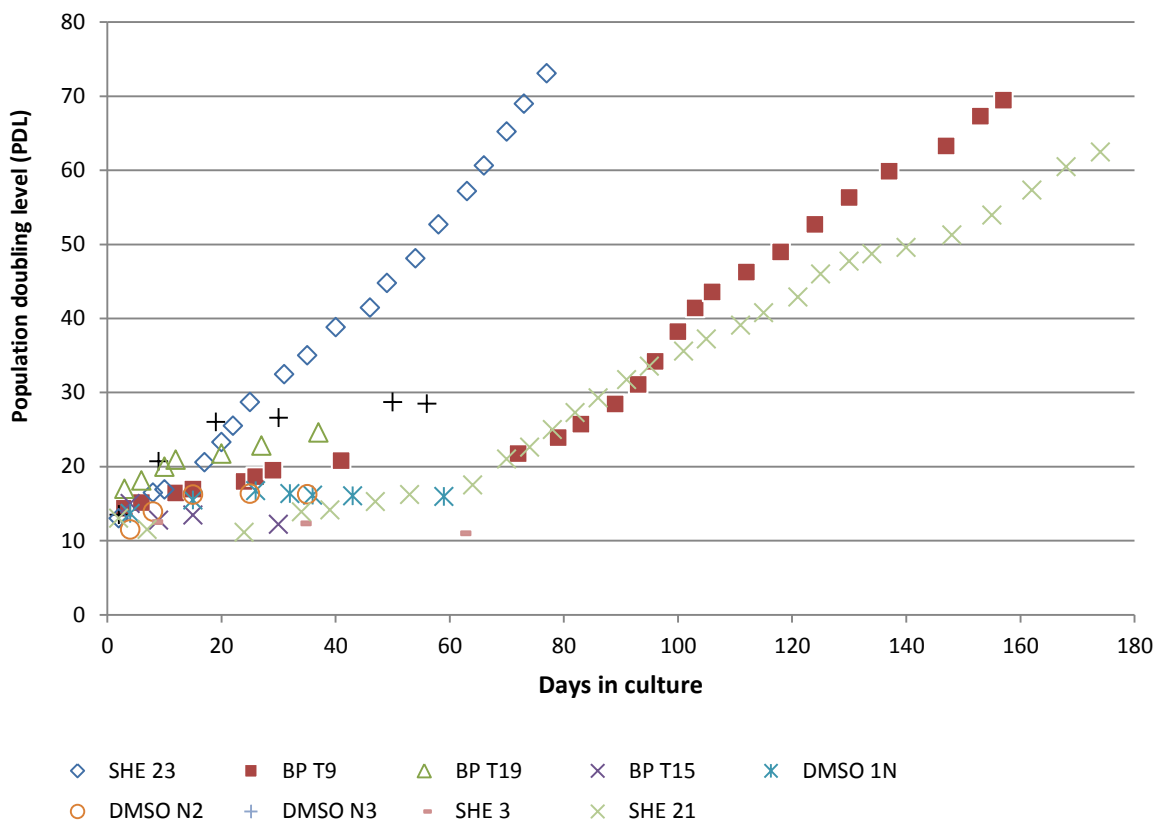


Figure 16- Most colony-derived SHE cells senesced by 35 population doublings

Whole SHE-MT colonies were picked at BioReliance using cloning cylinders and, on arrival at the Brunel laboratory; colony-derived cells were serially sub-cultured to study their growth characteristics. Detached cells were counted using a haemocytometer and calculated PDL values were plotted against number of days in culture. All DMSO and B(a)P non-transformed colony-derived cells that grew senesced before 35 PD (or 7 passages). 14 BP MT colony derived cultures also did not proliferate beyond P+7 or 35 PD; examples are BP T15 and BP T19. A total of 4 B(a)P-treated MT colonies immortalised and continued to proliferate beyond 35 PD: SHE 21, SHE 23, BP T4 (not plotted) and BP T9.

Morphologically transformed (MT) colony-derived SHE cells that were shown to have reduced rates of proliferation were noted to lose their MT characteristics following the decrease in population doubling times. As shown in Figure 17 but also in Figure 15 (right-most images), once clonal growth emerged from the senescent background, B(a)P-induced cells no longer had criss-crossed patterns of growth but were organised and contact inhibited at high cell densities. A similar observation was identified in SHE 14, the

DMSO-induced spontaneous MT clone too had an extensive incubation period where the cells did not divide but then a rare clone without MT characteristics continued to grow and took over the cell population, progressing to immortality (imaged previously, in Figure 13). In contrast, cells derived from B(a)P MT colonies that were immortal from the outset with continuous exponential growth (e.g. SHE 23, D22 #2 and D37 #1) retained their MT characteristics with obvious cell stacking and star-like growth (Figure 18).

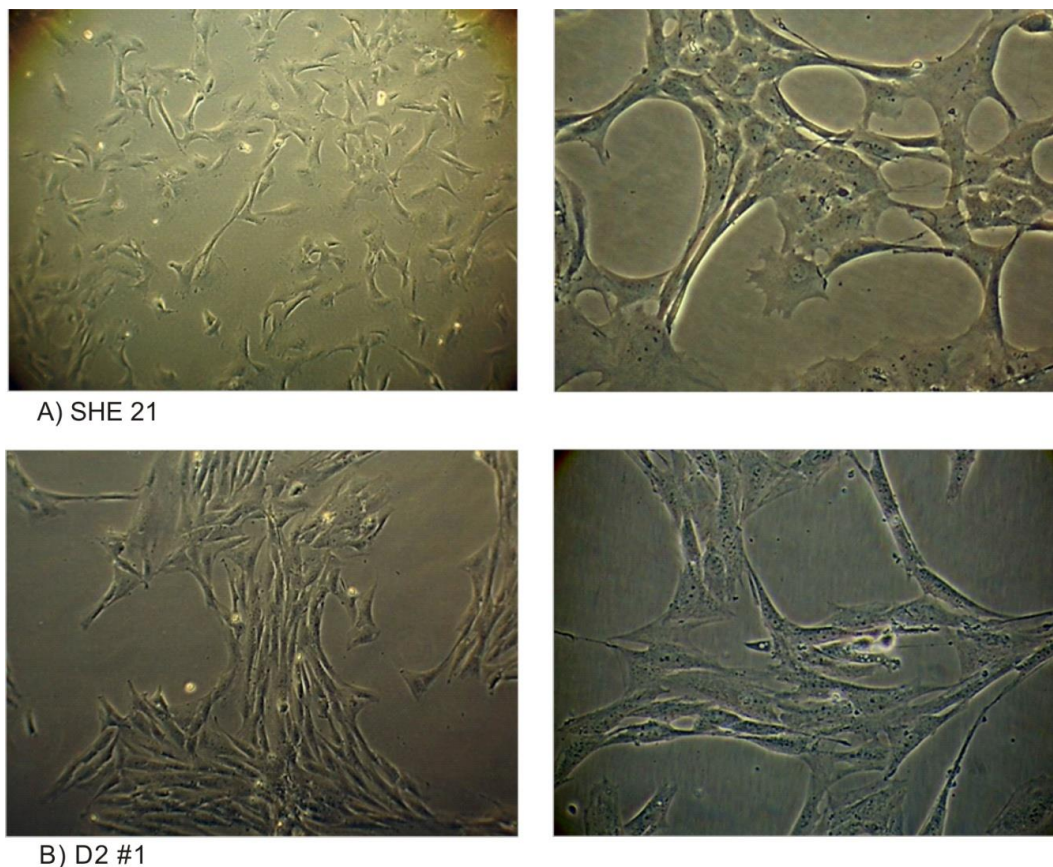
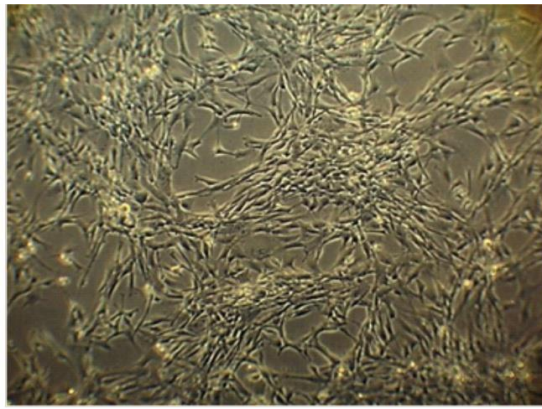
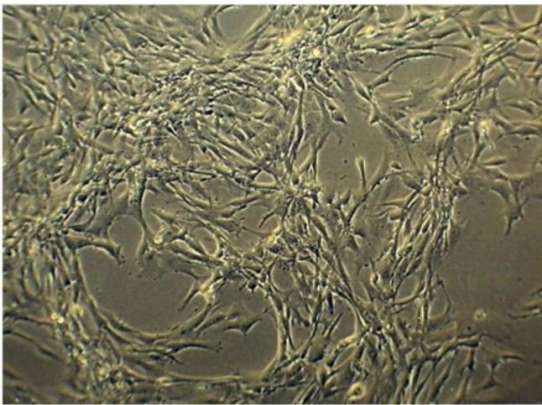
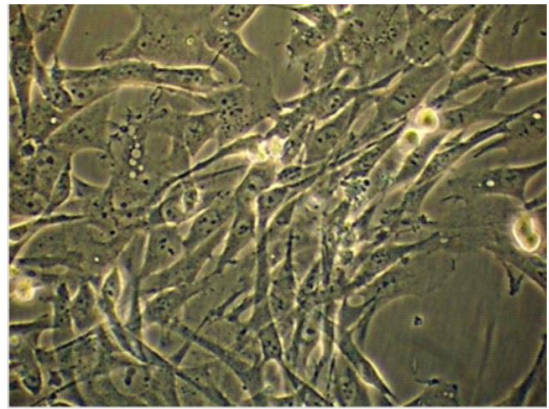


Figure 17 – Morphologically transformed (MT) characteristics are lost in two immortal BP MT colony-derived SHE cells obtained following crisis

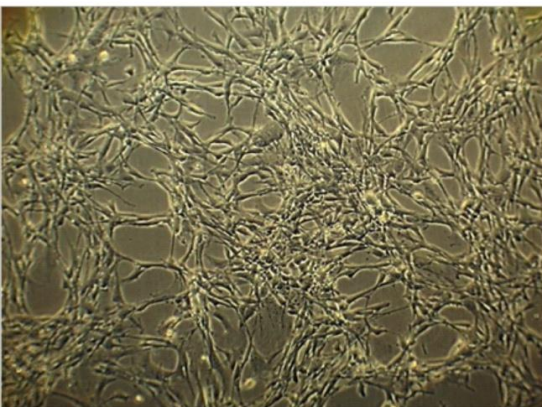
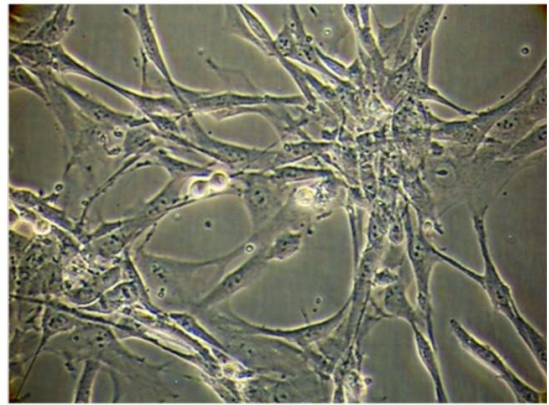
The B(a)P treated colonies which generated SHE 21 and D2#1 immortal cell lines were morphologically transformed. As the cells from these clones were cultured, MT characteristics in were lost. SHE 21 (A) grew in non-overlapping clusters and D2#1 (B) displays fibroblastic-like growth. Both of these cell lines had to overcome a cell crisis where no proliferation took place for prolonged period of time before immortalising. (A) SHE 21 P+26; (B) SHE BP B4 D2 #1 P22. Phase contrast images were taken with a Canon PowerShot G6 camera adapted onto a Carl Zeiss AxioVert CFL Microscope (images to the left taken using a 10 X objective and images to the right using a 40 X objective).



A) SHE 23



B) D37 #1



C) D22 #2

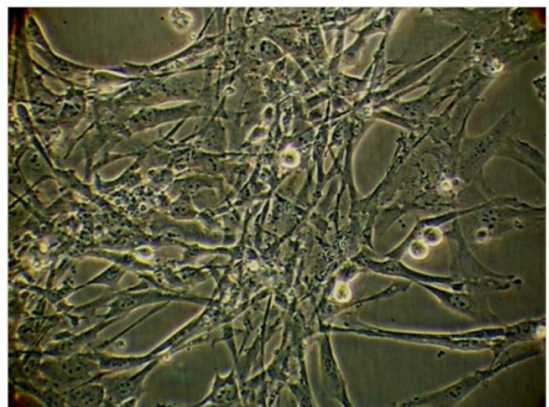


Figure 18 –MT characteristics are retained in clones derived from MT colonies that were immortal from the outset

Immortal cell lines generated from B(a)P treated MT colonies generally retained disorganised MT characteristics. Transformation was identified by overlapping criss-crossed growth and a lack of cell contact inhibition. The following representative cell lines are imaged: (A) SHE 23 P+6: 10X and 40X; (B) D37 #1 P13: 10X and 40X; (C) D22 #2 P12: 10X and 40X. Phase contrast images were taken with Canon PowerShot G6 camera adapted onto a Carl Zeiss AxioVert CFL Microscope (images to the left taken using a 10 X objective and images to the right using a 40 X objective).

In the table below (Table 8) all of the immortal SHE clones studied in this project are listed. This includes those that were obtained from BioReliance (5 cell lines), those prepared *de novo* at Brunel (6 cell lines), plus existing immortalised colony-derived lines previously prepared at Brunel by Dafou (2003), (2 cell lines). In total there were 12 B(a)P-treated MT immortal lines and 1 DMSO-treated MT immortal clone. Five lines had an observable cell crisis that was overcome before progressing to immortality. For simplicity, the SHE-MT colony derived cultures have been renamed and from this point on will be referred as stated in Table 8.

Table 8 – Summary of immortal MT colony derived SHE cells

| Name | Sample | Prepared by | Treatment | Crisis |
|-----------------|---------------|--------------------|------------------|---------------|
| DMSO MT1 | SHE 14 | BioReliance | DMSO | Y |
| BP MT1 | SHE 21 | BioReliance | B(a)P | Y |
| BP MT2 | SHE 23 | BioReliance | B(a)P | N |
| BP MT3 | BP T4 | BioReliance | B(a)P | Y* |
| BP MT4 | BP T9 | BioReliance | B(a)P | Y* |
| BP MT5 | D36 #4 | JCP | B(a)P | N |
| BP MT6 | D2 #1 | JCP | B(a)P | Y |
| BP MT7 | D22 #2 | JCP | B(a)P | N |
| BP MT8 | D37 #1 | JCP | B(a)P | N |
| BP MT9 | D34#2 | JCP | B(a)P | N |
| BP MT10 | D60#1 | JCP | B(a)P | Y* |
| BP MT11 | 8B-BP1 | DD | B(a)P | Unknown |
| BP MT12 | 8B-BP2 | DD | B(a)P | Unknown |

From SHE-MT assays conducted at BioReliance and Brunel, a total of 13 independent clones derived from morphologically transformed colonies bypassed senescence and immortalised. Of these, one had received treated with DMSO during the CTA and spontaneously immortalised; the remaining 12 had been exposed to the carcinogen B(a)P at the start of the MT CTA. The table gives the origin of each cell type and if they entered a cell crisis during stages of senescence bypass. The detailed growth characteristics of cultures prepared by Dafou (2003) were unknown as only late passage cell stocks were available. (*) did not show characteristics of crisis (cytoplasmic enlargement) but the cumulative population doublings indicate there was a lag phase before exponential cell growth.

3.4 Discussion

The first objective in this project was to investigate the relationship between morphological transformation and known hallmarks of malignant transformation (e.g. immortalisation) in Syrian hamster embryo cells (SHE cells) obtained from the SHE cell transformation assay. For this study, unstained colonies were picked and the cells used to establish colony-derived SHE cultures to investigate if there was a link between MT and cell immortalisation.

The average lifespan in culture of a normal primary SHE cells is 20-30 population doublings at which point the cells no longer possess any proliferative potential and undergo permanent growth arrest (Carman et al., 1998). Cellular senescence is typified by enlarged cytoplasm and flattened cellular morphologies often with stress fibres and increased lysosomal activity (Chandler and Peters, 2013). However, in reduced pH medium (such as DMEM-L, pH 6.7) the lifespan of SHE cells has been shown to be extended, reaching around 50 population doublings (Kerckaert et al., 1996c). In work by Dafou (2003) primary SHE cells underwent 55 PD before senescing but colony-derived cells entered senescence more readily. Growth studies presented here on SHE CTA colonies show that all non-transformed DMSO-treated colony-derived clones senesced before 35 population doublings, as did all B(a)P treated non-transformed colony-derived SHE cells. Senescent cells showed no signs of cellular division in culture for a month or more, despite regular fresh media changes. A common marker for senescence is lysosomal activity which is thought to increase with cell ageing and can be detected by senescence-associated beta-galactoside (SA- β gal) staining (Kurz et al., 2000). Although SA- β gal staining was used to confirm senescence in SHE cells, the formation of the blue precipitate was inconsistent and may have been affected by culture of cells in a low pH culture medium. Actively proliferating cells were often positive for the stain which was noted to form when the cells were at higher cell densities. Immunofluorescence with a marker of proliferation (Ki-67) was briefly attempted as an alternative (Schluter et al., 1993) but this was also unsuccessful in highly proliferating SHE cells (e.g. BP MT2) and was probably due to incompatibility of the human and mouse antibodies tested with the Syrian hamster. Therefore to confirm senescence in the colony-derived SHE cells, cells were kept in culture between one to two months and checked for any signs of growth.

The vast majority of morphologically transformed (MT) SHE cells also stopped proliferating and entered senescence. Over 90 % of B(a)P-induced MT colonies picked at Brunel entered growth arrest and almost 80 % of those from BioReliance also ceased to divide. It is therefore clear that MT characteristics alone are insufficient for cellular immortalisation and that subsequent additional event(s) are necessary for evasion of senescence barriers. The remaining 10-20 % of BP MT clones did bypass senescence whereas no non-transformed colony-derived cells were found to immortalise. In total (and from three different sources) twelve morphologically transformed B(a)P-treated clones picked from SHE-CTA colonies continued to proliferate and can be considered immortal. Thus the MT phenotype does seem to correlate with an increased likelihood of unlimited proliferative potential. When cells derived from the same colony were re-grown from early population doubling time points, immortality was not always acquired, indicating a stochastic nature of senescence bypass.

The event of unlimited growth was secondary to MT in at least 45 % of immortalised MT colony-derived SHE cells. Cultures requiring secondary events flattened and remained without signs of division for a period of 20 days, observable by a lack of telophase cells and long population doubling times. Subsequently cell division increased and, after a cell-crisis period reminiscent of senescence, areas of clonal growth emerged from a background of cytoplasmically enlarged cells. From this point onwards no signs of senescence or increased doubling times were observed but MT characteristics were lost in these cases so that cells became contact inhibited and did not overlap. These observations point towards necessary secondary events required by MT cells to bypass senescence and acquire unlimited growth potential. In those MT cells that stopped dividing, it is postulated that secondary events did not take place. In contrast, the remaining BP MT colony-derived SHE cells proliferated without any known incubation period (doubling times around 30 hours) and can be considered immortal at the outset. An interesting point is that these populations retained MT characteristics throughout their time in culture and were not contact-inhibited. This indicates that underlying molecular events and clonal evolution occurring during crisis had an effect on cell morphology which again highlights how the scored MT phenotype is not sufficient for the bypass of senescence barriers nor are criss-crossed patterns of growth required long-

term. Information on the generation of immortal clones BP MT11 and 12 was not available as these cultures were established by a previous PhD student (Dafou, 2003).

One single DMSO-treated MT colony established a spontaneously immortalised line and also followed growth kinetics similar to the two-step kinetics described earlier whereby rare clonal growth took over a population of mostly senescent cells. All other DMSO-MT clones irreversibly senesced. It is believed that this is an extremely rare event as spontaneous immortalisation is very uncommon in the Syrian hamster and largely unrecorded in previous findings (LeBoeuf et al., 1990, Trott et al., 1995). Along with previously described data from BP MT clones, we can conclude that morphologically transformed characteristics must predispose or prime SHE cells towards overcoming senescence barriers but that this is by no means guaranteed.

In terms of assay evaluation, the SHE CTA is a highly subjective assay which relies on a visual interpretation of each individual colony. What was apparent from conducting the assay is the heterogeneous nature of the colonies obtained, which can be explained by the target cells being derived from embryo cells. This is innately beneficial to screening as a mixture of cell types can be simultaneously tested. However, the resulting variety of colony types further complicates the scoring process (Bohnenberger et al., 2012, Maire et al., 2012c). Basic training did greatly aid my ability to discriminate between normal and morphologically transformed colonies but the actual scoring process can occasionally be ambiguous even for scientists familiar with conducting the assay. In these cases a second opinion is often sought (personal communication with BioReliance).

Frequencies of morphological transformation (MTF) have been shown to vary slightly between laboratories; this has been addressed with recent efforts to standardise the assay's protocol, improving assay reproducibility and transferability (Corvi et al., 2012). It is apparent from SHE CTA data from Brunel that the calculated MTF for the vehicle control DMSO (0.2 %) is greater than that stated in the ECVAM guidelines, as is the expected MTF for benzo(a)pyrene (5µg/µl) (Pant et al., 2012). This suggests an overestimation of those colonies that were scored MT and could be down to a number of factors (in the first instance attributed to lack of experience and lack of assay objectivity). However, other factors affecting the MTF cannot be excluded. Seeding density may have

had an effect. From previous experiments, using the same batches of primary SHE cells (Dafou, 2003) a seeding density of 80 cells per 60 mm dish was shown to produce an increased MTF of 4.1 % using 6 $\mu\text{g}/\mu\text{l}$ B(a)P compared to an average MTF of 1.7 % when 150 cells were seeded, indicating that a lower seeding density increases the observed MTF and vice versa. In my hands, when 150 cells per dish were seeded, colony picking became problematic as the colonies overlapped after the 7 day incubation period. A lower seeding density of 80 cells per dish was optimal in order to facilitate picking individual SHE colonies. Another factor to be taken into consideration is that MTFs were shown to be slightly higher in SHE CTAs performed using conditioned media compared with assays employing feeder layers (Pant et al., 2008, 2010). ECVAM's pre-validation study, which uses feeder layers of x-ray irradiated SHE cells instead of conditioned medium, places an upper limit of DMSO MTF at <0.6 %, and the observed MTF using B(a)P 5 $\mu\text{g}/\text{mL}$ was between 1-4 % depending on laboratory. In another SHE MT study by Pant (2008) using conditioned medium and not feeder cells, the vehicle control DMSO MTF was between 0.52 % and 0.80 % whereas the MTF for the positive control B(a)P at the same concentration was also higher, i.e. between 2.56 % and 2.85 %. The main purpose of performing the SHE CTA in-house was to generate an increased number of MT immortalised colonies for further analysis. Despite increased frequencies of MT in our samples, together with colony-derived SHE cells obtained from BioReliance, it can nonetheless be concluded that the vast majority of morphologically transformed colonies stopped dividing before 35 PD in reduced pH media. It is probable that the frequency of immortality in MT B(a)P cells picked in-house of <10 % reflects the higher proportion of colonies scored MT.

In conclusion, morphological transformation (MT) does not guarantee senescence bypass but may predispose cells within the MT colony to subsequently evade senescence. In almost half of the colonies studied, secondary events following MT were necessary for cellular immortalisation. MT cell characteristics were not necessarily retained in clones acquiring unlimited growth potential but all colony-derived SHE scored as non-transformed cells stopped dividing.

CHAPTER 4

4 The Syrian Hamster *CDKN2A/B* Locus

4.1 Introduction

The *CDKN2A-CDKN2B* locus is located on chromosome 9p21 in humans and spans over 40 Kb of genomic DNA. It is found in a gene desert but contains three important tumour genes, each under the control of separate promoters (*p16*, *p15* and *ARF*), which are involved in regulating cell growth and senescence pathways (Gil and Peters, 2006). The genomic region is frequently subject to loss of heterozygosity (LOH) and homozygous deletion in tumours (van der Riet et al., 1994, Gray et al., 2006, Florl and Schulz, 2003). During early stages of development the locus is silenced by polycomb protein repressor complexes (PRC1 and PRC2) which are then progressively removed over the course of the cell's lifespan pushing the cell towards senescence (Bracken et al., 2007, Martin et al., 2013). Targeting of Polycomb proteins by microRNAs (miRNAs) has been shown to activate expression of *p16* and entry into senescence (Overhoff et al., 2014). *ARF* is known to modulate the activity of the tumour suppressor protein p53 by regulating protein turnover via Mdm2, whereas *p16* activates senescence pathways via the retinoblastoma protein (pRB) (Kuilman et al., 2010). *ARF* and *p16* have their second exonic region in common which uses an alternative reading frame to generate proteins with distinct functions. The *p15* gene is thought to have arisen by duplication of *p16* and is believed to have similar functional roles (Krimpenfort et al., 2007); *p15* is located ~8 Kb upstream of *ARF* exon1 β which is another 20 Kb upstream of *p16* exon 1 α . A large anti-sense long non-coding RNA element ANRIL has been identified to overlap with the *CDKN2B* locus (Aguilo et al., 2011) which may co-ordinate regulation of all three tumour suppressors.

Up until recently the Syrian hamster (*Mesocricetus auratus*) genome had not been sequenced and only very limited sequence information has been available. The lack of accessible genomic data for this rodent model has been experimentally restrictive and has hindered studies concerning molecular mechanisms (Li et al., 2008, Yasaei et al., 2013, Creton et al., 2012). In 2013, the Broad Institute of MIT and Harvard University recently completed genomic shotgun sequencing of the Syrian hamster genome using the Illumina HiSeq 2000 platform (WGS Project APMT01). The project generated 237,700 unannotated whole genome shotgun sequences (WGS) containing nucleotide information which can be accessed via the NCBI database. Although not yet fully assembled, genomic information is now available for *Mesocricetus auratus* and very recently, predicted gene

transcripts inferred from protein alignments (personal communication with NCBI Help Desk) have also been uploaded. Previous to WGS Project APMT01, messenger transcripts were available for *p16*, *p15* and *ARF* genes but non-coding information was very limited. Taking advantage of the latest genomic knowledge, intergenic information can be sourced from the WGS files (APMT01). This chapter focuses on discussing coding regions of genes located within the *CDKN2A/B* locus. Inferred alignments between known Syrian hamster coding sequences and genomic WGS now permit a comparison of the genomic structure of the *CDKN2A/B* locus in hamster with other species. Additionally, non-coding regions upstream of the *p16* gene containing its promoter were further identified (Hanaoka et al., 2005) which enabled prediction of regulatory DNA sequences and characteristics.

4.2 Materials and methods

4.2.1 Annotated *CDKN2A/B* sequences available via NCBI

The following known mRNA sequences were identified via the NCBI nucleotide database for genes located in the Syrian hamster *CDKN2A/B* locus: *p16* (GenBank: AF292567), *ARF* (GenBank: AF443796) and *p15* (GenBank: NM_001281539). Additionally, for the *p16* gene two extra sequences containing limited genomic information were sourced: *p16* promoter (Hanaoka et al., 2005) and *p16* partial coding region (GenBank: AH010240.2) which contained incomplete intragenic information.

4.2.2 WGS sequences available via NCBI

Whole genome shotgun sequences (WGS) for the Syrian hamster were obtained via NCBI. Existing and known coding sequences for *p16*, *p15* and *ARF* were entered into nucleotide BLAST (BLASTn) to identify which WGS contained them, by selecting *Mesocricetus auratus* (taxid: 10036) and limiting the search to WGS contigs. Contig sequences were then downloaded into CLC Main Workbench software v6.9 (CLCbio, Aarhus, Denmark) for further alignments and sequence analysis.

4.2.3 Sequence alignments

Coding nucleotide sequences for *p16*, *p15* and *ARF* in human, rat and mouse were searched for via the NCBI nucleotide database and protein sequences were inferred. Sequences were aligned to Syrian hamster coding sequences using ClustalX v2.1 (Larkin et al., 2007) in the multiple alignment mode. Once aligned, the file was opened in Jalview v2.8.1 (Waterhouse et al., 2009) and residues were coloured according to their identity (i.e. conservation across sequences). Pairwise alignments in Jalview calculated the similarity between species, given as percentage identities. CLC Main Workbench software v6.9 (CLCbio, Aarhus, Denmark) was also used for simplicity to visualise the sequences.

4.2.4 Sequencing of ~1.6 Kb upstream of the *p16* transcriptional start site (TSS)

WGS contig sequences containing the upstream region to *p16* were confirmed by PCR and sent for Sanger sequencing (Beckman Coulter Genomics). Overlapping primers were designed to the immediately upstream sequences of contig085774 (GenBank: APMT01085774.1) located adjacent to the known 300 bp containing the 5' SH *p16* promoter.

Primer design

Primers were designed using Primer-BLAST (available via NCBI) and the suggested primer oligonucleotides were checked for specificity by 'blasting' them back into the SH WGS database. Three overlapping primer pairs were generated to cover a total of 1,674 bp just upstream of the *p16* gene's transcriptional start site and including 380 bp of known *p16* promoter region. Primer specificity was confirmed by PCR and gel electrophoresis (refer to section 2.7).

Confirming WGS sequence

A further PCR for each primer pair was then performed on wild-type Syrian hamster genomic DNA (gDNA); amplified products were extracted from a 1.5 % agarose gel and purified for sequencing as described in sections 2.8 and 2.9 respectively. For each PCR reaction, 100 ng gDNA was added to 25 µl AmpliTaq Gold[®] 360 master mix (Applied Biosystems[®]), 5 µl GC enhancer, 0.5 µM forward primer, 0.5 µM reverse primer made to 50 µl in RNase/DNase free dH₂O. Cycling conditions were as follows: denaturation at 95 °C

for 10 min followed by 40 cycles of 94 °C for 45 sec, 59 °C for 30 sec and 72 °C for 45 sec, then final extension at 72 °C for 7 min before holding at 4 °C. Reactions were performed in duplicate so as to load up to 100 µl of each PCR product on a 1.5 % agarose gel made in 1 X TBE buffer with EtBr. The resulting Sanger sequences were aligned back to the original WGS sequence (contig085774) using CLC Main Workbench software v6.9 (CLCbio, Aarhus, Denmark).

4.2.5 Investigating the *p16* gene promoter

Confirmed WGS sequence information was input into MethPrimer (Li and Dahiya, 2002), to identify potential CpG islands located in the *p16* promoter. The criteria for identification of a CpG island were (i) that it had to be over 100 bp in length and (ii) that its CG content had to be higher than 50 %. Similarly, data was input into GPMiner (Lee et al., 2012) to identify any promoter regulatory motifs. As there was no setting specific for hamster genomes included on the program, both human and mouse settings were tested and they gave the same output.

4.3 Results

4.3.1 Conservation of *CDKN2A-CDKN2B* coding regions

Gene coding regions of the *CDKN2A/B* locus in *Mesocricetus auratus* were aligned to corresponding mouse, rat and human sequences identified via the NCBI databases. Figure 19 shows the aligned mRNA (A) and protein (B) sequences for the *p16* coding regions of Syrian hamster (AF292567), mouse (AF044335), rat (L81167), human variant 1 (NM_000077) and 5 (NM_001195132). Hamster *p16* was found to be 474 nucleotides in length and was shown to have 71.78 % identity in common with mouse, 77.11 % with rat and 73.47 % and 72.06 % identity with human variant 1 and 5 respectively. *p16* identity to human transcript variants 1 and 5 was marginally higher than mouse (67.81 % and 66.73 % respectively) and rat (71.78 % and 70.27 % respectively); the highest identity was between mouse and rat orthologues (82.05 %). At a protein level, hamster *p16* shared

69.59 % identity to human *Ink4a* and 66.24 % to *p16-gamma*, 68.13 % identity to rat and 65.61 % identity to mouse.

Nucleotide and protein alignments performed with Clustal X for *ARF* are shown in Figure 20. Between Syrian hamster *p13ARF* and mouse *p19ARF* there was 77.63 % nucleotide sequence identity. This is compared to 81.27 % identity with rat and 76.36 % identity with human *p14ARF*. The coding region of Syrian hamster *ARF* appears to hold two extra codons encoding arginine residues in exon 1 β . The second exon is shorter in length leading to a total hamster *p13/ARF* polypeptide of 123 amino acids compared to 132 residues in human (*p14/ARF*) and over 160 residues in mouse and rat (*p19/ARF*). This difference in length helps explain the low sequence homology between the amino acid sequences; Syrian hamster *ARF* protein held 53.66 % identity with mouse, 54.47 % with human and 61.79 % with rat.

Finally, SH *p15* is 393 nucleotides in length and aligned to both human isoforms but showed the highest homology to the CDS of human *p15* transcript variant 1 (NM_078487) with 83.37 % identity. The coding transcript of hamster *p15* was highly conserved across species and had 88.89 % identity with mouse nucleotide sequences and 89.20 % with rat, see Figure 21. The gene's first exon was the most homologous. Between the *p15* Syrian hamster protein sequence there was 91.54 % identity with both rat and mouse sequences compared with 86.15 % identity with human *p15*.



Figure 20 – Alignment of Syrian hamster ARF coding regions

Sequence information was inferred from GenBank via NCBI nucleotide and protein databases, alignments were performed using ClustalX2 before exporting into Jalview v2.8.1. Regions shaded in blue are those of identity, with darker blue indicating the highest conservation. A) Nucleotide alignment of: hamster (AF443796), mouse (NM_009877), rat (AY679727), human variant 4(NM_058195). B) Derived amino acid alignment from nucleotide sequences.

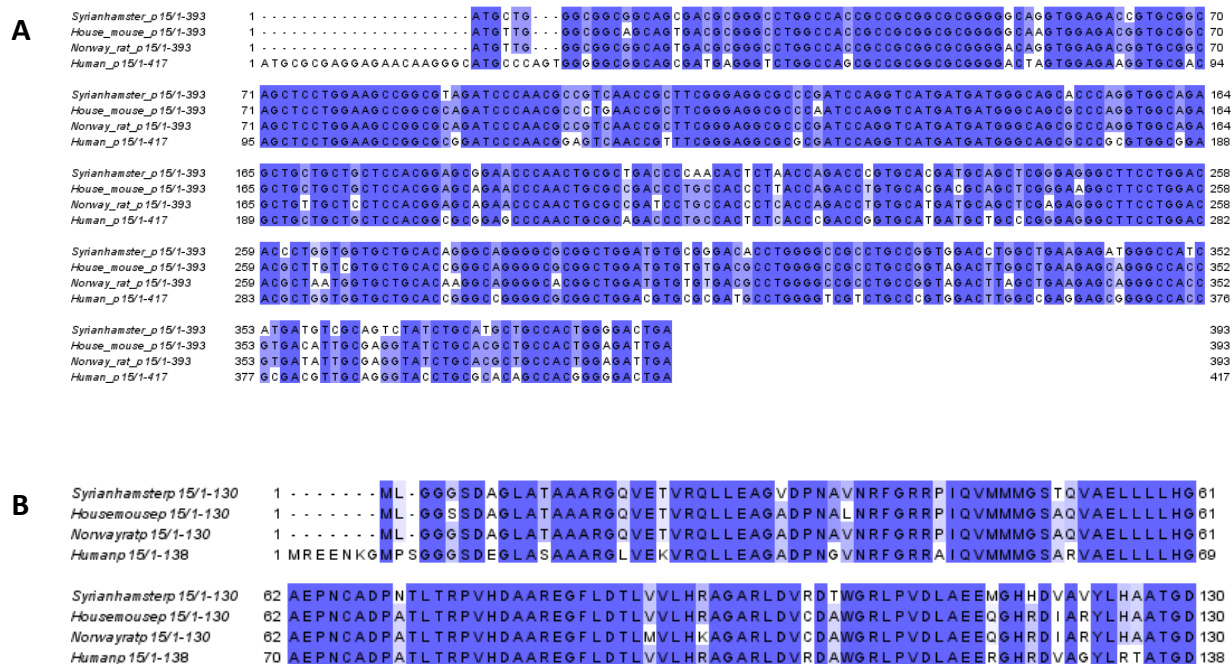


Figure 21 – Alignment of Syrian hamster *p15* coding regions

Sequence information was inferred from GenBank via NCBI nucleotide and protein databases, alignments were performed using ClustalX2 before exporting into Jalview v2.8.1. Regions shaded in blue are those of identity, with darker blue indicating the highest conservation. A) Nucleotide alignment of: Hamster (NM_001281539), mouse (NM_007670), rat (NM_130812), human variant (NM_004936). B) Derived amino acid alignment from nucleotide sequences.

4.3.2 Identification of genomic *CDKN2A* sequences in Syrian hamster

Recent completion of the *Mesocricetus auratus* whole genome shotgun (WGS) sequencing project (accession number GenBank: APMT01000000) has enabled the availability of unannotated SH genomic DNA sequences via the NCBI website. It is therefore possible to infer which assembled WGS sequences, also known as contigs, contain known nucleotide sequences belonging to genes of interest, in the case of this project, those belonging to the *CDKN2A/B* locus.

Using nucleotide BLAST (BLASTn), a search for WGS sequences with homology to Syrian hamster *p16* (GenBank: AF292567) identified two contigs: APMT01085773.1 and APMT01085774.1. The two WGS did not align together but instead contained separate regions of the *p16* coding sequence. Additional nucleotide sequences were therefore necessary to align *p16* correctly to the WGS and to infer exonic and intronic regions. The additional sequences were a partial SH coding region of *p16* (GenBank: AH010240.2) which also contains incomplete intragenic information between *p16* exons 1 α and 2, plus a 380 bp genomic sequence of the SH 5' upstream *p16* promoter region which has been identified by RACE PCR (Hanaoka et al., 2005). Together the known nucleotide sequences were used to align correctly the two SH WGS sequences found to contain *p16* transcripts.

Figure 22A schematically represents the nucleotide alignments; regions in common are those which hold identity. The first WGS (contig085774) contained *p16*'s promoter region, 128 bp nucleotides of its coding region and the first half of the partial *p16* sequence which also contained intronic information. Conversely, the reverse complement of the second WGS (contig085773) aligned to the outstanding half of non-coding DNA and partial *p16* coding sequence (GenBank: AH010240.2), and aligned to the remaining 346 bp of *p16* (GenBank: AF292567); these were inferred as exons 2 (305 bp) and 3 (41 bp). The positioning of the exonic regions identified in the WGS is schematically represented in Figure 22B. The identity between the respective sequences was 99 % with minor nucleotide differences mostly in non-coding regions, which are likely to be due to sample variation and single nucleotide polymorphisms (SNP).

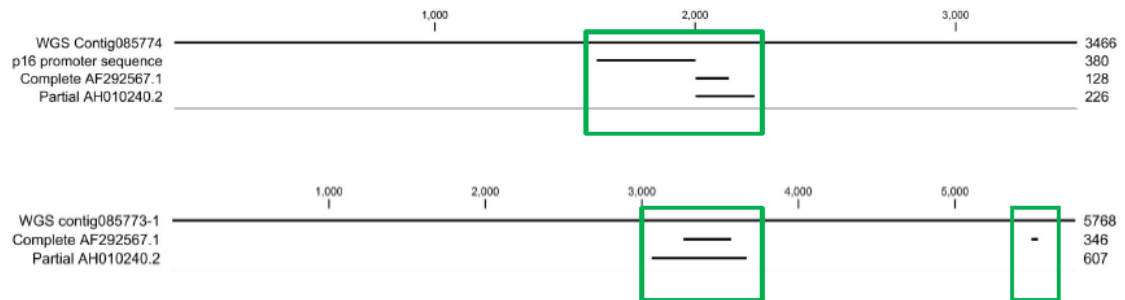
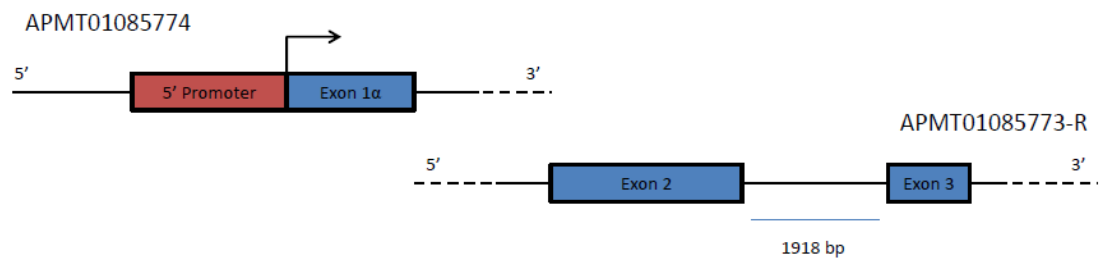
A) *p16* alignments to whole-genome shotgun sequencesB) Location of *p16* exons in whole-genome shotgun sequences

Figure 22 – *p16* nucleotide sequence alignments with unannotated *Mesocricetus auratus* WGS sequences

The CDS of SH *p16* aligned to WGS sequences in three distinct regions, corresponding to 3 exonic regions. (A) Two WGS contigs were identified using BLASTn that contained known *p16* nucleotide sequences GenBank: AF292567, AH010240.2 and its 5' promoter region PCR (Hanaoka et al., 2005). Aligned regions are highlighted in green. (B) Contig085774 aligned to promoter and coding regions containing exon 1 and the reverse complement of contig085773 aligned to exons 2 and 3. The two contigs did not align to each other (dashed lines). Alignments were performed using nucleotide BLASTn available via the NCBI website and CLC sequence viewer software v 6.9.

Coding sequences for Syrian hamster *p16* (AF292567), *ARF* (AF443796) and *p15* (NM_001281539) were subsequently aligned to WGS contigs to compare the genomic structure of the *CDKN2A/B* locus between hamster and human. A schematic of the SH locus is found in Figure 23. As gathered from earlier alignments, shown in Figure 22, in total hamster *p16* has 3 exonic regions. The second exonic region is common to both *p16* and *ARF*, but their resulting protein sequences do not align and their gene transcripts are read in different reading frames. Both tumour suppressor genes hold distinct first exons

as in the human genome and are regulated by separate transcriptional start sites. WGS nucleotide alignments showed that exon 1 β , which is unique to *ARF* and exon 1 α , which is unique to *p16* were located in separate contigs from each other (APMT01085775 and APMT01085774 respectively), suggesting they could be quite far apart. On the other hand, the Syrian hamster *p15* coding transcript is 393 bp long and maps to a single assembled WGS (APMT01085778) in 2 discrete sections, indicating 2 exonic regions which are located over 3 Kb away from each other. There are two known isoforms of human *p15*, one which is of a similar length of 417 bp nucleotides with two exons and the other one of which has 1 exon with its CDS spanning 237 bp.

From the inferred pairwise alignments, the genomic structure of *p16* and *ARF* appeared to be very similar to that in humans (Figure 23). In humans, the intronic distance between *p14/ARF* exon 1b and exon 2 is in the order of 20 Kb, whereas exons encoding *p16* are located 2-3 Kb from each other. Using WGS sequences it was not possible to deduce the distances between SH *p16* exon 1 α , exon1 β and exon 2 as the WGS did not overlap and all 3 exonic regions were found to be contained in separate contigs. However, the distance between SH *p16* exon 2 and exon 3 was just under 2 Kb which encompasses the gene's second intron and is comparable in length to human *p16* intron 2. Presupposing that assembled WGS are in sequence and numerically in the same order as the Syrian hamster genome, then the *CDKN2A/B* locus containing *p15*, *ARF* and *p16* could span up to 6 WGS contigs (085773-085778) which together are in the order of 45 Kb in length.

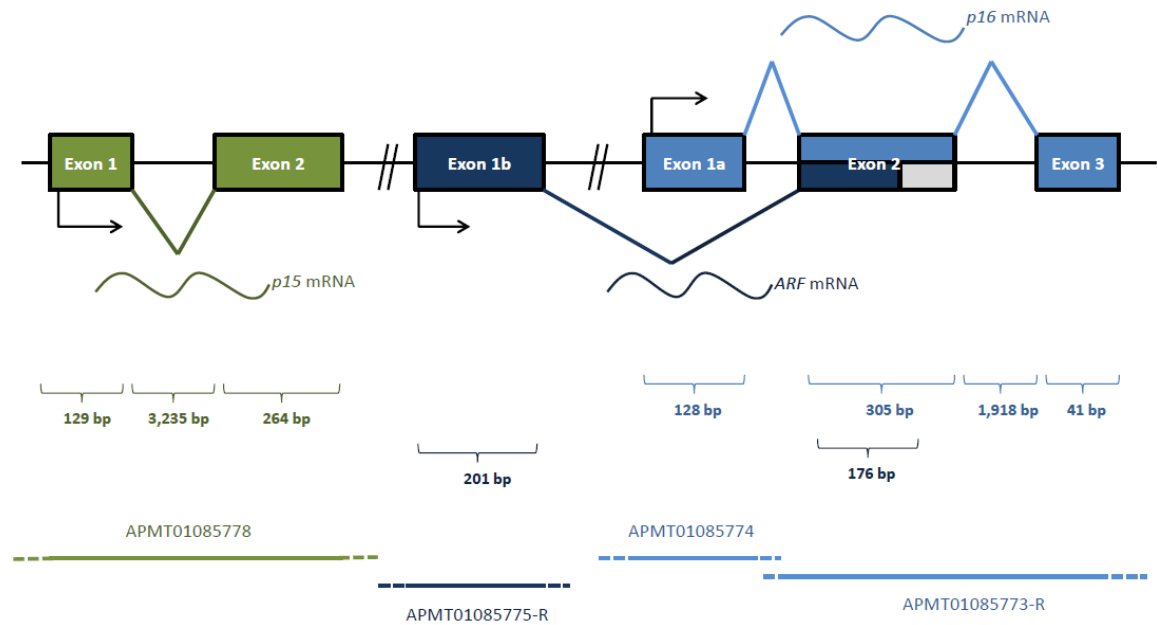


Figure 23 – Suggested genomic structure of the *CDKN2A-CDKN2B* locus in *Mesocricetus auratus*

Gene transcripts of the *CDKN2A/B* locus in the Syrian hamster mapped to 4 different WGS contigs. Coding sequences for *p16*, *p15* and *ARF* were aligned to WGS available via the NCBI nucleotide database using CLC sequence viewer v6.9. The number of exons in each gene was comparable to their human counterparts and the alignments suggested a very similar genomic layout of *p16*, *p15* and *ARF*. The figure is not to scale.

To confirm the upstream alignment of contig085774 to the 5' sequences of *p16*, overlapping sequencing primers were designed to the WGS sequence spanning a total of 1674 bp which included the known 5' 380 bp promoter region. Figure 24A is a schematic of the overlapping regions amplified. The PCR products were purified and sent for sequencing before re-aligning the forward and reverse nucleotide reads back to contig085774. The generated sequences closely matched the WGS assembly and confirmed the extended upstream region of *p16* in Syrian hamster. This information was necessary for subsequent experiments described in Chapter 8 which focus on the *p16* promoter site.

Finally, additional information regarding regulatory motifs and regions upstream of the *p16* transcriptional start site was obtained using online predictive software tools. MethPrimer (Li and Dahiya, 2002) identified two putative CpG islands over

100 nucleotides long with over 50 % GC content; these are shown in Figure 24B. The first CpG island is positioned upstream of the *p16* gene's transcriptional start site (-139 to -263 bp) and the second spans both the promoter site and exon 1 α (-88 to +51 bp). As seen in Figure 24B, the number of CpG sites diminishes further away from the promoter site with the majority located in the first 500 bp upstream of the start site. No additional CpG islands were found further upstream of this; however, Gene Promoter Miner or GPMiner (Lee et al., 2012) predicted a single large CpG site in the WGS confirmed sequence spanning around 700 bp (from -1008 bp to +306 bp).

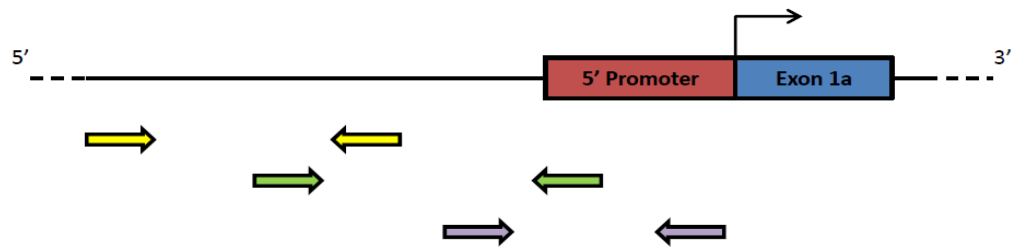
Regulatory motifs belonging to the promoter region were also sought using GPMiner (Lee et al., 2012); a list of the sites closest to the transcriptional start site are listed in Table 9. A palindromic TATA box was identified -160 bp upstream of *p16* start time and regulatory GC boxes were found either side of it at -53 bp and -151 bp, and -216 bp and -243 bp. Additional putative regulatory DNA motifs were located in close proximity to the start site (-24 and -64 bp).

Table 9 – Identification of predicted upstream regulatory motifs located in the *p16* promoter

| Location | Strand | TATA box | GC box | Pattern |
|--------------|--------|----------|--------|-----------|
| -24 to -31 | + | | | AGGCGATC |
| -53 to -58 | + | | GGGGCG | |
| -64 to -70 | + | | | TCACGCG |
| -108 to -114 | + | | | CCCCCCCC |
| -151 to -156 | + | | GCGGGC | |
| -157 to -162 | + | CCTATA | | |
| -216 to -221 | + | | GGGGCG | |
| -243 to -248 | - | | CGGCGG | |
| -276 to -284 | + | | | AGACCTAGG |
| -315 to -320 | + | | GCGCCG | |

Summary of results from GPMiner (Lee et al., 2012) when the upstream sequences of *p16* were input. Regulatory promoter motifs and patterns including TATA and GC boxes were identified in regions upstream of the *p16* start site.

A) Primers designed to *p16* upstream regions



B) GC content of *p16* upstream regions

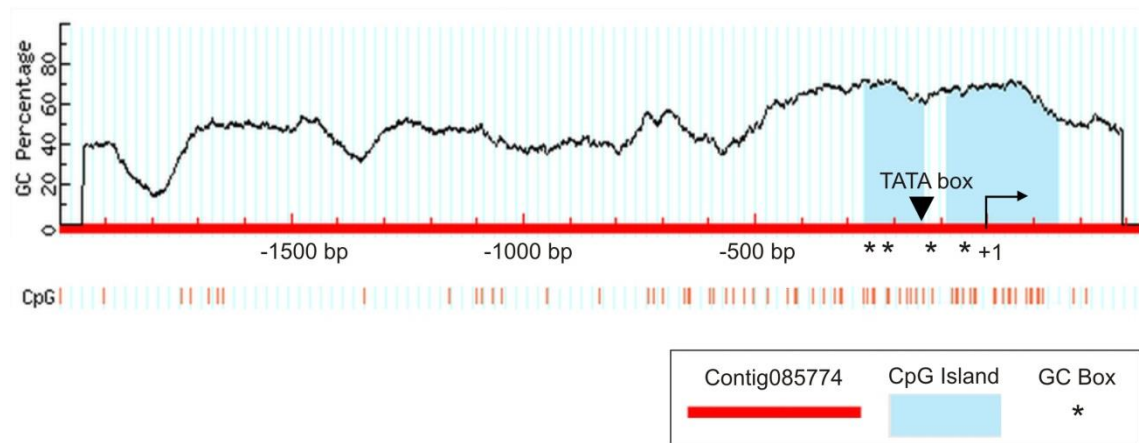


Figure 24 – Regulatory motifs and GC content of sequences upstream of *p16* in the Syrian hamster

Overlapping sequencing primer pairs (A) were designed using the WGS contig085774 to span upstream *p16* genomic sequences, including its known 5' promoter. The sequences generated by Sanger sequencing were aligned back to the contig and confirmed as far as -1641 bp upstream of the start site (+1). CpG islands (B) are shaded in blue and regulatory TATA and GC boxes indicated. Each CpG site is represented by a red line and the frequency of CpG sites increased with proximity to the start site.

4.4 Discussion

The analysis reveals the similarity of the Syrian hamster (SH) *CDKN2A-CDKN2B* locus to that found in humans (which spans around 43 Kb on chromosome 9p21 and encompasses *p16*, *ARF* and *p15* genes). Considering only *CDKN2A/B* exons, SH retained an average of over 70 % nucleotide identity for all three genes when compared with human transcripts and, although *ARF* proteins were considerably distinct from each other (only 54 %

identity), p15 and p16 amino acid sequences were well conserved, with 91 % and 69 % identity to their human counterparts respectively (Figure 19, Figure 20 Figure 21). These results are not dissimilar to those obtained by Muscarella et al., (2001) who originally identified the coding transcripts of Syrian hamster *p16* and *p15*. However, any discrepancies between the results can be explained by differences in calculating identity; sequence identities presented here accounted for both similarity and coverage. Secondly, analysis of sequence homology will have been affected by the initial selection of human GenBank nucleotide sequences leading to differences in sequence identities. A single *p16* transcript variant is available for the Syrian hamster, whereas there are at least 4 known coding human *p16^{CDKN2A}* transcript variants (excluding *ARF*). The inferred alignments may actually under-represent the homologies between species if there are additional, currently unknown, transcript variants belonging to the Syrian hamster which are more homologous to that of human.

From the gene alignments, *ARF* is the least conserved gene at the *CDKN2A/B* locus. A paper by Szklarczyk et al. (2007) describes higher than average selective pressures in mammals occurring across the *INK4A/ARF* locus. It was noted that at a protein level *ARF* orthologues were not well conserved. However, the number of residues in common between *ARF* and *p16* was shown to be retained to between 67-68 amino acids. This implies selection against stop codons in both reading frames as well as a functional significance of *ARF*'s second exon. However in chickens, *ARF* is solely encoded by exon 1 β and does not share overlapping reading frames with *p16* which is actually not present (Kim et al., 2003). Evolutionary studies on the *INK4A/ARF* locus discuss the paradox of two key tumour suppressor genes sharing a second exon despite the region being a common target of deletion in primary human tumours. Consequently, although the frequency of aberrations in *INK4A/ARF* is comparable to that in *p53*, the vast majority of *INK4A/ARF* aberrations are homozygous deletions, and less commonly *p16*-specific point mutations (Sharpless and DePinho, 1999). Mutations that do affect *ARF* tend to be in the shared second exon and are rarely exclusive to *ARF*. Interestingly, in evolutionary terms, *p16* tends to accumulate synonymous mutations whereas *ARF* acquires non-synonymous mutations so long as they have limited impact on its function (Szklarczyk et al., 2007). In this way the two tumour suppressor genes can evolve separately while still sharing

alternative reading frames. Conversely, *p15* which is considered a gene paralogue of *p16* (Gilley and Fried, 2001) and is located in a distinct region upstream of *INK4A/ARF*, has a reduced rate of gene evolution (Szklarczyk et al., 2007) which to some extent is reflected in the highly similar alignments shown in Figure 21.

By aligning known Syrian hamster sequences to genomic WGS sequences it was possible to infer their intronic gene regions and to estimate the position of each exon in relation to one another. Interestingly the WGS sequence containing coding regions for *p16* matched the strain variant identified in the *p16* specific portion of exon 2 in colony-derived SHE cells described in the next Chapter (section 5.2.1).

It cannot be assumed that separate WGS are continuous nor is it possible to state in which direction the contigs align, especially as the assemblies contain regions of ambiguity which, until the Syrian hamster genome is fully assembled and annotated, will not be clarified. However it is reassuring that the identified WGS sequences shown here that contain the known regions for *the CDKN2A/B* locus were in numerical order (see contigs in Figure 23) and the positions of SH *p15*, *ARF* and *p16* were comparable to those in human and mouse (Gil and Peters, 2006). When taking into account the 6 WGS contigs (WGS 085773-085778) the Syrian hamster *CDKN2A/B* locus can be estimated as spanning < 45 Kb; this contains all coding regions plus those sequences assumed to be intragenic. Even given that this raw estimate is derived from WGS sequences that are not fully annotated, the estimated genomic size of the SH locus is likely to be very similar, at least in length, to that in humans.

Having confirmed part of the genomic WGS, regulatory motifs were searched for in the genomic region surrounding hamster *p16*. A palindromic putative TATA box was found - 160 bp upstream of the *p16* transcriptional start site, flanked by regulatory GC boxes, which together act as recognition sites for RNA polymerase II and transcriptional machinery. The TATA box identified was found to be in closer proximity to the TSS than that in the rat, (Abe et al., 2002) which was predicted at -360 bp upstream of the start site. CpG islands were also identified encompassing the majority of the first -300 bp upstream of the *p16* gene promoter, the initiation codon and part of exon 1 α . CpG sites were mostly located near the transcriptional start site (Figure 24) indicating that the

methylation status of these sites may play a role in *p16* regulation as discussed in Chapter 6, and this was not dissimilar to findings in rat (Abe et al., 2002).

The additional genomic information presented in this chapter means that a larger amount of sequence directly upstream of the *p16* locus is now accessible for promoter studies using the Syrian hamster (see Chapter 6). Ultimately, the release of the *Mesocricetus auratus* genome will inevitably have a positive impact on future hamster-based work and aid mechanistic insight into the underlying events involved in the Syrian hamster embryo cell transformation assay (SHE CTA).

CHAPTER 5

5 Molecular Characteristics of SHE-MT Colony-Derived Cells

5.1 Introduction

There are two known cellular senescence barriers that act as safeguards against uncontrolled growth leading to cancer. The first (and most robust) is replicative senescence, whereby a cell with finite lifespan enters growth arrest following telomere shortening to a critical length, triggering a DNA damage response via p53. In most large mammals this is an important intrinsic barrier as it restricts cell growth to a finite number of population doublings. Acquisition of unlimited growth potential necessitates the reactivation of the ribonucleoprotein telomerase (responsible for maintaining telomere length) via transcriptional derepression of the gene encoding its catalytic component, known as hTERT in humans (Sealey et al., 2010). hTERT expression is constitutively switched off in adult human somatic cells. The other senescence barrier relies on the activation of anti-proliferating signalling pathways that regulate senescence in response to aberrant internal and/or external signalling. For example, stress-induced premature senescence (SIPS) is known to occur in cell cultures, due to unfavourable culture conditions, whereas oncogene-induced senescence (OIS) takes place when oncogenes become deregulated. Both of these telomerase-independent pathways involve similar mechanisms that activate ARF-p53 or p16-pRB signalling, which mutually block proliferation and can drive senescence. While human cells possess both classes of senescence barrier, small rodents constitutively express telomerase, meaning that for cell immortalisation to take place only a single barrier (SIPS or OIS) must be bypassed. This makes rodent models like the Syrian hamster (SH) ideal for studying senescence barriers in isolation from the requirement for telomerase activation (Russo et al., 1998). Unlike mice, the Syrian hamster is known to have a very low frequency of spontaneous immortalisation (Trott et al., 1995) which makes it a favourable model for carcinogen screening.

Bypass of senescence involves the inactivation or abrogation of cellular pathways regulating cell cycle progression. Both p53 and p16 signalling ultimately converge on the retinoblastoma protein (pRB) which when inactivated permits entry to S phase from G1. Unsurprisingly in cancers, components of the pathways are found to be mutated or subject to deregulation, thus permitting extended somatic cellular lifespans and subsequent clonal evolution and cancer development. p16 is a cyclin-dependent kinase

inhibitor which is upregulated in senescing cells; it acts by sequestering Cdk4/6 from Cyclin D1 leaving pRB in an active, unphosphorylated state. Rb1 is a member of the pocket protein family along with related proteins p107 and p130 which together act cooperatively and preferentially to bind E2F factors (Cobrinik, 2005). When active, pRB reversibly binds to and inhibits the E2F transcription factors responsible for promoting progression through G1 to S phase, thus restricting replication. Pocket proteins can also recruit histone deacetylases to E2F-responsive promoters via additional co-repressors to actively inhibit transcription. Inactivation of *p16* is commonly identified in tumour types mostly via homozygous deletion and/or silencing by epigenetic mechanisms. Like *p16*, *ARF* is another so called 'INK4' protein (Cdk4/6 inhibitors) (Canepa et al., 2007) which together with *p15* is found at the *CDKN2A/B* locus on chromosome 9p21.3 in humans. *ARF* also functions in regulating cell growth but via the p53 pathway. In mice, *ARF* expression increases as cells reach senescence and deletion is associated with extended lifespan whereas in humans *p16* seems to be the predominant driver of senescence (Sherr and DePinho, 2000, Weber et al., 2000). The expression of tumour suppressor protein p53 is tightly regulated post-transcriptionally and is subject to varying turnover rates influenced by its surrounding molecular environment. Expression of *ARF* increases with oncogenic stimuli and it serves to stabilise p53 by sequestering Mdm2 which otherwise marks p53 for ubiquitination and degradation. Amongst others, the downstream target of circulating p53 is transcription of *p21*, another cyclin-dependent kinase inhibitor, which results in the dephosphorylation of Rb1 and cell cycle arrest (Campisi and d'Adda di Fagagna, 2007, Larsson, 2011).

Previous work using Syrian hamster dermal (SHD) mass cultures has characterised molecular mechanisms underlying carcinogen-induced immortalisation, including benzo(a)pyrene and nickel as well as low-LET and high-LET ionising radiation (e.g. x-rays and fast neutrons). Common targets were the *CDKN2A/B* locus which was found to be subject to deletions, the *p16* promoter methylation, as well as point mutations in the tumour suppressor gene *p53* (Yasaei et al., 2013). The work presented in this chapter expands on these findings using heterogeneous embryonic cells cultures (SHE cells) treated with benzo(a)pyrene (see previous Chapter 3).

5.2 Materials and methods

5.2.1 Mutation screening of *p53* and *p16*

Coding regions of two key tumour suppressor genes *p16* and *p53* were sequenced for mutations in SHE immortalised lines derived from the SHE-MT assay (see Chapter 3). Overlapping primers for sequencing were used spanning exon 1 α and 2 of *p16* and exons 2-9 of *p53*; these are listed in the appendix (section 8).

Table 10– Regions sequenced of tumour suppressor transcripts and their expected band sizes.

| Gene | Exons | Expected amplicon (bp) |
|----------------|--------------------|------------------------|
| <i>p16/ARF</i> | Exon 1 α –2 | 459 |
| <i>p53</i> | Exons 2-4 | 388 |
| | Exons 4-6 | 377 |
| | Exons 6-9 | 383 |

Three overlapping sequencing primer pairs were used to sequence exons 2 to 9 of *p53* and one primer pair was used for *p16*.

Polymerase chain reaction (PCR)

A total volume of 40 μ l cDNA reactions were prepared from 2 μ g of DNase treated RNA as described in section 2.4) using the Applied Biosystems® cDNA kit. From this, 4 μ l cDNA was amplified with 0.5 μ M gene specific forward and reverse sequencing primers using 25 μ l DreamTaq green PCR master mix (2X) (Thermo Scientific™) in a final reaction volume of 50 μ l. For primer specific annealing temperatures see appendix. Example cycling conditions: denature at 95 °C for 2 min followed by 35 cycles of: 95 °C for 30 sec, annealing at 57 °C for 30 sec and extension at 72 °C for 45 sec. Final extension was for 7 min at 72 °C. For each sample, two PCR reactions were run in parallel and combined before loading ~100 μ l PCR product on a 1.5 % agarose gel. 10 μ l of 1 Kb⁺ DNA ladder (Invitrogen™) was also loaded as a reference. Gel electrophoresis took place at 75 V for around 1.5 hours before imaging.

Gel extraction

After visualising and imaging the gel, the expected band of interest (see Table 10) was excised and purified as described previously in section 2.8. The resulting purified DNA fragments were quantified using a NanoDrop and stored at -20°C until needed for sequencing.

Sequencing

Quantified PCR fragments above $15\text{ ng}/\mu\text{l}$ were outsourced for Sanger sequencing at Beckman Coulter Genomics using ABI3730XL (Beckman Coulter Genomics) according to shipment guidelines, along with appropriate sequencing primers diluted to $5\text{ }\mu\text{M}$. The nucleotide reads were analysed using CLC Main Workbench software V5.5 (CLCbio, Aarhus, Denmark) as previously described section 2.9. Forward and reverse alignments from SHE cells were compared to wild type primary Syrian hamster (*Mesocricetus auratus*) sequences as well as published reference sequences: *p16* (GenBank: AF292567.1) and *p53* (GenBank: U07182.1). Sequencing profiles were analysed for clarity of the read, individual peaks and minimal background. Mutations were accepted only if found in both forward and reverse reactions.

5.2.2 Gene expression analysis

RNA extraction

RNA was extracted using phenol-chloroform based methods as described in section 2.3. Extracted RNA quality and quantity was recorded and stored at -80°C .

First strand synthesis (cDNA)

cDNA was synthesised from DNase I treated RNA samples as described in section 2.4. cDNA samples were stored at -20°C until required, when they were thawed on ice.

Primer quality control

Primers for real-time qPCR were optimised using appropriate cycling conditions and tested at a range of different annealing temperatures (between $55\text{-}62^{\circ}\text{C}$) using DreamTaq green PCR master mix (2X) (Thermo ScientificTM). The appropriate annealing temperature was established by running the PCR products on an agarose gel and selecting the strongest band intensity. Primer specificity and working concentrations were

determined using real-time PCR and SYBR green chemistry. If two or more peaks were present in the dissociation curves following amplification then the primers were rejected. The presence of primer dimers in the non-template control (NTC) was only accepted if their Ct value was 10 Ct values higher than reactions containing cDNA.

Quantitative real-time PCR (qPCR) using SYBR chemistry

Real-Time PCR was performed as described in section 2.5 using 10 µl reactions and a 96-well plate format. Following amplification a dissociation curve was performed to check amplicon specificity. Gene targets analysed were *p16*, *p15*, *ARF*, *p53*, *Rb1*, *Mdm2*, *BMI-1*. *GAPDH* and *beta-actin* were used as reference targets or endogenous controls (see below). Gene expression in colony-derived SHE cells was compared to that of early passage and dividing, non-transformed SHE-MT assay derived SHE cells treated with vehicle control (DMSO). Time points were taken over the course of the cellular lifespan, so as to have a continuous analysis of transcript expression. Data was analysed according to the delta delta Ct equation using qbase^{PLUS} v2.6.1 (Biogazelle) software.

Selection of reference genes

qPCR data were normalised to *GAPDH* and *beta-actin* for improved reliability of gene expression quantification. Reference genes were selected from a panel of candidate genes from a variety of cellular processes to ensure their expression stability. The gene targets tested were: *beta-actin*, *SDHA*, *TBP*, *GAPDH*, *B2M* and *YWHAZ* as provided by geNormTM Reference Gene Selection Kit (Primerdesign Ltd). Transcript expression of these six genes was measured by standard qPCR on twelve representative samples (six untreated and six treated) including SHD and SHE samples treated with carcinogens benzo(a)pyrene, nickel chloride (NiCl₂), N-nitroso-N-methylurea (MNU) and high doses of X-ray radiation.

Standard qPCR reactions were performed in a MicroAmp Fast Optical 96-well reaction plate (Applied Biosystems®) and the amplification protocol performed using a Real-time HT9700 Applied Biosystems®). Per reaction, 5 µl cDNA diluted to 5 ng/µl was added to 1 µl resuspended primer mix, 10 µl PrimerDesign PrecisionPLUS 2X qPCR Mastermix (Primerdesign Ltd) and 4 µl RNase/DNase free water to give a total final volume of 20 µl per reaction. Amplification conditions were as follows: enzyme activation for 2 min at

95 °C, 50 cycles of denaturation for 15 sec at 95 °C and amplification for 1 min at 60 °C. Fluorogenic data was collected through the SYBR green channel during the annealing phase. A dissociation protocol was also performed (section 2.5) to check the melt curve for the amplified gDNA products.

Absolute quantification (AQ) data were exported and overall average gene stability was assessed by analysing Cq values on qbase^{PLUS} (Biogazelle) software using the geNORM function. Based on each gene's average expression, stability and pairwise variation the most stably expressed genes and optimum number of reference genes required were determined according to Handbook HB01.02.02 and MIQE guidelines (Vandesompele et al., 2002). An optimum geNORM experiment contains at least ten representative samples and eight candidate reference targets (Primer Design only provided six suitable for Syrian hamster) and all samples were measured in the same run for a given reference target (Hellemans et al., 2007).

5.2.3 Gene copy number variation (CNV) analysis

Genomic DNA samples were analysed for selected gene duplications or deletions using qPCR and Taqman style detection chemistry.

DNA extraction

DNA was extracted using methods previously described in sections 2.6 and RNase treated. DNA pellets were stored at -20 °C.

Selection of reference gene for CNV analysis

Gene stability at a gDNA level was assessed using the geNORM Reference Gene Selection Kit (Primerdesign Ltd) using SYBR chemistry and developed for the Syrian hamster. A panel of six reference genes was used to ensure that the most stable gene from these was selected for accurate normalisation at later experimental stages. These genes included: *beta-actin*, *SDHA*, *TBP*, *GAPDH*, *B2M* and *YWHAZ*. Given that these primers were originally developed by Primerdesign for use with Syrian hamster RNA samples, a standard PCR was performed to ensure the specificity of the primers to cDNA and gDNA samples along with establishing the position of these primers in relation to intron-exon boundaries. Only reference primers amplifying the same primer products in gDNA and cDNA were

considered for CNV analysis (i.e. those recognising exonic regions without intron/exon boundaries).

qPCR reactions took place in a MicroAmp fast optical 96-well reaction plate (Applied Biosystems®) and the amplification protocol run using a Real-time HT9700 Applied Biosystems®). Per reaction, 5 µl gDNA diluted to 5 ng/µl was added to 1 µl resuspended primer mix, 10 µl PrimerDesign PrecisionPLUS 2X qPCR Mastermix (Primerdesign Ltd) and 4 µl RNase/DNase-free water to give a total final volume of 20 µl per reaction. Amplification conditions were as follows: enzyme activation for 2 min at 95 °C, 50 cycles of denaturation for 15 sec at 95 °C and amplification for 1 min at 60 °C. Fluorogenic data was collected through the SYBR green channel. A dissociation protocol was also performed to check the melt curve for the amplified gDNA products.

A total of 14 gDNA samples were included to assess overall gene stability across untreated normal SHE cells, B(a)P treated immortal SHE cells and control x-ray and B(a)P SHD cells. For the analysis, qbase^{PLUS} (Biogazelle) software and the geNORM function was used. All samples for each reference gene were run on a single plate and each sample per gene was run in duplicate (Hellemans et al., 2007, Vandesompele et al., 2002). *SDHA* was selected as the most suitable reference gene for CNV analysis in SHE colony-derived cells.

CNV Taqman primer/probe design

Gene-specific double dye (Taqman style) probes for CNV analysis were designed and validated by PrimerDesign. Taqman probes were fluorescently labelled with FAM or VIC at their 5' end and a non-fluorescent quencher ('Black Hole') at the 3' end. Unlike SYBR green which detects all dsDNA, the Taqman style probe is specific to the gene amplicon amplified by the primer pair, ensuring specificity. Separate FAM labelled assays were designed for specifically for *p16* (NCBI ref. AH010240.2) exon 1 α , *ARF* (AF443796.1) exon 1 β and exon 2 which is common to both *p16* and *ARF*, *p15* (NM_001281539.1), *p53* (NM_001281661.1) and *BMI-1* (transcript variants 1 and 2 only: XM_005082709.1 and XM_005082710.1 respectively). *SDHA* (DQ402977.1) was used as the reference gene and its assay was labelled with the fluorophour VIC so as to simultaneously run its amplification with a gene of interest (i.e. duplexing). All primers for CNV were synthesised

by PrimerDesign Ltd and remain their intellectual property. Primer sequence information can be found in the appendix.

CNV using Taqman probes

Real-time qPCR for copy number variation analysis was performed using SHE gDNA as described above except that per reaction, 5 µl gDNA diluted to 5 ng/µl was added to 1 µl FAM-labelled gene specific probe, 1 µl VIC-labelled reference probe (*SDHA*), 10 µl PrimerDesign PrecisionPLUS 2X qPCR Mastermix (Primerdesign Ltd) and 3 µl RNase/DNase free water to give a total final volume of 20 µl per reaction. Amplification conditions were as follows: enzyme activation for 2 min at 95 °C, 50 cycles of denaturation for 15 sec at 95 °C and amplification for 1 min at 60 °C. Fluorogenic data was collected through the FAM channel. Amplification values for each gene of interest were normalised internally to the *SDHA* reference gene. In addition to wild type calibrator samples, immortalised SH dermal gDNA samples were used as references as their copy number for *p53*, *p16*, *ARF* and *p15* are known. Each sample was run in quadruple PCR replicates per plate and where possible each cell line was tested at an early and late population doubling time point. The experiment was performed in duplicate (two separate gDNA dilutions prepared from the same sample). Copy Caller Software v2.0 (Life Technologies) and qBASE plus premium (Biogazelle) were used to analyse the data.

5.3 Results

5.3.1 Mutation screening of *p53* and *p16/ARF* in immortalised transformed SHE cells

Previous studies using Syrian hamster dermal (SHD) cells indicated that benzo(a)pyrene-induced senescence bypass is mediated primarily through point mutations and specifically base pair transversions affecting the *p53* and *p16* tumour suppressor genes, at equivalent human mutational hotspots (Yasaei et al., 2013). Sanger sequencing was carried out for tumour suppressor genes *p53* and *p16* in colony-derived SHE cells as an initial screen to identify any potential mutations which could permit bypass of senescence barriers. An example of a good quality sequencing profile is shown in Figure 25; each peak is clear and corresponds to an individual nucleotide while the background in the trace is minimal. Generated sequencing reads were aligned to complete coding regions for *p16* and *p53* (GenBank: AF292567.1 and GenBank: U07182.1 respectively) and any point mutations identified were only accepted if found in both forward and reverse sequencing reactions.

SH samples were scanned for mutations in the coding regions of tumour suppressor gene *p53* (exons 2-9) using three overlapping primer pairs and a single primer pair for *p16* (exon 1 α -exon 2). Controls derived from early passage wild type SH dermal cells (SHD), primary SHE cells (SHE 2B) and colony-derived non-transformed cells initially exposed to DMSO which were picked following the SHE-MT assay (DMSO N). Mutational analysis took place on all immortalised SHE cells to include: 1 colony-derived DMSO-treated MT clone (DMSO MT1), and 12 BP-treated colony-derived clones scored as morphologically transformed (BP MT1 to BP MT12 and listed in section 3.3.4, Table 8). B(a)P treated, MT-scored colony-derived SHE cells that did not immortalise were also sequenced for gene mutations.

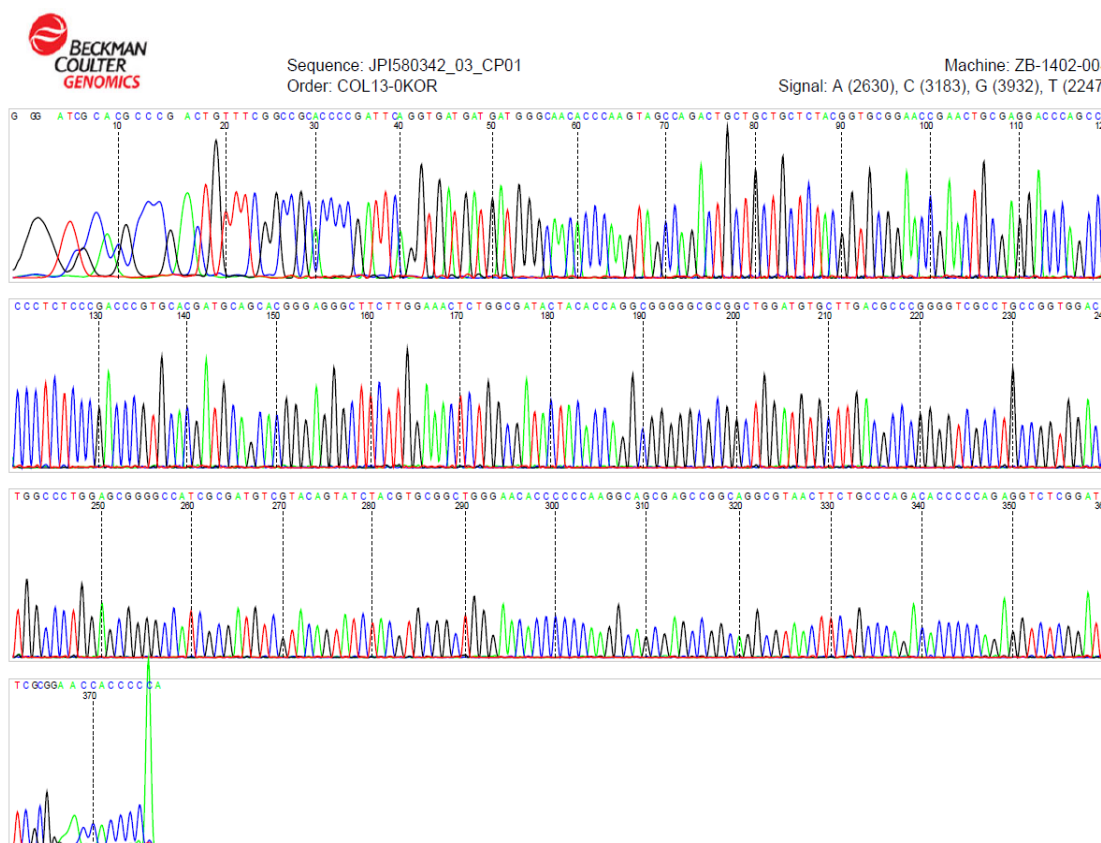


Figure 25 – A good quality Sanger sequencing profile example

This is a sequencing trace example for the forward reaction of the *p16* coding region of BP MT1. Sanger sequencing reactions were outsourced to Beckman and Coulter Genomics. A good sequencing profile consisted of clear peaks with little or no background and regular signal intensity throughout the read.

When aligned to reference sequences, all samples including untreated controls and B(a)P-treated MT immortal and finite lifespan SHE cells held a common variation in *p16* at 345-346 bp from its ATG transcriptional start site (CT>TC). The base change was identified in both forward and reverse sequencing reactions; aligned examples are shown in **Error! Reference source not found.** The transcriptional change spanned two codons located in the second portion of *p16/ARF* exon 2, which is unique to *p16*, causing a non-synonymous or translational change only in the proteins 116th amino acid (refer to Table 11) as the alteration to the second codon is silent. Because these changes were common to all samples analysed when compared to reference sequences available via NCBI, they are an

assumed strain variation or single-nucleotide polymorphisms (SNP). No other alterations to the *p16* coding region sequenced were identified in immortal SHE-MT cultures or controls.

Table 12 summarises mutations identified via Sanger sequencing for the coding regions of *p53* in benzo(a)pyrene-induced SHE-MT clones. As with *p16*, a common inversion was also identified which was located at position 561-562 bp from its transcriptional start site (GA>AG) and is highlighted in **Error! Reference source not found.**. This was located in the sequence encoding the DNA binding domain and also spanned 2 codons causing a change in the transcribed protein in only 1 of the two amino acids (Ser>Gly). Again, it is assumed this is a strain variant as the change was noted in all samples tested. A synonymous base change located at 195 bp from the transcriptional start site (TSS) was found in all Brunel-derived SHE colonies, including the SHE primary cell of origin (SHE 2B). This mapped to the *p53* proline-rich domain and is equivalent to amino acid 66 in human *p53*, which is not considered a mutational hotspot (**Error! Reference source not found.**), and is likely to be an inter-laboratory strain variant between Brunel and BioReliance-derived SHE colonies.

Finally, 4 different non-synonymous *p53* point mutations were found in 4 separate immortal SHE lines, which had been derived following treatment with benzo(a)pyrene; they had been scored as morphologically transformed and had bypassed senescence (**Error! Reference source not found.**). These were: BP MT9, BP MT10, BP MT11 and BP MT12. Point mutations in each cell line were identified in both the forward and reverse sequencing reactions; Figure 28 identifies a single peak on the sequencing profile observed, relating to the nucleotide base change. As noted in Table 12, three out of four mutations were transversions, which is a characteristic fingerprint of benzo(a)pyrene exposure (Toyooka et al., 2003) and 3 out of 4 point mutations targeted arginine amino acid residues. The resulting translational changes were all located in the DNA binding domain of *p53* which, when mapped to the orthologous human *p53* protein, were identified in known mutational hotspots. For example the SH point mutation *p53* c752 G>T (Figure 28C) which corresponds to human *p53* amino acid 248, occurring in SHE BP MT11, has been identified in 121 human cancers (IARC *p53* database) and human codon 248 has been mutated in 1544 known instances (Beroud et al., 2000).

| | | | | | | | | | |
|---------------|------------|------------|------------|------------|------------|-------------|-------------|-----|-----|
| | | | 20 | | 40 | | 60 | | 70 |
| SH p16 (NCBI) | ATGGAGCCCT | CTGCGGACGG | GCTGGCTAGG | GCGGCTGCC | AGGGCCGCGA | GCAAGAGGTT | CGGGCTTTGC | | |
| DMSO N F | ----- | ----- | ----- | ----- | ----- | ----- | ----- | | |
| DMSO N R | ----- | ----- | ----- | ----- | ----- | ---AGAGGTT | CGGGCTTTGC | | 17 |
| BP MT2 F | ----- | ----- | ----- | ----- | ----- | ----- | ----- | | |
| BP MT2 R | TC----- | ----- | ----- | ----- | ----- | ---AGAGGTT | CGGGCTTTGC | | 19 |
| BP MT6 F | ----- | ----- | ----- | ----- | ----- | ----- | ----- | | |
| BP MT6 R | TC----- | ----- | ----- | ----- | ----- | ---AGAGGTT | CGGGCTTTGC | | 19 |
| | | 80 | | 100 | | 120 | | 140 | |
| SH p16 (NCBI) | TGGAAGCAGG | GGTTTCGCC | AACGCCCGA | ACTGTTTCGG | CCGCACCCCG | ATTCAGGTGA | TGATGATGG | | 140 |
| DMSO N F | -----G | AGA-TGCG-- | -ACG--CCGA | ACTGTTTCGG | CCGCACCCCG | ATTCAGGTGA | TGATGATGG | | 55 |
| DMSO N R | TGGAAGCAGG | GGTTTCGCC | AACGCCCGA | ACTGTTTCGG | CCGCACCCCG | ATTCAGGTGA | TGATGATGG | | 87 |
| BP MT2 F | -----G | GGATT-GC-- | -ACG--CCGA | -CTGTTTCGG | CCGCACCCCG | ATTCAGGTGA | TGATGATGG | | 54 |
| BP MT2 R | TGGAAGCAGG | GGTTTCGCC | AACGCCCGA | ACTGTTTCGG | CCGCACCCCG | ATTCAGGTGA | TGATGATGG | | 89 |
| BP MT6 F | -----AGG | GG-TT-GC-- | AACGCCCGA | ACTGTTTCGG | CCGCACCCCG | ATTCAGGTGA | TGATGATGG | | 58 |
| BP MT6 R | TGGAAGCAGG | GGTTTCGCC | AACGCCCGA | ACTGTTTCGG | CCGCACCCCG | ATTCAGGTGA | TGATGATGG | | 89 |
| | | 160 | | 180 | | 200 | | 210 | |
| SH p16 (NCBI) | CAACACCCAA | GTAGCCAGAC | TGCTGCTGCT | CTACGGTGCG | GAACCGAACT | GCGAGGACCC | AGCCACCCTC | | 210 |
| DMSO N F | CAACACCCAA | GTAGCCAGAC | TGCTGCTGCT | CTACGGTGCG | GAACCGAACT | GCGAGGACCC | AGCCACCCTC | | 125 |
| DMSO N R | CAACACCCAA | GTAGCCAGAC | TGCTGCTGCT | CTACGGTGCG | GAACCGAACT | GCGAGGACCC | AGCCACCCTC | | 157 |
| BP MT2 F | CAACACCCAA | GTAGCCAGAC | TGCTGCTGCT | CTACGGTGCG | GAACCGAACT | GCGAGGACCC | AGCCACCCTC | | 124 |
| BP MT2 R | CAACACCCAA | GTAGCCAGAC | TGCTGCTGCT | CTACGGTGCG | GAACCGAACT | GCGAGGACCC | AGCCACCCTC | | 159 |
| BP MT6 F | CAACACCCAA | GTAGCCAGAC | TGCTGCTGCT | CTACGGTGCG | GAACCGAACT | GCGAGGACCC | AGCCACCCTC | | 128 |
| BP MT6 R | CAACACCCAA | GTAGCCAGAC | TGCTGCTGCT | CTACGGTGCG | GAACCGAACT | GCGAGGACCC | AGCCACCCTC | | 159 |
| | | 220 | | 240 | | 260 | | 280 | |
| SH p16 (NCBI) | TCCCGACCCG | TGCACGATGC | AGCACGGGAG | GGCTTCTTGG | AAACTCTGGC | GATACTACAC | CAGGCGGGGG | | 280 |
| DMSO N F | TCCCGACCCG | TGCACGATGC | AGCACGGGAG | GGCTTCTTGG | AAACTCTGGC | GATACTACAC | CAGGCGGGGG | | 195 |
| DMSO N R | TCCCGACCCG | TGCACGATGC | AGCACGGGAG | GGCTTCTTGG | AAACTCTGGC | GATACTACAC | CAGGCGGGGG | | 227 |
| BP MT2 F | TCCCGACCCG | TGCACGATGC | AGCACGGGAG | GGCTTCTTGG | AAACTCTGGC | GATACTACAC | CAGGCGGGGG | | 194 |
| BP MT2 R | TCCCGACCCG | TGCACGATGC | AGCACGGGAG | GGCTTCTTGG | AAACTCTGGC | GATACTACAC | CAGGCGGGGG | | 229 |
| BP MT6 F | TCCCGACCCG | TGCACGATGC | AGCACGGGAG | GGCTTCTTGG | AAACTCTGGC | GATACTACAC | CAGGCGGGGG | | 198 |
| BP MT6 R | TCCCGACCCG | TGCACGATGC | AGCACGGGAG | GGCTTCTTGG | AAACTCTGGC | GATACTACAC | CAGGCGGGGG | | 229 |
| | | 300 | | 320 | | 340 | | 360 | |
| SH p16 (NCBI) | CGCGGCTGGA | TGTGCTTGAC | GCCCGGGGTC | GCCTGCCGTT | GGACCTGGCC | CTGGAGCGGG | GCCATCSCGA | | 350 |
| DMSO N F | CGCGGCTGGA | TGTGCTTGAC | GCCCGGGGTC | GCCTGCCGTT | GGACCTGGCC | CTGGAGCGGG | GCCATCSCGA | | 265 |
| DMSO N R | CGCGGCTGGA | TGTGCTTGAC | GCCCGGGGTC | GCCTGCCGTT | GGACCTGGCC | CTGGAGCGGG | GCCATCSCGA | | 297 |
| BP MT2 F | CGCGGCTGGA | TGTGCTTGAC | GCCCGGGGTC | GCCTGCCGTT | GGACCTGGCC | CTGGAGCGGG | GCCATCSCGA | | 264 |
| BP MT2 R | CGCGGCTGGA | TGTGCTTGAC | GCCCGGGGTC | GCCTGCCGTT | GGACCTGGCC | CTGGAGCGGG | GCCATCSCGA | | 299 |
| BP MT6 F | CGCGGCTGGA | TGTGCTTGAC | GCCCGGGGTC | GCCTGCCGTT | GGACCTGGCC | CTGGAGCGGG | GCCATCSCGA | | 268 |
| BP MT6 R | CGCGGCTGGA | TGTGCTTGAC | GCCCGGGGTC | GCCTGCCGTT | GGACCTGGCC | CTGGAGCGGG | GCCATCSCGA | | 299 |
| | | 360 | | 380 | | 400 | | 420 | |
| SH p16 (NCBI) | TGTCGTACAG | TATCTACGTG | CGGCTGGGAA | CACCCCCCAA | GGCAGCGAGC | CGGCAGGC -G | TAACTTCTGC | | 419 |
| DMSO N F | TGTCGTACAG | TATCTACGTG | CGGCTGGGAA | CACCCCCCAA | GGCAGCGAGC | CGGCAGGC -G | TAACTTCTGC | | 334 |
| DMSO N R | TGTCGTACAG | TATCTACGTG | CGGCTGGGAA | CACCCCCCAA | GGCAGCGAGC | CGGCAGGC -G | TAACT-CTGC | | 365 |
| BP MT2 F | TGTCGTACAG | TATCTACGTG | CGGCTGGGAA | CACCCCCCAA | GGCAGCGAGC | CGGCAGGC -G | TAACTTCTGC | | 333 |
| BP MT2 R | TGTCGTACAG | TATCTACGTG | CGGCTGGGAA | CACCCCCCAA | GGCAGCGAGC | CGT CAGGCTG | TAACGTCTG - | | 368 |
| BP MT6 F | TGTCGTACAG | TATCTACGTG | CGGCTGGGAA | CACCCCCCAA | GGCAGCGAGC | CGGCAGGC -G | TAACTTCTGC | | 337 |
| BP MT6 R | TGTCGTACAG | TATCTACGTG | CGGCTGGGAA | CACCCCCCAA | GGCAGCGAGC | CGGCAGGC -G | TAACT-CTG - | | 366 |
| | | 440 | | 460 | | | | | |
| SH p16 (NCBI) | CCAGACACCC | CCAGAGGTCT | CGGATTTTCG | GGACCACCCC | CTAGGGCCCT | ACTAA | 474 | | |
| DMSO N F | CCAGACACCC | CCAGAGGTCT | CGGATTTTCG | GGACCACCCC | CA----- | ----- | 376 | | |
| DMSO N R | C-AGACCTC | CCT----- | ----- | ----- | ----- | ----- | 377 | | |
| BP MT2 F | CCAGACACCC | CCAGAGGTCT | CGGATTTTCG | GGACCACCCC | C----- | ----- | 374 | | |
| BP MT2 R | CCAGTCTCC | GC----- | ----- | ----- | ----- | ----- | 380 | | |
| BP MT6 F | CCAGACACCC | CCAGAGGTCT | CGGATTTTCG | GGACCACCCC | ----- | ----- | 377 | | |
| BP MT6 R | CCAGACGCC | CCG----- | ----- | ----- | ----- | ----- | 379 | | |

Figure 26 – Sanger sequencing of *p16* mRNA identified a strain variation in SHE colony-derived cells compared to the published NCBI sequence.

No mutations were detected in the coding regions of *p16* analysed in SHE samples. However, a strain variation common to all cells analysed was identified which differs to the reference sequence available via NCBI (GenBank: AF292567.1). The inverted base changes are highlighted above in red (c.345 CT>TC).

Table 11 – No mutations in *p16* gene coding regions were identified

| No. | MUTATION | CODON CHANGE | TRANSLATED MUTATION | HUMAN EQUIVALENT | HOTSPOT | LOCATION |
|--------------------|------------|---------------------|---------------------|---------------------|---------------|-------------|
| All samples | c345 CT>TC | CAC/TGC> CAT/CGC | 115-116aa | HIS/CYS> HIS/ARG | 116aa HIS/ARG | 0 Exon 2 |

No gene mutations leading to an altered protein structure were identified in the coding regions of *p16* by Sanger sequencing. However, a strain variant common to all SHE samples analysed was located at 345-346 bp found in exon 2 which leads to a cysteine being changed to an arginine at the 116th amino acid in the p16 protein.

Table 12 – Mutations identified in *p53* gene coding regions

| No. | MUTATION | CODON CHANGE | TRANSLATED MUTATION | HUMAN EQUIVALENT | HOTSPOT ^a | LOCATION |
|--------------------|------------|---------------------|---------------------|---------------------|----------------------|----------------------------------|
| All samples | c561 GA>AG | GAG/AGC> GAA/GGC | 187-188aa | GLU/SER> GLU/GLY | 185aa ASP/SER | 18 (0) DNA binding domain |
| 7 | c195 G>A | GCG>GCA | 65aa | ALA>ALA | 66aa MET | 2 (0) Proline Rich |
| 1 | c482 G>T | CGT>CTT | 161aa | ARG>LEU | 158aa ARG | 264 (102) DNA binding domain |
| 1 | c734 G>C | TGC>TCC | 245aa | CYS>SER | 242aa CYS | 198 (20) DNA binding domain |
| 1 | c752 G>T | CGG>CTG | 251aa | ARG>LEU | 248aa ARG | 1544 (121) DNA binding domain |
| 1 | c808 C>T | CGG>TGG | 270aa | ARG>TRP | 267aa ARG | 65 (34) DNA binding domain |

Brunel-derived samples analysed held a synonymous point mutation in the proline rich domain of *p53* and all SHE samples analysed contained what we believe to be a strain variation. Four immortal SHE lines held *p53* point mutations which lead to an altered translated protein sequence. All non-synonymous point mutations were located in the DNA binding domain of the p53 protein and can be considered to be found in corresponding human mutational hotspots. ^a number of human *p53* mutations found at that codon according to the Universal mutation database(UMD) (Beroud et al., 2000) and numbers in brackets represent the number of known human tumours with the same amino-acid mutation according to IARC *p53* database R17.

| | | | | | | | | | |
|---------------|------------|------------|------------|------------|------------|------------|------------|-----|--|
| | | -20 | | 1 | | 20 | | 40 | |
| SH p53 (NCBI) | TGAAGCCTGG | CTGACTTCCT | GAGTGTGCC | ATGGAGGAGC | CACAGTCAGA | CCTCAGCATC | GAGCTCCCTC | 70 | |
| DMSO N F | -----TCCT | -----TCCT | GAATGTGTC | ATGGAGGAGC | CACAGTCAGA | CCTCAGCATC | GAGCTCCCTC | 53 | |
| DMSO N R | TGAAGCCTGG | CTGACTTCCT | GAGTGTGCC | ATGGAGGAGC | CACAGTCAGA | CCTCAGCATC | GAGCTCCCTC | 70 | |
| BP MT9 F | -----TG | -----TG | GAGTGTGCC | ATGGAGGAGC | CACAGTCAGA | CCTCAGCATC | GAGCTCCCTC | 51 | |
| BP MT9 R | TGAAGCCTGG | CTGACTTCCT | GAGTGTGCC | ATGGAGGAGC | CACAGTCAGA | CCTCAGCATC | GAGCTCCCTC | 70 | |
| BP MT10 F | -----T-T | -----T-T | CGTGTGTC | ATGGAGGAGC | CACAGTCAGA | CCTCAGCATC | GAGCTCCCTC | 57 | |
| BP MT10 R | TGAAGCCTGG | CTGACTTCCT | GAGTGTGCC | ATGGAGGAGC | CACAGTCAGA | CCTCAGCATC | GAGCTCCCTC | 70 | |
| BP MT11 F | -----TGCT | -----TGCT | GC-----C | ATGGAGGAGC | CACAGTCAGA | CCTCAGCATC | GAGCTCCCTC | 47 | |
| BP MT11 R | TGAAGCCTGG | CTGACTTCCT | GAGTGTGCC | ATGGAGGAGC | CACAGTCAGA | CCTCAGCATC | GAGCTCCCTC | 70 | |
| BP MT12 F | -----TGCT | -----TGCT | G-----C | ATGGAGGAGC | CACAGTCAGA | CCTCAGCATC | GAGCTCCCTC | 46 | |
| BP MT12 R | TGAAGCCTGG | CTGACTTCCT | GAGTGTGCC | ATGGAGGAGC | CACAGTCAGA | CCTCAGCATC | GAGCTCCCTC | 70 | |
| | | 60 | | 80 | | 100 | | | |
| SH p53 (NCBI) | TGAGTCAGGA | GACATTTTCA | GACCTGTGGA | AACTACTTCC | TCCAAACAAT | GTTCTGTCCA | CCTTGCCGTC | 140 | |
| DMSO N F | TGAGTCAGGA | GACATTTTCA | GACCTGTGGA | AACTACTTCC | TCCAAACAAT | GTTCTGTCCA | CCTTGCCGTC | 123 | |
| DMSO N R | TGAGTCAGGA | GACATTTTCA | GACCTGTGGA | AACTACTTCC | TCCAAACAAT | GTTCTGTCCA | CCTTGCCGTC | 140 | |
| BP MT9 F | TGAGTCAGGA | GACATTTTCA | GACCTGTGGA | AACTACTTCC | TCCAAACAAT | GTTCTGTCCA | CCTTGCCGTC | 121 | |
| BP MT9 R | TGAGTCAGGA | GACATTTTCA | GACCTGTGGA | AACTACTTCC | TCCAAACAAT | GTTCTGTCCA | CCTTGCCGTC | 140 | |
| BP MT10 F | TGAGTCAGGA | GACATTTTCA | GACCTGTGGA | AACTACTTCC | TCCAAACAAT | GTTCTGTCCA | CCTTGCCGTC | 121 | |
| BP MT10 R | TGAGTCAGGA | GACATTTTCA | GACCTGTGGA | AACTACTTCC | TCCAAACAAT | GTTCTGTCCA | CCTTGCCGTC | 140 | |
| BP MT11 F | TGAGTCAGGA | GACATTTTCA | GACCTGTGGA | AACTACTTCC | TCCAAACAAT | GTTCTGTCCA | CCTTGCCGTC | 117 | |
| BP MT11 R | TGAGTCAGGA | GACATTTTCA | GACCTGTGGA | AACTACTTCC | TCCAAACAAT | GTTCTGTCCA | CCTTGCCGTC | 140 | |
| BP MT12 F | TGAGTCAGGA | GACATTTTCA | GACCTGTGGA | AACTACTTCC | TCCAAACAAT | GTTCTGTCCA | CCTTGCCGTC | 116 | |
| BP MT12 R | TGAGTCAGGA | GACATTTTCA | GACCTGTGGA | AACTACTTCC | TCCAAACAAT | GTTCTGTCCA | CCTTGCCGTC | 140 | |
| | | 120 | | 140 | | 160 | | 180 | |
| SH p53 (NCBI) | CTCTGATTCC | ATTGAAGAAC | TGTTCCGTGC | CGAGAATGTT | GCAGGCTGGC | TAGAAGACCC | AGGTGAAGCT | 210 | |
| DMSO N F | CTCTGATTCC | ATTGAAGAAC | TGTTCCGTGC | CGAGAATGTT | GCAGGCTGGC | TAGAAGACCC | AGGTGAAGCT | 193 | |
| DMSO N R | CTCTGATTCC | ATTGAAGAAC | TGTTCCGTGC | CGAGAATGTT | GCAGGCTGGC | TAGAAGACCC | AGGTGAAGCT | 210 | |
| BP MT9 F | CTCTGATTCC | ATTGAAGAAC | TGTTCCGTGC | CGAGAATGTT | GCAGGCTGGC | TAGAAGACCC | AGGTGAAGCT | 191 | |
| BP MT9 R | CTCTGATTCC | ATTGAAGAAC | TGTTCCGTGC | CGAGAATGTT | GCAGGCTGGC | TAGAAGACCC | AGGTGAAGCT | 210 | |
| BP MT10 F | CTCTGATTCC | ATTGAAGAAC | TGTTCCGTGC | CGAGAATGTT | GCAGGCTGGC | TAGAAGACCC | AGGTGAAGCT | 191 | |
| BP MT10 R | CTCTGATTCC | ATTGAAGAAC | TGTTCCGTGC | CGAGAATGTT | GCAGGCTGGC | TAGAAGACCC | AGGTGAAGCT | 210 | |
| BP MT11 F | CTCTGATTCC | ATTGAAGAAC | TGTTCCGTGC | CGAGAATGTT | GCAGGCTGGC | TAGAAGACCC | AGGTGAAGCT | 187 | |
| BP MT11 R | CTCTGATTCC | ATTGAAGAAC | TGTTCCGTGC | CGAGAATGTT | GCAGGCTGGC | TAGAAGACCC | AGGTGAAGCT | 210 | |
| BP MT12 F | CTCTGATTCC | ATTGAAGAAC | TGTTCCGTGC | CGAGAATGTT | GCAGGCTGGC | TAGAAGACCC | AGGTGAAGCT | 186 | |
| BP MT12 R | CTCTGATTCC | ATTGAAGAAC | TGTTCCGTGC | CGAGAATGTT | GCAGGCTGGC | TAGAAGACCC | AGGTGAAGCT | 210 | |
| | | 200 | | 220 | | 240 | | | |
| SH p53 (NCBI) | CTCCAAGGGT | CGGCGCTGCG | GGCAGCGCCG | GCGGCTCCTG | CAGCAGAGGA | CCCTGTAGCT | GAGACTCCTG | 280 | |
| DMSO N F | CTCCAAGGGT | CGGCGCTGCG | GGCAGCGCCG | GCGGCTCCTG | CAGCAGAGGA | CCCTGTAGCT | GAGACTCCTG | 263 | |
| DMSO N R | CTCCAAGGGT | CGGCGCTGCG | GGCAGCGCCG | GCGGCTCCTG | CAGCAGAGGA | CCCTGTAGCT | GAGACTCCTG | 280 | |
| BP MT9 F | CTCCAAGGGT | CGGCGCTGCG | GGCAGCGCCG | GCGGCTCCTG | CAGCAGAGGA | CCCTGTAGCT | GAGACTCCTG | 261 | |
| BP MT9 R | CTCCAAGGGT | CGGCGCTGCG | GGCAGCGCCG | GCGGCTCCTG | CAGCAGAGGA | CCCTGTAGCT | GAGACTCCTG | 280 | |
| BP MT10 F | CTCCAAGGGT | CGGCGCTGCG | GGCAGCGCCG | GCGGCTCCTG | CAGCAGAGGA | CCCTGTAGCT | GAGACTCCTG | 261 | |
| BP MT10 R | CTCCAAGGGT | CGGCGCTGCG | GGCAGCGCCG | GCGGCTCCTG | CAGCAGAGGA | CCCTGTAGCT | GAGACTCCTG | 280 | |
| BP MT11 F | CTCCAAGGGT | CGGCGCTGCG | GGCAGCGCCG | GCGGCTCCTG | CAGCAGAGGA | CCCTGTAGCT | GAGACTCCTG | 257 | |
| BP MT11 R | CTCCAAGGGT | CGGCGCTGCG | GGCAGCGCCG | GCGGCTCCTG | CAGCAGAGGA | CCCTGTAGCT | GAGACTCCTG | 280 | |
| BP MT12 F | CTCCAAGGGT | CGGCGCTGCG | GGCAGCGCCG | GCGGCTCCTG | CAGCAGAGGA | CCCTGTAGCT | GAGACTCCTG | 256 | |
| BP MT12 R | CTCCAAGGGT | CGGCGCTGCG | GGCAGCGCCG | GCGGCTCCTG | CAGCAGAGGA | CCCTGTAGCT | GAGACTCCTG | 280 | |
| | | 260 | | 280 | | 300 | | 320 | |
| SH p53 (NCBI) | CACCGGTGGC | CTCTGCGCCA | GCCACTCCCT | GGCCCTCTC | ATCTTCTGTC | CCATCCTATA | AAACCTACCA | 350 | |
| DMSO N F | CACCGGTGGC | CTCTGCGCCA | GCCACTCCCT | GGCCCTCTC | ATCTTCTGTC | CCATCCTATA | AAACCTACCA | 333 | |
| DMSO N R | CACCGGTGGC | CTCTGCGCCA | GCCACTCCCT | GGCCCTCTC | ATCTTCTGTC | CCATCCTATA | AAACCTACCA | 350 | |
| BP MT9 F | CACCGGTGGC | CTCTGCGCCA | GCCACTCCCT | GGCCCTCTC | ATCTTCTGTC | CCATCCTATA | AAACCTACCA | 331 | |
| BP MT9 R | CACCGGTGGC | CTCTGCGCCA | GCCACTCCCT | GGCCCTCTC | ATCTTCTGTC | CCATCCTATA | AAACCTACCA | 350 | |
| BP MT10 F | CACCGGTGGC | CTCTGCGCCA | GCCACTCCCT | GGCCCTCTC | ATCTTCTGTC | CCATCCTATA | AAACCTACCA | 331 | |
| BP MT10 R | CACCGGTGGC | CTCTGCGCCA | GCCACTCCCT | GGCCCTCTC | ATCTTCTGTC | CCATCCTATA | AAACCTACCA | 350 | |
| BP MT11 F | CACCGGTGGC | CTCTGCGCCA | GCCACTCCCT | GGCCCTCTC | ATCTTCTGTC | CCATCCTATA | AAACCTACCA | 327 | |
| BP MT11 R | CACCGGTGGC | CTCTGCGCCA | GCCACTCCCT | GGCCCTCTC | ATCTTCTGTC | CCATCCTATA | AAACCTACCA | 350 | |
| BP MT12 F | CACCGGTGGC | CTCTGCGCCA | GCCACTCCCT | GGCCCTCTC | ATCTTCTGTC | CCATCCTATA | AAACCTACCA | 326 | |
| BP MT12 R | CACCGGTGGC | CTCTGCGCCA | GCCACTCCCT | GGCCCTCTC | ATCTTCTGTC | CCATCCTATA | AAACCTACCA | 350 | |
| | | 340 | | 360 | | 380 | | | |
| SH p53 (NCBI) | GGGCGACTAT | GGTTTCCGTC | TGGGCTTCC | GCACTCGGGG | ACGGCCAAAT | CTGTACATG | CACGTA | 420 | |
| DMSO N F | GGGCGACTAT | GGTTTCCGTC | TGGGCTTCC | GCACTCGGGG | ACGGCCAAAT | CTGTACATG | CACGTA | 403 | |
| DMSO N R | GGGCGACTAT | GGTTTCCGTC | TGGGCTTCC | GCACTCGGGG | ACGGCCAAAT | CTGTACATG | CACGTA | 420 | |
| BP MT9 F | GGGCGACTAT | GGTTTCCGTC | TGGGCTTCC | GCACTCGGGG | ACGGCCAAAT | CTGTACATG | CACGTA | 401 | |
| BP MT9 R | GGGCGACTAT | GGTTTCCGTC | TGGGCTTCC | GCACTCGGGG | ACGGCCAAAT | CTGTACATG | CACGTA | 420 | |
| BP MT10 F | GGGCGACTAT | GGTTTCCGTC | TGGGCTTCC | GCACTCGGGG | ACGGCCAAAT | CTGTACATG | CACGTA | 401 | |
| BP MT10 R | GGGCGACTAT | GGTTTCCGTC | TGGGCTTCC | GCACTCGGGG | ACGGCCAAAT | CTGTACATG | CACGTA | 420 | |
| BP MT11 F | GGGCGACTAT | GGTTTCCGTC | TGGGCTTCC | GCACTCGGGG | ACGGCCAAAT | CTGTACATG | CACGTA | 397 | |
| BP MT11 R | GGGCGACTAT | GGTTTCCGTC | TGGGCTTCC | GCACTCGGGG | ACGGCCAAAT | CTGTACATG | CACGTA | 420 | |
| BP MT12 F | GGGCGACTAT | GGTTTCCGTC | TGGGCTTCC | GCACTCGGGG | ACGGCCAAAT | CTGTACATG | CACGTA | 396 | |
| BP MT12 R | GGGCGACTAT | GGTTTCCGTC | TGGGCTTCC | GCACTCGGGG | ACGGCCAAAT | CTGTACATG | CACGTA | 420 | |
| | | 400 | | 420 | | 440 | | 460 | |
| SH p53 (NCBI) | CCTTCCCTCA | ATAAGCTGTT | CTGCCAGCTG | GCGAAAACAT | GCCCCGTGCA | GCTGTGGGTC | AGTCCACAC | 490 | |
| DMSO N F | CCTTCCCTCA | ATAAGCTGTT | CTGCCAGCTG | GCGAAAACAT | GCCCCGTGCA | GCTGTGGGTC | AGTCCACAC | 473 | |
| DMSO N R | CCTTCCCTCA | ATAAGCTGTT | CTGCCAGCTG | GCGAAAACAT | GCCCCGTGCA | GCTGTGGGTC | AGTCCACAC | 490 | |
| BP MT9 F | CCTTCCCTCA | ATAAGCTGTT | CTGCCAGCTG | GCGAAAACAT | GCCCCGTGCA | GCTGTGGGTC | AGTCCACAC | 471 | |
| BP MT9 R | CCTTCCCTCA | ATAAGCTGTT | CTGCCAGCTG | GCGAAAACAT | GCCCCGTGCA | GCTGTGGGTC | AGTCCACAC | 490 | |
| BP MT10 F | CCTTCCCTCA | ATAAGCTGTT | CTGCCAGCTG | GCGAAAACAT | GCCCCGTGCA | GCTGTGGGTC | AGTCCACAC | 471 | |
| BP MT10 R | CCTTCCCTCA | ATAAGCTGTT | CTGCCAGCTG | GCGAAAACAT | GCCCCGTGCA | GCTGTGGGTC | AGTCCACAC | 490 | |
| BP MT11 F | CCTTCCCTCA | ATAAGCTGTT | CTGCCAGCTG | GCGAAAACAT | GCCCCGTGCA | GCTGTGGGTC | AGTCCACAC | 467 | |
| BP MT11 R | CCTTCCCTCA | ATAAGCTGTT | CTGCCAGCTG | GCGAAAACAT | GCCCCGTGCA | GCTGTGGGTC | AGTCCACAC | 490 | |
| BP MT12 F | CCTTCCCTCA | ATAAGCTGTT | CTGCCAGCTG | GCGAAAACAT | GCCCCGTGCA | GCTGTGGGTC | AGTCCACAC | 466 | |
| BP MT12 R | CCTTCCCTCA | ATAAGCTGTT | CTGCCAGCTG | GCGAAAACAT | GCCCCGTGCA | GCTGTGGGTC | AGTCCACAC | 490 | |
| | | 480 | | 500 | | 520 | | | |
| SH p53 (NCBI) | CTCCACCTGG | CACCCGTGTC | GCGCATGG | CCATCTACAA | GAAGTTACAA | TACATGACGG | AAGTTGTAAG | 560 | |
| DMSO N F | CTCCACCTGG | CACCCGTGTC | GCGCATGG | CCATCTACAA | GAAGTTACAA | TACATGACGG | AAGTTGTAAG | 543 | |
| DMSO N R | CTCCACCTGG | CACCCGTGTC | GCGCATGG | CCATCTACAA | GAAGTTACAA | TACATGACGG | AAGTTGTAAG | 560 | |
| BP MT9 F | CTCCACCTGG | CACCCGTGTC | GCGCATGG | CCATCTACAA | GAAGTTACAA | TACATGACGG | AAGTTGTAAG | 541 | |
| BP MT9 R | CTCCACCTGG | CACCCGTGTC | GCGCATGG | CCATCTACAA | GAAGTTACAA | TACATGACGG | AAGTTGTAAG | 560 | |
| BP MT10 F | CTCCACCTGG | CACCCGTGTC | GCGCATGG | CCATCTACAA | GAAGTTACAA | TACATGACGG | AAGTTGTAAG | 541 | |
| BP MT10 R | CTCCACCTGG | CACCCGTGTC | GCGCATGG | CCATCTACAA | GAAGTTACAA | TACATGACGG | AAGTTGTAAG | 560 | |
| BP MT11 F | CTCCACCTGG | CACCCGTGTC | GCGCATGG | CCATCTACAA | GAAGTTACAA | TACATGACGG | AAGTTGTAAG | 537 | |
| BP MT11 R | CTCCACCTGG | CACCCGTGTC | GCGCATGG | CCATCTACAA | GAAGTTACAA | TACATGACGG | AAGTTGTAAG | 560 | |
| BP MT12 F | CTCCACCTGG | CACCCGTGTC | GCGCATGG | CCATCTACAA | GAAGTTACAA | TACATGACGG | AAGTTGTAAG | 536 | |
| BP MT12 R | CTCCACCTGG | CACCCGTGTC | GCGCATGG | CCATCTACAA | GAAGTTACAA | TACATGACGG | AAGTTGTAAG | 560 | |

| | | | | | | | | | |
|---------------|------------|-------------|------------|-------------|------------|------------|------------|------------|-----|
| | | 540 | | 560 | | 580 | | 600 | |
| SH p53 (NCBI) | ACGCTGTCCC | CACCACGAGC | GCTCCTCCGA | GA | SCGATGGT | TTGGCTCCTC | CTCAGCATCT | TATCCGAGTG | 630 |
| DMSO N F | ACGCTGTCCC | CACCACGAGC | GCTCCTCCGA | AG | SCGATGGT | TTGGCTCCTC | CTCAGCATCT | TATCCGAGTG | 613 |
| DMSO N R | ACGCTGTCCC | CACCACGAGC | GCTCCTCCGA | AG | SCGATGGT | TTGGCTCCTC | CTCAGCATCT | TATCCGAGTG | 630 |
| BP MT9 F | ACGCTGTCCC | CACCACGAGC | GCTCCTCCGA | AG | SCGATGGT | TTGGCTCCTC | CTCAGCATCT | TATCCGAGTG | 611 |
| BP MT9 R | ACGCTGTCCC | CACCACGAGC | GCTCCTCCGA | AG | SCGATGGT | TTGGCTCCTC | CTCAGCATCT | TATCCGAGTG | 630 |
| BP MT10 F | ACGCTGTCCC | CACCACGAGC | GCTCCTCCGA | AG | SCGATGGT | TTGGCTCCTC | CTCAGCATCT | TATCCGAGTG | 611 |
| BP MT10 R | ACGCTGTCCC | CACCACGAGC | GCTCCTCCGA | AG | SCGATGGT | TTGGCTCCTC | CTCAGCATCT | TATCCGAGTG | 630 |
| BP MT11 F | ACGCTGTCCC | CACCACGAGC | GCTCCTCCGA | AG | SCGATGGT | TTGGCTCCTC | CTCAGCATCT | TATCCGAGTG | 607 |
| BP MT11 R | ACGCTGTCCC | CACCACGAGC | GCTCCTCCGA | AG | SCGATGGT | TTGGCTCCTC | CTCAGCATCT | TATCCGAGTG | 630 |
| BP MT12 F | ACGCTGTCCC | CACCACGAGC | GCTCCTCCGA | AG | SCGATGGT | TTGGCTCCTC | CTCAGCATCT | TATCCGAGTG | 606 |
| BP MT12 R | ACGCTGTCCC | CACCACGAGC | GCTCCTCCGA | AG | SCGATGGT | TTGGCTCCTC | CTCAGCATCT | TATCCGAGTG | 630 |
| | | 620 | | 640 | | 660 | | | |
| SH p53 (NCBI) | GAAGGAAATA | TGCATGCCGA | ATACCTGGAT | GACAAGCAGA | CTTTTCGGCA | CAGTGTGGTG | GTGCCCATG | 700 | |
| DMSO N F | GAAGGAAATA | TGCATGCCGA | ATACCTGGAT | GACAAGCAGA | CTTTTCGGCA | CAGTGTGGTG | GTGCCCATG | 683 | |
| DMSO N R | GAAGGAAATA | TGCATGCCGA | ATACCTGGAT | GACAAGCAGA | CTTTTCGGCA | CAGTGTGGTG | GTGCCCATG | 700 | |
| BP MT9 F | GAAGGAAATA | TGCATGCCGA | ATACCTGGAT | GACAAGCAGA | CTTTTCGGCA | CAGTGTGGTG | GTGCCCATG | 681 | |
| BP MT9 R | GAAGGAAATA | TGCATGCCGA | ATACCTGGAT | GACAAGCAGA | CTTTTCGGCA | CAGTGTGGTG | GTGCCCATG | 700 | |
| BP MT10 F | GAAGGAAATA | TGCATGCCGA | ATACCTGGAT | GACAAGCAGA | CTTTTCGGCA | CAGTGTGGTG | GTGCCCATG | 681 | |
| BP MT10 R | GAAGGAAATA | TGCATGCCGA | ATACCTGGAT | GACAAGCAGA | CTTTTCGGCA | CAGTGTGGTG | GTGCCCATG | 700 | |
| BP MT11 F | GAAGGAAATA | TGCATGCCGA | ATACCTGGAT | GACAAGCAGA | CTTTTCGGCA | CAGTGTGGTG | GTGCCCATG | 677 | |
| BP MT11 R | GAAGGAAATA | TGCATGCCGA | ATACCTGGAT | GACAAGCAGA | CTTTTCGGCA | CAGTGTGGTG | GTGCCCATG | 700 | |
| BP MT12 F | GAAGGAAATA | TGCATGCCGA | ATACCTGGAT | GACAAGCAGA | CTTTTCGGCA | CAGTGTGGTG | GTGCCCATG | 676 | |
| BP MT12 R | GAAGGAAATA | TGCATGCCGA | ATACCTGGAT | GACAAGCAGA | CTTTTCGGCA | CAGTGTGGTG | GTGCCCATG | 700 | |
| | | 680 | | 700 | | 720 | | 740 | |
| SH p53 (NCBI) | AGCCACCTGA | GGTTGGCTCT | GACTGTACCA | CCATCCACTA | TAACACATG | TGTAATAGTT | CC | GCATGGG | 770 |
| DMSO N F | AGCCACCTGA | GGTTGGCTCT | GACTGTACCA | CCATCCACTA | TAACACATG | TGTAATAGTT | CC | GCATGGG | 753 |
| DMSO N R | AGCCACCTGA | GGTTGGCTCT | GACTGTACCA | CCATCCACTA | TAACACATG | TGTAATAGTT | CC | GCATGGG | 770 |
| BP MT9 F | AGCCACCTGA | GGTTGGCTCT | GACTGTACCA | CCATCCACTA | TAACACATG | TGTAATAGTT | CC | GCATGGG | 751 |
| BP MT9 R | AGCCACCTGA | GGTTGGCTCT | GACTGTACCA | CCATCCACTA | TAACACATG | TGTAATAGTT | CC | GCATGGG | 770 |
| BP MT10 F | AGCCACCTGA | GGTTGGCTCT | GACTGTACCA | CCATCCACTA | TAACACATG | TGTAATAGTT | CC | GCATGGG | 751 |
| BP MT10 R | AGCCACCTGA | GGTTGGCTCT | GACTGTACCA | CCATCCACTA | TAACACATG | TGTAATAGTT | CC | GCATGGG | 770 |
| BP MT11 F | AGCCACCTGA | GGTTGGCTCT | GACTGTACCA | CCATCCACTA | TAACACATG | TGTAATAGTT | CC | GCATGGG | 747 |
| BP MT11 R | AGCCACCTGA | GGTTGGCTCT | GACTGTACCA | CCATCCACTA | TAACACATG | TGTAATAGTT | CC | GCATGGG | 770 |
| BP MT12 F | AGCCACCTGA | GGTTGGCTCT | GACTGTACCA | CCATCCACTA | TAACACATG | TGTAATAGTT | CC | GCATGGG | 746 |
| BP MT12 R | AGCCACCTGA | GGTTGGCTCT | GACTGTACCA | CCATCCACTA | TAACACATG | TGTAATAGTT | CC | GCATGGG | 770 |
| | | 760 | | 780 | | 800 | | | |
| SH p53 (NCBI) | GGGCATGAAC | CGCGGCCCTA | TCCTCACCAT | CATCACGCTG | GAGGACCCCA | GTGGGAACCT | GCTGGG | ACGG | 840 |
| DMSO N F | GGGCATGAAC | CGCGGCCCTA | TCCTCACCAT | CATCACGCTG | GAGGACCCCA | GTGGGAACCT | GCTGGG | ACGG | 823 |
| DMSO N R | GGGCATGAAC | CGCGGCCCTA | TCCTCACCAT | CATCACGCTG | GAGGACCCCA | GTGGGAACCT | GCTGGG | ACGG | 840 |
| BP MT9 F | GGGCATGAAC | CGCGGCCCTA | TCCTCACCAT | CATCACGCTG | GAGGACCCCA | GTGGGAACCT | GCTGGG | ACGG | 821 |
| BP MT9 R | GGGCATGAAC | CGCGGCCCTA | TCCTCACCAT | CATCACGCTG | GAGGACCCCA | GTGGGAACCT | GCTGGG | ACGG | 840 |
| BP MT10 F | GGGCATGAAC | CGCGGCCCTA | TCCTCACCAT | CATCACGCTG | GAGGACCCCA | GTGGGAACCT | GCTGGG | ACGG | 821 |
| BP MT10 R | GGGCATGAAC | CGCGGCCCTA | TCCTCACCAT | CATCACGCTG | GAGGACCCCA | GTGGGAACCT | GCTGGG | ACGG | 840 |
| BP MT11 F | GGGCATGAAC | CGCGGCCCTA | TCCTCACCAT | CATCACGCTG | GAGGACCCCA | GTGGGAACCT | GCTGGG | ACGG | 817 |
| BP MT11 R | GGGCATGAAC | CGCGGCCCTA | TCCTCACCAT | CATCACGCTG | GAGGACCCCA | GTGGGAACCT | GCTGGG | ACGG | 840 |
| BP MT12 F | GGGCATGAAC | CGCGGCCCTA | TCCTCACCAT | CATCACGCTG | GAGGACCCCA | GTGGGAACCT | GCTGGG | ACGG | 816 |
| BP MT12 R | GGGCATGAAC | CGCGGCCCTA | TCCTCACCAT | CATCACGCTG | GAGGACCCCA | GTGGGAACCT | GCTGGG | ACGG | 840 |
| | | 820 | | 840 | | 860 | | 880 | |
| SH p53 (NCBI) | AACAGCTTTG | AGGTTTCGTAT | TTGTGCCTGC | CCTGGGAGAG | ACCGTCGTAC | AGAGGAAAAA | AATTTCCAAA | 910 | |
| DMSO N F | AACAGCTTTG | AGGTTTCGTAT | TTGTGCCTGC | CCTGGGAGAG | ACCGTCGTAC | AGAGGAAAAA | AATTTCCAAA | 893 | |
| DMSO N R | AACAGCTTTG | AGGTTTCGTAT | TTGTGCCTGC | CCTGGGAGAG | ACCGTCGTAC | AGAGGAAAAA | AATTTCCAAA | 910 | |
| BP MT9 F | AACAGCTTTG | AGGTTTCGTAT | TTGTGCCTGC | CCTGGGAGAG | ACCGTCGTAC | AGAGGAAAAA | AATTTCCAAA | 891 | |
| BP MT9 R | AACAGCTTTG | AGGTTTCGTAT | TTGTGCCTGC | CCTGGGAGAG | ACCGTCGTAC | AGAGGAAAAA | AATTTCCAAA | 910 | |
| BP MT10 F | AACAGCTTTG | AGGTTTCGTAT | TTGTGCCTGC | CCTGGGAGAG | ACCGTCGTAC | AGAGGAAAAA | AATTTCCAAA | 891 | |
| BP MT10 R | AACAGCTTTG | AGGTTTCGTAT | TTGTGCCTGC | CCTGGGAGAG | ACCGTCGTAC | AGAGGAAAAA | AATTTCCAAA | 910 | |
| BP MT11 F | AACAGCTTTG | AGGTTTCGTAT | TTGTGCCTGC | CCTGGGAGAG | ACCGTCGTAC | AGAGGAAAAA | AATTTCCAAA | 887 | |
| BP MT11 R | AACAGCTTTG | AGGTTTCGTAT | TTGTGCCTGC | CCTGGGAGAG | ACCGTCGTAC | AGAGGAAAAA | AATTTCCAAA | 910 | |
| BP MT12 F | AACAGCTTTG | AGGTTTCGTAT | TTGTGCCTGC | CCTGGGAGAG | ACCGTCGTAC | AGAGGAAAAA | AATTTCCAAA | 886 | |
| BP MT12 R | AACAGCTTTG | AGGTTTCGTAT | TTGTGCCTGC | CCTGGGAGAG | ACCGTCGTAC | AGAGGAAAAA | AATTTCCAAA | 910 | |
| | | 900 | | 920 | | 940 | | | |
| SH p53 (NCBI) | AGAAGGGAGA | ACCTTGCCCA | GAACTACCCC | CAAA -GAGTG | CTAAACGAGC | ATTGCTTACC | AACACAAGCT | 979 | |
| DMSO N F | AGAAGGGAGA | ACCTTGCCCA | GAACTACCCC | CAAA -GAGTG | CTAAACGAGC | ATTGCTTACC | AACACAAGCT | 962 | |
| DMSO N R | AGAAGGGAGA | ACCTTGCCCA | GAACTACCCC | CAAA -GAGTG | CTAAACGAGC | ATTGCTTACC | AACACAAGCT | 968 | |
| BP MT9 F | AGAAGGGAGA | ACCTTGCCCA | GAACTACCCC | CAAA -GAGTG | CTAAACGAGC | ATTGCTTACC | AACACAAGCT | 960 | |
| BP MT9 R | AGAAGGGAGA | ACCTTGCCCA | GAACTACCCC | CAAA -GAGTG | CTAAACGAGC | ATTGCTTACC | AACACAAGCT | 964 | |
| BP MT10 F | AGAAGGGAGA | ACCTTGCCCA | GAACTACCCC | CAAA -GAGTG | CTAAACGAGC | ATTGCTTACC | AACACAAGCT | 960 | |
| BP MT10 R | AGAAGGGAGA | ACCTTGCCCA | GAACTACCCC | CAAA -GAGTG | CTAAACGAGC | ATTGCTTACC | AACACAAGCT | 966 | |
| BP MT11 F | AGAAGGGAGA | ACCTTGCCCA | GAACTACCCC | CAAA -GAGTG | CTAAACGAGC | ATTGCTTACC | AACACAAGCT | 956 | |
| BP MT11 R | AGAAGGGAGA | ACCTTGCCCA | GAACTACCCC | CAAA -GAGTG | CTAAACGAGC | ATTGCTTACC | AACACAAGCT | 961 | |
| BP MT12 F | AGAAGGGAGA | ACCTTGCCCA | GAACTACCCC | CAAA -GAGTG | CTAAACGAGC | ATTGCTTACC | AACACAAGCT | 955 | |
| BP MT12 R | AGAAGGGAGA | ACCTTGCCCA | GAACTACCCC | CAAA -GAGTG | CTAAACGAGC | ATTGCTTACC | AACACAAGCT | 966 | |

Figure 27 – Sanger sequencing of *p53* mRNA identified non-synonymous point mutations in 30 % of immortal MT colony-derived SHE cells and a common strain variation in all samples compared to the published NCBI sequence.

Four immortal lines harboured different point mutations which lead to changes in the amino acid sequence of *p53*; these are highlighted in boxes with an asterisk above. A synonymous point mutation was also identified common to all Brunel-derived clones; indicated with two asterisks. A strain variation in *p53* was identified in all samples (GA>AG inversion, no asterisk). Sequences were aligned to the reference sequence available via NCBI (GenBank: U07182.1).

Samples that were found to harbour mutations were re-sequenced at earlier population doubling time points so as to establish if the mutations were a direct result of benzo(a)pyrene exposure. A summary of point mutations identified in colony-derived B(a)P-induced SHE cells is shown in Table 11 and Table 12 and any changes between early and late passage cells noted in Table 13. At early population doubling times, the point mutation located in the DNA binding domain of colony-derived immortal BP MT9 and BP MT10 was identified in both forward and reverse sequencing reactions which points to a direct mutational event. However, at early population doubling time points, 2 overlapping profile peaks were identified in *p53* c482 and c808 bp transcripts respectively for BP MT9 and BP MT10, shown in Figure 28. Conversely, at later passage time points the respective mutations were noted as clear individual peaks. The height of the two peaks for BP MT9 at early passages was not equal, suggesting that there was heterogeneity for *p53* within the cell population which was lost over time. At later time points only the mutated form of *p53* c482 bp was identified in BP MT9 cells suggesting the wild type sequence had been lost. In BP MT10, the height of the Sanger sequencing peaks was equal at early time points, suggesting either an equal number of colony-derived cells containing wild-type and mutated *p53* or that in each cell only one allele encoded wild type *p53*. Given that the number of peaks was reduced from 2 to 1 it is suggestive of the wild-type copy being lost and the mutated allele selected for. Conclusions over any *p53* transcript changes concerning SHE BP MT11 and BP MT12 could not be made as only later population doubling time points for these colony-derived cells were available (Dafou, 2003).

Finally, the base-pair change in *p53* at c195 bp was synonymous but analysis of the sequencing profiles revealed that in some cases it was not present in all transcripts sequenced within a given sample, and overlapping sequencing peaks were present (an example is shown in Figure 29). In the primary SHE 2B used to perform the SHE CTA at Brunel; adenine bases (A) was mostly identified on the sequencing profiles at c195 bp, but a very small peak corresponding to guanine was also present at the same site. Two SHE-MT lines has only a single peak corresponding to adenine at c195 bp, but 3 lines showed two peaks: one for A and one for G nucleotide residues. At the later time points testing only the synonymous 'mutated' corresponding peak was identified (Table 13).

Table 13 – Re-sequencing of *p53* transcripts at earlier time points reveals changes in population.

| Origin | Cell line | Mutation | In Early Passage | In Late Passage | No. peaks |
|-------------|-----------|-----------------------|------------------|-----------------|-----------|
| BioReliance | DMSO N | none | n/a | n/a | n/a |
| Brunel | SHE 2B | 195bp (G>A) | 90 % | n/a | 2 |
| Brunel | BP MT5 | 195bp (G>A) | 50 % | 50 % | 2 |
| Brunel | BP MT6 | 195bp (G>A) | 50 % | 50 % | 2 |
| Brunel | BP MT7 | 195bp (G>A) | 100 % | 100 % | 1 |
| Brunel | BP MT8 | 195bp (G>A) | 50 % | 50 % | 2 |
| Brunel | BP MT9 | 195bp (G>A) | 50 % | 100 % | 2→1 |
| | | 482bp (G>T) | 25 % | 100 % | 2→1 |
| Brunel | BP MT10 | 195bp (G>A) | 100 % | 100 % | 1 |
| | | 808bp (C>T) | 50 % | 100 % | 2→1 |
| Brunel* | BP MT11 | 734bp (G>C) | n/a | 100 % | 1 |
| Brunel* | BP MT12 | 752bp (G>T) | n/a | 100 % | 1 |

In samples found to harbour mutations *p53*, sequences derived from cDNA samples were re-sequenced at earlier passage time points. The sequencing profiles revealed that cultures analysed at earlier time points were heterogeneous for the mutations identified at later time points. This suggests that populations of colony derived SHE cells change over time with cells containing wild type *p53* falling out of the population and there may be selective pressures favouring cells harbouring *p53* mutations. Non-synonymous mutations are in bold typeface. (*) B(a)P-induced SHE clones prepared at Brunel by a previous PhD student (Dafou, 2003) and only late passage cells were available.

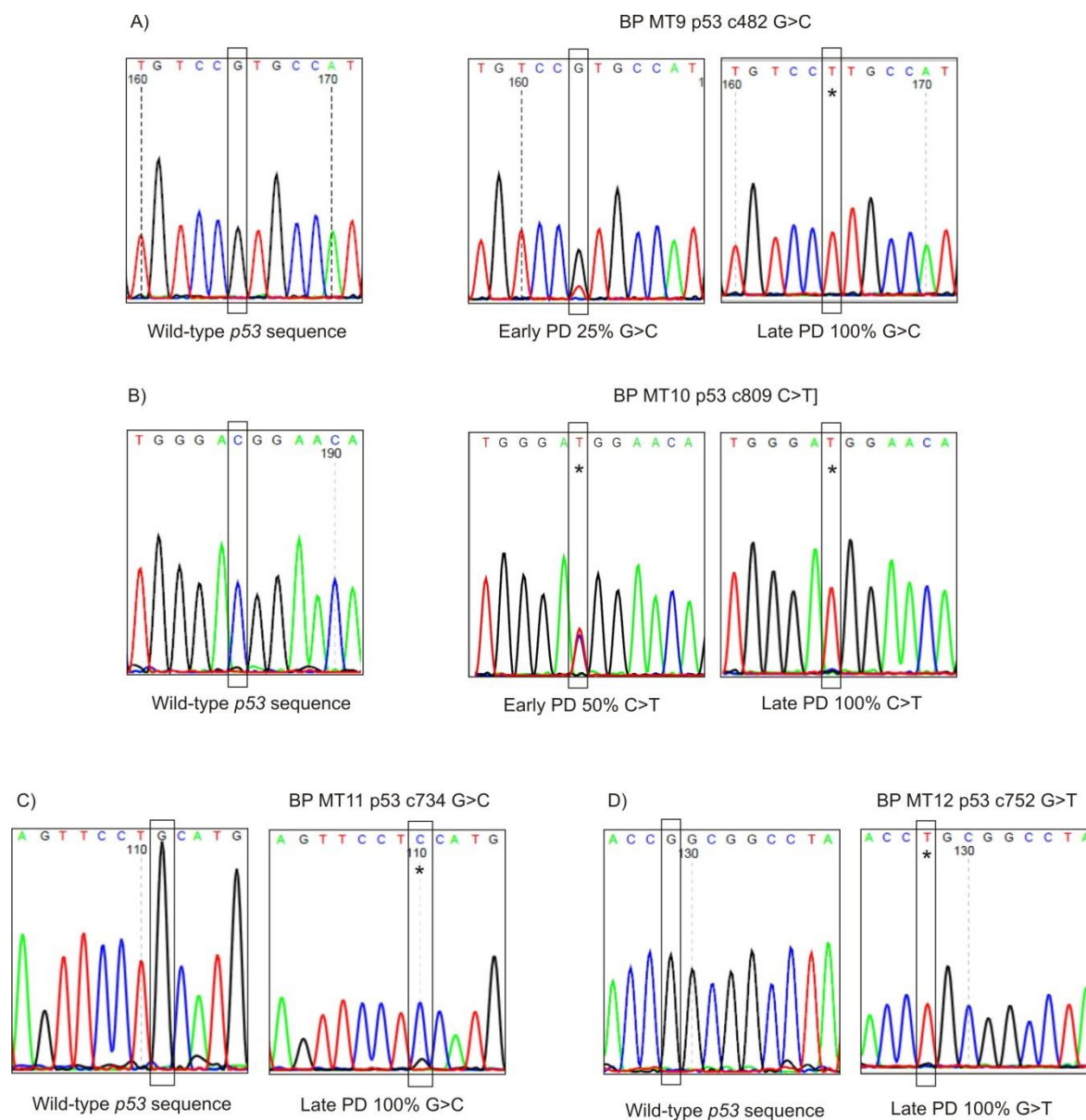


Figure 28 – Sanger sequencing profile sections containing non-synonymous *p53* mutations

In total, four mutations leading to changes in the translated *p53* amino acid sequence were identified. The profile to the left for figures A-D is the corresponding wild type sequence and highlighted peaks are those which were subject to mutation; the star indicates that the nucleotide file generated contained the point mutation. At early population doublings BP MT9 and BP MT10 sequencing profiles revealed superimposed peaks indicating both wild type and mutated versions of *p53* were present in the samples tested. Only forward sequencing reactions are shown; corresponding complementary mutations were identified in the reverse sequencing reactions.

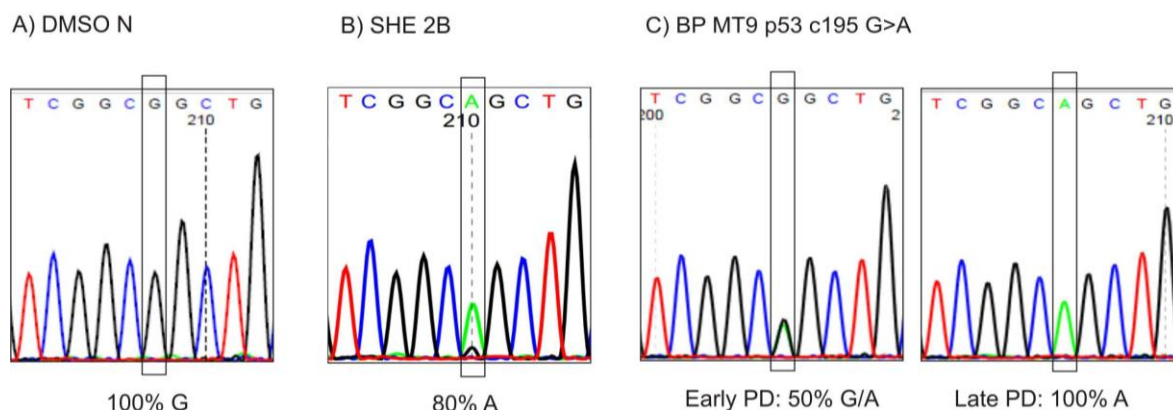


Figure 29 – Synonymous base change *p53* c195 bp is selected for in SHE MT BP9 over time in B(a)P-induced immortalised colony-derived SHE cells

Sequence profiles at coding region 195 bp for *p53* in SHE colony-derived cells (highlighted by a black box). The wild-type codon GCG is identified in BioReliance-derived DMSO and BP-treated clones (A) but GCA was the predominant transcript in the untreated primary SHE line from Brunel SHE 2B (B). G>A at 195 bp was also identified in Brunel-derived B(a)P-treated MT clones. (C) In BP MT9 cells at early population doubling time points, a green peak is just visible behind the black one and at later time points a single green peak (adenine) was shown in late passage BP MT9.

5.3.2 Gene expression analysis of immortal colony derived cells

Cells derived from the SHE cell transformation assay (CTA) were analysed for patterns of gene expression following colony picking and clonal establishment. The gene targets analysed, potentially relevant to senescence-bypass, were from the ARF-p53 and p16-Rb signalling pathways. Amplification values were normalised to housekeeping genes *beta-actin* and *GAPDH* and then compared to proliferating early passage DMSO-treated cells derived from non-transformed colonies scored in the SHE CTA. Expression for each target gene varied across the DMSO-treated non-transformed group, so that alone no single sample was an appropriate control given that expression patterns in colony-derived cells was unknown. The RQ values for the DMSO-group controls (N1-N6) are plotted in Figure 30. *Mdm2* and *p16* (because of one significant outlier) showed the largest variation whereas *ARF* and *p53* expression was most similar. The mean relative value for each target gene was assigned a relative value of 1 and used as the overall calibrator to compare gene expression fold changes.

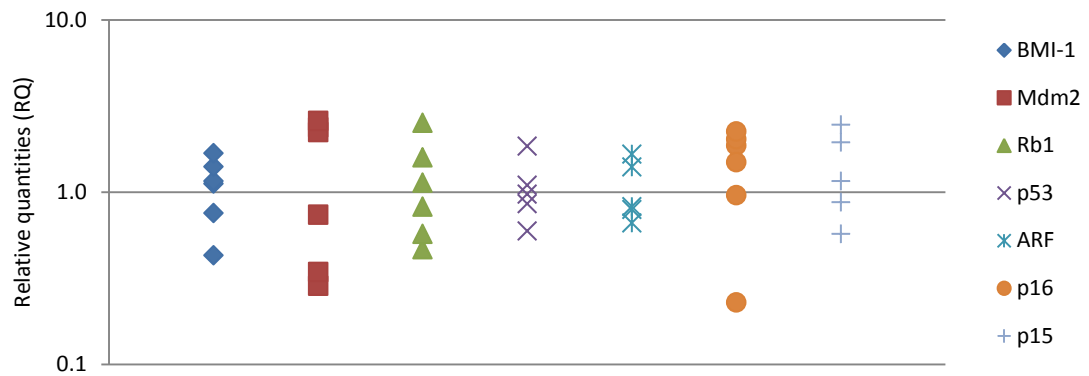


Figure 30 – Gene expression in proliferating DMSO-treated non-transformed SHE colony-derived SHE cells

DMSO-treated non-transformed colony-derived cells were used as the control group (N1-N6). These were proliferating and early passage (P2-P3) clones. The mean expression of N1-N6 for each gene target was assigned a relative value (RQ) of 1 and used to calculate the RQ values of other samples. Values were normalised to the reference genes *GAPDH* and *beta-actin*.

Gene expression was analysed over successive passages of colony-derived SHE cells during their lifespans. In colonies obtained from BioReliance, the initial thawed vial was assigned passage P+1 whereas for colonies picked in-house at Brunel passage 5 (P5) represents the time point at which colony-derived cells were first transferred to a 100 mm² dish. A summary of all the data is presented as a 'heat-map' in Figure 31 and will be referred to during this section along with additional plotted graphs. Cell lines BP MT11 and BP MT12 were previously established (Dafou, 2003) and thus RNA from early passages could not be sourced, hence the single row of expression data (Figure 31). SHE clones BP MT9 and BP MT10 were generated towards the end of the project and their gene expression analysis was not undertaken.

SHE untreated primary cells were over 100-fold downregulated for *p16* and *ARF* expression and over 50-fold downregulated for *p15* when compared to the DMSO control group mean. Elevated levels of *BMI-1* were noted in these cells and *Mdm2* transcription was downregulated in comparison with the DMSO control group. This was in contrast to DMSO-treated non-transformed colony-derived senescing cells which showed a 6-8 fold overexpression in *p16* along with a 3-4-fold increase in *ARF* and *p15* (Figure 31).

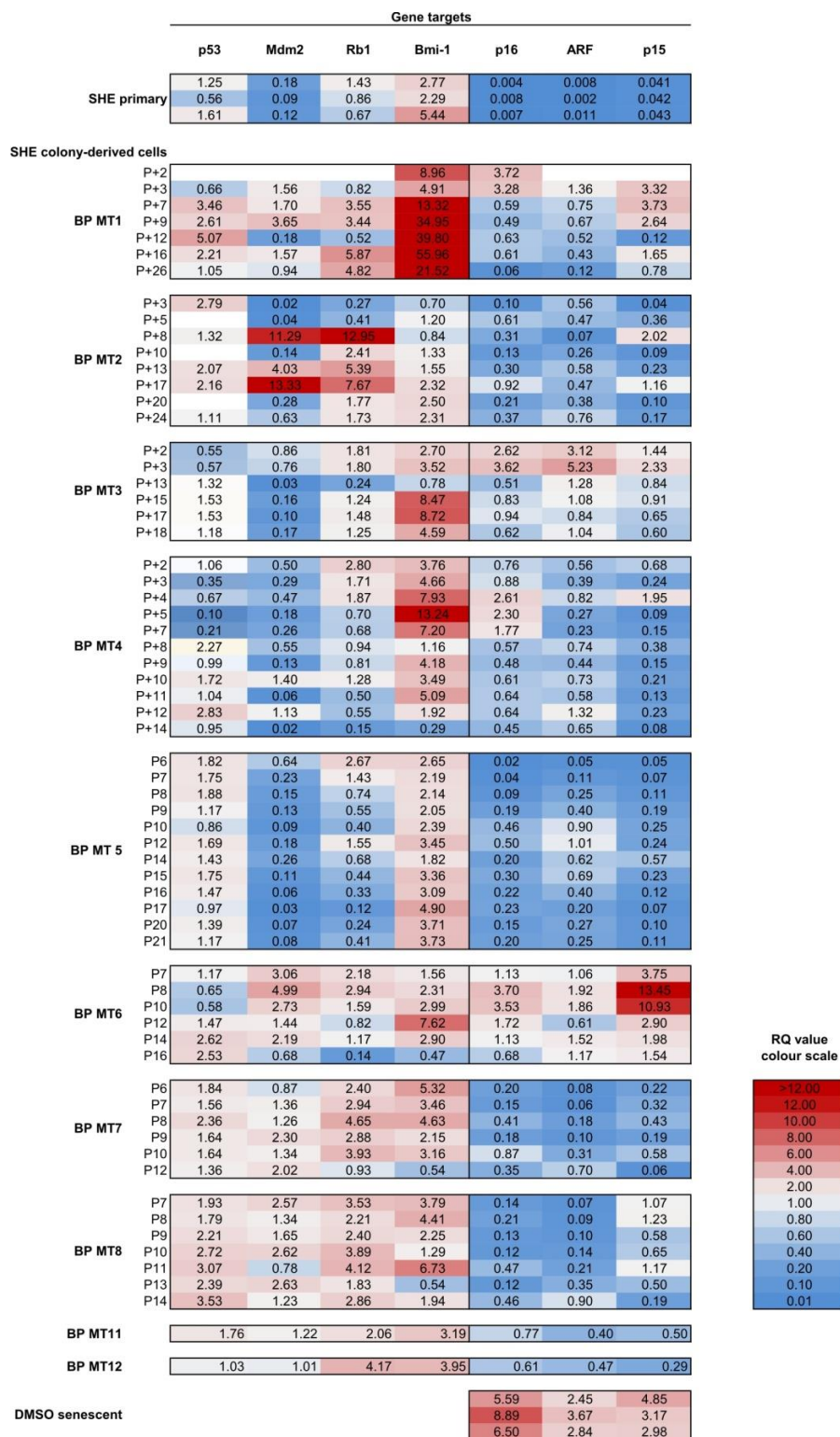


Figure 31 - Heat map of gene expression patterns in all B(a)P-treated MT immortalised SHE cells

Summary of gene expression in all B(a)P-induced colony-derived SHE MT cells tested at successive passages during their lifespan. *p53*, *Mdm2*, *Rb1*, *BMI-1*, *p16*, *ARF* and *p15* were assayed for and normalised to the reference genes *GAPDH* and *beta-actin*. Overexpressing genes are in red and downregulated ones are in blue. Early time points for BP MT11 and BP MT12 were unavailable as these colony were isolated previously (Dafou, 2003) and BP MT10 and BP MT9 were not analysed.

p16 gene expression is attenuated in at least 30 % of benzo(a)pyrene-induced immortal MT colony-derived SHE cells

Gene expression analysis of colony-derived cells from the SHE-MT CTA revealed that *p16* was generally reduced when compared with average RQ values from the control group of proliferating DMSO-treated non-transformed colony-derived cells. In four immortalised B(a)P-induced SHE cell lines *p16* expression levels were downregulated 5 to 10-fold when assayed at early passage time points (RQ values between 0.2 and 0.1 respectively) and *p16* transcripts levels remained below 50 % compared to the average DMSO-treated controls following multiple subcultures (Figure 31). An example of *p16* transcripts with RQ values for BP MT2 and BP MT8 are plotted in Figure 32A. Results indicated that, at later passages, *p16* was not overexpressed, as was the case in normal finite lifespan SHE cells; the latter showed a 6-8 fold increase but continued to transcribe *p16* at a baseline level (ie. at least 10-fold higher than primary SHE cells - see RQ values in Figure 32C). No cell crisis was observed in BP MT2, BP MT5, BP MT7 or BP MT8 which proliferated exponentially. RNA extracts at early PD were not available for BP MT11 and BP MT12 as the MT colonies had been isolated earlier by a previous PhD student (Dafou, 2003). Relative quantities of *p16* expression were also below the DMSO-treated controls average in both immortal cell lines. Their gene expression profiles at earlier time points following colony picking were not determined.

Secondary events following MT lead to the down regulation of p16 and p15

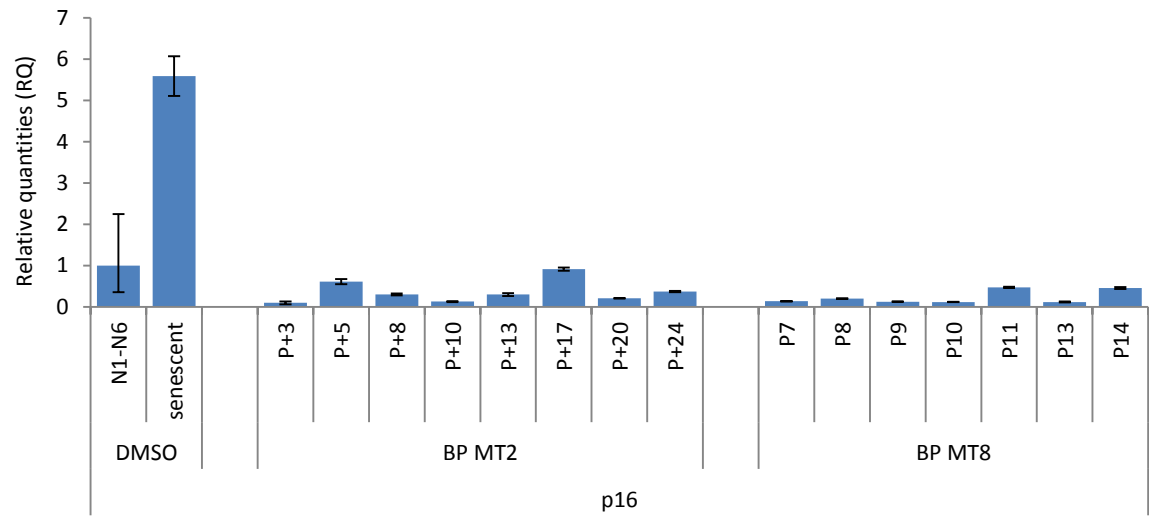
In 50 % (4 out of 8) of B(a)P-treated MT colony-derived cells analysed over successive passages, it was found that *p16* transcript levels at early population doublings were temporarily elevated by 2-5 fold compared with the control group of proliferating DMSO-treated non-transformed colony-derived cells. This was accompanied by a change in observed cellular characteristics towards an increasing senescent-like phenotype and reduced levels of cell growth. After a period of cell-crisis which lasted up to a month, proliferation rates increased and coincided with an abrupt reduction in the relative quantities of *p16* mRNA detected by qPCR. Such low *p16* levels were stably retained in subsequent population doublings to levels below the average DMSO-treated non-transformed control RQ value as shown in Figure 32B. The sudden drop in expression was not limited to *p16*; in BP MT1, BP MT4 and most strikingly BP MT6 (see Figure 32B) the

downregulation of *p16* was accompanied by a reduction of *p15*. In BP MT3 the expression of *ARF* and *p15* were simultaneously affected. The data is indicative of secondary events taking place following morphological transformation permitting evasion of senescence barriers.

Similar patterns of gene expression at the CDKN2A/B locus

The *CDKN2A/B* locus encodes three tumour suppressor genes under the control of independent promoters. Gene expression analysis indicated that the observed patterns of *p16* expression were generally recapitulated with *ARF* and *p15* following increasing population doublings. This was especially evident in BP MT5, as shown in Figure 32C. At the earliest point of RNA extraction following colony picking and expansion (passage 6; around 18 population doublings) all three genes were significantly downregulated compared to DMSO controls to levels almost comparable to those observed in primary SHE cells. All three *CDKN2A/B* locus transcripts then steadily increased by 10-fold until passage 10; *p16* and *p15* were still downregulated compared with the DMSO control average, but were within the lowest expression range of the DMSO panel, whereas *ARF* reached an RQ value of 1 between passages 10 and 12 (no change compared with the controls). Thereafter, *p16* gene expression decreased slightly and reached a plateau, as did that of *ARF* and *p15*. At the latest time point recorded (P 21) average RQ values were ≤ 0.2 for all three genes. The Spearman rank correlation coefficient (R_s) was close to 1 between expression of *ARF* to *p16* and to *p15* (R_s 0.80, $p < 0.005$ and R_s 0.92 $p < 0.001$ respectively) and R_s 0.65 $p < 0.025$ between *p16* and *p15*, indicating a positive correlation. Common trends of *CDKN2A/B* expression were also observed in other BP MT clones but were mostly confirmed between *p16* and *p15* as shown in Figure 32B.

A) *p16* expression is maintained at levels permissive for proliferation in B(a)P-induced SHE immortalised cells



B) Secondary events following morphological transformation (MT) leading to senescence bypass

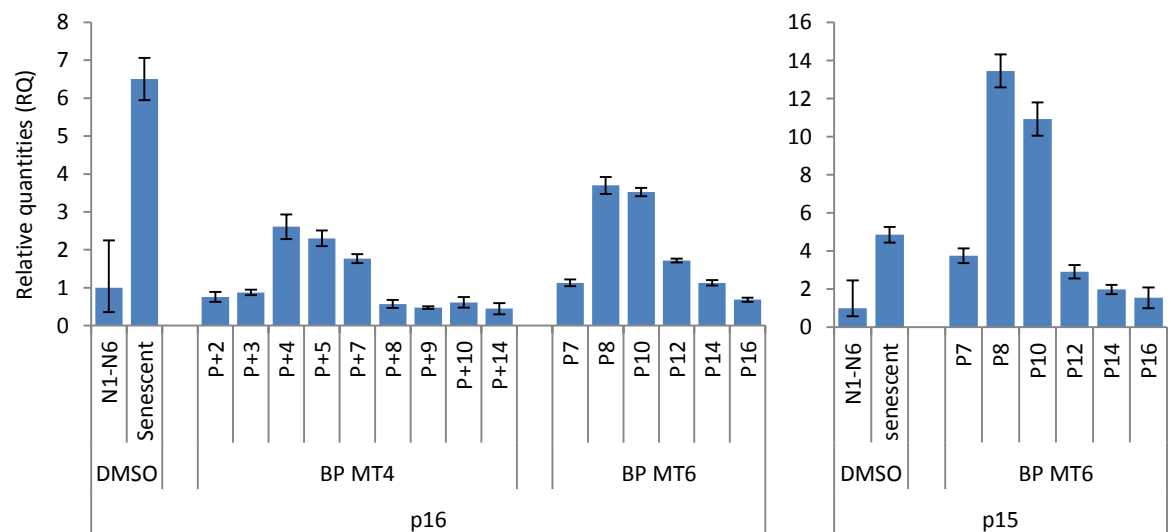
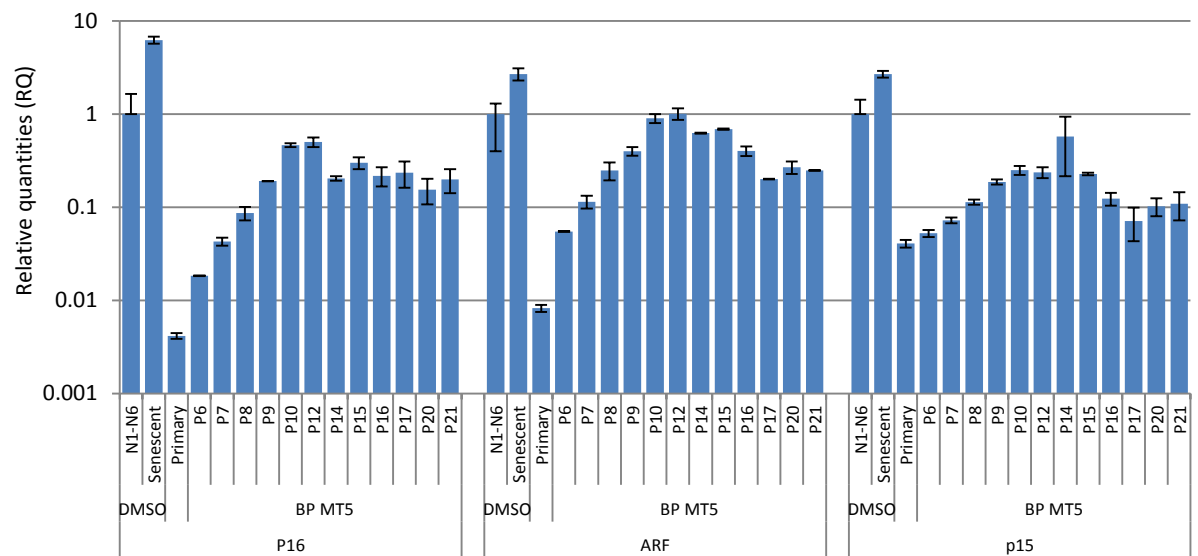


Figure 32 – mRNA transcripts in SHE colony-colony derived cells (cont. on next page)

(A) mRNA expression of *p16* in colony-derived SHE cell clones BP MT2 and BP MT8. (B) mRNA expression of *p16* and *p15* in colony-derived SHE BP MT4 and BP MT6.

C) Similar patterns of gene expression of *p16*, *ARF* and *p15* located at the *CDKN2A/B* locus in B(a)P-induced immortal colony-derived SHE cells



D) *BMI-1* overexpression in B(a)P-induced immortal SHE colony-derived cells

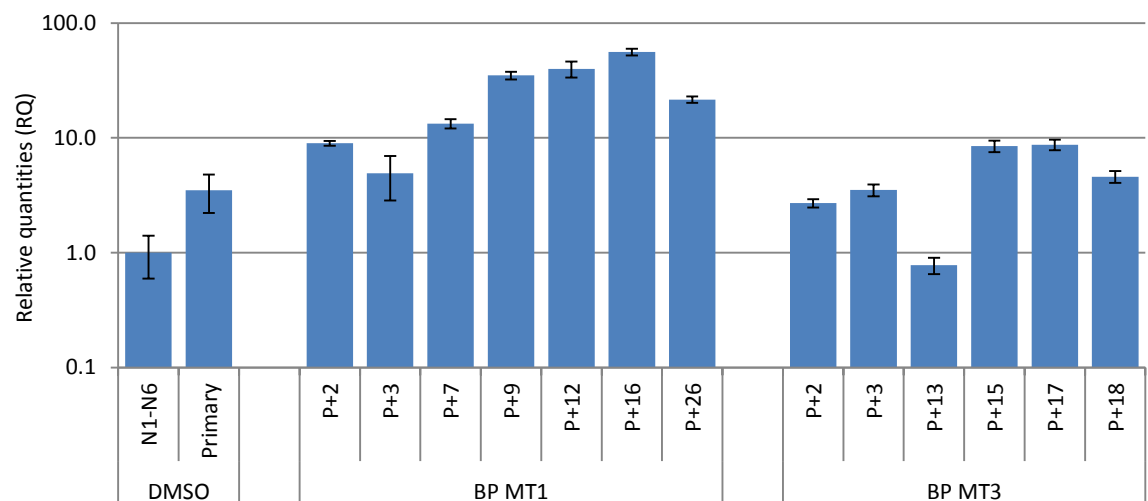


Figure 32 - mRNA transcripts in SHE colony-colony derived cells (cont.)

(C) mRNA expression of genes *p16*, *p15* and *ARF* (located in close proximity to each other in the *CDKN2A/B* locus on chr9p21.3 in humans) in colony-derived SHE clone BP MT5. (D) mRNA expression of *BMI-1* in colony-derived SHE BP MT1 and BP MT3. DMSO N are the control group (N1-N6) of proliferating, early passage (P+2-P+3) DMSO treated non-transformed colonies. The mean of N1-N6 was assigned a value of 1 and used to calculate the RQ values of other samples. Relative quantities of amplified product were normalised to the reference genes *GAPDH* and *beta-actin*. Error bars represent the standard deviation of $2^{-\Delta\Delta Ct}$.

BMI-1 expression is upregulated in B(a)P-induced immortal MT colony-derived SHE cells

BMI-1 is a member of the Polycomb group proteins (PcG) which act to repress the expression of other genes by epigenetic mechanisms. BMI-1 expression was found to be increased by 2 to 5-fold in primary SHE cells compared with proliferating non-transformed DMSO-treated colony-derived cells (shown in Figure 32D). An abundance of *BMI-1* transcripts was identified in 90 % of the B(a)P-induced immortal MT colonies assayed and in 3 instances the increase was above 8-fold that in non-transformed control SHE cells (see Figure 31). In all immortalised MT colonies assayed for *BMI-1* gene expression, transcription was generally above the DMSO-controls mean relative values. These ranged from a modest increase (2.5-fold in BP MT2) to much larger increases in other MT clones. For example, in BP MT1 an initial 8-fold increase continued to rise reaching up to 50-fold; in BP MT3 BMI-1 was overexpressed 8-fold in time points measured after P+15 (Figure 32D) and in BP MT4 *BMI-1* rose to 13 fold and at later time points decreased (Figure 31).

p53 expression is subtly altered in B(a)P-induced SHE MT cells and its upstream regulators Mdm2 and ARF are downregulated

As shown in Figure 31, gene expression levels of the tumour suppressor gene *p53* did not greatly vary when compared to the DMSO-control group. However, differences in expression within each cell type did change over time points analysed. For example, BP MT1 displayed a 3-5-fold increase in its expression at early time points but this was reduced to control levels in the later time points assayed. Conversely, BP MT3 and BP MT4 displayed reduced *p53* expression at early time points which then increased to values similar to the DMSO non-transformed control group from passages 13 and 8 respectively.

Upstream regulators of *p53*, *ARF* and *Mdm2* were generally found to be downregulated at the transcriptional level (Figure 31). In the case of *Mdm2* (which marks *p53* for ubiquitination and degradation) its transcripts were reduced to levels similar to untreated primary SHE cells in 40 % of B(a)P-induced colony-derived cells (4 out of 10) and the remaining immortalised cell lines were positive for *Mdm2* but generally below 2.5 fold above the DMSO control group mean. Reduced expression of *Mdm2*'s upstream binding partner *ARF* was observed in 80 % of B(a)P-induced clones (normal expression levels in BP MT3 and BP MT6) as discussed earlier in this section. There was no common

correlation (Spearman rank coefficient, R_s) between *Mdm2*, *ARF* or *p53* gene expression across colony-derived clones assayed at successive time points. However, *ARF* and *p53* did have a positive correlation of expression in BP MT4 and BP MT8 (R_s 0.74, p value <0.01 and R_s 0.86, p value <0.025 respectively) whereas in BP MT3 an inverse correlation between *ARF* and *p53* (R_s -0.77, p value <0.1) and *Mdm2* and *p53* expression (R_s -0.83, p value <0.05) was noted.

Rb1 follows similar expression patterns to Mdm2, and its downregulation is cell line specific

Rb1 gene expression varied across immortalised B(a)P-induced colony-derived SHE cells (shown in Figure 33 and Figure 31). There were 3 to 6-fold *Rb1* transcript increases in 50 % of the cell lines and SHE clone BP MT2 overexpressed up to 12-fold compared with the DMSO non-transformed group. In the case of BP MT5 *Rb1*, gene expression became progressively downregulated, with only 10 % expression compared to the DMSO control average at passage 17 (Figure 33). This is in contrast to BP MT7 and BP MT8 which overall retained a marginal overexpression of *Rb1* at the consecutive time points measured.

It was observed that *Rb1* and *Mdm2* gene expression followed the same trends in four SHE B(a)P-induced cell lines during the course of the time points measured (BP MT2, BP MT3, BP MT5 and BP MT6). For example, the fluctuations in *Rb1* gene expression evident in BP MT5 (shown in Figure 33) were mirrored in the cell line's *Mdm2* expression (not shown, but see Figure 31). The genes shared a positive correlation (p value <0.01) which is shown in Figure 34.

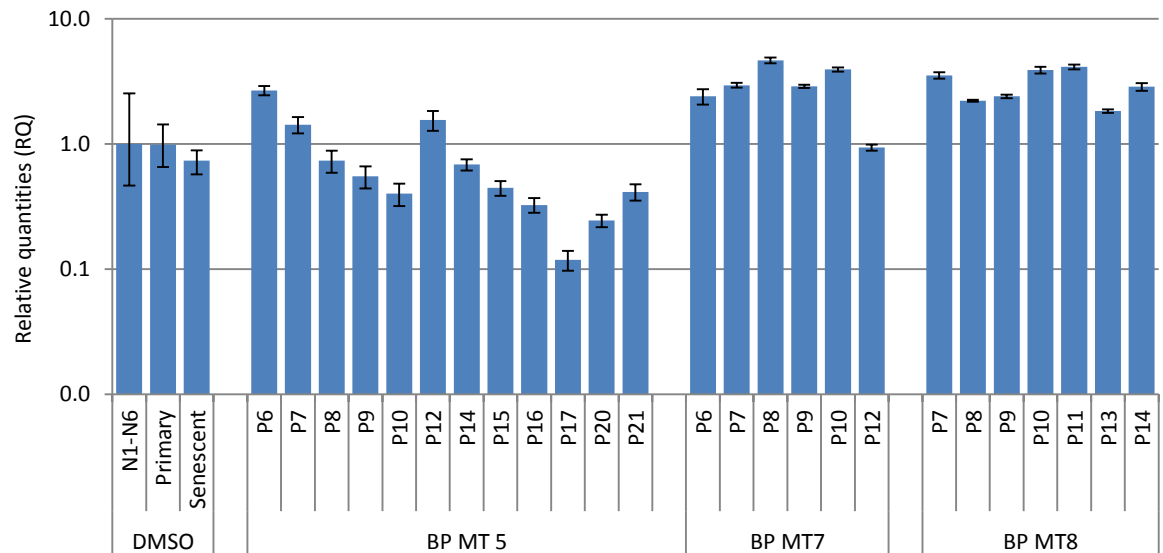


Figure 33 – Rb1 gene expression in B(a)P-induced immortal SHE colony-derived cells

mRNA expression of *Rb1* in colony-derived SHE BP MT5 BP MT7 and BP M8. DMSO N is the control group (N1-N6) of proliferating, early passage (P+2-P+3) DMSO treated non-transformed colonies. The mean of these was assigned a value of 1 and used to calculate the RQ values of other samples. Relative quantities of amplified product were normalised to the reference genes *GAPDH* and *beta-actin*. Error bars represent the standard deviation of $2^{-\Delta\Delta C_t}$. Note that the y-axis scale is log10.

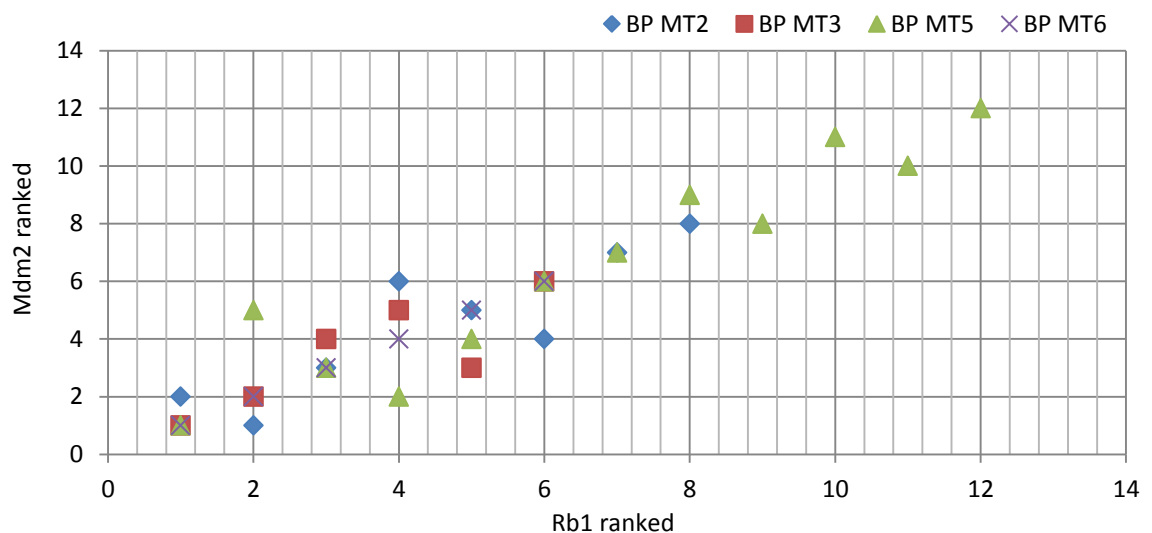


Figure 34 – Mdm2 and Rb1 gene expression is positively correlated

Gene expression of Mdm2 and Rb1 at successive time points followed the same trends in SHE clones BP MT2, BP MT3, BP MT5 and BP MT6. RQ values were ranked per gene and cell type, the Spearman rank correlation coefficient (R_s) was calculated for the ranked expression between *Mdm2* and *Rb1*; R_s was above 0.83 in all four cases and p values were <0.01 .

5.3.3 Copy number variation (CNV) in immortal colony-derived SHE cells

Numerical gene changes (gains or losses) in immortalised colony-derived SHE cells were studied using copy number variation (CNV) analysis with TaqMan-style probes. The stability of the reference gene succinate dehydrogenase subunit A (*SDHA*) was verified using SHE treated and untreated genomic DNA (gDNA) samples (see section 5.2.3). Amplification values for the reference gene *SDHA* were duplexed alongside the target genes which were those encoded by the *CDKN2A/B* locus (*p16* exon 1 α , *p16/ARF* exon 2, *ARF* exon 1 β and *p15*) and *p53*. Positive calibrator samples were presumed to contain 2 allelic copies of each target gene and included wild-type primary SHE cells and a panel of finite lifespan non-transformed SHE colony-derived cells, initially treated with DMSO in the SHE-MT assay. Additionally, gDNA samples from carcinogen-induced Syrian hamster dermal (SHD) cells known to have allelic copy loss were included. The entire *CDKN2A/B* locus is deleted in the X-ray-immortalised SHD line 4XH11 but this line still retains both gene copies of *p53*, whereas line SHD 5BP2 carries a single allelic loss of *p53* and also single copy loss across the *CDKN2A/B* locus (Yasaei et al., 2013).

Figure 35 shows the gene copy numbers (CN) for the panel of controls used in the CNV analysis. An overall CNV value of 2 was assigned to the average value from the SHE primary sample and used as the calibrator for unknown samples. No fluorescence amplification was observed in *p16*, *p15* or *ARF* for the X-ray-treated sample SHD 4XL1 but two copies of *p53* were identified (Yasaei et al., 2013). SHD 5BP2 had a single copy of *p53*, *p16/ARF* exon 2 and *ARF* exon 1 β but was found to have retained both copies of *p16* exon 1 α and *p15*. As shown in Figure 35, sample variation was evident amongst the calibrator SHE DMSO samples when compared to the SHE primary calibrator. The average predicted CN across all gene targets was 2.01 and the CNV range across all targets measured was between 1.12 and 3.21 copies. Given this large range, stringent criteria were used to call gene amplifications or deletions in unknown samples. For MT colony-derived immortalised SHE cells, single allelic loss was called when copy number values were observed to be lower than 1.0 predicted copies and gene amplification called when greater than 3.5 copies. The CNV range for each unknown sample was taken into consideration to make each copy number call.

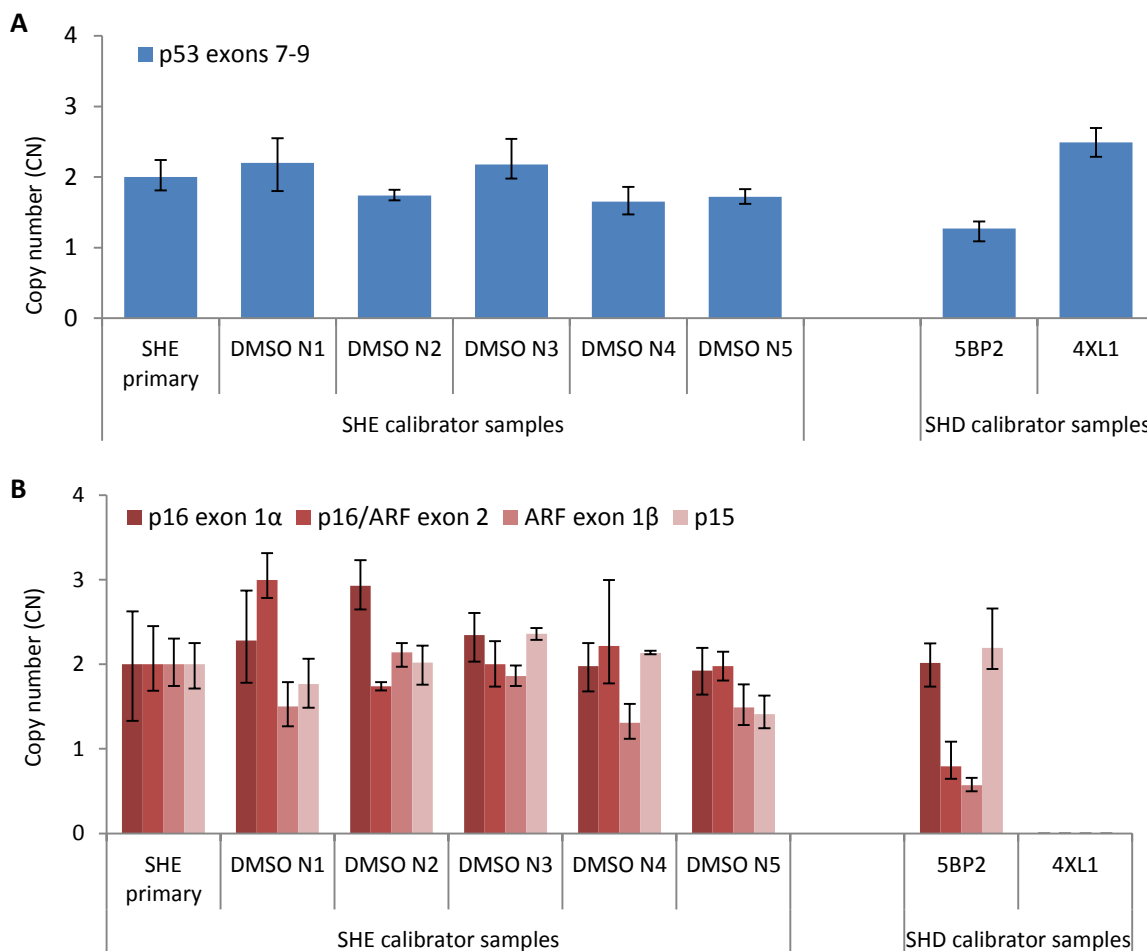


Figure 35 - Copy numbers for SHE and SHD calibrator samples used for CNV analysis

Genomic DNA from wild type SHE cells and SHE cells derived from non-transformed DMSO treated colonies were used as calibrator samples for copy number variation (CNV) analysis. SHD with known CNV were also analysed. SDHA was identified as the most stable reference gene (GeNorm) and was assayed in parallel to the target assay. Primers were designed and validated by PrimerDesign. CNVs were analysed for *p53* exons 7-9 (A) and (B) *p16* exon1 α , *p16/ARF* exon 2, *ARF* exon 1 β and *p15* using CopyCaller software v 2.0. Error bars represent the copy number variation range between sample replicates.

Copy number variation analysis was carried out on MT colony-derived SHE cells. In cell lines that immortalised, DNA samples were analysed at 'early' and 'late' passages to account for any allelic gains or losses during the cell population's lifespan. Early passages include cells below ~35 population doublings and late include cells above ~50 population doublings. The *p53* CNV data shown in Figure 36 was calibrated against non-transformed SHE samples with both normal copies of *p53* (Figure 35A) and suggests that nearly all MT colony-derived SHE cells carry 2 *p53* alleles at early and late time points. Gene

amplification was observed in only one SHE sample, namely B(a)P treated MT SHE 24, which did not immortalise; its predicted *p53* CNV was 4 copies. BP MT7 at the early time point had an estimated *p53* copy number of 0.6 but the allelic loss was not identified at the later time point in the same cell type (CNV of 2.15 copies). As mentioned earlier a cut off of 1.0 copy was used to determine allelic loss so, although BP MT11 and BP MT12 were calculated to have 1.20 and 1.29 copies of *p53* respectively, they are predicted to have 2 gene copies when taking into account the CNV range.

Separate copy number variation assays were carried out for *p16* exon1 α , *p16/ARF* exon 2, *ARF* exon 1 β and *p15*; all encoded by the *CDKN2A/B* locus. Amplification data was calibrated against primary SHE gDNA and non-transformed colony-derived SHE samples which were assumed to have both normal allelic copies of the locus (Figure 35B). BP MT3 (Figure 37) displayed single allelic loss of *ARF* exon 1 β and exon 2 (common to *p16*) (CNV values were between 0.5 and 0.7 copies) and 2 copies of *p16* exon1 α and *p15*; although *p15* values were borderline, possibly indicating one copy. BP MT6 retained a single copy of the entire *CDKN2A/B* locus but only at the later time point suggesting that one allele was deleted in these cell lines during the process of immortalisation; the result was similar for BP MT1, although *p16/ARF* exon 2 was borderline as its maximum CNV was predicted as 1.23 at the later time point. BP MT11 and BP MT12 also had a single copy of the whole locus encompassing *p16*, *ARF* and *p15* (CNV values all below 0.8). No genomic alterations at the selected loci were observed in the spontaneously immortal DMSO MT1 at either time points.

Two of the four morphologically transformed B(a)P-treated SHE cells that entered senescence and did not immortalise were predicted to have two copies of the genes located at the *CDKN2A/B* locus. Interestingly, *p15* was amplified in SHE 24 and BP T15 (see Figure 37) with CNV ranges above the 3.5 copy threshold. The CNV analysis predicted 5-6 copies at early time points of *ARF* exon 1 β and *p16/ARF* exon 2 in BP MT2 and BP MT5 whereas BP MT7 was predicted to carry more than 8 copies of exon 2 at the early time point analysed. Curiously, the amplifications were generally not observed in gDNA samples tested from the same cell lines at later time points, with all genomic regions in BP MT2, BP MT5 and BP MT7 showing a predicted 2 gene copies except for 3.82 copies of *p16/ARF* exon 2 in BP MT5.

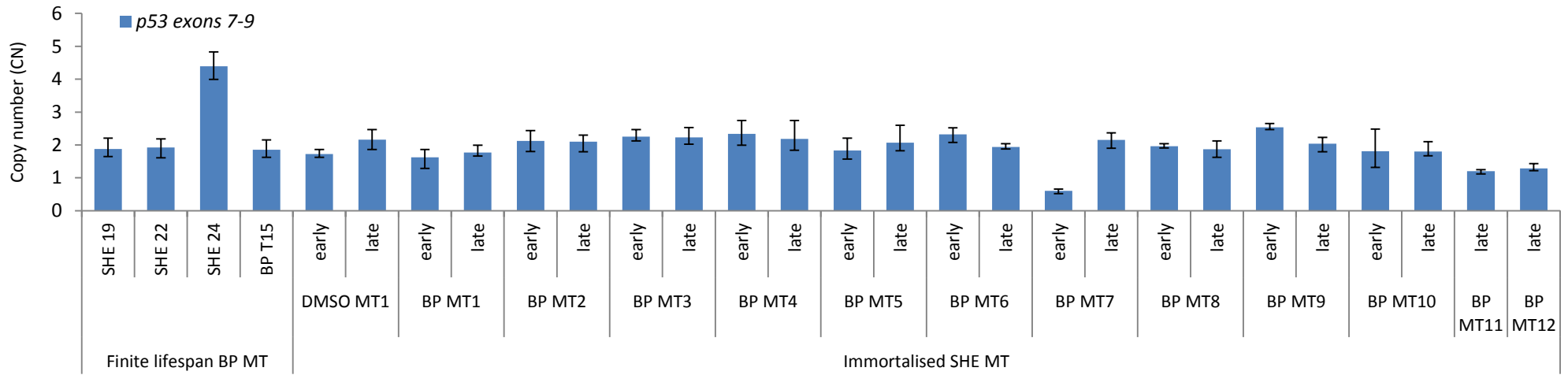


Figure 36 - Copy number variation of *p53* in immortalised colony-derived SHE-MT cells

The allelic status of *p53* was measured using qPCR and Taqman style probes in morphologically transformed (MT) colony-derived SHE cells. DNA from finite lifespan and immortalised MT SHE cells was analysed. Calibrator SHE samples shown in Figure 35 were used as controls with an average copy number of 2 copies. Values above 3.5 copies were considered gene amplification and below 1.0 copies single allele loss. Amplification data was analysed using CopyCaller software v 2.0. The error bars represent the maximum and minimum CNV range.

| | | p16 exon 1 α | | | p16/ARF exon 2 | | | ARF exon 1 β | | | p15 | | |
|-----------------------|--------|---------------------|------|------|----------------|------|------|--------------------|------|-------|------|------|------|
| | | CNV | Min | Max | CNV | Min | Max | CNV | Min | Max | CNV | Min | Max |
| BP MT1 | early | 3.14 | 2.55 | 3.82 | 1.25 | 0.89 | 1.90 | 4.03 | 3.21 | 4.71 | 4.18 | 3.69 | 4.79 |
| | late | 0.78 | 0.68 | 0.89 | 0.88 | 0.70 | 1.23 | 0.69 | 0.61 | 0.78 | 0.86 | 0.76 | 0.99 |
| BP MT3 | late | 1.33 | 1.25 | 1.44 | 0.54 | 0.44 | 0.65 | 0.59 | 0.53 | 0.67 | 1.04 | 0.90 | 1.25 |
| BP MT6 | early | 2.77 | 2.61 | 2.98 | 2.45 | 2.31 | 2.65 | 2.54 | 2.12 | 2.78 | 2.75 | 2.52 | 3.01 |
| | late | 0.49 | 0.42 | 0.66 | 0.97 | 0.90 | 1.05 | 0.85 | 0.72 | 1.00 | 0.41 | 0.40 | 0.42 |
| BP MT10 | early | 1.03 | 0.94 | 1.16 | 0.82 | 0.70 | 1.02 | 1.07 | 0.86 | 1.38 | 0.59 | 0.48 | 0.72 |
| | late | 2.47 | 2.29 | 2.65 | 1.66 | 1.50 | 1.91 | 1.71 | 1.55 | 1.87 | 2.08 | 1.79 | 2.42 |
| BP MT11 | late | 0.67 | 0.51 | 0.80 | 0.51 | 0.42 | 0.57 | 0.81 | 0.68 | 0.97 | 0.51 | 0.41 | 0.61 |
| BP MT12 | late | 0.45 | 0.40 | 0.57 | 0.30 | 0.26 | 0.37 | 0.38 | 0.35 | 0.42 | 0.44 | 0.22 | 0.52 |
| DMSO MT1 | early | 2.41 | 2.20 | 2.76 | 2.68 | 2.26 | 3.24 | 3.56 | 3.18 | 4.07 | 2.11 | 1.44 | 2.91 |
| | late | 1.87 | 1.79 | 1.93 | 1.59 | 1.37 | 1.80 | 1.33 | 1.25 | 1.48 | 1.73 | 1.28 | 2.25 |
| BP MT4 | early | 2.41 | 2.07 | 2.8 | 3.22 | 2.85 | 3.65 | 3.35 | 2.74 | 3.94 | 3.00 | 2.78 | 3.24 |
| | late | 1.81 | 1.67 | 1.93 | 1.66 | 1.56 | 1.76 | 1.66 | 1.48 | 1.99 | 1.81 | 1.59 | 1.96 |
| BP MT8 | early | 1.53 | 1.36 | 1.82 | 1.64 | 1.41 | 2.00 | 1.22 | 1.12 | 1.35 | 1.40 | 1.28 | 1.56 |
| | late | 3.02 | 2.79 | 3.39 | 3.04 | 2.86 | 3.29 | 2.13 | 1.93 | 2.36 | 3.13 | 3.05 | 3.26 |
| BP MT9 | early | 2.41 | 2.32 | 2.48 | 1.47 | 1.34 | 1.76 | 1.52 | 1.41 | 1.65 | 2.33 | 2.17 | 2.56 |
| | late | 2.43 | 1.94 | 2.88 | 1.84 | 1.54 | 2.12 | 1.72 | 1.39 | 2.15 | 2.63 | 2.27 | 2.97 |
| Finite lifespan BP MT | SHE 19 | 1.80 | 1.61 | 2.12 | 2.26 | 1.87 | 2.70 | 2.23 | 1.91 | 2.55 | 1.77 | 1.45 | 2.23 |
| | SHE 22 | 2.28 | 1.77 | 2.91 | 3.42 | 3.30 | 3.61 | 1.89 | 1.63 | 2.27 | 2.34 | 1.79 | 4.09 |
| | SHE 24 | 3.08 | 2.82 | 3.24 | 2.23 | 1.86 | 2.85 | no data | | | 4.35 | 4.06 | 4.63 |
| | BP T15 | 3.88 | 3.74 | 4.01 | 1.55 | 1.09 | 2.20 | 3.07 | 2.73 | 3.46 | 5.67 | 4.66 | 7.28 |
| BP MT2 | early | 3.2 | 3.08 | 3.42 | 6.2 | 5.88 | 6.41 | 6.16 | 5.59 | 6.7 | 3.44 | 3.37 | 3.48 |
| | late | 1.97 | 1.76 | 2.24 | 1.85 | 1.65 | 2.14 | 1.23 | 1.04 | 1.45 | 1.81 | 1.48 | 2.11 |
| BP MT5 | early | 3.07 | 2.69 | 3.44 | 6.34 | 5.93 | 6.7 | 7.21 | 6.39 | 7.94 | 3.47 | 3.35 | 3.54 |
| | late | 2.68 | 2.57 | 2.83 | 3.82 | 3.62 | 4.05 | 2.58 | 2.29 | 2.88 | 3.78 | 3.31 | 4.21 |
| BP MT7 | early | 2.31 | 2.04 | 2.49 | 4.93 | 2.99 | 6.51 | 9.33 | 8.25 | 10.49 | 2.47 | 2.24 | 2.65 |
| | late | 2.46 | 2.41 | 2.51 | 2.62 | 2.37 | 2.95 | 1.64 | 1.43 | 1.90 | 2.75 | 2.64 | 2.90 |

| | |
|------|------------------|
| ++++ | >4.5 |
| +++ | >3.5 |
| ++ | 1.0 - 3.5 |
| +/- | <1.0 |
| -/- | no amplification |

Figure 37 – Copy number variation at the *CDKN2A/B* locus in immortalised colony-derived SHE-MT cells

The allelic status of *p16* exon1 α , *p16/ARF* exon 2, *ARF* exon 1 β and *p15* were measured using qPCR and Taqman-style probes in morphologically transformed (MT) colony-derived SHE cells. DNA from finite lifespan and immortalised MT SHE cells was analysed. Calibrator SHE samples shown in Figure 35 were used as controls with an average copy number of 2 copies. Values above 3.5 copies were considered gene amplification and below 1.0 copies single allele loss; the CNV range was taken into account. Amplification data was analysed using CopyCaller software v 2.0.

5.4 Discussion

This chapter describes in detail the results of work in which colony-derived cells from the SHE cell transformation assay were analysed for their patterns of gene expression, copy number variation and gene mutations in p53- and p16-tumour suppressor pathways. The objective was to provide molecular insight to events leading to senescence bypass in morphologically transformed (MT) SHE cells sourced directly from the SHE cell transformation assay (CTA). The results focus on molecular alterations in SHE cells treated with the carcinogen benzo(a)pyrene which is commonly used as the SHE CTA's positive control carcinogen. The data presented here may also expand on current knowledge of the mode of action of benzo(a)pyrene as a cell transforming agent and potent human carcinogen.

p53 mutations in SHE MT B(a)P-induced clones

The metabolic activation of benzo(a)pyrene commonly leads to the formation of DNA adducts, which if incorrectly repaired, will mispair on DNA replication leading to characteristic point mutations. The majority of B(a)P-induced mutations are thought to be G to T transversions. Such mutations are commonly identified in lung cancers (Toyooka et al., 2003) and when present in the critical tumour suppressor gene *p53*, are influenced by a strand bias whereby guanine base nucleotides on the non-coding strand are targeted more than those on the transcribed strand (Hollstein et al., 1991). The tumour suppressor *p53* is frequently mutated in human cancers and in chemically-immortalised Syrian hamster cell lines (Chang et al., 1995, 2000, Oreffo et al., 1993). Here in this analysis, four *p53* point mutations were identified in separate B(a)P-induced MT colony-derived SHE clones (Figure 38). Two of these were G>T transversions, one a G>C transition and the other a C>T transition which if targeted via a B(a)P adduct on the opposite strand is also a guanine residue (G>A). The resulting changes in the translated protein were all predicted to localise to human mutational hotspots within the p53 DNA binding domain. One SH *p53* mutation (p.C245S) was identical to a point mutation found in an SH dermal B(a)P-induced cell line (Yasaei et al., 2013) indicating a commonly targeted site in hamster cell immortalisation. Using PredictProtein with SNAP2 (Yachdav et al., 2014) to assess the impact that each mutational event might have on protein function, all point mutations had a score above +70 and a high probability of impacting p53 function, (R161L = +82;

R270W = +74; C245S = +88; R251L = +71) this was in stark contrast to the strain variant S188G which was predicted no change in protein function (score of -86). According to the IARC p53 database all mutated codons were deleterious missense mutations that would alter the vast majority of the ten predicted human *p53* isoforms ($\Delta p53\alpha$ was not affected by R267W), whereas the strain variant was predicted a neutral effect on protein function did not affect the transactivation domain. This suggests that p53 activity was compromised in 33 % of BP-induced immortal SHE MT cells (4 out of 12) and moreover, confirms that the base change common to all samples sequenced is indeed a strain variant. Given the mutational frequency induced by benzo(a)pyrene at a single gene locus is about 3 in 10,000 cells (Newbold et al., 1977) which despite being more than 30-fold higher than spontaneous mutations occurring is still very low, the outcome of a relatively high proportion of immortal SHE MT clones containing a *p53* mutation might be unexpected.

Sequencing profiles revealed that *p53* mutations in BP MT9 and BP MT10 were present at early population doublings (under passage 10) indicative of the mutation likely being a direct effect of benzo(a)pyrene treatment, although only two were characteristic G>T transversions. The sequencing profiles also indicated that the mutated form of *p53* was only present in the whole cell population or in all transcripts at the later time point when the clone fully acquired immortality, suggesting the mutated p53 conferred growth advantages and evasion of senescence barriers. Only one B(a)P-induced SHE MT clone had amplification in *p53* (4 copies, tetraploid) but no gene mutations and it failed to bypass senescence. The overall p53 mutation frequency was lower in SHE compared to that observed in SHD immortal B(a)P-induced lines (Yasaei et al., 2013) but the lack of CNV in B(a)P-induced clones was concordant with senescence bypass studies in induced SHD cells, where 5 out of 7 B(a)P-induced lines were found to carry *p53* DNA binding domain point mutations, although only one line sustained single allele loss of *p53* (Yasaei et al., 2013).

| Treatment | Scoring | Cell clones | Immortal | p16 exon 1a status | p16/ARF exon 2 status | ARF exon 1b status | p15 status | p53 status | p16 point mutation | p53 point mutation |
|--------------------|--------------------|-------------|----------|--------------------|-----------------------|--------------------|------------|------------|--------------------|--------------------|
| None | n/a | SHD (WT) | No | +/+ | +/+ | +/+ | +/+ | +/+ | No | No |
| None | n/a | SHE (WT) | No | +/+ | +/+ | +/+ | +/+ | +/+ | No | No |
| B(a)P | n/a (mass culture) | SHD 5BP2 | Yes | +/+ | +/- | +/- | +/+ | +/+ | No | No |
| X-rays (high dose) | n/a (mass culture) | SHD 4XH2 | Yes | -/- | -/- | -/- | -/- | +/+ | Deleted | No |
| DMSO | Non-transformed | SHE 2 | No | +/+ | +/+ | +/+ | +/+ | +/+ | No | No |
| | MT | SHE 3 | No | +/+ | +/+ | +/+ | +/+ | +/+ | No | No |
| B(a)P | MT | DMSO MT1 | Yes | +/+ | +/+ | +/+ | +/+ | +/+ | No | No |
| | | SHE 19 | No | +/+ | +/+ | +/+ | +/+ | +/+ | No | No |
| | | SHE 22 | No | +/+ | +/+ | +/+ | +/+ | +/+ | No | No |
| | | SHE 24 | No | +/+ | +/+ | +/+ | +/+ | +/+ | No | No |
| | | BP T15 | No | +/+ | +/+ | +/+ | +/+ | +/+ | No | No |
| | | BP MT1 | Yes | +/- | +/+ | +/- | +/- | +/+ | No | No |
| | | BP MT2 | Yes | +/+ | +/+ | +/+ | +/+ | +/+ | No | No |
| | | BP MT3 | Yes | +/+ | +/- | +/- | +/+ | +/+ | No | No |
| | | BP MT4 | Yes | +/+ | +/+ | +/+ | +/+ | +/+ | No | No |
| | | BP MT5 | Yes | +/+ | +/+ | +/+ | +/+ | +/+ | No | Syn |
| | | BP MT6 | Yes | +/- | +/- | +/- | +/- | +/+ | No | No |
| | | BP MT7 | Yes | +/+ | +/+ | +/+ | +/+ | +/+ | No | Syn |
| | | BP MT8 | Yes | +/+ | +/+ | +/+ | +/+ | +/+ | No | Syn |
| | | BP MT9 | Yes | +/+ | +/+ | +/+ | +/+ | +/+ | No | Syn |
| BP MT10 | Yes | +/+ | +/+ | +/+ | +/+ | +/+ | No | Syn | | |
| BP MT11 | Yes | +/- | +/- | +/- | +/- | +/+ | No | Syn | | |
| BP MT12 | Yes | +/- | +/- | +/- | +/- | +/+ | No | Syn | | |

Figure 38 – Copy number variation (CNV) and point mutations in *p53* and *CDKN2A/B* genes in SHE colony-derived cells

A summary of gene copy numbers and mutations identified in colony-derived cells derived from the SHE CTA at 'late' passages (population doublings ~above 50 Pd). Mutations were screened by Sanger sequencing and CNV was performed using qPCR with TaqMan-style primers designed by Primerdesign. A strain variation common to all cells tested was identified in both *p16* and *p53* but point mutations were only found in *p53*. The synonymous mutation refers to *p53* c195 G>A which was silent at the amino acid level. Separate CNV assays were designed for *p53* spanning exons 7-9, *p15*, *p16* exon 1 α , *ARF* exon 1 β and *p16/ARF* shared exon 2. One gene copy was called when ≤ 1.0 copies were predicted, 3 copies called when ≥ 3.5 copies and 4 copies called when ≥ 4.5 copies predicted using CopyCaller v2.0, Applied Biosystems.

From the copy number variation analysis (CNV), both BP MT9 and BP MT10-immortalised cell lines were shown to have two copies of *p53*, at least between exons 7 and 8. In cancer, *p53* inactivating mutations are often accompanied by single allele loss on the remaining wild-type allele. This may have been the case in BP MT11 and BP MT12 as predicted *p53* gene copies were 1.20 and 1.29 respectively. However, in BP MT9 and BP MT10 the data would in fact be suggestive of two *p53* alleles both with a point

mutation (see Figure 38). The likelihood of two mutations taking place at exactly the same place in two alleles separately is next to impossible, unless there was chromosome loss followed by duplication of the remaining chromosome. One explanation could be due to differences in sample population doublings taken between RNA and DNA extracts in these instances; CNV was analysed around 5-6 population doublings (2 passages) before RNA was extracted for cDNA synthesis. It may be that in that over time cells lost a copy of *p53* giving rise to only one peak on the sequencing profile; but this would need to be confirmed. Also, the CNV analysis takes place at a DNA level whereas mRNA transcripts (not DNA) were sequenced for mutations. DNA sequencing might reveal additional allelic *p53* mutations or upstream deletions that could interfere or block transcription on the other allele, allowing transcription of only the first mutated allele. In this case amplified cDNA will have only contained one allelic version of *p53* even though the clones contain two *p53* gene copies. Gene copy analysis by fluorescence in situ hybridisation (FISH) with multiple probes to *p53* would verify the gene copy number across the gene and now that the Syrian hamster genome has been sequenced, genomic DNA encompassing the whole gene locus could be analysed.

The synonymous point mutation in *p53* c195 G>A was identified in all Brunel-derived SHE colonies and also involved a guanine residue (a transition mutation) but resulted in no predicted change in the protein conformation and was not found to be in a mutational hotspot (Figure 38). c195 G>A was identified in the original primary SHE population suggesting a further strain variant, different from the *p53* NCBI sequence and from clones obtained from BioReliance. The sequence profiles often showed two unequal peaks at c195 which is suggestive of either two populations of cells with alternative versions of *p53* or possibly allelic variants with a transcription bias. The mRNA transcripts sequenced suggest that the adenine (A) variant was preferred as at later time points the guanine (G) variant was not identified. One more speculative suggestion could be selection of the synonymous mutation or single-nucleotide polymorphism (SNP) in favour of its impact on splicing machinery. Silent mutations can promote cancer and in *p53* such aberrations are specifically located in close proximity to *p53* splice sites (Supek et al., 2014). Although not located at a splice junction, the corresponding wild-type codon in humans (human codon 66) is located in a predicted splicing enhancer motif (Cartegni et al., 2003) which, if

mutated, could influence the transcription of *p53* splice variants by affecting the assembly of spliceosome complexes. These splice enhancer sequences are not well-conserved recognition sequences but rather are loosely defined regions that can promote exon skipping or inclusion depending on their capacity to recruit splice factors. This was not investigated further.

Loss of CDKN2A/B locus in SHE colony-derived cells

In 50 % of B(a)P-induced immortal clones (6 out of 12) single copy loss was observed (CNV <1.0) and in these instances *ARF* exon 1 β was also commonly affected (Figure 38). In three of these cases the whole locus was subject to a single allelic deletion which was not observed at the early time point tested in BP MT6. It is likely that BP MT1 also lost the whole locus (*p16*, *ARF* and *p15*) as its CNV value for exon 2 was 0.88 but with a maximum range of 1.23 copies. Initial upregulation of *p16* and *p15* was noted in BP MT1 and BP MT6 which corresponded to a temporary cell crisis. A secondary event is presumed then to have taken place that resulted in increased cell growth and reduced expression levels of the *CDKN2A/B* locus which is consistent with the observed copy number loss only at the later time point. The reduction in mRNA expression of Cdk inhibitors can be explained by the deletion of one allele containing the *CDKN2A/B* locus that resulted in a lower level of *p16*, *p15* and *ARF* gene expression permissive for proliferation to continue.

BP MT3 lacked one allele of *ARF* exon 1 β and of exon 2 which is shared in alternative reading frame with *p16*. However, due to a lack of cell material (the cells could only be replated between passages +3 and P+12) DNA could not be extracted from the cells at the early passage time point. It too showed downregulation of *p16*, *p15* and *ARF* gene expression at later time points. Given the patterns of expression, it is likely that BP MT3's change in gene expression was linked to the loss of *p16/ARF* exon 2 and *ARF* exon 1 β . BP MT11 and BP MT12 on average expressed *p16*, *p15* and *ARF* at around 50 % of that measured in the non-transformed DMSO group and also carried a *p53* point mutation. Monoallelic expression of *CDKN2A/B* may not have been sufficient to activate senescence pathways causing haploinsufficiency; in fact gene transcript levels were akin to those in non-primary proliferating cells. In some SHD B(a)P-induced cell lines, monoallelic (heterozygous) deletions were commonly identified at the *CDKN2A/B* locus but were accompanied by increased levels of *p16* gene expression. Unlike in colony-derived SHE

cells, *p16* mutations were identified and gene silencing was only observed in a single B(a)P-induced SHD line, which was explained by DNA methylation at the gene promoter (Yasaei et al., 2013). Deletions spanning the 9p21.3 region are commonly associated with melanoma and multiple tumour types (Gu et al., 2013) and have also been identified in patients suffering from the very rare melanoma-astrocytoma syndrome (Frigerio et al., 2014).

Gene amplifications at the CDKN2A/B locus in SHE colony-derived cells

Gene amplification at chromosome 9p21.3 in humans is uncommon although it has been identified in urinary bladder cancers and associated with poor prognosis (Berggren de Verdier et al., 2006). Chromosomal aberrations as a result of benzo(a)pyrene exposure in SHE morphologically transformed cells have been recorded although normal SHE cells are well known for maintaining diploidy. From a single B(a)P-induced MT cell line, 83 % of cells counted were abnormal and included hypotetraploid, and hypo-octaploid cells along with aneuploid cells with fewer than 23 chromosomes (Markovits et al., 1975).

Results from the CNV analysis in SHE colony-derived cells suggested that there was amplification in genes found at the *CDKN2A/B* locus in 25 % of B(a)P-induced immortal SHE clones (3 out of 12) and also in two of the finite lifespan clones treated with benzo(a)pyrene (CNV >3.5). In B(a)P MT cells amplification was limited to *p16/ARF* exon 2 and *ARF* exon 1 β , mostly observed at early time points. This was not dissimilar from earlier observations in B(a)P-induced SHD immortal clones (Yasaei et al., 2013) which also noted CNV amplification limited to *ARF*. In samples predicted to have acquired *p16/ARF* amplification, there were two copies of *p53* at both early and later time points so amplification at the locus is unlikely to be explained by genome-wide amplification or polyploidy. Given that the predicted copy numbers were unequal across the locus, for example BP MT7 had over 8 copies of the *ARF* specific exon but two copies of *p16* exon 1 α , it is indicative of gene- or locus-specific amplification and not whole chromosomal amplification. If the cell population is viewed as initially genetically heterogeneous when derived from the MT colony, only those with selective growth advantage would continue to divide and overcome senescence barriers. If the CNV amplification at early time points is true (would need to be verified) then at later time points with clonal expansion, extra copies were lost from the overall cell population, indicating cell cycle arrest in those

amplified cells. Only BP MT5 retained an extra copy of exon 2, although the CNV minimum range was borderline.

Reliability of the CNV assay

More repeats of the CNV analysis would be needed to remove sample variation. The increase in predicted copy number did not generally correlate with increases in gene expression, which indeed questions the quantitative reliability of the assay. The variability within the control group (*p16*, *p15* and *ARF* assays) was high and noticeably so compared with the *p53* assay. To take this into account, it was necessary to allocate a large CNV range to attempt to gain a meaningful interpretation of the predicted copy number variation data, probably at the cost of assay sensitivity. One potential influencing factor could be remnant traces of PCR inhibitors within the gDNA samples derived from the extraction process. Although the gDNA used was diluted to 5 ng/μl and sample quality checked, this may not have been sufficient, leading to variable interference of the PCR reaction and resulting Cq values. The reference gene (*SDHA-VIC*) and target of interest (labelled with FAM) were duplexed in the same reaction to account for pipetting variability, which could have led to misinterpreted results. It was noted that the overall fluorogenic data recorded by the qPCR machine was quite low, and readings may have been dampened by running both simultaneously. This could have had unpredictable effects on the relative amplification, if the reduction in fluorescence did not take place evenly between the two fluorophores. Alternative methods to measure copy numbers to complement the CNV assay would be ideally performed although until recently a lack of genomic sequence information was limiting. Fluorescence in situ hybridisation (FISH) using gene specific probes would help visualise the gene copies and karyotyping the cell lines would aid identification of any gross chromosomal loss or gain in the resulting immortalised clones.

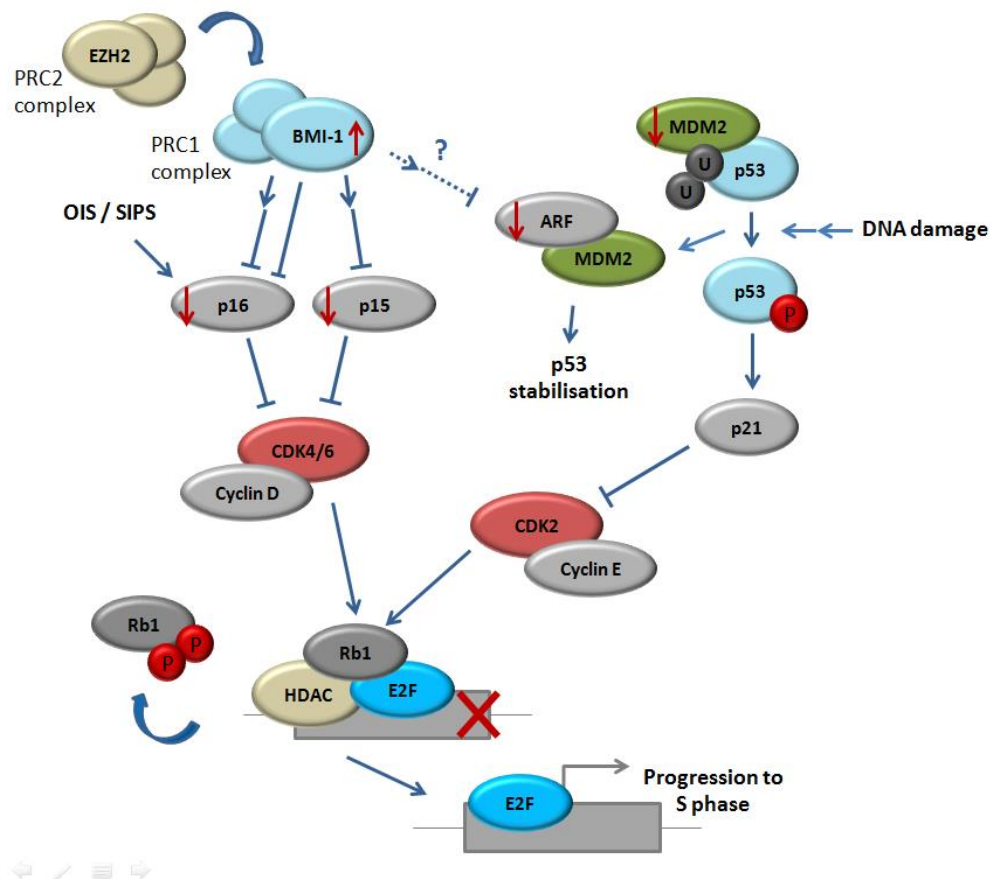


Figure 39 - Transcriptional changes potentially leading to immortalisation and senescence bypass

A schematic representation of transcriptional alterations identified in morphologically transformed SHE cells that had bypassed senescence, and which may help explain underlying molecular mechanisms of immortalisation. Genes assayed included components of the p16-pathway (*BMI-1*, *p16*, *p15* and *Rb1*) and the p53-pathway (*p53*, *ARF*, *Mdm2*). Red arrows indicate common transcriptional changes identified in this project by qPCR.

Transcriptional changes in p16- and p53-senescence pathways

A basic pathway network diagram is shown in Figure 39 for p16- and p53-senescence promoting pathways incorporating commonly observed transcriptional changes seen in B(a)P-induced morphologically transformed colony-derived SHE cells. Both pathways ultimately influence progression of the cell cycle from G1 to S phase via the inactivation of cyclin dependent kinases that keep pRb in an active, phosphorylated state (Henley and Dick, 2012). The pathway analysis was limited to mRNA level assessment as there was

difficulty in identifying reliable antibodies for western blotting specific to the Syrian hamster. In order to confirm the low levels of p16 transcripts, several human and mouse antibodies specific to *p16* were tested in samples found to have high levels of *p16* transcripts (for example DMSO controls) but protein detection was not achieved in hamster samples despite multiple optimisation attempts. Ideally transcriptional changes would be confirmed by protein analysis and where relevant quantified both at total and phosphorylated protein level to gauge protein activity.

BMI-1 upregulation in MT B(a)P-induced SHE cells

Data presented in this chapter provide insight into the possible mechanisms underlying upstream regulation of members of the *CDKN2A/B* locus that drive senescence pathways. Increased expression of *BMI-1* in immortal benzo(a)pyrene-induced morphologically transformed (MT) SHE cells could partly account for how *p16* and *p15* are transcriptionally downregulated compared to non-transformed SHE cells. BMI-1 is a ring-finger protein and a member of the Polycomb repressive complex 1 (PRC1) which, along with other complexed proteins such as CBX7 (chromobox homologue 7) and RING1B (ring finger protein 2), recognise epigenetic marks imposed by other Polycomb group (PcG) proteins. There is evidence that a steady release of PRC1 proteins bound to the *CDKN2A/B* locus has an activating effect on *p16* transcription during senescence (Itahana et al., 2003) whereas *BMI-1* overexpression extends replicative cell lifespan by disrupting the Rb1-pathway (Itahana et al., 2003). Arsenic-induced cell transformation in immortalised BALB/c 3T3 cells was shown to correlate with increased levels of PRC2 protein components EZH2, SUZ12 and EED as well as elevated protein levels of BMI-1. When PcG proteins were knocked-down, *ARF* and *p16* levels were rescued in transformed cells (Kim et al., 2012) although there was no mention of any proliferation rate differences following transfection. Additionally, an upstream DNA element of *p16* is recognised and bound by BMI-1 (BRE-element) which acts as a negative transcription factor directly influencing *p16* transcription in humans (Meng et al., 2010). Further investigation is required in immortalised SHE MT cells to confirm *BMI-1* overexpression at the protein level, and a knockdown via short-hairpin RNAs would confirm its upstream role in regulating *p16*, *p15* and possibly *ARF*, which is also located at the *CDKN2A/B* locus.

Downregulation of p16 and p53 compensation

The monoallelic loss of the *CDKN2A/B* locus identified by copy number variation analysis was linked to the downregulation of one or more of its gene products in MT clones BP MT1, BP MT3 and BP MT6. As this secondary event took place, there were changes in gene expression of members of the *p53* pathway (Figure 31). For example, there was a 3-fold increase in *p53* expression noted in BP MT3 and BP MT6 after P+3 and P10 respectively. A higher fold increase was observed in BP MT1 after P+3 which correlated to when *p16* was downregulated; a further increase in *p53* was noted at P+12 when *p15* transcripts were also reduced. This is suggestive of members of the *p53*-pathway sensing the silencing of senescence regulators in some instances, possibly causing the observed slight increase in *p53* expression in compensation. A similar observation was made for BP MT4 between passages +7 and +8, which retained both copies of the *CDKN2A/B* locus but also suffered from attenuated levels of *p16*, *ARF* and *p15* (Figure 32), suggesting alternative regulatory mechanisms.

Both *p53* and *p16*-pathways converge on the retinoblastoma protein which when active maintains cells in their resting state, limiting progression of the cell cycle from G1 to S phase (Henley and Dick, 2012). In BP MT4 and BP MT6 *Rb1* expression was reduced at the same passages as when *p15* downregulation was commonly observed, implicating its role in senescence. Transcripts of *p16* were reduced concomitantly with *Rb1* and *p15* in BP MT6 and in BP MT4 *p16* was downregulated following a 2.5-fold decrease in *Rb1* (Figure 31). No information was generated with regards to pRB1 protein levels or phosphorylation state in colony-derived clones which limits conclusions drawn on the activity of pRB1. The mRNA data suggests the deregulation of senescence activating pathways, permitting uncontrolled growth despite increased *p53* transcription in B(a)P-induced MT SHE cells with downregulated *p16* and *p15*.

On the other hand *Rb1* expression was also shown to be upregulated in several immortal SHE lines, including BP MT7, BP MT8 and *p53* mutants BP MT11 and BP MT12. If *p53* was non-functional due to inactivating DNA binding domain mutations in the latter two lines, it is conceivable that its downstream target *p21* failed to activate RB1, allowing progression through to S phase. With low levels of *p16* and *p15*, cyclin D may remain activate and thus RB1 further inactive despite higher mRNA transcripts circulating due to

its protein phosphorylation via cyclin dependent kinases. Further work is needed to prove the posttranslational regulation of RB1 in immortal B(a)P-induced SHE cells but the data suggests that regulation of the restriction checkpoint into S phase is compromised. *CDKN2A/B* transcripts were downregulated in BP MT7 and BP MT8 however these cells were found to have both wild type copies of *p53*, *p16*, *ARF* and *p15*. There may be additional unknown inactivating events taking place in the p53-pathway or the reduced expression of the locus including *ARF*, which affects p53 protein turnover by sequestering Mdm2, may have been sufficient to bypass senescence barriers.

***Mdm2* gene expression**

Mdm2 was minimally expressed in BP MT5, which would suggest stabilisation of the p53 protein (as it is not marked for ubiquitination) and the resulting increased p21 activity could then lead to the inactivation of Cdk2 and cell cycle arrest. However, this was not the case as the cells reached over 100 population doublings and showed no signs of entering senescence. Indeed *Mdm2* is often overexpressed and amplified in cancers (Rayburn et al., 2005) which is inconsistent with its striking downregulation detected in BP MT5. A gradual increase in transcription of its upstream regulator *ARF* to levels comparable of the DMSO-control group was observed (Figure 32) but its expression was later downregulated by about 80 % along with *p16* and *p15*. Transcript levels of *Mdm2* in BP MT5 were comparable to those identified in primary SHE cells, suggesting that its silencing is compatible with proliferation, and low levels were also common to BP MT3 and BP MT4. It possible that downregulation of Mdm2 is the cell's way of trying to activate the p53 pathway and initiate cell cycle arrest.

Downstream effectors like *p21* and *Cdks* were not transcriptionally quantified in this study but may be drastically altered thus evading cell cycle checkpoints. Recent papers argue that the function of Mdm2 goes beyond negatively regulating p53 activity and that it may not always be oncogenic (Manfredi, 2010, Nag et al., 2013). A role for Mdm2 in promoting cell cycle arrest has been implicated, as stabilisation of p53 activity by silencing *Mdm2* with small interfering RNAs, did not impact cell cycle progression (Giono and Manfredi, 2007). Despite increased p53 and p21 levels, *Mdm2* knockdowns continued to proliferate indicating that it may be required for a full cell cycle arrest via the p53-pathway. It is also worth noting that *Mdm2* has multiple isoforms plus binding partners

(Nag et al., 2013) and it is possible that the qPCR primers used in this analysis may encompass only a subset of all transcript variants.

Sample variability in qPCR analysis

Relative quantities of gene transcripts were compared to a group of non-transformed DMSO-treated colony-derived cells (Figure 30). RNA was extracted from DMSO controls which were early passage (P2-P3), that were proliferating and had visible mitotic telophase pairs. It was found that most of the DMSO N group did not grow very well and many cells on recovery (following shipment from BioReliance) or following colony picking were senescent and could not be further expanded for analysis. This limited the number of controls that were available for analysis; ideally sample size would have been larger and more representative. Variation was not sample specific so that there were no obvious outliers that over- or under-expressing all genes which could be commonly removed to minimise the range observed. From the available DMSO controls with good growth, substantial variation was identified between colony-derived cells (N1-N6), especially for *p16* mRNA transcripts. To a certain extent this was to be expected given the heterogeneous nature of the SHE CTA also exemplified by the differences in BP MT clone expression profiles. Slight differences in population doublings across the DMSO clones may have influenced their transcriptional levels; in the case of clones from BioReliance, population doublings or number of passages were unknown at point of recovery (assigned P+1). Whereas for *p16*, if only the highest RQ values had been assigned as the calibrators, the fold difference observed would have been much greater with stronger gene downregulation in BP MT clones. On the other hand if the lower RQ values for *Mdm2* DMSO controls had been assigned an RQ of 1 then the low levels of *Mdm2* gene expression would not have been observed, but certain clones would have been interpreted as having upregulated transcripts. Patterns of gene expression within the same BP MT clone at different time points would remain largely unchanged, except that changes might be increased or diminished depending on the calibrator's expression. Without a 'normal' DMSO CTA clone transcription profile as a reference point, it was necessary to group the control samples together. Primary SHE cells were not used as calibrators as they were not considered to be representative of cells derived from the SHE CTA which have gone through assay specific growth conditions such as plating at low

seeding density, colony formation and at least 13 or more population doublings. It was hoped that by grouping the controls together a closer to normal representation of non-transformed DMSO-treated controls would be obtained.

Chapter summary

Colony-derived cells from the SHE MT cell transformation assay (CTA) were analysed for gene mutations, copy number variation and gene expression in potentially relevant genes from the p53- and p16-pathways. MT cells analysed continued to proliferate beyond 100 population doublings and can be considered fully immortal, in marked contrast to untreated SHE primary cells which entered senescence after ~35-45 population doublings (Dafou, 2003). We identified *p53* point mutations in 4 out of 12 immortal B(a)P-induced MT SHE cells which altered the translated protein sequence and were likely to be functionally inactivating. Two of the mutations were transversions and consistent with benzo(a)pyrene's mutational fingerprint. No point mutations were observed in *p16* or in any of the finite lifespan clones. A single allele loss was observed in 40 % of BP MT immortalised lines which was not limited to *p16* but was extended to the whole *CDKN2A/B* locus, i.e. including the tumour suppressor genes (TSGs) *p15* and *ARF*. Gene expression analysis indicated that the entire locus was expressed at low levels, unlike in senescent cells which overexpressed all three TSGs. In those instances where *p15* or *p16* were initially upregulated, the timing of (CNV) gene copy loss seems to have coincided with a reduction in mRNA transcripts and the appearance of clonal cell growth. The negative *CDKN2A* regulator *BMI-1* was shown to be upregulated in most SHE MT cells which can, at least in part, explain the silencing of the *CDKN2A/B* locus. In some instances, *p53* was slightly upregulated along with *Rb1* transcription but cell cycle arrest did not take place, probably indicating further signalling pathway abrogation in the lines containing wild type *p53*. Surprisingly, the p53 negative regulator *Mdm2* was expressed at very low levels but this may have been due to highly expressing control samples.

CHAPTER 6

6 The Role of DNA Methylation in Regulating *p16* in Immortal SHE MT Colony-Derived Cells

6.1 Introduction

DNA methylation is a known epigenetic regulator of transcription, most widely associated with gene silencing but also with imprinting and X-chromosome inactivation. Occurring non-exclusively at CpG dinucleotide sites the addition of methyl groups takes place on cytosine residues and is catalysed by various methyltransferase enzymes belonging to the *Dnmt* family (Rhee et al., 2002). The dynamic process of DNA methylation is regulated by the synergistic activation of Dnmt enzymes which catalyse *de novo* methylation whilst maintaining existing methyl groups (Okano et al., 1999). DNA methylation is reversible and demethylating TET enzymes play a role in remodelling methylation patterns (Kohli and Zhang, 2013, Jeltsch and Jurkowska, 2014). Epigenetic methyl marks can be stably inherited following cellular replication, since hemimethylated DNA is recognised by Dnmt enzymes such that unmethylated strands are remethylated. Changes to an organism's methylome can lead to gene dysregulation and disease (Ehrlich, 2002) and, in cancer, metastatic cell types have been shown to have genome-wide altered patterns of methylation (Reyngold et al., 2014).

Hypermethylation of the *p16* promoter has been identified as a risk factor in the development of breast cancer (Wang et al., 2012). Aberrant patterns of DNA methylation in this region have been shown to cause transcriptional inactivation of *p16* in a number of cell types and species; including human oral cancer cells (Cody et al., 1999), head and neck cancer (Demokan et al., 2012) prostate and renal cell carcinomas (Herman et al., 1995) as well as other *in vivo* cancer models such as rat and mouse, (Honoki et al., 2004, Wu et al., 2012) and the Syrian hamster. The 5' promoter region of SH *p16* was shown to be methylated in pancreatic carcinomas induced by N-nitrosobis(2-oxopropyl)amine (BOP) (Hanaoka et al., 2005, Li et al., 2004) and by 7,12-dimethylben(a)anthracene (DMBA) in SH cheek pouch tumours (Li et al., 2008) explaining the observed reduced expression levels of *p16*. In earlier studies, epigenetic silencing by extensive DNA methylation at the *p16* promoter was also identified in immortalised Syrian hamster dermal (SHD) cells, induced by exposure to the known epigenetic-carcinogen nickel chloride (Yasaei et al., 2013). Further, the *p16* gene in one benzo(a)pyrene-induced SHD cell line was also identified to be transcriptionally inactivated due to its heavily methylated promoter region. This raised the possibility that silencing of *p16* in

immortalised SHE colony-derived cells could also be explained epigenetically via DNA methylation at the 5' *p16* promoter. Thanks to the recent Syrian hamster whole genome sequencing performed by the Broad Institute, additional genomic information is now available via the NCBI website. Following on from sequencing alignments discussed in Chapter 7, (section 4.2.3) *p16* promoter analysis in cells derived from the SHE-MT assay could now be improved over that described previously (Hanaoka et al., 2005) by extending the upstream promoter sequence available for analysis.

In order to analyse the extent of methylation present, a bisulphite conversion of genomic DNA was carried out to discriminate between methylated and unmethylated cytosine bases. Treatment of genomic DNA with sodium bisulphite converts cytosine residues to uracil, but methyl groups (-CH₃) bound to cytosines are protective of the conversion process, meaning that methylated cytosines remain unchanged. Uracil is complementary to adenine which also base pairs with thymine; on subsequent rounds of PCR the present uracils are replaced by thymine. Therefore, post bisulphite conversion and desulphonation, any unmethylated cytosines are altered to thymines. This approach enabled the investigation of epigenetic silencing of *p16* in immortalised colony-derived SHE cells.

Immortalised colony-derived SHE cells positive for abnormal DNA methylation at the *p16* promoter were treated with 5'-Aza-2'-deoxycytidine (5-aza-dC), which inhibits methyltransferase activity, to ascertain whether the removal of aberrant methyl groups could restore *p16* expression and even lead to the reactivation of senescence barriers. 5-aza-dC, also known as decitabine or abbreviated to DAC, is a pro-drug which once activated by kinase phosphorylation becomes a substrate for replication and can be incorporated into the DNA in the place of cytosine bases. As methyltransferases recognise hemimethylated DNA they remain covalently bound to 5-azacytosine rings and their catalytic activity is blocked (Mompalmer, 2005). Methylation can no longer take place in treated cells but DNA damage response (DDR) pathways are initiated, trapped methyltransferases are degraded leading to a global loss of DNA methylation (Stresemann and Lyko, 2008).

6.2 Materials and methods

6.2.1 DNA methylation analysis of *p16*

Bisulphite conversion

Bisulphite conversions were performed using the Cells-to-CpG Bisulphite Conversion Kit (Applied Biosystems®) on genomic DNA, extracted by the methods described in 2.6. The following steps were performed:

DNA bisulphite conversion

Conversion reagent was freshly prepared by adding 26 µl denaturation reagent and 800 µl ddH₂O to one conversion tube, mixing and then adding 50 µl conversion buffer. The mixture was then incubated at 60 °C for 10 min with brief vortexing, to properly solubilise the conversion reagent. A total of 1 µg purified genomic DNA was made to 45 µl in ddH₂O and 5 µl denaturation reagent was added before mixing and then incubating at 50 °C for 10 min. Volumes of 100 µl prepared conversion reagent was then added to each denatured sample, the reaction was mixed well and then two 75 µl aliquots per sample were placed in the thermal cycler. The thermal cycling conditions for bisulphite conversion were as follows: two cycles of 65 °C for 30 min and 95 °C for 1.5 min, followed by a final incubation at 65 °C for 30 min before holding at 4 °C for a maximum of 4 hours.

Desalting and desulphonation

Volumes of 600 µl binding buffer was first added to a binding column, followed by the converted DNA, before inverting the column to mix. The sample was passed through the column at 10,000 RPM for 1 min and the flow-through discarded. Subsequently gDNA bound to the column was washed with 600 µl wash buffer and the DNA then desulphonated by incubating the column with 200 µl desulphonation reagent for 15 min at room temperature with the lid closed. After 1 min of centrifugation at 10,000 RPM the column was again washed and the flow-through fully discarded. The bisulphite converted and desalted DNA was then eluted into 40 µl pre-warmed elution buffer and stored at 4 °C for up to three months.

Methyl-specific PCR (MSP)

PCR was performed on bisulphite-converted samples using methyl-specific primers (MSP) and primers specific to non-methylated genomic DNA for the 5' upstream promoter region and exon 1 α of *p16*. Primer sequences for exon 1 α were sourced from published papers (Li et al., 2004, 2008) as were primers for the *p16* promoter (Yasaei et al., 2013). Primer sequences are located in the appendix. A total of 3 μ l bisulphite converted gDNA was amplified to a final reaction volume of 50 μ l with 0.5 μ l Phusion U polymerase (Thermo ScientificTM), 200 μ M dNTPs, 0.5 μ M forward and reverse *p16* MSP primers along with 10 μ l 5 X GC Buffer and 1.5 μ l 100 % DMSO. Samples were kept on ice and mixed well. Thermal cycling was as follows: denaturation at 98 °C for 30 s followed by 45 cycles of 98 °C for 5 s 54 °C for 20 s and 72 °C for 15 s, then final extension at 72 °C for 10 min before holding at 4 °C. For each MSP experiment two PCR reactions were performed based on the bisulphite conversion of unmethylated cytosine nucleotides: one specific to methylated DNA and one specific to non-methylated DNA. Products were then run on a 2 % agarose gel with EtBr in 1X TBE buffer at 70 V for 2-3 hours before imaging.

CpG site analysis of p16 promoter

Designing BS sequencing primers

Additional sequence information upstream of *p16* permitted the design of bisulphite sequencing primer pairs spanning a larger promoter region. MethPrimer (Li and Dahiya, 2002) was used to design suitable oligonucleotides which recognise bisulphite-converted gDNA. These sequences are designed to complement bisulphite converted DNA and were selected based on their lack of CpG sites so as to avoid amplification bias of methylated or unmethylated sequences. The input sequence was a 1 Kb sequence directly upstream of *p16*, which included the previously identified 300 bp belonging to the *p16* 5' promoter region (Hanaoka et al., 2005). From this candidate BS sequencing primer pairs were obtained. Optimal primer annealing temperatures were assessed by performing gradient PCRs with annealing temperatures between 52 °C and 62 °C. Primers generating a 457 bp amplicon held good DNA specificity and were suitable for sequencing. The MethPrimer software also predicted two CpG islands (over 50 % GC content) within the input sequence: the first being 125 bp and the second 110 bp in length.

Amplification

Phusion U Polymerase worked best at amplifying the 457 bp amplicon upstream to *p16*, so it was necessary to use a vector capable of inserting blunt ended PCR products. Two 50 μ l PCR reactions were set up per sample using bisulphite sequencing primers. Each reaction contained 4 μ l bisulphite converted gDNA, 0.5 μ M forward and reverse bisulphite *p16* promoter primers, 200 μ M dNTPs, 10 μ l 5X GC Buffer, 1.5 μ l 100 % DMSO and 0.5 μ l Phusion U polymerase (Thermo Scientific). Samples were kept on ice and mixed well. Thermal cycling involved denaturation at 98 °C for 30 s followed by 40 cycles of: 98 °C for 10 s, 56 °C for 30 s and 72 °C for 30 s, then final extension at 72 °C for 10 min before holding at 4 °C.

Gel extraction

Products were run on a 1.5 % agarose gel with EtBr in 1X TBE buffer at 70 V for 1.5 hours before imaging. Then using a sterile scalpel and UV box, the band of interest was excised for extraction and purification as described in section 2.8. The resulting DNA was quantified using a NanoDrop 2000 and stored at -20 °C until required for ligation steps.

Plasmid preparation

The pJET1.2/blunt linearised vector (Figure 40A, Thermo Scientific) was modified by Dr Evgeny Makarov by ligation of a double stranded 19 bp DNA product into its insertion site (Figure 40B). This sequence contained four restriction sites (see Figure 40C) which was used to produce a 'home-brew' vector suitable for the incorporation of blunt-ended DNA fragments.

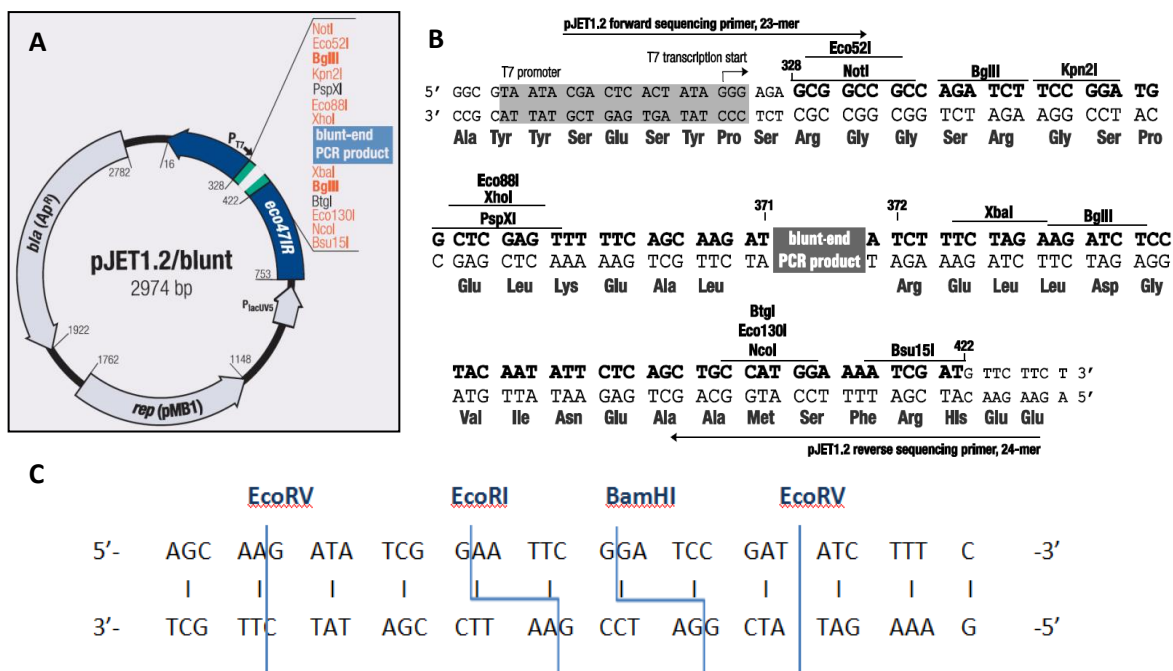


Figure 40 – The pJET1.2 blunt cloning vector

A) Commercially available pJET 1.2/blunt vector map (Thermo Scientific) B) DNA sequence of multiple cloning site (MCS) region containing the insertion site and forward and reverse sequencing primers C) Restriction sites in modified linearised pJET propo plasmid. The cloning vector contains an ampicillin resistance gene as well as a lethal restriction enzyme gene which is disrupted by ligation of the insert into the MSC.

10 µg of the ligated vector with short insert was first digested with 100 units of Eco321 (EcoRV) (Fermentas) for 2 hours 30 min at 37 °C in a final volume of 200 µl to cut the plasmid at two recognition sites producing a vector with blunt ends. To minimize re-circularisation of the plasmid, the reaction was then further ligated with 50 Units of EcoRI (Fermentas) in the same buffer solution for an hour at 37 °C. The plasmid was then extracted by adding 200 µl phenol, chloroform and isoamyl alcohol (Sigma-Aldrich®) in a ratio of 25:24:1 respectively to the sample, briefly vortexing before centrifuging at 13,000 RPM for 5 min. The upper aqueous phase was then transferred to a new tube and 20 µl of 3 M NaAc (pH 5) was added to precipitate the DNA. 500 µl of 100 % EtOH (2.5 x volume of sample) was added and the reaction incubated at -20 °C for 30 min. The vector was then precipitated at 14,000 RPM at 4 °C for 30 min before washing the pellet with 70 % EtOH and re-centrifuging. Once air dried, the pellet was resuspended in 175 µl

RNase/DNase-free dH₂O. A final restriction digest was performed with BamHI (Fermentas) again to reduce the chances of plasmid re-ligation and circularisation. 50 Units of BamHI was added to the resuspended vector along with 20 µl 10X BamHI buffer, LspII091 (with BSA) (Fermentas) made to a final volume of 200 µl. The digestion was performed at 37 °C for 2 hours before a subsequent phenol/chloroform extraction as described above. The final pellet containing modified vector was resuspended in 100 µl to give a concentration of ~50 ng/ml.

Blunt-ended insert ligation

Ligation reactions were performed on ice with a final volume of 20 µl and an insert to vector ratio of 3:1 was maintained for all reactions. The insert was mixed well with 2 µl PEG 4000, 10 X ligase buffer, 1 µl T4 DNA Ligase (all Fermentas) and 1 µl 50 ng/ul pJET prepared vector. The ligation reaction was allowed to proceed overnight at 4 °C.

Transformation

2.5 µl of the incubated ligation reaction was added to a vial of One Shot TOP10 chemically competent *E. coli*, (Invitrogen™) thawed on ice. The reaction was then incubated on ice for 30 min before heat-shocking the bacteria for 45 s at 42 °C. The cells were allowed to recover on ice for 2 min before shaking at 200 RPM for 1 hour at 37 °C in 250 µl S.O.C. medium. 10 µl and 20 µl of transformed bacteria were then spread evenly on pre-warmed LB-agar plates prepared with 50 µg/ml ampicillin. The plates were then inverted and incubated overnight at 37 °C.

Colony picking and growth

Fifteen or more individual colonies were picked per transformation reaction using sterile pipette tips. Each colony was added directly into a clean PCR tube for colony PCR and the pipette tip then placed into a sterile Falcon tube containing 2 mL LB-broth with 50 µg/ml ampicillin and cultures grown overnight at 37 °C and 200 RPM. Colony PCR was set up in 20 µL reactions as follows: 10 µl DreamTaq green PCR master mix (2X), (ThermoScientific™) 0.25 µM forward and reverse pJET 1.2 plasmid primers. Thermal cycling parameters: bacterial cells were lysed at 94 °C for 10 min, denatured at 94 °C for 2 min, then subjected to 30 cycles of 94 °C for 30 s, 60 °C for 30 s and 72 °C for 1 min,

followed by final extension at 72 °C for 10 min and holding at 4 °C. Products were run on a 1.5 % agarose gel with EtBr in 1X TBE buffer at 80 V for 1.5 hours before imaging. Colonies containing the expected promoter insert were identified and up to twelve of the positive cultures selected for plasmid purification.

Plasmid purification

Bacterial cultures in 2 mL LB-broth were pelleted at 8,000 RPM for 3 min and the supernatant removed before plasmid extraction using a column based miniprep kit (Qiagen). The cell pellet was resuspended and lysed before neutralisation; RNA was degraded with RNaseA and the resulting cell lysates pelleted. The supernatant containing nucleotides was applied and centrifuged through a spin column in order to bind the DNA, and the column was then washed several times before eluting in 40 µl of elution buffer. Typical DNA concentrations were of good purity suitable for sequencing ($A_{260/280}$ ratio > 1.8) and of concentrations >200 ng/µl.

Sequencing and Analysis

Purified plasmids were sent to Beckman and Coulter for Sanger sequencing using the pJET 1.2 reverse vector primer. For each bisulphite converted sample, a minimum of 10 picked colonies were analysed to estimate the methylation status of each CpG site within the 457 bp upstream region of the *p16* promoter. The nucleotide reads were analysed in CLC Sequence viewer as described in section 2.9 and aligned to the corresponding 500 bp region of upstream sequence of *p16* identified in WGS contig085774 (APMT01085774.1).

6.2.2 Demethylation Analysis

To confirm *p16* gene regulation via DNA methylation, immortalised SHE cells were treated with 5'-Aza-2'-deoxycytidine (5-aza-dC) and monitored over a period of 4 weeks following treatment. Time points for RNA and DNA extraction were taken at days 1, 2, 4 and 8.

Drug treatment

The following immortalised late passage SHE colony-derived MT cell lines were selected for demethylation analysis: BP MT2, BP MT6, BP MT7 and BP MT8. An untreated primary SHE cell line (SHE 2B, prepared and frozen by Dr Debbie Trott) was also treated in the same way.

6×10^5 cells were seeded per 100 mm dish in complete DMEM-L in 10 % CO₂ at 37 °C as described in the General Materials and Methods, Chapter 4. After 24 hours, a final concentration of 5 µM 5-aza-dC in fresh media was added at T₀. After 4 hours media was replaced again containing a final concentration of 5 µM 5-aza-dC. Treatment of SHE cells was performed in duplicate, untreated and vehicle control (DMSO) plates were also included in the analysis for each cell type.

Cell culture

Culture of demethylated cells was as described in the General Materials and Methods, (Chapter 4) with the exception of using TrypLE Express enzyme (1X) without phenol red (Gibco®) instead of Trypsin-EDTA. This was to facilitate cell counting and limit damage to the cells that may result from frequent detachment. Representative treated, untreated and DMSO control SHE cells were routinely counted using a haemocytometer after detaching and total cell counts were recorded. Cumulative population doublings were calculated as described in section 3.2.5.

SA-βgal staining

Representative treated, untreated and DMSO exposed SHE cells were fixed and stained with x-gal to detect their beta-galactosidase activity, which is associated with the cellular senescence phenotype. For this purpose, cells were plated in duplicate in 6-well plates and after 2-3 days in culture were fixed and stained as per the protocol described in section 2.2. Cells were then scored for their SA-βgal activity detected as a blue precipitate. From each plate 3 different areas were counted for βgal-positive cells and their average expressed as a percentage of the total number of cells.

RNA extraction

RNA was extracted from untreated, treated and DMSO control plates at time points between T_{24hrs} and T_{3weeks} after the first 5-aza-dC treatment. After washing in 3-4 mL cold

CMF-HBSS (Invitrogen Gibco®), 1 mL peqGOLD TriFast (PeqLab) was added per plate and the cell lysate was added to a 1.5 mL Eppendorf tube. At this point the samples were frozen at - 80°C until proceeding to the RNA extraction step as described in section 2.3.

Quantitative Real-Time PCR (qPCR) using SYBR chemistry

cDNA was prepared in 20 µl reactions as previously described from DNaseI treated RNA samples. Prior to qPCR, cDNA was diluted 1:2 in DNase/RNase free water to a final volume of 40 µl. *p16* and *p15* gene expression was detected using real-time qPCR and the reference genes *GAPDH* and *ACTB* were used as described in section 2.5, with SYBR chemistry. Typical working reactions were made from 5 µl iTaq universal SYBR green supermix (BioRad), 1 µl 5 µM primer mix (forward and reverse primers), 2 µl diluted cDNA and 2 µl DNase/RNase free H₂O. Ct values of treated cells and DMSO controls were normalised to the average Ct values of untreated cells of the same cell type taken at different time points. Expression levels were calculated according to the delta delta Ct method. PCR replicates were run in triplicate and two separate cDNA synthesis reactions were performed on each sample for a total of 6 technical replicates per sample and 2 biological replicates.

DNA extraction

DNA was extracted from untreated, 5-aza-dC treated and DMSO treated plates at time points between T_{24hrs} and T_{3weeks} after the first 5-aza-dC treatment. After washing in CMF-HBSS (Gibco®), cells were trypsinised and pelleted before further washing in 2 mL CMF-HBSS. Cell pellets were stored at - 80 °C until proceeding to the DNA extraction step as described in General Materials and Methods (section 2.6).

CpG site analysis of demethylated p16 promoter

To confirm the demethylation of the SH 5' *p16* promoter after treatment with 5 µM 5-aza-dC, DNA samples were bisulphite-converted (see section 6.2.1) to detect and compare the methylation status of the 457 bp region of interest that was previously shown to be methylated.

The upstream promoter region of *p16* was PCR amplified, purified by gel extraction and cloned into the pJET 1.2 vector described above in section 6.2.1. Colonies containing the bisulphite-converted region were sent for sequencing to Beckman and Coulter using

pJET 1.2 Reverse primers and obtained sequences were analysed using CLC Main Workbench software v5.5 (CLCbio, Aarhus, Denmark) as described in section 2.9.

6.3 Results

6.3.1 Silencing of *p16* by DNA methylation

Previous studies have shown that immortal SHD clones induced by nickel chloride and benzo(a)pyrene had epigenetically downregulated *p16* by DNA methylation of its 5' promoter region (Yasaei et al., 2013). These studies were extended here to determine whether the downregulation of *p16* transcripts observed in the immortal MT colony-derived SHE cells could be explained by a common mechanism. Methyl-specific PCR (MSP) was initially carried out in SHE CTA colony-derived cells in two regions of *p16*, schematically represented in Figure 41. Methyl-specific MSP1 primers targeted the *p16* 5' upstream promoter and MSP2 primers were targeted to the 5' region of the *p16* gene body in exon 1 α . Subsequently, bisulphite sequencing of the 5' promoter region which contains two predicted CpG islands was performed (see Figure 41) to confirm the MSP1 result.

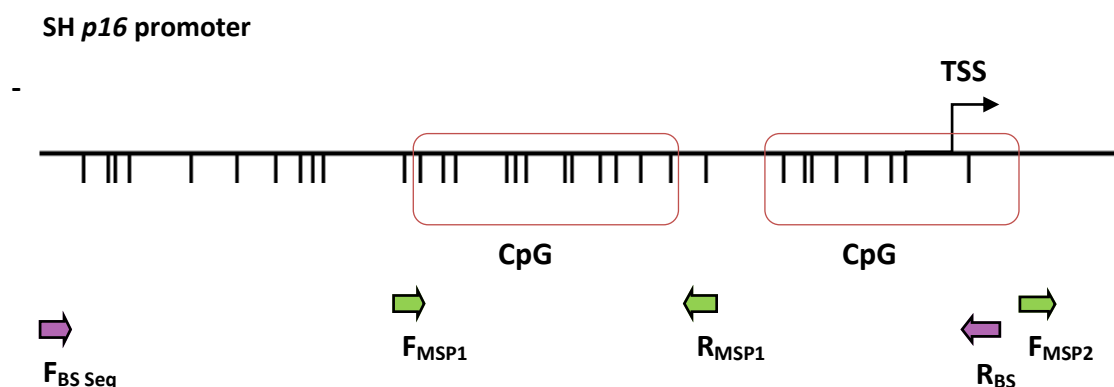


Figure 41 – Diagram of the *p16* promoter in the Syrian hamster

The upstream 5' promoter region of *p16* contains 2 predicted CpG islands (Primer Meth) indicated by the red boxes. CpG dinucleotide sites analysed are represented by vertical black lines. Primers used to analyse this region were designed to bisulphite converted DNA and included two sets of methyl-specific primers which amplified in the promoter region (MSP1 green arrows, both amplicons of 150 bp) and in exon 1 α (MSP2 green arrows, 100 bp and 143 bp). Bisulphite sequencing primers are also positioned (BS Seq. purple arrows, 457 bp product).

Methyl-specific PCR

MSP was carried out on bisulphite converted genomic DNA from immortalised MT colony-derived cells. Bisulphite-specific MSP primers were designed to discriminate between methylated and unmethylated gDNA based on the bisulphite conversion process. The first set of primers recognised CpG island 1, located in the *p16* promoter (MSP1) and a second set were used to identify methylation in *p16* exon 1 α (MSP2). For each MSP experiment, two separate PCR reactions were prepared: one to selectively recognise unmethylated DNA (converted) and the other to amplify methylated DNA (unconverted). Figure 42 contains representative images of the electrophoresis MSP products. Presence of both amplicons in the two PCR reactions per MSP experiment indicates DNA methylation whereas a single unmethylated band indicates no methylation.

The data from methyl-specific PCR gels indicated that there were different patterns of DNA methylation across immortal colony-derived SHE cells in the tumour suppressor gene *p16*. With reference to the gel in Figure 42A, there was no amplification in primers amplifying methylated DNA but amplicons of the expected weight (150 bp) were present in all unmethylated wells and also a non-specific PCR product of around 100 bp. In non-

amplified wells the bright bands of very low molecular weight are due unincorporated primers. This data was suggestive of no methylation in the *p16* promoter; however this conclusion is solely applicable to CpG sites found within the primer pairs used for PCR. Additionally, the lack of amplification of MSP1 methyl-specific PCR products was inconsistent across repeated PCRs, which raised concerns. Primer annealing and extension was occasionally observed in the *p16* promoter using MSP1 methyl-primers but was not consistent across repeats, necessitating further investigation. Figure 42B suggests that there was DNA methylation present within the coding region of *p16* (exon 1 α), especially in the positive control and BP MT1. This was reproducible across different batches of bisulphite converted DNA and in separate PCRs. Finite lifespan B(a)P-induced MT colony-derived cells from SHE 19 which did not immortalise but were senescent was not shown to be methylated and the negative control (SHE 2B) only had amplification in unmethylated wells.

Bisulphite sequencing of the p16 promoter

To further investigate the presence of DNA methylation in SHE samples, bisulphite sequencing was performed on the immediately upstream region of *p16* which contains the gene's transcriptional promoter. The primers used are those indicated by purple arrows in Figure 41 and their product spans a 457 bp of gDNA containing 32 CpG dinucleotides which could be sites of potential methylation. Examples of excised PCR products containing amplified *p16* promoter fragments are imaged in Figure 43. After ligation and transformation of competent *E.coli* bacteria with the fragment of interest, bacterial colonies were checked by colony PCR to confirm that they contained the correct insert, an example of which is shown in Figure 44. The correct colonies were then purified and Sanger sequenced using the reverse pJET1.2 vector sequencing primer, so as to amplify the whole *p16* promoter insert. The resulting bisulphite converted *p16* sequences were then aligned and analysed for the presence of methylation at 32 CpG sites as shown in Figure 45.

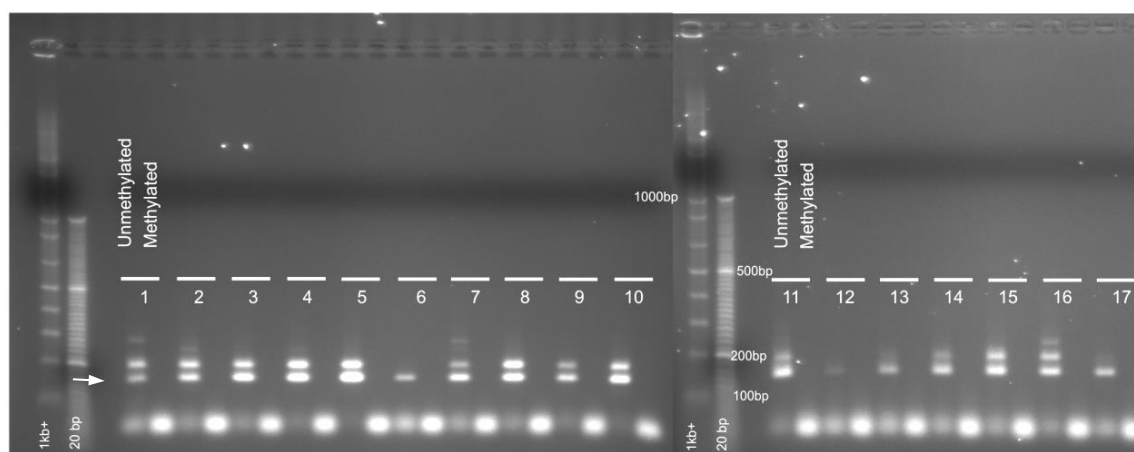
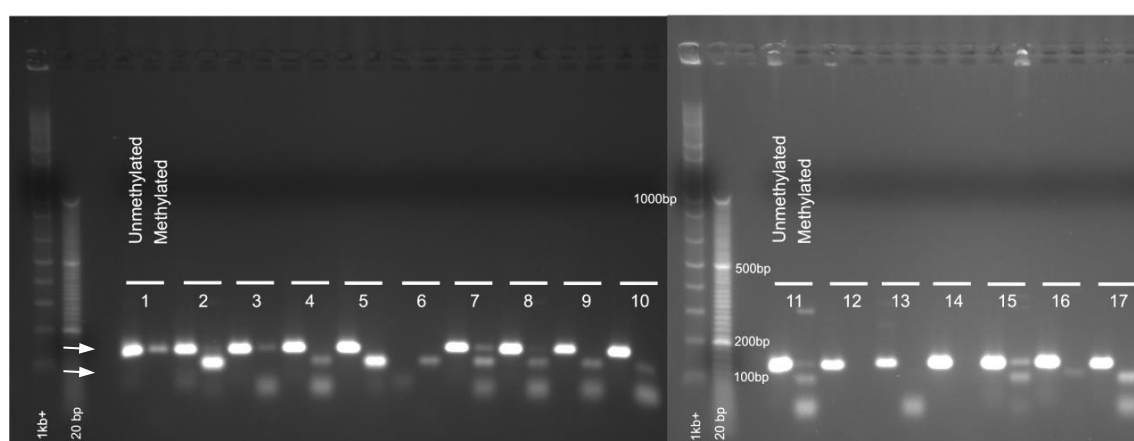
A) *p16* 5' promoter MSP1B) *p16* exon 1a MSP2

Figure 42 – Analysis of DNA methylation in *p16* 5' promoter and exon 1a using methyl specific PCR (MSP)

Bisulphite converted gDNA was amplified with two sets of primers designed to either methylated or unmethylated DNA. Both *p16* exon 1a and a 5' *p16* promoter regions were analysed using MSP primer sets to give an indication of the extent of methylation of *p16*. Expected band sizes for unmethylated and methylated products were 150 bp for both primer pairs for the promoter amplicon (A) and 143 bp and 100 bp for exon1a (B). Products in methylated wells indicate the presence of methylated cytosine in the primer set and products in unmethylated wells indicate amplification of unmethylated DNA. PCR products were run on a 2 % agarose gel in TBE buffer along side a 1 kb and 20 bp ladder.

- | | | |
|----------------------------|---------------------|-----------------|
| 1) SHE 2B (-ve control) | 7) BP MT3 P+16 | 13) BP MT6 P13 |
| 2) SHD BP1.2 (+ve control) | 8) BP MT4 P+8 | 14) BP MT8 P23 |
| 3) BP MT SHE19P+2 | 9) BP MT11 P16 | 15) BP MT7 P16 |
| 4) DMSO MT1 P+18 | 10) BP MT12 P15 | 16) BP MT10 P16 |
| 5) BP MT1 P+21 | 11) BP MT SHE24 P+3 | 17) BP MT9 P16 |
| 6) BP MT2 P+26 | 12) BP MT5 P26 | |

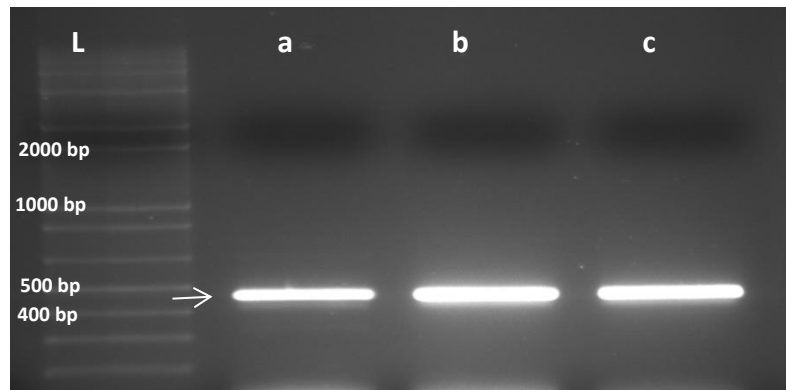


Figure 43 – Excision of bisulphite-converted *p16* promoter PCR products

Following a bisulphite conversion, 457 bp upstream of the *p16* start site including its 5' promoter, was amplified by PCR using bisulphite sequencing primers (purple arrows, Figure 41). The PCR products were run on a 1.5% agarose TBE gel containing ethidium bromide at 70 V for 1.5 hours. Three example excised products are imaged above (a-c) and the correct band size of 459 bp was excised (indicated by the arrow), purified and quantified for subsequent cloning steps. A 1 Kb^{plus} DNA ladder (Invitrogen) was loaded alongside PCR products as a reference (L).

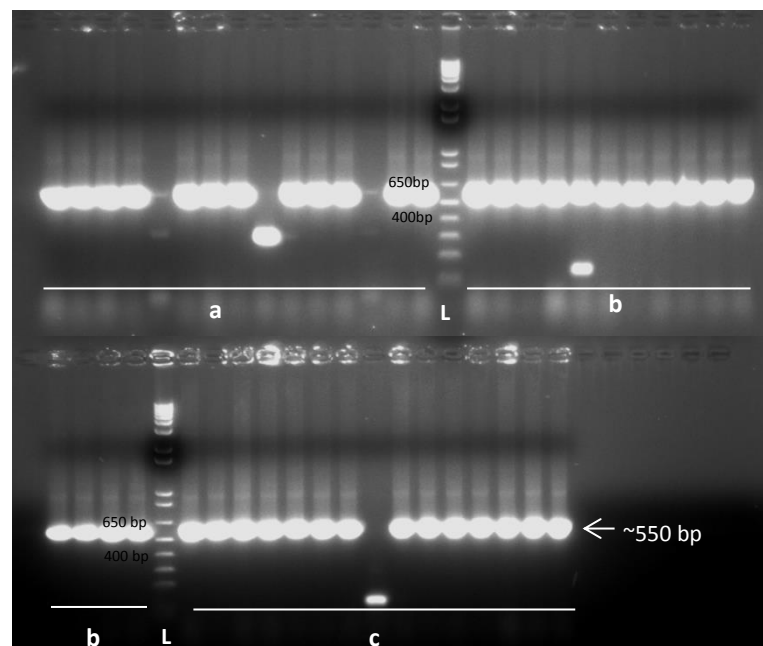


Figure 44 – Bacterial colony PCR to confirm the correct *p16* promoter insert into pJET1.2 vector

Up to 15 bacterial colonies were picked per sample and their inserts checked by colony PCR using pJET1.2 vector sequencing primers flanking the insert. Only colonies containing the correct insert were purified by miniprep and then Sanger sequenced. Imaged are three representative samples that were cloned. The expected band size containing insert and flanking vector regions was ~550 bp (arrow). A 1 Kb^{plus} DNA ladder (Invitrogen) was loaded alongside PCR products as a reference (L).

For each sample, 10 or more colonies were sequenced so as to obtain an estimated percentage of DNA methylation within each MT SHE line. Each CpG site was analysed individually and are represented by the 32 circles in Figure 45; the right-most CpG site is 3', which is closest to the *p16* transcriptional start site (TSS). A CpG site was considered to be methylated when unconverted cytosines were identified in above 50 % of colonies sequenced for each CG dinucleotide. Data is also shown for the presence of methylation in fewer than 50 % of the colonies as this was identified to take place at common CpG sites. SHD BP1.2 is known to have a methylated *p16* promoter (Yasaei et al., 2013) and was used as the positive control whereas gDNA from a DMSO-treated non-MT colony and untreated SHD samples were used as the negative controls.

Extensive methylation was identified in the CpG island closest to the *p16* promoter region in 5 out of 12 immortal B(a)P treated MT colony derived cell lines and in the positive control SHD BP1.2. Figure 45 shows that certain CpG sites were commonly methylated across the immortal SHE samples. BP MT6, 7, 8, 9 and 10 were methylated at CpG sites 6 to 8, which are clustered together in the *p16* upstream promoter sequence. In these clones ten or more colonies analysed were methylated, except for BP MT6 which was methylated in 50 % of colonies analysed. Sites 4, 12, 14 and 18 were noted to be regularly targeted by the addition of methyl groups. BP MT2 was shown to have additional DNA methylation at the most upstream CpG site (site 32). Interestingly, partial methylation was also observed in another 3 immortal BP MT cells at the same CpG sites (BP MT1, BP MT2, BP MT5) as those that were fully methylated; possibly indicating a regulatory role in *p16* expression, depending on the methyl state of CpG sites within the CpG island.

No methylation was observed in the DMSO-MT immortal colony DMSO MT1, possibly indicating that DNA methylation could be an epigenetic effect caused by the initial exposure of SHE colonies to benzo(a)pyrene. BP MT colony SHE 19 that was not immortal (i.e. senesced) did not show signs of methylation and neither did BP-induced, immortal BP MT4, BP MT11 and MT12. The BP MT line SHE 24 that was lost to infection but did show signs of clonal growth following a cell crisis phase was partially methylated.

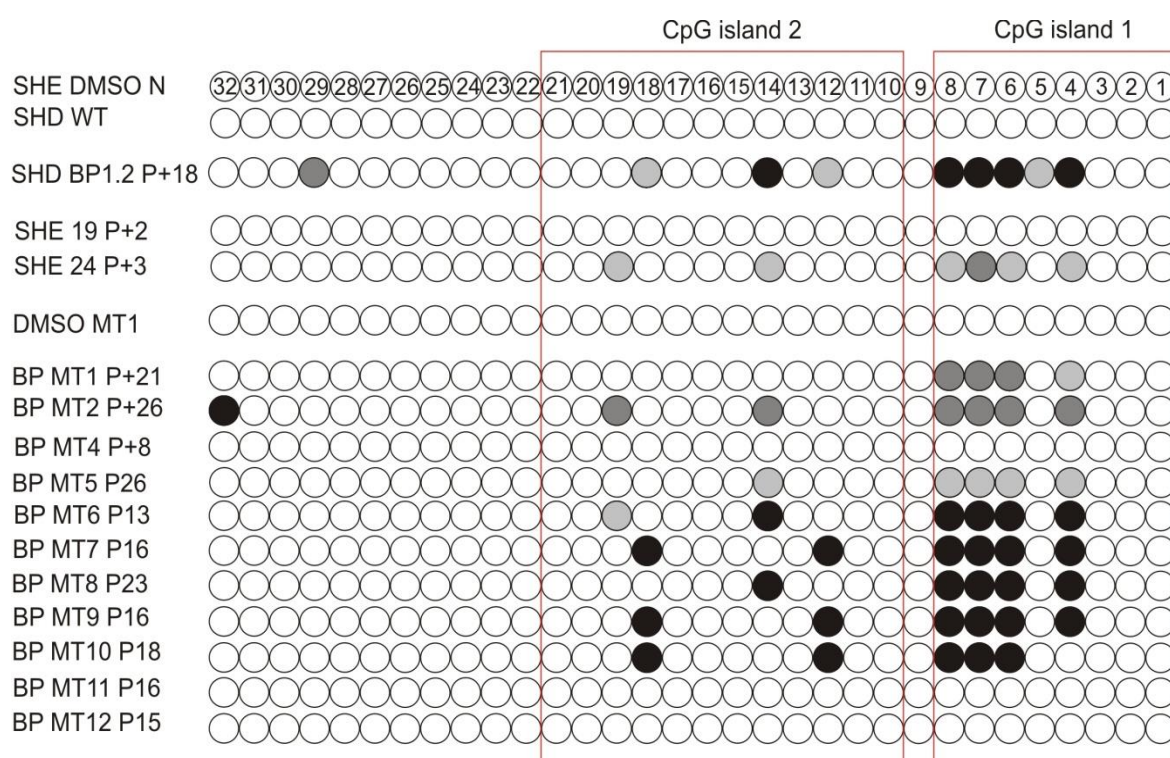


Figure 45– DNA methylation status of CpG sites in -457 bp upstream region of the SH *p16* transcriptional start site (TSS)

Bisulphite converted gDNA was amplified using bisulphite sequencing primers and *p16* 5'-promoter sequences analysed for DNA methylation at 32 CpG sites; CpG site 1 is downstream of the ATG start site (+14 bp) and CpG site 32 the most upstream (-440 bp). Empty (white) symbols indicate no methylation present. Black symbols represent those CpG sites in which over 50% of the 10 bacterial colonies analysed were methylated, dark grey symbols indicate methylation at CpG sites in 30 to 40 % of samples and light grey symbols indicate methylation in 20 % of samples at each CpG site. The negative controls included a SHD untreated sample and a non-transformed colony-derived SHE cell culture from the DMSO treated group. The positive control (SHD BP1.2) is known to be methylated from work on SHD cells (Yasaei et al., 2013).

Demethylation of immortal SHE MT colony derived cells increases p16 expression

To generate further evidence linking DNA methylation with the regulation of *p16* expression, 4 immortal SHE MT colony-derived SHE cell types were demethylated using the methyltransferase inhibitor 5'-Aza-2'-deoxycytidine (5-aza-dC). Immortal BP MT2, BP MT6, BP MT7, BP MT8 plus a wild type SHE primary control (SHE 2B) were treated twice with 5 μ M 5-aza-dC and then monitored for the following 3 weeks. All treatments per cell type were performed simultaneously and in duplicate.

Cell counts of treated plates were taken after 24, 48 and 96 hours following exposure to 5-aza-dC and from then on every two to three days (Figure 46). After plating and treatment total cell numbers increased and only a few floating cells were present in treated groups between 24 and 48 hours. There was no measurable difference in the rate of growth in cells treated with the vehicle control DMSO compared with untreated SHE cells of the same cell type, with the exception of SHE 2B where DMSO (Figure 46A) seemed to have a positive effect on proliferation in the first two days following treatment. Differences in the numbers of cells counted between day 1 and day 2 in SHE 2B may have been a result of unequal seeding as cell counts were taken from different plates that were harvested for RNA or DNA. Following 48 hours, the rate of growth was the same between untreated and DMSO treated SHE 2B cells otherwise indicating the cells behaved in the same way.

Following treatment with 5-aza-dC, the immortal cell cultures' rate of population doubling decreased dramatically from day 4 compared with their untreated and DMSO-treated controls. This was accompanied by a change in cell morphology shown in images taken at day 4 and day 10 after exposure to 5-aza-dC (Figure 47). Morphological changes were especially pronounced in BP MT7 (D) treated cells which became enlarged, flat and senescent. After 10 to 12 days in culture, treated cells started to recover and patches of mitotic cells became visible across the cell dishes (Figure 48). However, BP MT7 did not recover and remained senescent. Cell proliferation was also decreased in the control primary SHE 2B culture despite its unmethylated *p16* promoter status (Figure 46A).

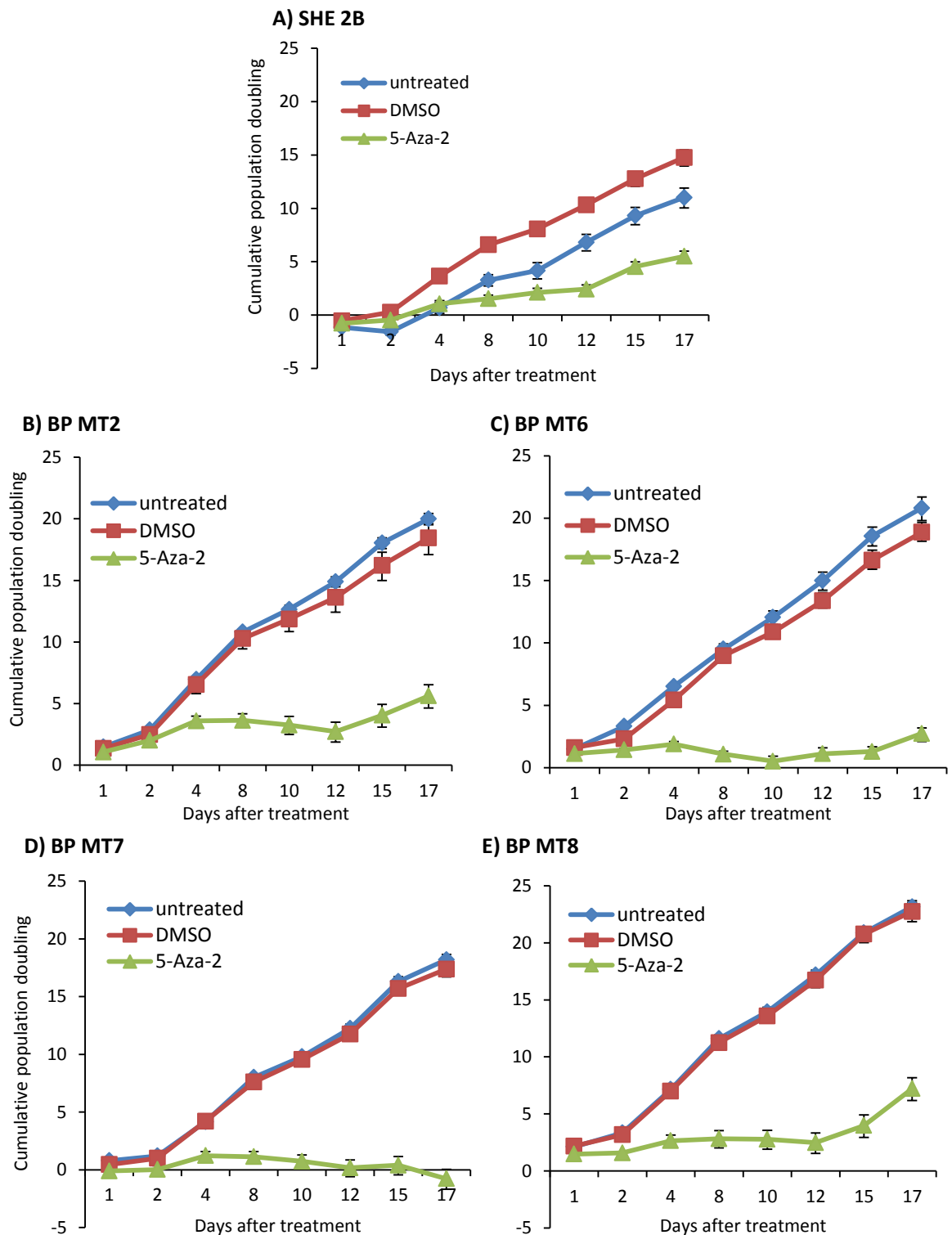
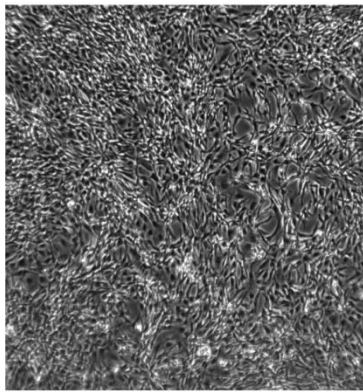


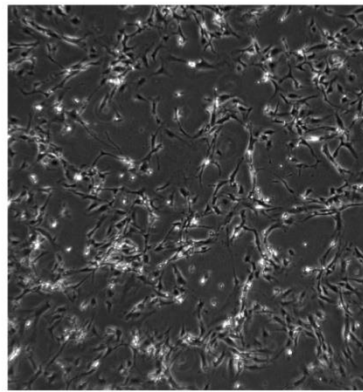
Figure 46 – Growth curves for SHE cells treated with the demethylating agent 5-aza-dC

SHE cell growth was monitored following a 24 hour exposure to 5 μ M 5-aza-dC for a period of 3 weeks. Cells were counted over a period of 17 days; population doublings (PD) were calculated and plotted. Error bars represent the standard deviation from the cumulative PD mean.

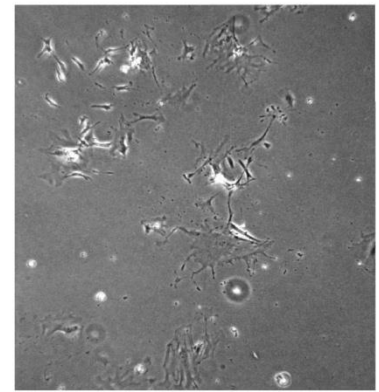
A) SHE 2B



untreated day 4

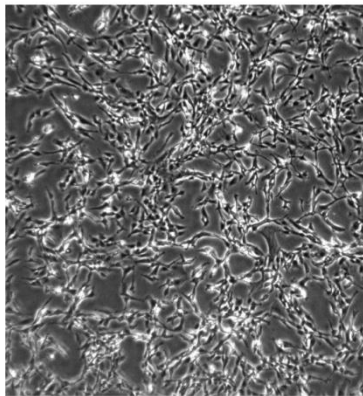


treated day 4

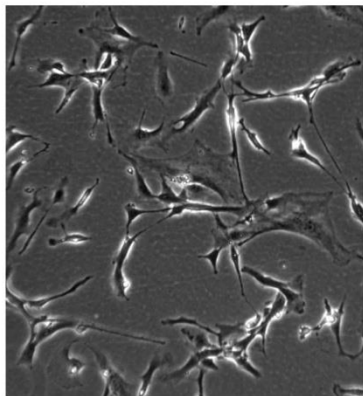


treated day 10

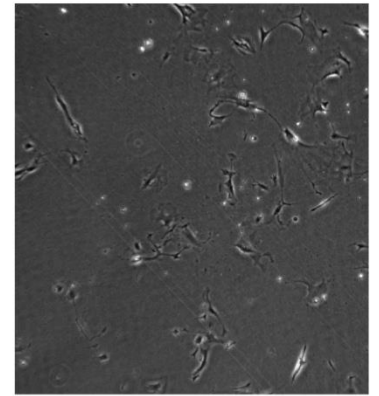
B) BP MT2



untreated day 4

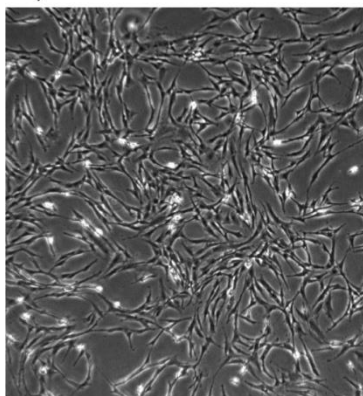


treated day 4 200 μ m

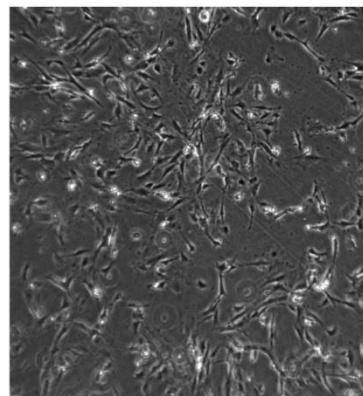


treated day 10

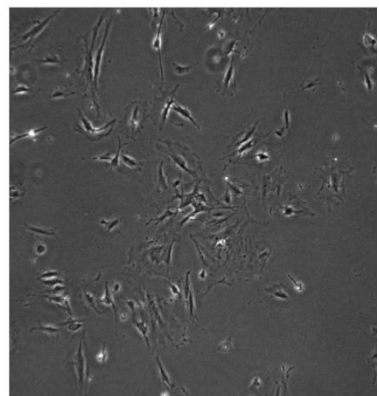
C) BP MT6



untreated day 4



treated day 4

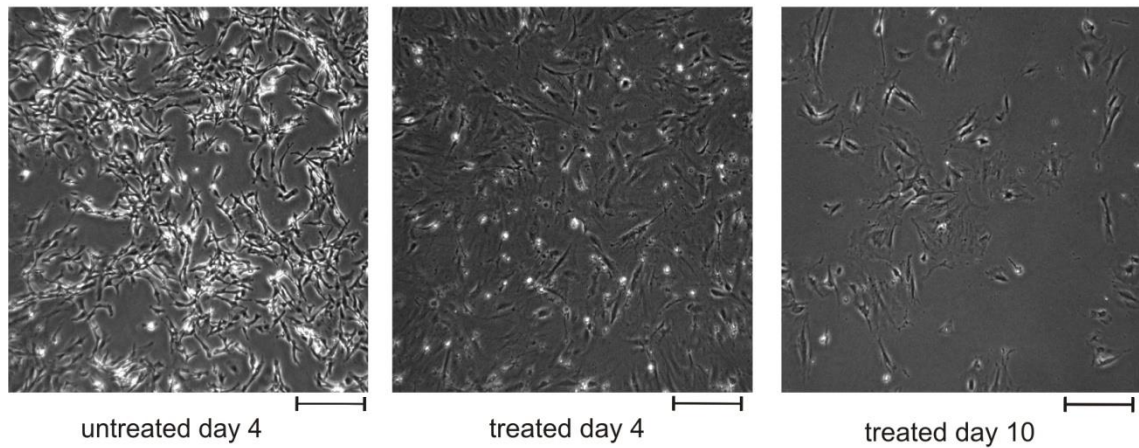


treated day 10

500 μ m

Continued on next page

D) BP MT7



E) BP MT8

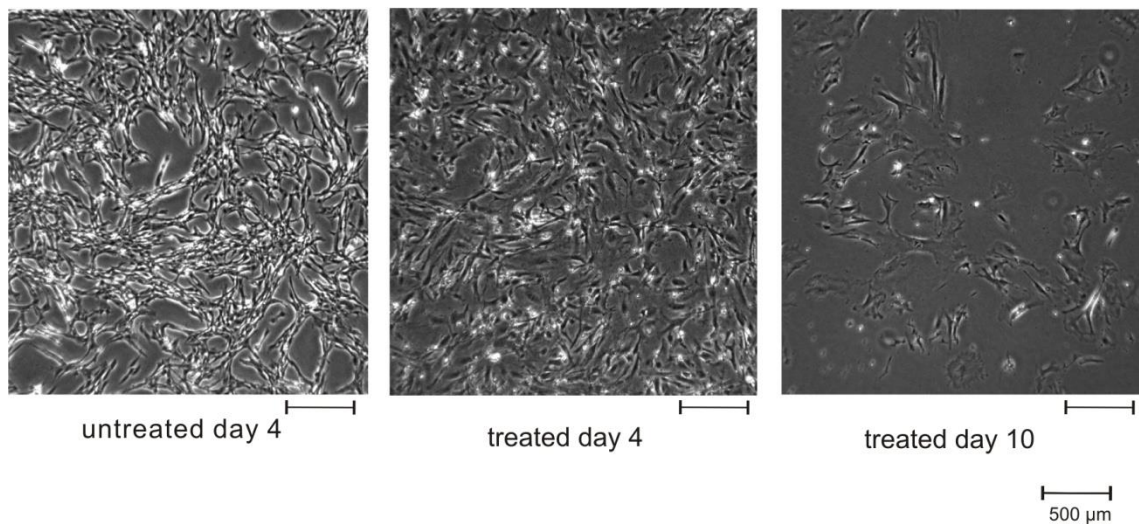


Figure 47 - SHE cells treated with the demethylating agent 5-aza-dC are visibly altered

SHE cell growth was monitored following two doses of 5 μ M 5-aza-dC for a period of 3 weeks. After 4 days, changes in cell appearance were noticeable and more so 10 days following treatment treated cells became enlarged, contained fewer visible mitotic cells compared with the untreated and vehicle control treated (not shown) counterparts and the population doubling level decreased. Phase contrast images were taken using a Carl Zeiss microscope at 4 X magnification.

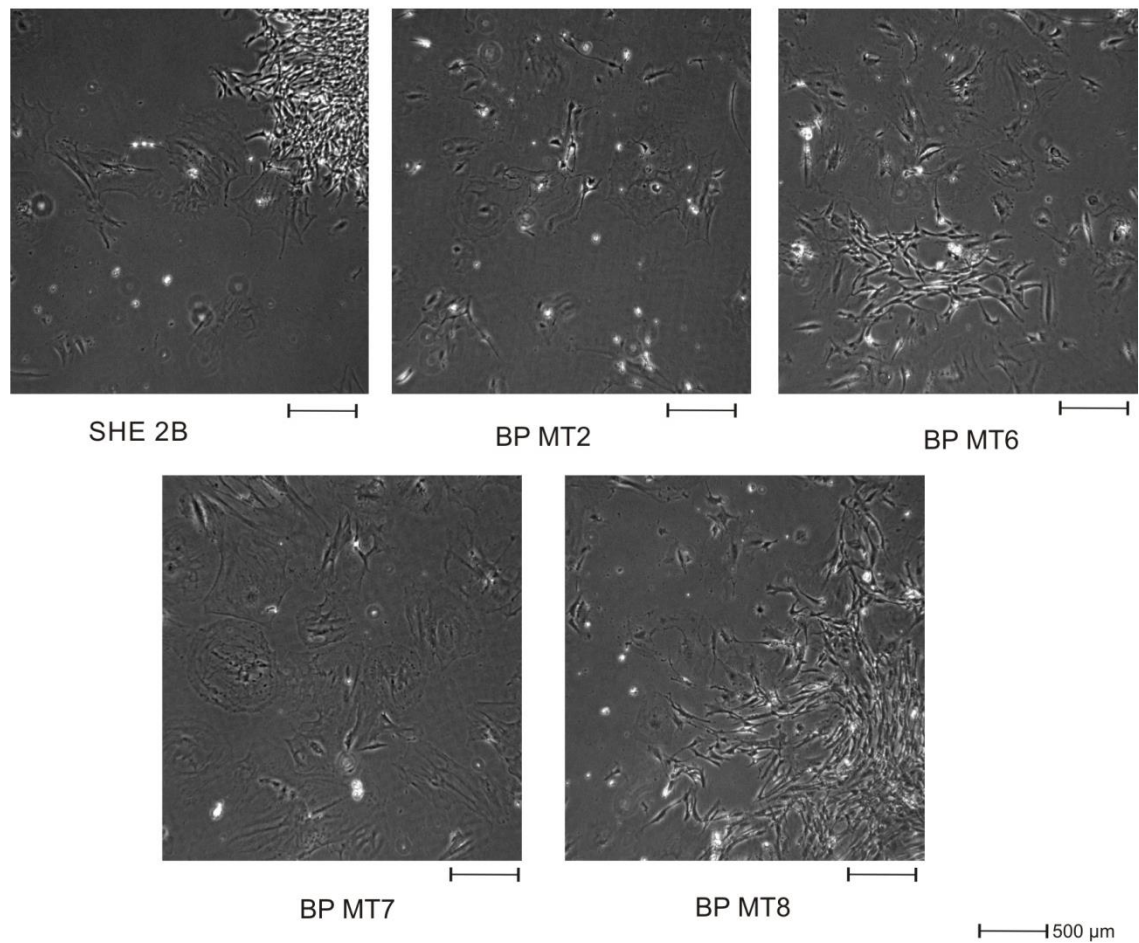


Figure 48 – Cell recovery occurs after 10 to 17 days following methyltransferase inhibition

After 17 days in culture cell recovery from treatment and demethylation was clearly visible as patches of proliferating cells on the cell dishes were identified. However, this was not the case for BP MT7 (D22 #2) which ceased to proliferate following treatment and stained positive for SA- β gal.

Senescence-associated beta-galactosidase staining (SA- β gal) was carried out on 5-aza-dC treated cells. Senescent cells are thought to have increased lysosomal activity which decreases the cytosolic pH levels and reacts with the SA- β gal stain producing a blue precipitate (Kurz et al., 2000). The proportion of SA- β gal positively-stained cells increased in 5-aza-dC treated SHE cells compared with the same untreated cell type and DMSO treated control. Representative images of stained colony-derived SHE cells from BP MT2 (A) and BP MT7 (B) are shown in Figure 49, there is little or no blue precipitate formation in the untreated and vehicle control stained dishes. Figure 50 shows the average percentage of cells that stained positive for senescence after 10 days in culture following exposure to the demethylating agent. The overall average staining background for untreated and DMSO treated SHE cells was 4.3 % and 5.1 % respectively indicating that the vehicle control had little if any effect on senescence induction, and this was confirmed in the growth curves shown in Figure 46. The treated control SHE 2B had the lowest percentage of stained cells (22.7 %) whereas the cell line that did not recover BP MT7 (D22 #2) had the highest percentage of SA- β gal cells (45.3 %) the staining of which is shown in Figure 49B. Similar results were identified after 16 days of treatment although the percentage of positively stained demethylated cells was reduced due to recovery and increased growth rates. In the case of BP MT7 treated cells however, after 16 days 70.0 % of cells stained positive for SA- β gal which correlated with a further increase in the number of senescent cells over time as a result of 5-aza-dC exposure.

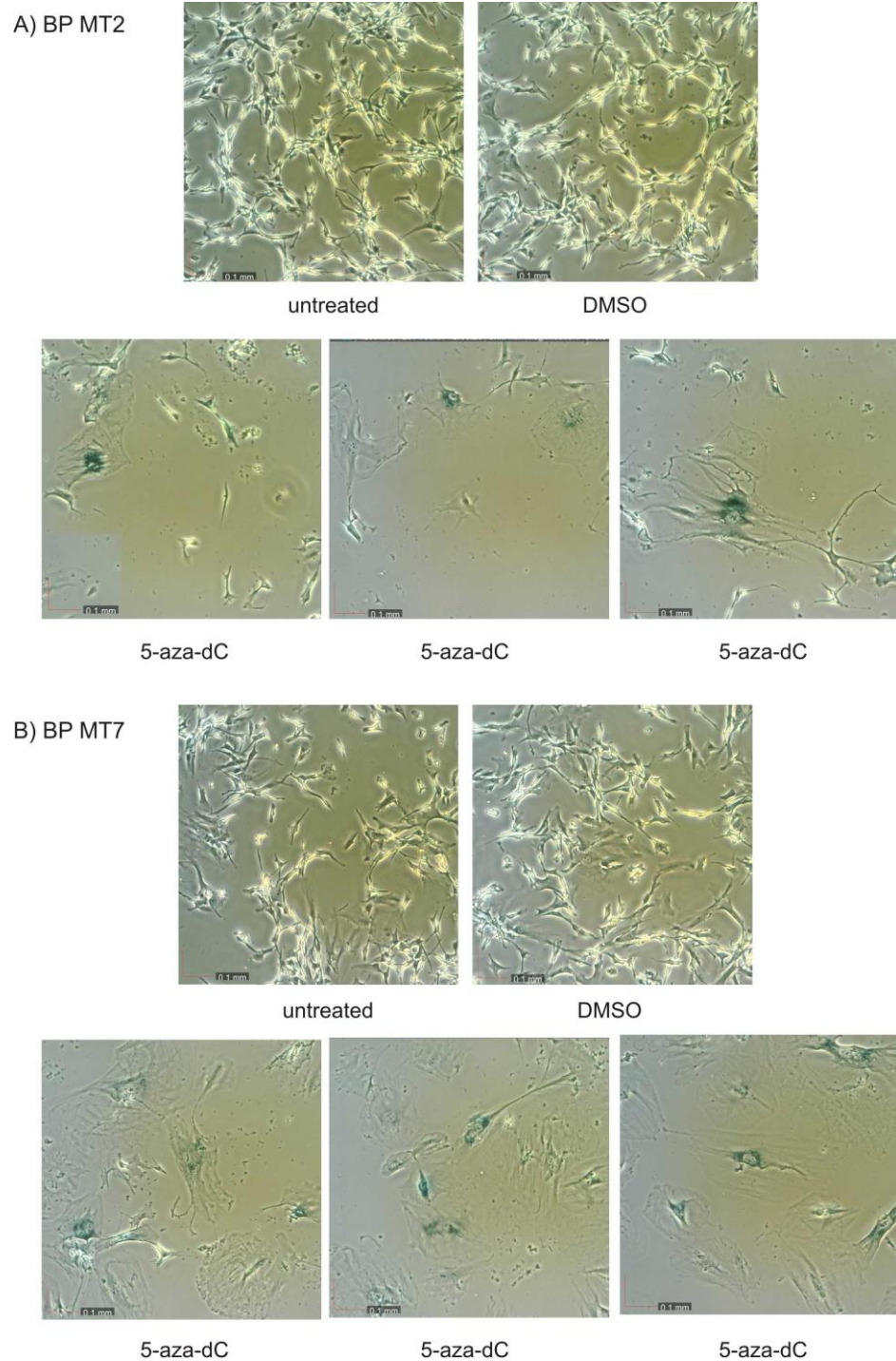


Figure 49 – Senescence associated beta-galactosidase (SA- β gal) staining increases following treatment with 5-aza-dC

Representative images of untreated and 5-aza-2'-deoxycytidine treated immortalised colony-derived SHE cells stained for SA- β gal after 10 days. 24 hours after seeding, cells were treated with 5 μ M 5-aza-dC for 24 hours and grown for up to 3 weeks. Senescent cells stain positive for SA- β gal and a blue precipitate is formed. Images were taken with a Olympus CK40 microscope with a Dino-Eye digital eyepiece (Dino-Lite) and DinoCapture v2.0 Software (magnification 4 X).

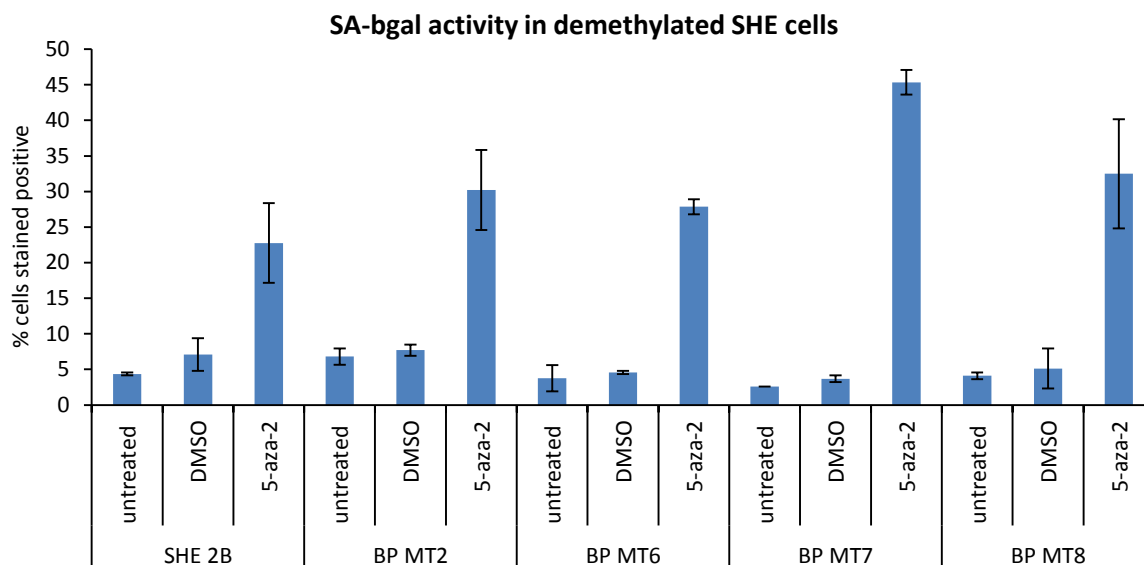


Figure 50– Demethylated SHE cells stain positive for SA- β gal

Percentage of SA- β gal positive population in immortalised colony-derived SHE cells treated with 5 μ M 5-aza-dC after 10 days in culture. Positive cells stain blue and an increase in beta-galactosidase activity is thought to be a general marker of cellular senescence. Plates for each treatment were stained in duplicate and the percentage of blue cells calculated; at least three different areas per plate were counted, (minimum of 100 cells counted) and the average values taken for each replicate. Error bars represent the standard deviation from the mean.

Gene expression levels of *p16* in demethylated SHE MT colony derived cells were measured using qPCR to establish if the observed increases in cellular senescence and reduced rates of division could be explained by an elevation of *p16* gene expression; *p15* gene expression was also quantified to see if it too may have been regulated by DNA methylation (data not included). cDNA was prepared from RNA samples taken from treated cells between 24 hours and 8 days after treatment with 5-aza-dC. Two biological replicates were prepared per 5-aza-dC treated time point and the average expression value compared to untreated cells taken at 24h, 48h, day 4 and day 8. Cells treated with DMSO were also included to account for changes in gene expression following exposure

to the vehicle control at the same time points. As with the untreated control, the average relative quantities (RQ values) are plotted for DMSO treated-cells in Figure 51.

Following the supposed inhibition of methyltransferase enzymes, there was an increase in gene expression of *p16* compared to untreated controls in B(a)P-induced immortalised SHE cells at 4 and 8 days after 5-aza-dC treatment; but not before 48 hours (see Figure 51). This was the case for all five cell lines treated, including the primary wild type SHE cells (Figure 51A, SHE 2B). The relative quantities of *p16* transcripts between untreated and DMSO controls were virtually equal amongst each cell type tested, indicating the vehicle control had little or no effect on the cells in terms of *p16* expression. The increase in expression was most noticeable after 8 days in SHE BP MT8 (E) where there was a statistically significant 15 fold difference in transcript levels compared to untreated SHE BP MT8. SHE BP MT2 (B) and BP MT 7 (D) showed an 8 and 6 fold increase in expression compared with their untreated controls after 8 days following demethylation respectively, which was also found to be significant. Lastly, treatment with 5-aza-dC led to higher levels of *p16* in BP MT6 (C) after 4 and 8 days, but the increase was reduced (under 4 fold) compared with the other cell lines with known methylated *p16* promoters. This was akin to the increase in gene expression identified in the wild type primary SHE cell type which is not methylated at the *p16* promoter.

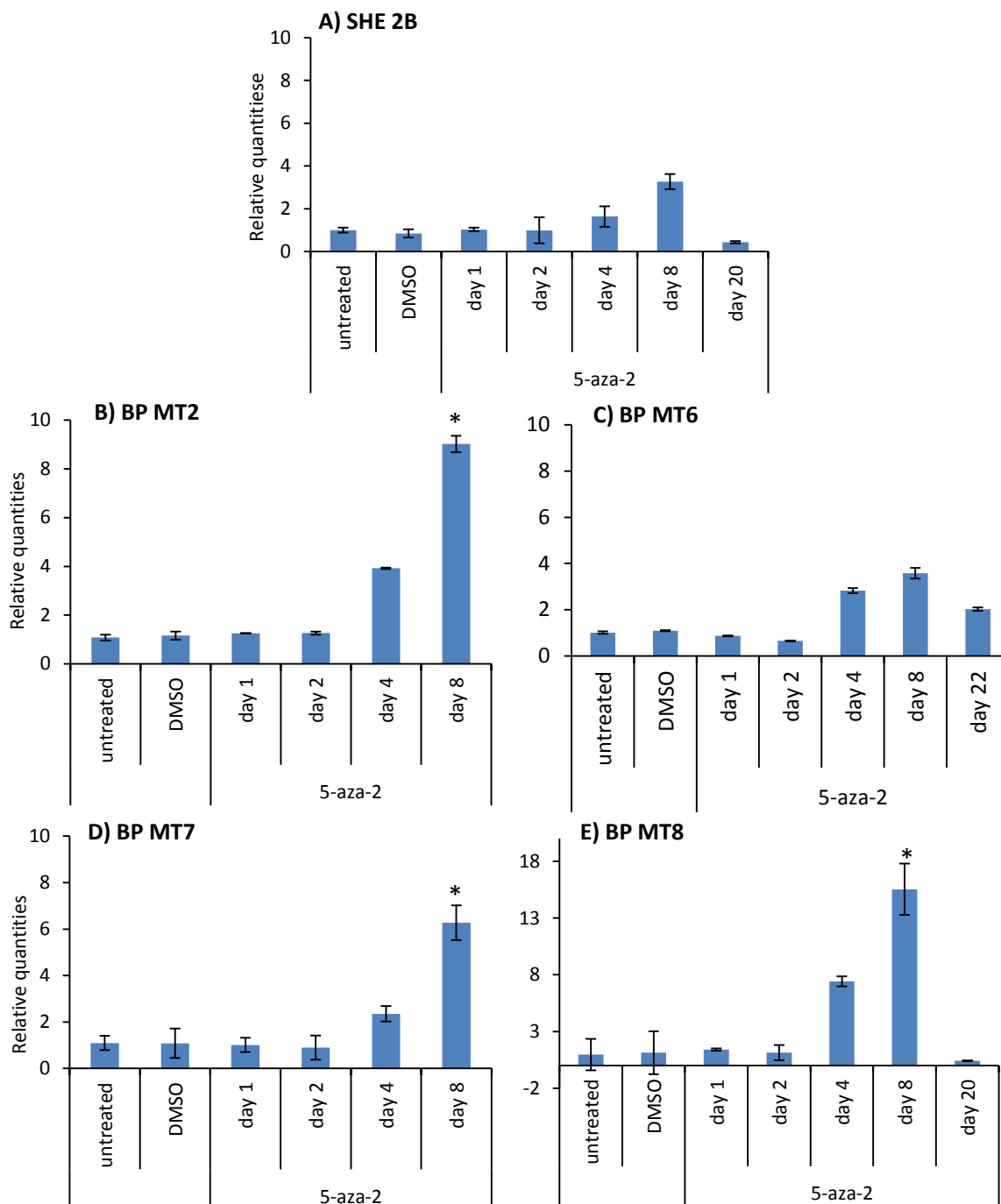


Figure 51 – *p16* transcript levels following treatment with 5-aza-dC

At various time points following treatment with 5-aza-dC, *p16* mRNA expression was measured by qPCR (SYBR green) in selected BP-induced SHE immortal clones with known methylated *p16* promoters. Expression was normalised to reference genes *beta-actin* and *GAPDH*, samples were calibrated to the average NRQ value of untreated controls (n=4) of the same cell type. Treated time points plotted are the average of n=2 with each cDNA prepared in duplicate and run in triplicate (6 technical repeats per biological sample). Error bars represent the standard deviation from the average. Significance (*) was calculated using unpaired t-tests ($p < 0.02$).

To confirm that the exposure of immortalised SHE-MT cells to 5-aza-dC caused demethylation of the *p16* promoter (Figure 51) bisulphite sequencing was repeated on the treated SHE samples 4 and 8 days after treatment using the same bisulphite sequencing primers. (The experiments for this section were carried out with the help of undergraduate student Lisa McGinty). As described in section 6.2.1, a minimum of 10 colonies per gDNA sample and time point were sequenced to estimate the percentage of genomic DNA that is methylated at CpG sites immediately upstream of the *p16* gene promoter. Given that 5-aza-dC acts by inhibiting the enzymes responsible for transferring methyl groups its effects should be expected to take place after at least one population doubling, as DNA methyl groups ought only to have been lost once the genome has gone through a full round of replication.

Figure 52 compares the *p16* promoter methylation profile of untreated SHE BP MT cells with the respective 5-aza-dC treated cells after 4 and 8 days. As expected there was no methylation in the primary untreated SHE cells (SHE 2B) and this remained unchanged following demethylation. Incubation of BP-induced, immortal SHE cells with 5-aza-dC strongly reduced the extent of methylation in *p16* 5' CpG Island 1 in BP MT7 and BP MT8 from 100 % methylation in picked colonies to 20 % or less. Demethylation correlated well with the previously observed increase in *p16* expression from day 4 after treatment with the methyltransferase inhibitor (Figure 51). Demethylation in colony-derived cultures was retained for up to 8 days following treatment. Partial methylation in CpG island 1, identified in untreated BP MT2 (grey dots, Figure 51 and Figure 52) was removed by methyltransferase inhibition for up to 4 days but re-instated after 8 days following treatment. This indicates the reversibility of demethylation caused by treatment with 5-aza-dC, and proved that treatment with 5-aza-dC can lead to a loss of DNA methylation at the *p16* promoter which was retained for at least 4 days. However, immortal BP MT6 retained its methylated promoter status (methylation at CpG sites in black were found in 50 % of bacterial colonies) suggesting that in this cell line, either methyl groups at CpG sites were replaced before 4 days following treatment or that demethylation by 5-aza-dC did not take place at the *p16* promoter in this cell line.

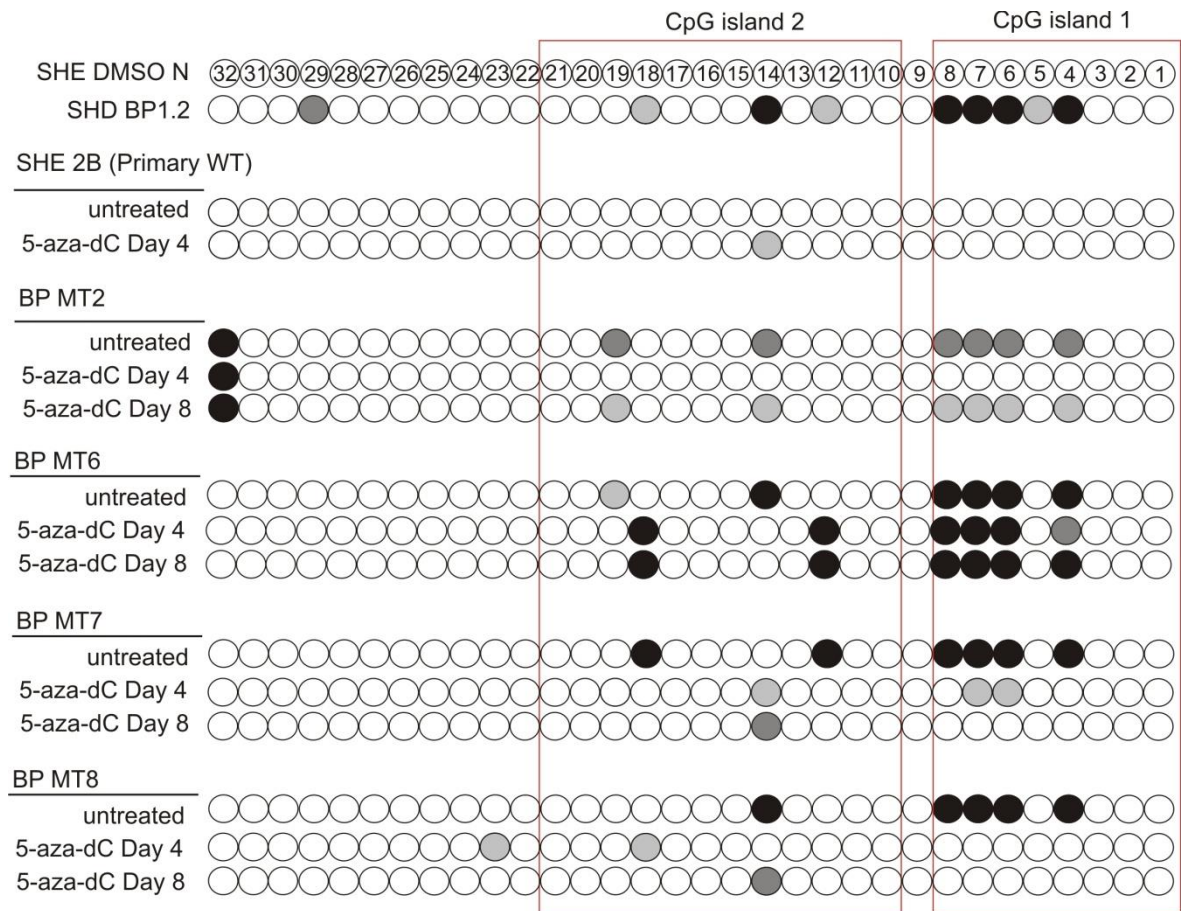


Figure 52 – Following exposure to 5-aza-dC there is a reduction of DNA methylation in the *p16* promoter after 4 and 8 days

Cells were treated with the methyltransferase inhibitor 5-aza-dC and DNA was extracted from cells 4 and 8 days after exposure. Bisulphite converted gDNA was then amplified using bisulphite sequencing primers and *p16* 5'-promoter sequences were analysed for DNA methylation at 32 CpG sites; CpG site 1 is closest to the ATG start site and CpG site 32 is the most distant. A minimum of 10 colonies per sample were analysed. White (empty) symbols indicate no methylation, black symbols represent >50% methylation, dark grey symbols represent methylation at 30-40% of samples and light grey symbols in 20% of samples at each CpG site.

6.4 Discussion

In this Chapter it was sought to establish if *p16* expression in immortalised SHE-MT colony-derived cultures was regulated by DNA promoter methylation and if removal of aberrant methyl groups in its promoter region could restore *p16* transcript levels or even reactivate senescence pathways.

Strong patterns of DNA methylation at the *p16* promoter were initially observed in 40 % of immortal, morphologically transformed (MT) samples originally induced by benzo(a)pyrene. Almost all B(a)P-induced MT clones tested (methylated or unmethylated) expressed low levels of *p16* compared to DMSO-treated non-transformed clones and failed engage senescence pathways. Two B(a)P-clones with extensive methylation at their *p16* promoter site (100 % of colonies tested at 5-6 CpG sites – BP MT7 and BP MT8) on average expressed 20-40 % of *p16* transcripts found in DMSO-non transformed control levels. Whereas BP MT1, BP MT2 and BP MT5 that were partially methylated at similar targeted CpG sites expressed 20-50 % of control *p16* mRNA levels. In BP MT immortal clones with unmethylated DNA, BP MT11 and BP MT12 *p16* transcripts were slightly reduced to 70 %-80 % of transcripts. However, the *p16* promoter in BP MT6 was found to be 50 % methylated and its gene expression was similar to the DMSO-control group following secondary events. Therefore the methyl status of the *p16* promoter was not fully predictive of its expression in SHE cells and nor was the determined extent of methylation.

Following incubation with the demethylating agent 5-Aza-2'-deoxycytidine, *p16* expression was strongly upregulated in BP MT2, BP MT7 and BP MT8, even when its promoter locus was originally not fully methylated (BP MT2 <50 % methylated). The temporary removal of methyl groups probably due to methyltransferase inactivation, correlated to an increase in *p16* expression, a reduced level of growth, and an increase in the proportion of senescent cells. In one instance, treatment had a permanent effect on the BP MT7 clone which following demethylation ceased to proliferate completely. Removal of methyl groups in BP MT6 was not confirmed but *p16* expression did increase 4-fold compared to untreated BP MT6; the relative increase was similarly observed in the

treated unmethylated control (SHE 2B). It is unknown if methyl groups were reinstated before the 4 days following treatment in this cell line or if they were never removed.

Methyl-specific PCR and bisulfite sequencing

Data obtained from bisulphite sequencing offers a more comprehensive and reliable view of the extent of DNA methylation compared to methyl-specific PCR (MSP) across a larger number of CpG sites which are individually analysed. In contrast, data generated by MSP only targets CpG sites contained in MSP primer sequences irrespective of the methyl-status of amplified PCR products, but can be considered suitable as an initial indicative screen. Both *p16* promoter and exon 1 α were tested using MSP primers in colony-derived SHE-MT cells (Figure 42) and PCRs for each were repeated several times. Amplification via MSP of methylated products for *p16* exon 1 α (MSP2) in colony-derived SHE cells (Figure 42B) was reproducible across different batches of bisulphite converted DNA. B(a)P-induced, immortal SHE BP MT1 was found to be methylated in exon 1 α as was the SHD positive control and both were shown to have reduced levels of *p16* transcript when analysed via real-time PCR [Figure 31 and (Yasaei et al., 2013)]. Aberrant methylation of *p16* exon 1 α has also been associated with downregulation of gene expression in SH pancreatic tumours at a frequency of 46.7 % induced by BOP (Li et al., 2004) and of 26.5 % induced by DMBA (Li et al., 2008). In B(a)P-induced immortalised SHE cells, the frequency of methylation in the *p16* exon 1 α was only of 8.3 % (1 out of 12) albeit this sample (BP MT1) was downregulated for *p16*.

On the other hand, MSP data generated using MSP1 *p16* promoter primers and immortalised SHE samples were inconsistent depending on the batch of bisulphite converted gDNA generated and also between PCR replicates. Unmethylated promoter primer targets were always amplified and the inconsistency noted from methylated promoter MSP primers. This could be due either to incomplete bisulphite conversion or unspecific primer annealing by oligonucleotide binding to both methylated and unmethylated DNA. Bisulphite sequencing provided more reliable data concerning the methylation status of CpG sites from -440 bp and +14 bp to the *p16* TSS (Figure 45). This compensated for the unreliability of the MSP data, although a CG rich sequence could have been incorporated in the analysis to assess the efficiency of the bisulphite conversion process in addition to the positive control. Bisulphite sequencing confirmed

that the CpG sites recognised by MSP1 primers were not methylated but fully converted to thymines, explaining why no PCR amplicons were visualised in reactions containing methylated DNA primers, as shown in Figure 42A.

Sites of DNA methylation

It has been suggested from DNA methylation studies in rats, that the status of the promoter of *p16* is more predictive of gene expression levels than the methylation status of exon 1 α , with particular importance assigned to CpG sites between the regulatory TATA box and *p16* transcriptional start site (TSS) (Abe et al., 2002, Honoki et al., 2004). In B(a)P-induced SHE immortal clones it was observed that commonly targeted CpG sites were flanked by the predicted TATA box and known TSS for SH *p16* (Figure 45). No methylation took place at the TATA box itself but the sites immediately upstream of it were methylated. From the bisulphite sequencing data it was shown that 40 % of immortal SHE cultures induced with B(a)P were extensively methylated in CpG island 1 of the *p16* promoter and a further 27 % of B(a)P-induced samples were partially methylated at the same CpG sites (4-8). Data obtained from chemically induced SHD clones (Yasaei et al., 2013) also identified similar CpG sites of methylation in close proximity to the *p16* TSS induced by soluble nickel and B(a)P.

Reversibility of treatment

Treatment of SHE cells with 5-aza-dC was performed on proliferating cells for 24 hours to allow at least one round of DNA replication to take place within the whole population. As a result silencing methyl groups located at the *p16* promoter were lost in 3 out of 4 BP-induced colony-derived SHE cells treated with the pro-drug 5-aza-dC. Following incubation with the pro-drug, metabolised 5-azacytosine rings are incorporated into DNA instead of cytosine residues. As methyltransferases target DNA to catalyse the addition of methyl groups, the covalent bond between enzyme and azanucleoside cannot be eliminated meaning that they remain attached. This causes a depletion of methyltransferases and thus the addition of methyl groups cannot take place (Stresemann and Lyko, 2008). Removal of epigenetic methyl marks was observed after 4 days and mostly retained for up to 8 days before recovery and re-instatement of methyl groups at CpG sites. Treated cells became phenotypically enlarged and senescent with increased percentages of cells staining positive for SA- β gal, along with dramatic

reductions in proliferating cells compared to DMSO vehicle controls and untreated counterparts. Consequently, expression of *p16* was stimulated after 4 days of treatment, which tied in with removal of methylation only taking place after several rounds of replication and following methyltransferase inhibition. Inhibitory effects of 5-aza-dC were not permanent as patches of cell growth emerged after 2 weeks from treatment. Transcript levels of *p16* after 20 days were again substantially reduced suggesting reinstatement of promoter methylation. Interestingly, the re-instatement of methyl marks at the *p16* promoter after 8 days in demethylated samples was not identical to patterns identified in their untreated counterparts. Differences were found in CpG sites located in CpG Island 2 which were not commonly methylated in all BP-induced immortal SHE cells (i.e. not CpG sites 4-8). These may be secondary regulatory CpG sites.

Biological effects

Finally, there are a number of publications suggesting that the association between 5-aza-2'-deoxycytidine and demethylation, leading to the induction of senescence, is non-causal and that, in fact, its mode of action is methylation-independent. These studies mostly focus on the cytotoxicity of the pro-drug and describe demethylation as just one consequence of the treatment. Unsurprisingly, cellular responses vary greatly depending on the administered concentrations as well as the length of exposure (Liu et al., 2013), which may also impact the drug's mode of action. Using embryonic stem (ES) cells, (Juttermann et al., 1994) observed that the reduced enzymatic activity of methyltransferases led to increased resistance of 5-aza-dC-induced cytotoxicity. The study concluded that demethylation was a secondary event and that 5-aza-dC-induced cytotoxicity is primarily a DNA damage response caused by binding of azacytosines to the DNA. Activation of ATM and ATR pathways were observed following a 72-hour time course of 5-aza-dC treatment along with increased double strand breaks and G₂ growth arrest (Palii et al., 2008), indicative of direct DNA damage. 5-aza-dC was cytotoxic in *p16* and *ARF* siRNA knockdowns and caused growth arrest in cells without methylated *INK4a/ARF* promoters as well as in lines overexpressing *p16* and *ARF* (Xiong and Epstein, 2009). This led to the prediction of a 5-aza-dC *p16*-independent mechanism that is capable of causing growth-arrest. In the same study, exposure to 5-aza-dC restored *INK4a/ARF* expression in a cell line with promoter methylation, but restoration of

expression was not enough to inhibit cell growth. These results to a certain degree are similar to those presented here, in so far as there was a decrease in cell proliferation following 5-aza-dC treatment in the primary SHE wild-type cell line SHE 2B that was shown to have an unmethylated *p16* promoter. This suggests 5-aza-dC influences cell growth and possibly senescence by *p16*-independent mechanisms and is consistent with the findings of Xiong and Epstein (2009) although data presented here in this Chapter do not extend beyond the influence of 5-aza-dC on the expression and methyl status of *p16*. Conversely, cell growth was inhibited in one immortal SHE cell line (BP MT7) following a 24 hour exposure to 5-aza-dC. Given that methylated SHE lines were shown to be demethylated at the *p16* promoter and gene expression increased after 4–8 days of treatment, the data presented here supports the idea that 5-aza-dC effects cell proliferation via the *p16* status. However, it must also have additional modes of action, such as activation of the DNA damage response or other pathways, since attenuated changes in proliferation and expression were also noted in the non-methylated control.

Conclusion

In conclusion, 40 % of B(a)P-induced clones were found to be abnormally methylated at the *p16* promoter and 27 % were partially methylated at common CpG sites. DNA demethylation was observed following treatment with 5-aza-dC at the *p16* 5' promoter which was retained for up to 8 days. This correlated with upregulation of *p16*, an increase in senescent cells and growth inhibition suggesting suppressive transcriptional role of DNA methylation in SHE cells. Given that treatment will have targeted methylation globally, we cannot state that 5-aza-dC treatment solely targeted *p16* to generate a reduction in cell growth or, indeed, that the drug acts via demethylation alone. In fact, the data supports the idea that additional regulatory pathways might be targeted other than those involving *p16*. Promoter methylation was not fully predictive of *p16* gene silencing, but was associated with a suppressive transcriptional role in SHE cells. In one instance a 6-fold increase in *p16* expression cells following treatment and demethylation seemed sufficient to induce terminal senescence (BP MT7). However, other MT BP lines also under-expressed *p16* and bypassed senescence barriers but were found to be unmethylated (e.g. BP MT4). It is proposed that DNA methylation of the *p16* promoter

can co-operate with other regulatory mechanisms to repress its transcriptional expression and induce senescence bypass in B(a)P-induced SHE clones.

CHAPTER 7

7 General Discussion

Conclusion and Future Perspectives

7.1 Discussion

Alternative methods of safety testing (i.e. to replace rodent bioassays) are in demand driven by recent EU legislation requiring a substantial reduction of animals used for carcinogenicity assessments, and a complete ban on their use in the cosmetic industry (EC, 2003a, EC, 2007a). The implementation of safety assessment in the context of the consumer, and our surrounding environment, is crucial for the development of novel drugs, chemicals and healthcare products. For successful *in vitro* screening, the selected test battery must be predictive of mutagenic/genotoxic agents plus ideally have the ability to detect non-genotoxic carcinogenicity. Previously, a positive result from standard *in vitro* assays (bacterial mutagenicity, mammalian cell cytogenetics/micronucleus tests) would normally have been confirmed by *in vivo* rodent bioassays which are now banned for cosmetics and becoming increasingly regulated for other chemical classes (Creton et al., 2012). Genotoxicity tests such as the Ames and micronucleus assays, which assess mutation rates and chromosome damage respectively, pick up genetic insult but can give *in vitro*-specific false positives and are not predictive of non-genotoxic carcinogenic modes of action such as transcriptional changes and epigenetic alterations (Vanparys et al., 2012). Cell transformation assays (CTAs) have been proposed as promising cell-based systems for chemical screening, although their routine implementation has not been supported by regulatory bodies, because an understanding of their molecular underpinnings is lacking (Farmer, 2002, Creton et al., 2012).

The Syrian hamster embryo cell transformation assay is an established CTA which has recently been pre-validated by ECVAM (Maire et al., 2012b, Pant et al., 2012, Corvi et al., 2012) and the formulation of OECD Test Guidelines is well advanced (Vasseur and Lasne, 2012). These pre-validation studies assessed the assay's reproducibility under two commonly used pH conditions (pH 6.70 and pH 7.0-7.35) (Maire et al., 2012b, Pant et al., 2012) and resulted in a standardised recommended protocol (Maire et al., 2012a) along with colony photo-catalogues to try and address the subjective nature of the assay's endpoint (Bohnenberger et al., 2012, Maire et al., 2012c). Certainly, without proper training and expertise, the SHE CTA is troublesome due to its subjectivity; every colony must be independently scrutinised for its growth patterns and scoring is performed by eye. The heterogenic nature of the embryo-derived cell population is one of the assay's

strengths as more than one cell type can be tested simultaneously, but this diversity means that the variety of colony morphologies complicates the scoring process. Discrimination between non-transformed (N) and morphologically transformed (MT) colonies is subject to several influencing factors which, depending on the toxicologist performing the assay, may be given more or less weight in making the decision (i.e. transformed versus non-transformed). As noted in the case of the MT colonies scored during this project (presented in Chapter 3) there exists a range of MT phenotypes and this is also addressed in the published photo-catalogues (Bohnenberger et al., 2012, Maire et al., 2012c). The frequency of MT (MTF) induced by benzo(a)pyrene (5 µg/mL) in the pre-validation studies varied slightly across the different laboratories involved; 1-3 % MTF at pH 6.7 (Pant et al., 2012) and 2-6 % MTF at pH 7.0 (Maire et al., 2012b) and highlights the importance of standardising the cell batch for testing (the highest MTFs at pH 7.0 were obtained using a different batch of SHE cells). MTF values (presented in section 3.3) were substantially higher which in part is likely to have been due to a lower seeding density used (Dafou, 2003) to permit accurate colony picking and the replacement of irradiated feeder layers with conditioned medium, which was observed to produce a minimal increase on MTF (Pant et al., 2008, Maire et al., 2012a). Scoring of colonies in my experience was far from straightforward and, although the differences between normal and transformed colonies in many cases were clear-cut, the call between MT and 'altered' phenotypes (LeBoeuf et al., 1990, Bohnenberger et al., 2012) was on occasion difficult to make with any confidence. Altered colonies are those that display 'partially transformed' phenotypes but their lack of cell organisation and criss-crossed growth is less pronounced than in fully MT clones (LeBoeuf et al., 1990); scoring is highly subjective. Altered colonies are not to be included in the MTF calculation (Maire et al., 2012a) which, depending on the stringency of the criteria for scoring MT, dramatically changes the frequency of MTF. Hence, assay standardisation and thorough training are critical features to ensure success and reproducibility of this assay. The body of recent publications including pre-validation studies have addressed this and concluded that the SHE CTA is reproducible across laboratories. Therefore, with strict adherence to the appropriate OECD test guidelines, the assay could be fit for assessment purposes (Corvi et al., 2012).

Despite appropriate efforts to increase the SHE CTA's reproducibility, mechanisms underlying the assay's endpoint of morphological transformation (MT), and explaining the relationship of MT to genotoxic and non-genotoxic carcinogenesis, remain mostly undefined. This has further fuelled uncertainties in implementing the SHE CTA into regulatory applications (Creton et al., 2012) (DRP in progress – personal communication from Nathalie Delrue and Laurence Musset to RFN). Initial studies addressing neoplastic transformation in SHE cells, describe the induction of morphological transformation as an early event, linking it to the bypass of senescence which leads to unlimited growth potential. Immortal MT cell clones then progress further acquiring the ability to form anchorage independent foci in semi-solid agar and tumours when injected into nude mice (LeBoeuf et al., 1990, Isfort et al., 1996a). Although anchorage-independence assays were not performed in this project, the observed cell growth kinetics were similar to those previously identified, in so far as not all MT colonies immortalised (LeBoeuf et al., 1990). All normal colonies, regardless of exposure, entered senescence and stopped proliferating before they had undergone 35 population doublings from the single-cell stage (26 to 44 PD for LeBoeuf et al., 1990); in fact, a substantial proportion managed only one or two passages before entering senescence. Fewer than 10 % of B(a)P-induced MT colonies picked in the Brunel laboratories (6 in total) bypassed senescence barriers (and have reached over 100 PD of growth at the time of writing) whereas 22 % of BP MT clones sent to Brunel from BioReliance (4 out of 18) immortalised. LeBoeuf (1990) observed a background frequency of spontaneous immortalisation of 3 % in morphologically transformed colonies from control (DMSO-treated) dishes and similar frequencies in B(a)P non-transformed colonies. From the data obtained in this project only 1 DMSO MT colony continued to proliferate, giving a 5 % spontaneous immortalisation rate from the BioReliance cohort of colonies alone (there was no senescence bypass in any of the BP N colonies).

At least 45 % of MT colony-derived cells that immortalised were found to undergo and overcome a cell crisis phase, which took place between passages 4 and 12; at this point doubling times increased and cytoplasmic enlargement was observed in the majority of cells in culture; similar observations were made in previous SHE MT colony-derived studies conducted at pH 6.70 (LeBoeuf et al., 1990). Scoring of morphological

transformation, therefore, does not guarantee escape from senescence since over 70 % of MT SHE cells senesced before 35 population doublings. Senescence bypass was mostly attributed to MT cells that had been exposed to carcinogens and was much less common in spontaneously derived MT clones (10-22 % in BP MT compared to 0-5 % in DMSO MT). Observation of cellular crisis and a senescent-like phenotype in >45 % of MT colonies confirms that the acquisition of unlimited proliferative potential requires additional, probably stochastic, events (Trott et al., 1995, LeBoeuf et al., 1990).

Immortal SHE cell lines continued to proliferate beyond 100 population doublings but did not necessarily retain their MT phenotypes. Clonally-derived proliferating cells emerging after cell crisis eventually formed monolayers that had lost criss-crossed growth patterns and, when approaching high cell density, were contact inhibited. The same pattern was also seen with the single spontaneous immortal DMSO MT1 line that was generated. Retention of MT characteristics is not necessary for malignant transformation, although may be required for anchorage-independent growth *in vitro* (LeBoeuf et al., 1990). However studies by Barrett et al., (1979) indicated a strong relationship between anchorage independent growth (AIG) in semi-solid agar of immortal MT colony-derived cells and *in vivo* tumour formation; this tendency increases with passaging and was estimated to take between 32-75 population doublings to acquire (Barrett et al., 1979, LeBoeuf et al., 1990). This is consistent with the notion that immortalisation and senescence bypass are only the first necessary steps towards progression to malignancy. Further work would be needed to confirm the neoplastic potential of SHE MT colonies produced in this study.

The actual mechanisms that lie behind morphological transformation are still unclear (Creton et al., 2012). The data presented in this project highlight the fact that morphological changes are not sufficient for the cells to escape senescence, but that colonies containing transformed cells have a higher probability of generating immortal cell lines that may then go on to acquire malignant characteristics. No unique predictive attribute (prior to colony picking) was visually identified in MT colonies later capable of evading senescence that could enable them to be distinguished from those that ceased to proliferate (again subjective). Efforts by others have been made to render the scoring process more objective, such as the application of computerised image analysis to detect

changes in colour, cell organisation and texture (Ridder et al., 1997) and of Fourier-transform infrared (FTIR) microscopy, which has been employed to identify biochemical fingerprints in SHE MT cells (Walsh et al., 2009, Ahmadzai et al., 2012b). By using the colony scraping technique for MT colony isolation and further culture, half of each MT colony was propagated and the remaining half stained and observed microscopically to confirm the MT phenotype. By combining objective colony analysis and establishing colony-derived cultures, early stage differences might be identified between MT clones which have the capability to immortalise and those that are already programmed for entry into senescence. Another approach could be the use of alternative staining agents to Giemsa which may be more discriminatory. For example, given that many of the MT colonies picked underwent growth-arrest after only one or two passages from picking, senescence-associated beta-galactosidase staining might be predictive of cell growth potential (Kurz et al., 2000) although it has been known to be influenced by cell type and cell density.

Molecular analysis of the resulting immortal SHE colonies generated from the SHE CTA has provided further insight into induced carcinogenesis by benzo(a)pyrene and expands the evidence of the Syrian hamster being a mechanistically relevant model for studying the bypass of cellular senescence (Russo et al., 1998, Trott et al., 1995). Studies using SH dermal fibroblasts characterised events leading to senescence bypass induced by a panel of carcinogens using a mass culture approach (Yasaei et al., 2013); from this work it was evident that exposure to different carcinogens (both genotoxic and non-genotoxic) resulted in molecular fingerprints reflecting their mode of action. For example, irradiated SHD clones that immortalised suffered from a physical loss of the *CDKN2A/B* locus spanning over 37 KB of genomic content and encoding *p16*, *p15* and *ARF*, whereas the non-genotoxic human carcinogen nickel chloride induced transformation by silencing *p16* expression epigenetically by DNA methylation at its promoter (Yasaei et al., 2013). The immortal clones generated from soluble nickel and IR are presumed to have been generated by a single hit (classified by the authors as 'Type I immortalisation') (Trott et al., 1995, Newbold et al., 1982) ultimately silencing *p16* expression by homozygous deletion (X-rays) or promoter methylation combined with single copy number loss (nickel). In contrast, a two-step model was proposed for B(a)P-induced immortal SHD clones,

whereby the initial event was inactivation of *p53* by point mutations (primarily G to T transversions) followed by a 'second hit' after 20 population doublings which targeted the *p16-Rb* pathway, either by *p16* single copy allele loss or epigenetic silencing of its promoter, plus *p15* or *Rb1* transcript down-regulation (Yasaei et al., 2013).

Work presented in this thesis focused on the mechanisms by which senescence bypass was induced (via MT) by benzo(a)pyrene in primary SHE cells. In contrast to the SHD work described above, only 33 % of immortalised B(a)P MT clones contained potentially inactivating *p53* point mutations. In two or more instances (BP MT9 and BP MT10) the *p53* mutations conferred cellular growth advantages which were clonally selected for, and the *p16* gene promoter was shown to be heavily methylated, consistent with a 'two-step' (Type II – see explanation above) process leading to senescence bypass and the generation of established cell lines. This is also consistent with an observed decreased proliferation rate for BP MT10 during the first 20 population doublings, despite no actual senescence or crisis-like phenotype observed. (Expression analysis was unfortunately not completed for BP MT9 and BP MT10 due to time constraints). The growth kinetics of BP MT11 and BP MT12 were not characterised but, in addition to *p53* mutations, these clones are likely to be missing one allelic copy of the entire *CDKN2A/B* locus (more CNV repeats are necessary or use of other methods to confirm the result) and they expressed *p16* and *p15* at low levels which is also indicative of a two-step immortalisation process.

The remaining 67 % of BP-MT colony-derived SHE cells that immortalised did not carry *p53* mutations affecting the amino acid sequence or indeed even point mutations in *p16* transcripts. From the analysis performed on SH dermal cells, all but one B(a)P-induced SHD clone were shown to overexpress *p16* (Yasaei et al., 2013). In contrast the majority of SHE immortalised clones did not upregulate *p16* transcription; mRNA levels in BP MT clones were either comparable to the untreated DMSO control group or down-regulated by between 50% and 90 %. 40 % of BP MT immortal clones were found to be heavily methylated at the *p16* promoter, but this did not always correlate with gene silencing. However, as methylation could be specific to B(a)P-exposure this does indicate that, in addition to its well characterised mutational mechanism, B(a)P can induce epigenetic effects and thus act as a non-genotoxic carcinogen too.

BP MT7 and BP MT8 expressed *p16* minimally and their gene promoter was methylated. These colony-derived cells were spindle-shaped, retained MT characteristics reached high cell densities in culture without an observed cell crisis. When treated with the demethylating agent 5-aza-dC, there was increased expression of *p16* and removal of methyl groups at the *p16* promoter which, in BP MT7, was sufficient to induce senescence. The data suggest that DNA methylation can negatively regulate *p16* gene expression, although the presence of methylation was not always predictive of transcriptional silencing. This is reminiscent of Type I kinetics induced by nickel (Yasaei et al., 2013) but, given that *ARF* is also downregulated, there may be cooperative events additionally taking place to regulate *p53* negatively (via increased Mdm2 availability) despite increased levels of *Rb1* transcripts.

The cell crisis observed in MT clones that escaped senescence, but that appeared to require secondary events, correlated with a single allelic loss at two of more genomic regions within the *CDKN2A/B* locus in three BP MT colony-derived clones (BP MT1, BP MT3, BP MT6). Hemizyosity in these instances always involved *ARF* exon 1 β plus one of *p16*'s two exons and was linked to downregulation of *p16* over successive passages (i.e. over an estimated 20-40 population doublings). Senescence bypass in BP MT6 was seemingly more complex; despite *CDKN2A* allelic loss and a 50% reduction of *p16* expression in this clone, its mRNA levels were still comparable to the DMSO control group. Additionally, its *p16* gene promoter was methylated but this was not sufficient to reduce *p16* transcripts compared with the DMSO controls. Of the clones treated with 5-aza-dC, activation of *p16* in BP MT6 was similar to that observed in the treated SHE primary control, and methyl groups were not lost at the time points tested, thus demonstrating that methylation of the *p16* promoter is not always predictive of its expression. However, there was over 10-fold induction of *p15* expression during the cell crisis (compared to the DMSO group) which was subsequently heavily reduced (2-3 fold above the control) in BP MT6 cells post crisis. This secondary event was paralleled by a slight reduction in *p16* expression following crisis, and CNV analysis indicated hemizyosity of *p15*. This supports the importance of *p15* as a tumour suppressor gene in the regulation of senescence in Syrian hamster which was also hypothesised to have a role in SHD immortalisation when transcriptionally silenced (Yasaei et al., 2013).

A reduction of *p16* gene expression in BP MT4 was observed following a senescence-like cell crisis but transcriptional repression cannot be explained by mutation, allelic loss or DNA methylation. One possibility is that upregulation of *BMI-1* had a silencing effect either: (i) by acting as a transient negative transcription factor by directly binding to *p16* DNA elements (Meng et al., 2010), or (ii) acting indirectly, by recruitment and assembly of Polycomb group repressor complexes bound to chromatin (Jacobs et al., 1999) which, if maintained, could have a more long lasting effect. *BMI-1* was strongly expressed in two type II BP MT clones which had single copy number loss of the *CDKN2A/B* locus, and *BMI-1* transcripts was generally more abundant in BP MT clones than in the DMSO control group (3 to 4-fold increases). The data suggest that elements upstream of *p16* are altered in immortalised BP MT clones co-operating to suppress senescence pathways and extend cellular lifespan.

Finally in the remaining immortal clones (BP MT2 and BP MT5) expression of *p16*, *p15* or *ARF* was minimal but both cell lines retained both allelic copies of the *CDKN2A/B* locus and *p53*, were partially methylated at the *p16* promoter and possessed no known translated *p53* or *p16* inactivating point mutations. Additional unknown events may have cooperated towards the bypass of senescence. *Rb1* in BP MT5 was transcriptionally repressed and this could possibly have been due to inactivating gene mutations, copy number loss or deregulation of other upstream regulators. *p53* activity is controlled by post-transcriptional modifications that may have been be disrupted, so that increased transcription had little or no effect in activating cell cycle arrest and/or *Rb1* may have been hyperphosphorylation and deregulated. *Mdm2* downregulation is also largely unexplained as it is generally associated with oncogenic activity, but may be a compensatory cellular mechanism attempting to activate *p53*-mediated cell-cycle arrest. *ARF* signalling is also largely inactivated which may point towards upstream mediators failing to sense genetic damage and initiate signalling cascades. The cell cycle regulator *p21* was also not investigated and, similarly, expression of cyclin kinases was not examined; both of these studies would complement the work presented here.

CTAs based on the Syrian hamster allow the study of oncogene- and stress- induced senescence in isolation from that initialised by replicative senescence (caused by telomere attrition), as rodent models do not require the reactivation of telomerase for

immortalisation (Russo et al., 1998). This is favourable for a mechanistic understanding of senescence bypass but cannot fully predict the transforming potential of chemicals in a human model, which would be the ideal goal (Creton et al., 2012). The data presented here demonstrates the mechanistic relevance of the SHE CTA to carcinogen-induced senescence bypass. Despite the assay's subjectivity, MT characteristics did predispose colonies to evade senescence barriers and led to unlimited growth potential in 10-30 % of colonies (depending on the study) following exposure to B(a)P. It should be reassuring to toxicologists that morphological transformation in the Syrian hamster embryo system can lead to the deregulation of pathways regulating senescence, and these endpoints are in part shared by human systems. Certainly, the mode of action of various compounds and their concentrations is likely to influence the relationship between MT and immortality and pathway components may be targeted differently as seen with the SHD system (Yasaei et al., 2013). It would be unrealistic to expect all colonies to be picked from every CTA conducted, but it may be advantageous to isolate a statistically robust number of MT colonies and, as performed here, conduct a detailed molecular analysis to gauge an unknown compound's mode of action.

Now that the Syrian hamster genome has been sequenced it opens the door to more in-depth analysis of the model which would complement MT colony screening at a molecular level for pathway analysis. There is scope for improved primer design applicable to relevant gene targets and predicting protein structures in order to find suitable antibodies for protein expression. The sequence analysis presented here further confirms similarities between the human and SH genomes in terms of the *CDKN2A/B* gene structure, i.e. exonic regions of *p15*, *p16* and *ARF* (Muscarella et al., 2001). Its chromosomal location in the Syrian hamster is yet to be identified, but the locus is predicted to encompass under 45 Kb according to aligned but not continuous WGS sequences, a figure which is roughly comparable to the estimated 37-40 Kb *CDKN2A/B* locus in humans. Interestingly, the Syrian hamster *p16* gene is more homologous to its human counterpart than rat and mouse sequences, which might correlate more closely to conservation of structure to function. It is known that ARF plays an important role in regulating senescence bypass in mice (Kamijo et al., 1997, Sharpless et al., 2004) but, in humans, cell senescence seems to be effected mainly via p16. In hamsters it has been

suggested that *p16* is also the key player (Yasaei et al., 2013) but the reasons for the difference with mice are unclear.

One advantage of using the SHE-MT assay for predicting carcinogenicity is that it shows good concordance with rodent bioassay data (80-90 %) as well as sensitivity and specificity (LeBoeuf et al., 1996). Ideally, implementation of CTAs into regulatory testing should offer a highly predictive and sensitive assay representative of the human system (Vasseur and Lasne, 2012). Efforts are underway in our laboratory to understand fully the mechanisms of normal growth barriers using mammary epithelial cells (HMEC) in order to develop a human-based cell transformation assay. Normal HMECs will proliferate for 15-30 population doublings before overexpressing *p16* and entering senescence; this first stage is named 'stasis' (the equivalent of which in rodents is OIS/SIPS). Under stressful culture conditions like starvation, stasis can be spontaneously bypassed and the resulting post-selection cells do not express *p16* but continue to proliferate for a further 30-70 population doublings until telomere shortening induces cell cycle arrest. This stage is called 'agonescence' when p53 is functional, or 'crisis' if p53 is inactive, and corresponds to replicative senescence (Stampfer and Yaswen, 2003). Deletion or inactivation of *p53* has been associated with increased rates of acquiring immortality and coincides with the reactivation of telomerase (Stampfer et al., 2003). When treated with carcinogens, such a B(a)P, the second stringent barrier can be avoided by reactivating the catalytic component of telomerase (hTERT) and is associated with large but stable karyotype changes on the short arm of chromosome-3 (Linne et al, unpublished data). Carcinogenesis can therefore be modelled at different stages in the progression of HMEC to immortalisation by selecting pre- or post-stasis cells and would provide human mechanistic insight into bypass of premature senescence (SIPS/stasis) and replicative senescence respectively.

7.2 Conclusion and future perspectives

Understanding the molecular underpinnings of intrinsic barriers to uncontrolled cell growth opening the gate to tumour development is essential in order to model carcinogenesis. With an increased requirement for the reduction of rodent bioassays used in compound testing, toxicologists must rely on approved *in vitro* models for their safety assessments (Creton et al., 2012). The SHE CTA is a subjective assay by the nature of its endpoint of visual scoring of morphologically transformed colonies; good practice and standardised training can minimise laboratory variability (Vasseur and Lasne, 2012).

The experimental work conducted in this project and described in detail in this thesis demonstrates that, although MT does not always equate to senescence bypass and cell immortalisation in the Syrian hamster embryo model, it does increase the probability of the acquisition of unlimited growth potential in MT colony-derived cells. Inactivating mutations in *p53* were observed in 30 % of immortal MT B(a)P-induced clones and expression of *p16* was commonly downregulated. Growth kinetics indicated secondary events to MT were necessary for the evasion of senescence barriers, and these were associated with an allelic loss of *p16* at later time points along with its transcriptional repression. No inactivating mutations of *p16* were observed. However, the *p16* promoter was found to be subject to DNA methylation in immortal colony-derived cells but was not always associated with *p16* downregulation; removal of methyl groups using the demethylating agent 5-aza-dC was accompanied by increases in *p16* expression in some instances. Another common feature was overexpression of *BMI-1*, which lies upstream of *p16* in the same anti-proliferative signalling pathway and is likely to have contributed towards the repression of *p16*.

With the completion of the Syrian hamster genome sequencing, it was possible to perform a comparative analysis of the *CDKN2A/B* locus which confirmed its conserved genomic structure and sequence homology for *p16*, *p15* and *ARF* with humans. Increased sequence availability should now permit better molecular understanding of both SHD and SHE models, which was not previously possible. Repressive interactions between *BMI-1* and *p16* ought to be confirmed, for example by chromatin immunoprecipitation (ChIP) analysis, and other members of the Polycomb group repressor complexes such as *EZH2*

could also be examined. It is proposed that protein expression and modifications of key regulators of the cell cycle be further investigated, once the appropriate antibodies are identified, to include p16, pRb and p53. Downstream targets such as p21 and cyclin kinases may be abrogated and further explain mechanisms of senescence bypass.

The Syrian hamster remains an excellent cell model for studying OIS/SIPS and its bypass in isolation without to the requirement for reactivating telomerase (Russo et al., 1998, Trott et al., 1995). The extra genetic sequence information now available should aid the understanding of SH carcinogenesis at a molecular level and draw out any species-specific pathways. Both SHE and SHD assays have been shown to be mechanistically relevant in simulating human toxicological studies and respond to both genotoxic and non-genotoxic carcinogenic insults (Yasaei et al., 2013).

Eventually, implementation of a fully characterised human CTA would be highly advantageous for predictive toxicology, but caveats will still remain. Due to their cell-based nature, transformation assays are restricted to certain cell types and are not fully representative of how cells are organised in three-dimensional space let alone the human body. Ideally, a three-dimensional model might ultimately be implemented. By their very nature, such assays will always have their own limitations and shortcomings. Thus, as complete a picture as possible for safety testing (in multiple systems) is necessary to provide a 'weight-of-evidence' approach capable of covering different angles of risk assessment.

8 Appendix

Table 1: List of all primers and probes

| Gene expression real time PCR primers | T _m °C |
|--|-------------------|
| <i>GAPDH</i> | |
| 5'-TTGTTGCCATCAATGACCCCTT-3'(forward) | 59 |
| 5'-CGTTCTCAGCCTTGACTGTGCCTT-3' (reverse) | |
| <i>Beta-actin</i> | |
| 5'-ATGCCAGGTCATCACCATT-3'(forward) | 59 |
| 5'-TGTAGTTTCGTGGATGCCACA-3' (reverse) | |
| <i>p16 (Cdkn2a)</i> | |
| 5'- AGAGGTTCTGGGCTTTGCT-3' (forward) | 59 |
| 5'-CTACTTGGGTGTTGCCCATC-3' (reverse) | |
| <i>ARF (INK4A)</i> | |
| 5'-GCAGGTTCTGGTGACTGT-3' (forward) | 59 |
| 5'-CTCGCTAGCATCAACAGCAG-3' (reverse) | |
| <i>p53</i> | |
| 5'-CCCCCAAAGAGTGCTAAACGA-3' (forward) | 59 |
| 5'-CAGTTCCAAGGCCTCATTCAA-3' (reverse) | |
| <i>p15 (Cdkn2b)</i> | |
| 5'-CTGTGAGAGGAGGACAAGGG-3' (forward) | 57 |
| 5'-CATCATCATGACCTGGATCG-3' (reverse) | |
| <i>Mdm2</i> | |
| 5'-CACAGGTCCCTTTCCTTGA-3' (forward) | 57 |
| 5'-TGAATCCTGATCCAGCCAAT-3' (reverse) | |
| <i>Rb1</i> | |
| 5'-CGCCTTCTGTCTGATCATCCA-3' (forward) | 57 |
| 5'-TTGGTCCAAAT GCCGGTCT-3' (reverse) | |
| <i>BMI-1</i> | |
| 5'-CTGGAGAAGAAATGGCCCTCT-3' (forward) | 59 |
| 5'-TTCTCCCGCATTGTGTCAGC-3' (reverse) | |
| Sequencing primers | |
| <i>p53</i> | |
| Exons 2-4 | |
| 5'-GCTTCCCTGAAGACCTGAAG-3' (forward) | |
| 5'-CCAGACGGAAACCATAGTCG-3' (reverse) | 57 |
| Exons 4-6 | |
| 5'-CTGGCCCCTCATCTTCT-3' (forward) | |
| 5'-ACTGTGCCGAAAAGTCTGCT-3' (reverse) | 57 |
| Exon 6-9 | |
| 5'-CCGAGTGGAAGGAAATATGC-3' (forward) | |
| 5'-TGTTTTTCTTTGGCTGGG-3' (reverse) | 57 |
| <i>p16 (Cdkn2a)</i> | |
| 5'-ATGGAGCCCTCTGCGGACG-3' (forward) | 59 |
| 5'-GGGGTGGTCCGCGAAATCC-3' (reverse) | |

| Bisulphite sequencing primers | T _m °C |
|--|-------------------|
| p16 promoter (457 bp upstream region) | |
| 5'- TTGGTTTATTAGTTTAGGAGATTTA -3' (forward) | |
| 5'- ATACTACTCCAATACTCCCCTATC-3' (reverse) | 56 |
| | |
| Copy number variation primers (PrimerDesign Ltd) | |
| ARF exon 1β [AF443796]- FAM labelled | 60 |
| Undisclosed | |
| p16 (Cdkn2a) exon1α [AH010240] - FAM labelled | 60 |
| Undisclosed | |
| p16 (Cdkn2a) exon2 [AH010240] - FAM labelled | 60 |
| Undisclosed | |
| p15 (Cdkn2b) [NM_001281539] - FAM labelled | 60 |
| Undisclosed | |
| p53 (p53) exons 7-8 [NM_001281661] - FAM labelled | 60 |
| Undisclosed | |
| SDHA – VIC labelled | 60 |
| Undisclosed | |
| | |
| Methylation specific PCR primers | |
| Modified/methylated p16 exon 1α (100bp) | 54 |
| 5'-GCGGTTGTTTAGGGTCGC-3' (forward) | |
| 5'-CTACCTAAATCGAAATACGACCG-3' (reverse) | |
| Modified/un-methylated p16 exon 1α (143bp) | 54 |
| 5'-GGAGTAGTATGGAGTTTTTTGTGGAT-3' (forward) | |
| 5'-TATACCTAAATCAAATACAACCA-3' (reverse) | |
| | |
| Modified/methylated p16 promoter | 56 |
| 5'-TTTAGGTAGAAGATTCGATTGTCGT-3' (forward) | |
| 5'-AACGAACTCACTAAACCTCACGAA-3' (reverse) | |
| Modified/un-methylated p16 promoter | 56 |
| 5'-TTTAGGTAGAAGATTTGATGTTGT-3' (forward) | |
| 5'-AACAAAACCTCACTAAACCTCACAAA-3' (reserve) | |

9 References

- ABDELMOHSEN, K., SRIKANTAN, S., KANG, M. J. & GOROSPE, M. 2012. Regulation of senescence by microRNA biogenesis factors. *Ageing Res Rev*, 11, 491-500.
- ABE, M., OKOCHI, E., KURAMOTO, T., KANEDA, A., TAKATO, T., SUGIMURA, T. & USHIJIMA, T. 2002. Cloning of the 5' upstream region of the rat p16 gene and its role in silencing. *Jpn J Cancer Res*, 93, 1100-6.
- ADELEYE, Y., ANDERSEN, M., CLEWELL, R., DAVIES, M., DENT, M., EDWARDS, S., FOWLER, P., MALCOMBER, S., NICOL, B., SCOTT, A., SCOTT, S., SUN, B., WESTMORELAND, C., WHITE, A., ZHANG, Q. & CARMICHAEL, P. L. 2014. Implementing Toxicity Testing in the 21st Century (TT21C): Making safety decisions using toxicity pathways, and progress in a prototype risk assessment. *Toxicology*.
- AGHERBI, H., GAUSSMANN-WENGER, A., VERTHUY, C., CHASSON, L., SERRANO, M. & DJABALI, M. 2009. Polycomb mediated epigenetic silencing and replication timing at the INK4a/ARF locus during senescence. *PLoS One*, 4, e5622.
- AGUILO, F., ZHOU, M. M. & WALSH, M. J. 2011. Long noncoding RNA, polycomb, and the ghosts haunting INK4b-ARF-INK4a expression. *Cancer Res*, 71, 5365-9.
- AHMADZAI, A. A., TREVISAN, J., FULLWOOD, N. J., CARMICHAEL, P. L., SCOTT, A. D. & MARTIN, F. L. 2012a. The Syrian hamster embryo (SHE) assay (pH 6.7): mechanisms of cell transformation and application of vibrational spectroscopy to objectively score endpoint alterations. *Mutagenesis*, 27, 257-66.
- AHMADZAI, A. A., TREVISAN, J., PANG, W., PATEL, II, FULLWOOD, N. J., BRUCE, S. W., PANT, K., CARMICHAEL, P. L., SCOTT, A. D. & MARTIN, F. L. 2012b. Classification of test agent-specific effects in the Syrian hamster embryo assay (pH 6.7) using infrared spectroscopy with computational analysis. *Mutagenesis*, 27, 375-82.
- AL-KAABI, A., VAN BOCKEL, L. W., POTHEN, A. J. & WILLEMS, S. M. 2014. p16INK4A and p14ARF gene promoter hypermethylation as prognostic biomarker in oral and oropharyngeal squamous cell carcinoma: a review. *Dis Markers*, 2014, 260549.
- ALEXANDRE, S., RAST, C., MAIRE, M. A., ORFILA, L. & VASSEUR, P. 2003. ZnCl₂ induces Syrian hamster embryo (SHE) cell transformation. *Toxicol Lett*. Netherlands.
- AOUBALA, M., MURRAY-ZMIJEWSKI, F., KHOURY, M. P., FERNANDES, K., PERRIER, S., BERNARD, H., PRATS, A. C., LANE, D. P. & BOURDON, J. C. 2011. p53 directly transactivates Delta133p53alpha, regulating cell fate outcome in response to DNA damage. *Cell Death Differ*, 18, 248-58.
- AZQUETA, A. & COLLINS, A. R. 2013. The essential comet assay: a comprehensive guide to measuring DNA damage and repair. *Arch Toxicol*, 87, 949-68.
- BALLS, M., AMCOFF, P., BREMER, S., CASATI, S., COECKE, S., CLOTHIER, R., COMBES, R., CORVI, R., CURREN, R., ESKES, C., FENTEM, J., GRIBALDO, L., HALDER, M., HARTUNG, T., HOFFMANN, S., SCHECTMAN, L., SCOTT, L., SPIELMANN, H., STOKES, W., TICE, R., WAGNER, D. & ZUANG, V. 2006. The principles of weight of evidence validation of test methods and testing strategies. The report and recommendations of ECVAM workshop 58. *Altern Lab Anim*, 34, 603-20.
- BARRETT, J. C., CRAWFORD, B. D., MIXTER, L. O., SCHECTMAN, L. M., TS'O, P. O. & POLLACK, R. 1979. Correlation of in vitro growth properties and tumorigenicity of Syrian hamster cell lines. *Cancer Res*, 39, 1504-10.
- BARRETT, J. C. & TS'O, P. O. 1978. Evidence for the progressive nature of neoplastic transformation in vitro. *Proc Natl Acad Sci U S A*, 75, 3761-5.

- BEAUSEJOUR, C. M., KRTOLICA, A., GALIMI, F., NARITA, M., LOWE, S. W., YASWEN, P. & CAMPISI, J. 2003. Reversal of human cellular senescence: roles of the p53 and p16 pathways. *EMBO J*, 22, 4212-22.
- BELL, D. W. 2010. Our changing view of the genomic landscape of cancer. *J Pathol*, 220, 231-43.
- BENIGNI, R. & BOSSA, C. 2011. Alternative strategies for carcinogenicity assessment: an efficient and simplified approach based on in vitro mutagenicity and cell transformation assays. *Mutagenesis*, 26, 455-60.
- BERGGREN DE VERDIER, P. J., KUMAR, R., ADOLFSSON, J., LARSSON, P., NORMING, U., ONELOV, E., WIJKSTROM, H., STEINECK, G. & HEMMINKI, K. 2006. Prognostic significance of homozygous deletions and multiple duplications at the CDKN2A (p16INK4a)/ARF (p14ARF) locus in urinary bladder cancer. *Scand J Urol Nephrol*, 40, 363-9.
- BERGGREN, P., KUMAR, R., SAKANO, S., HEMMINKI, L., WADA, T., STEINECK, G., ADOLFSSON, J., LARSSON, P., NORMING, U., WIJKSTROM, H. & HEMMINKI, K. 2003. Detecting homozygous deletions in the CDKN2A(p16(INK4a))/ARF(p14(ARF)) gene in urinary bladder cancer using real-time quantitative PCR. *Clin Cancer Res*, 9, 235-42.
- BEROUD, C., COLLOD-BEROUD, G., BOILEAU, C., SOUSSI, T. & JUNIEN, C. 2000. UMD (Universal mutation database): a generic software to build and analyze locus-specific databases. *Hum Mutat*, 15, 86-94.
- BERWALD, Y. & SACHS, L. 1963. IN VITRO CELL TRANSFORMATION WITH CHEMICAL CARCINOGENS. *Nature*, 200, 1182-4.
- BLACKBURN, E. H. & COLLINS, K. 2011. Telomerase: an RNP enzyme synthesizes DNA. *Cold Spring Harb Perspect Biol*, 3.
- BODNAR, A. G., OUELLETTE, M., FROLKIS, M., HOLT, S. E., CHIU, C. P., MORIN, G. B., HARLEY, C. B., SHAY, J. W., LICHTSTEINER, S. & WRIGHT, W. E. 1998. Extension of life-span by introduction of telomerase into normal human cells. *Science*, 279, 349-52.
- BOHNENBERGER, S., BRUCE, S. W., KUNKELMANN, T., PANT, K., PERSCHBACHER, S., SCHWIND, K. R., SLY, J. & POTH, A. 2012. Photo catalogue for the classification of cell colonies in the Syrian hamster embryo (SHE) cell transformation assay at pH 6.7. *Mutat Res*, 744, 82-96.
- BOURDON, J. C., FERNANDES, K., MURRAY-ZMIJEWSKI, F., LIU, G., DIOT, A., XIRODIMAS, D. P., SAVILLE, M. K. & LANE, D. P. 2005. p53 isoforms can regulate p53 transcriptional activity. *Genes Dev*, 19, 2122-37.
- BRACKEN, A. P., KLEINE-KOHLBRECHER, D., DIETRICH, N., PASINI, D., GARGIULO, G., BEEKMAN, C., THEILGAARD-MONCH, K., MINUCCI, S., PORSE, B. T., MARINE, J. C., HANSEN, K. H. & HELIN, K. 2007. The Polycomb group proteins bind throughout the INK4A-ARF locus and are disassociated in senescent cells. *Genes Dev*. United States.
- BRUGAROLAS, J., CHANDRASEKARAN, C., GORDON, J. I., BEACH, D., JACKS, T. & HANNON, G. J. 1995. Radiation-induced cell cycle arrest compromised by p21 deficiency. *Nature*, 377, 552-7.
- BUAJEEB, W., POOMSAWAT, S., PUNYASINGH, J. & SANGUANSIN, S. 2009. Expression of p16 in oral cancer and premalignant lesions. *J Oral Pathol Med*. Denmark.
- CAMPISI, J. & D'ADDA DI FAGAGNA, F. 2007. Cellular senescence: when bad things happen to good cells. *Nat Rev Mol Cell Biol*. England.
- CANEPÀ, E. T., SCASSA, M. E., CERUTI, J. M., MARAZITA, M. C., CARCAGNO, A. L., SIRKIN, P. F. & OGARA, M. F. 2007. INK4 proteins, a family of mammalian CDK inhibitors with novel biological functions. *IUBMB Life*, 59, 419-26.
- CARMAN, T. A., AFSHARI, C. A. & BARRETT, J. C. 1998. Cellular senescence in telomerase-expressing Syrian hamster embryo cells. *Exp Cell Res*, 244, 33-42.
- CARTEGNI, L., WANG, J., ZHU, Z., ZHANG, M. Q. & KRAINER, A. R. 2003. ESEfinder: A web resource to identify exonic splicing enhancers. *Nucleic Acids Res*, 31, 3568-71.
- CARTER, S. & VOUSDEN, K. H. 2009. Modifications of p53: competing for the lysines. *Curr Opin Genet Dev*, 19, 18-24.
- CHANDLER, H. & PETERS, G. 2013. Stressing the cell cycle in senescence and aging. *Curr Opin Cell Biol*, 25, 765-71.

- CHANG, K. W., LACONI, S., MANGOLD, K. A., HUBCHAK, S. & SCARPELLI, D. G. 1995. Multiple genetic alterations in hamster pancreatic ductal adenocarcinomas. *Cancer Res*, 55, 2560-8.
- CHANG, K. W., SARRAJ, S., LIN, S. C., TSAI, P. I. & SOLT, D. 2000. P53 expression, p53 and Ha-ras mutation and telomerase activation during nitrosamine-mediated hamster pouch carcinogenesis. *Carcinogenesis*, 21, 1441-51.
- CHANG, S. 2005. Modeling aging and cancer in the telomerase knockout mouse. *Mutat Res*, 576, 39-53.
- CHAO, D. L., SANCHEZ, C. A., GALIPEAU, P. C., BLOUNT, P. L., PAULSON, T. G., COWAN, D. S., AYUB, K., ODZE, R. D., RABINOVITCH, P. S. & REID, B. J. 2008. Cell proliferation, cell cycle abnormalities, and cancer outcome in patients with Barrett's esophagus: a long-term prospective study. *Clin Cancer Res*. United States.
- CHEN, D., SHAN, J., ZHU, W. G., QIN, J. & GU, W. 2010. Transcription-independent ARF regulation in oncogenic stress-mediated p53 responses. *Nature*, 464, 624-7.
- COBRINIK, D. 2005. Pocket proteins and cell cycle control. *Oncogene*, 24, 2796-809.
- CODY, D. T., 2ND, HUANG, Y., DARBY, C. J., JOHNSON, G. K. & DOMANN, F. E. 1999. Differential DNA methylation of the p16 INK4A/CDKN2A promoter in human oral cancer cells and normal human oral keratinocytes. *Oral Oncol.*, 35, 516-22.
- COLACCI, A., MASCOLO, M. G., PERDICHIZZI, S., QUERCIOLO, D., GAZZILLI, A., ROTONDO, F., MORANDI, E., GUERRINI, A., SILINGARDI, P., GRILLI, S. & VACCARI, M. 2011. Different sensitivity of BALB/c 3T3 cell clones in the response to carcinogens. *Toxicol In Vitro*. 2011 Elsevier Ltd.
- COLLADO, M., BLASCO, M. A. & SERRANO, M. 2007. Cellular senescence in cancer and aging. *Cell*, 130, 223-33.
- COLLADO, M. & SERRANO, M. 2006. The power and the promise of oncogene-induced senescence markers. *Nat Rev Cancer*. England.
- COLLINS, K. & MITCHELL, J. R. 2002. Telomerase in the human organism. *Oncogene*, 21, 564-79.
- COMBES, R., BALLS, M. B., CURREN, R., FISCHBACH, M., FUSENIG, N., KIRKLAND, D., LASNE, C., LANDOLPH, J., LEOEUF, R., MARQUARDT, H., MCCORMICK, J., MULLER, L., RIVEDAL, E., SABBIONI, E., TANAKA, N., VASSEUR, P. & YAMASAKI, H. 1999. Cell Transformation Assays as Predictors of Human Carcinogenicity, The Report and Recommendations of ECVAM. Workshop 39. *ATLA*, 27, 745-767.
- COMBES, R. D. 2012. Cell transformation assays: are we barking up the wrong tree? *Altern Lab Anim*, 40, 115-30.
- COPELAND, N. G. & JENKINS, N. A. 2009. Deciphering the genetic landscape of cancer--from genes to pathways. *Trends Genet*, 25, 455-62.
- CORVI, R., AARDEMA, M. J., GRIBALDO, L., HAYASHI, M., HOFFMANN, S., SCHECHTMAN, L. & VANPARYS, P. 2012. ECVAM prevalidation study on in vitro cell transformation assays: general outline and conclusions of the study. *Mutat Res*, 744, 12-9.
- CRETON, S., AARDEMA, M. J., CARMICHAEL, P. L., HARVEY, J. S., MARTIN, F. L., NEWBOLD, R. F., O'DONOVAN, M. R., PANT, K., POTH, A., SAKAI, A., SASAKI, K., SCOTT, A. D., SCHECHTMAN, L. M., SHEN, R. R., TANAKA, N. & YASAEI, H. 2012. Cell transformation assays for prediction of carcinogenic potential: state of the science and future research needs. *Mutagenesis*, 27, 93-101.
- CUSTER, L., GIBSON, D. P., AARDEMA, M. J. & LEOEUF, R. A. 2000. A refined protocol for conducting the low pH 6.7 Syrian hamster embryo (SHE) cell transformation assay. *Mutat Res*. Netherlands.
- D'ADDA DI FAGAGNA, F. 2008. Living on a break: cellular senescence as a DNA-damage response. *Nat Rev Cancer*, 8, 512-22.
- D'ADDA DI FAGAGNA, F., REAPER, P. M., CLAY-FARRACE, L., FIEGLER, H., CARR, P., VON ZGLINICKI, T., SARETZKI, G., CARTER, N. P. & JACKSON, S. P. 2003. A DNA damage checkpoint response in telomere-initiated senescence. *Nature*, 426, 194-8.

- DAFOU, D. 2003. **Establishment of hamster and human cell systems for the study of malignant transformation**. Ph.D., Brunel University.
- DAI, C. & GU, W. 2010. p53 post-translational modification: deregulated in tumorigenesis. *Trends Mol Med*, 16, 528-36.
- DEBACQ-CHAINIAUX, F., ERUSALIMSKY, J. D., CAMPISI, J. & TOUSSAINT, O. 2009. Protocols to detect senescence-associated beta-galactosidase (SA-beta-gal) activity, a biomarker of senescent cells in culture and in vivo. *Nat Protoc*, 4, 1798-806.
- DEMOKAN, S., CHUANG, A., SUOGLU, Y., ULUSAN, M., YALNIZ, Z., CALIFANO, J. A. & DALAY, N. 2012. Promoter methylation and loss of p16(INK4a) gene expression in head and neck cancer. *Head Neck*, 34, 1470-5.
- DIETRICH, N., BRACKEN, A. P., TRINH, E., SCHJERLING, C. K., KOSEKI, H., RAPPILBER, J., HELIN, K. & HANSEN, K. H. 2007. Bypass of senescence by the polycomb group protein CBX8 through direct binding to the INK4A-ARF locus. *Embo j*, 26, 1637-48.
- DIMRI, G. P., LEE, X., BASILE, G., ACOSTA, M., SCOTT, G., ROSKELLEY, C., MEDRANO, E. E., LINSKENS, M., RUBEL, I., PEREIRA-SMITH, O. & ET AL. 1995. A biomarker that identifies senescent human cells in culture and in aging skin in vivo. *Proc Natl Acad Sci U S A*, 92, 9363-7.
- DIMRI, M., CARROLL, J. D., CHO, J. H. & DIMRI, G. P. 2013. microRNA-141 regulates BMI1 expression and induces senescence in human diploid fibroblasts. *Cell Cycle*, 12, 3537-46.
- DIPAULO, J. A., NELSON, R. L. & DONOVAN, P. J. 1969. Sarcoma-producing cell lines derived from clones transformed in vitro by benzo[a]pyrene. *Science*, 165, 917-8.
- DONEHOWER, L. A., HARVEY, M., SLAGLE, B. L., MCARTHUR, M. J., MONTGOMERY, C. A., JR., BUTEL, J. S. & BRADLEY, A. 1992. Mice deficient for p53 are developmentally normal but susceptible to spontaneous tumours. *Nature*, 356, 215-21.
- DOYLE, B., MORTON, J. P., DELANEY, D. W., RIDGWAY, R. A., WILKINS, J. A. & SANSOM, O. J. 2010. p53 mutation and loss have different effects on tumourigenesis in a novel mouse model of pleomorphic rhabdomyosarcoma. *J Pathol*, 222, 129-37.
- EC 2003a. Directive 2003/15/EC of the European Parliament and of the Council of 27 February 2003 amending Directive 78/786/EEC on the approximation of the laws of the member states relating to cosmetic products. Off. J. Eur. Union.
- EC 2003b. Directive 2003/15/EC of the European Parliament and of the Council of 27 February 2003 amending Directive 78/786/EEC on the approximation of the laws of the member states relating to cosmetic products. Off. J. Eur. Union L, 66: 26–35.
- EC 2007a. Corrigendum to regulation (EC) No 1907/2006 of the European Parliament and of the Council of 18 December 2006. Off. J. Eur. Union.
- EC 2007b. Corrigendum to regulation (EC) No 1907/2006 of the European Parliament and of the Council of 18 December 2006. Off. J. Eur. Union L 136, 50: 3–280.
- EHRlich, M. 2002. DNA methylation in cancer: too much, but also too little. *Oncogene*, 21, 5400-13.
- FARMER, P. B. 2002. Committee on Mutagenicity of Chemicals in Food, Consumer Products and the Environment ILSI/HESI research programme on alternative cancer models: results of Syrian hamster embryo cell transformation assay. International Life Sciences Institute/Health and Environmental Science Institute. *Toxicol Pathol*, 30, 536-8.
- FENECH, M. 2007. Cytokinesis-block micronucleus cytome assay. *Nat Protoc*, 2, 1084-104.
- FENG, L., HOLLSTEIN, M. & XU, Y. 2006. Ser46 phosphorylation regulates p53-dependent apoptosis and replicative senescence. *Cell Cycle*, 5, 2812-9.
- FERLAY, J., SOERJOMATARAM, I., DIKSHIT, R., ESER, S., MATHERS, C., REBELO, M., PARKIN, D. M., FORMAN, D. & BRAY, F. 2014. Cancer incidence and mortality worldwide: Sources, methods and major patterns in GLOBOCAN 2012. *Int J Cancer*.
- FERLAY, J., STELIAROVA-FOUCHER, E., LORTET-TIEULENT, J., ROSSO, S., COEBERGH, J. W., COMBER, H., FORMAN, D. & BRAY, F. 2013. Cancer incidence and mortality patterns in Europe: estimates for 40 countries in 2012. *Eur J Cancer*, 49, 1374-403.

- FINKEL, T., SERRANO, M. & BLASCO, M. A. 2007. The common biology of cancer and ageing. *Nature*, 448, 767-74.
- FLORL, A. R. & SCHULZ, W. A. 2003. Peculiar structure and location of 9p21 homozygous deletion breakpoints in human cancer cells. *Genes Chromosomes Cancer*, 37, 141-8.
- FORBES, S. A., TANG, G., BINDAL, N., BAMFORD, S., DAWSON, E., COLE, C., KOK, C. Y., JIA, M., EWING, R., MENZIES, A., TEAGUE, J. W., STRATTON, M. R. & FUTREAL, P. A. 2010. COSMIC (the Catalogue of Somatic Mutations in Cancer): a resource to investigate acquired mutations in human cancer. *Nucleic Acids Res*, 38, D652-7.
- FRIGERIO, S., DISCIGLIO, V., MANOUKIAN, S., PEISSEL, B., DELLA TORRE, G., MAURICHI, A., COLLINI, P., PASINI, B., GOTTI, G., FERRARI, A., RIVOLTINI, L., MASSIMINO, M. & RODOLFO, M. 2014. A large de novo 9p21.3 deletion in a girl affected by astrocytoma and multiple melanoma. *BMC Med Genet*, 15, 59.
- FUJITA, K., MONDAL, A. M., HORIKAWA, I., NGUYEN, G. H., KUMAMOTO, K., SOHN, J. J., BOWMAN, E. D., MATHE, E. A., SCHETTER, A. J., PINE, S. R., JI, H., VOJTESEK, B., BOURDON, J. C., LANE, D. P. & HARRIS, C. C. 2009. p53 isoforms Delta133p53 and p53beta are endogenous regulators of replicative cellular senescence. *Nat Cell Biol*, 11, 1135-42.
- FULLGRABE, J., KAVANAGH, E. & JOSEPH, B. 2011. Histone onco-modifications. *Oncogene*, 30, 3391-403.
- GIL, J. & PETERS, G. 2006. Regulation of the INK4b-ARF-INK4a tumour suppressor locus: all for one or one for all. *Nat Rev Mol Cell Biol*. England.
- GILLEY, J. & FRIED, M. 2001. One INK4 gene and no ARF at the Fugu equivalent of the human INK4A/ARF/INK4B tumour suppressor locus. *Oncogene*, 20, 7447-52.
- GIMENEZ-CONTI, I. B., LABATE, M., LIU, F. & OSTERNDORFF, E. 1996. p53 alterations in chemically induced hamster cheek-pouch lesions. *Mol Carcinog*, 16, 197-202.
- GIONO, L. E. & MANFREDI, J. J. 2007. Mdm2 is required for inhibition of Cdk2 activity by p21, thereby contributing to p53-dependent cell cycle arrest. *Mol Cell Biol*, 27, 4166-78.
- GIRE, V., ROUX, P., WYNFORD-THOMAS, D., BRONDELLO, J. M. & DULIC, V. 2004. DNA damage checkpoint kinase Chk2 triggers replicative senescence. *Embo j*, 23, 2554-63.
- GOLDSTEIN, A. M., CHAN, M., HARLAND, M., HAYWARD, N. K., DEMENAI, F., BISHOP, D. T., AZIZI, E., BERGMAN, W., BIANCHI-SCARRA, G., BRUNO, W., CALISTA, D., ALBRIGHT, L. A., CHAUDRU, V., CHOMPRET, A., CUELLAR, F., ELDER, D. E., GHIORZO, P., GILLANDERS, E. M., GRUIS, N. A., HANSSON, J., HOGG, D., HOLLAND, E. A., KANETSKY, P. A., KEFFORD, R. F., LANDI, M. T., LANG, J., LEACHMAN, S. A., MACKIE, R. M., MAGNUSSON, V., MANN, G. J., BISHOP, J. N., PALMER, J. M., PUIG, S., PUIG-BUTILLE, J. A., STARK, M., TSAO, H., TUCKER, M. A., WHITAKER, L. & YAKOBSON, E. 2007. Features associated with germline CDKN2A mutations: a GenoMEL study of melanoma-prone families from three continents. *J Med Genet*, 44, 99-106.
- GONZALEZ, S., KLATT, P., DELGADO, S., CONDE, E., LOPEZ-RIOS, F., SANCHEZ-CESPEDES, M., MENDEZ, J., ANTEQUERA, F. & SERRANO, M. 2006. Oncogenic activity of Cdc6 through repression of the INK4/ARF locus. *Nature*, 440, 702-6.
- GONZALEZ, S. & SERRANO, M. 2006. A new mechanism of inactivation of the INK4/ARF locus. *Cell Cycle*. United States.
- GRAY, S. E., KAY, E., LEADER, M. & MABRUK, M. 2006. Analysis of p16 expression and allelic imbalance / loss of heterozygosity of 9p21 in cutaneous squamous cell carcinomas. *J Cell Mol Med*, 10, 778-88.
- GRAY-SCHOPFER, V. C., CHEONG, S. C., CHONG, H., CHOW, J., MOSS, T., ABDEL-MALEK, Z. A., MARAIS, R., WYNFORD-THOMAS, D. & BENNETT, D. C. 2006. Cellular senescence in naevi and immortalisation in melanoma: a role for p16? *Br J Cancer*, 95, 496-505.
- GU, F., PFEIFFER, R. M., BHATTACHARJEE, S., HAN, S. S., TAYLOR, P. R., BERNDT, S., YANG, H., SIGURDSON, A. J., TORO, J., MIRABELLO, L., GREENE, M. H., FREEDMAN, N. D., ABNET, C. C., DAWSEY, S. M., HU, N., QIAO, Y. L., DING, T., BRENNER, A. V., GARCIA-CLOSAS, M., HAYES, R., BRINTON, L. A., LISSOWSKA, J., WENTZENSEN, N., KRATZ, C., MOORE, L. E., ZIEGLER, R. G., CHOW, W. H., SAVAGE, S. A., BURDETTE, L., YEAGER, M., CHANOCK, S. J.,

- CHATTERJEE, N., TUCKER, M. A., GOLDSTEIN, A. M. & YANG, X. R. 2013. Common genetic variants in the 9p21 region and their associations with multiple tumours. *Br J Cancer*, 108, 1378-86.
- GUMP, J., STOKOE, D. & MCCORMICK, F. 2003. Phosphorylation of p16INK4A correlates with Cdk4 association. *J Biol Chem*, 278, 6619-22.
- GUO, Y., YUAN, C., WEGHORST, C. M. & LI, J. 2010. IKKbeta specifically binds to P16 and phosphorylates Ser8 of P16. *Biochem Biophys Res Commun*, 393, 504-8.
- HANAHAHAN, D. & WEINBERG, R. A. 2000. The hallmarks of cancer. *Cell*, 100, 57-70.
- HANAHAHAN, D. & WEINBERG, R. A. 2011. Hallmarks of cancer: the next generation. *Cell*, 144, 646-74.
- HANAOKA, M., SHIMIZU, K., SHIGEMURA, M., KATO, A., FUJII, H., HONOKI, K. & TSUJIUCHI, T. 2005. Cloning of the hamster p16 gene 5' upstream region and its aberrant methylation patterns in pancreatic cancer. *Biochem Biophys Res Commun*, 333, 1249-53.
- HARLEY, C. B., FUTCHER, A. B. & GREIDER, C. W. 1990. Telomeres shorten during ageing of human fibroblasts. *Nature*, 345, 458-60.
- HAYFLICK, L. 1965. THE LIMITED IN VITRO LIFETIME OF HUMAN DIPLOID CELL STRAINS. *Exp Cell Res*, 37, 614-36.
- HELLEMANS, J., MORTIER, G., DE PAEPE, A., SPELEMAN, F. & VANDESOMPELE, J. 2007. qBase relative quantification framework and software for management and automated analysis of real-time quantitative PCR data. *Genome Biol*. England.
- HENIKOFF, S., FURUYAMA, T. & AHMAD, K. 2004. Histone variants, nucleosome assembly and epigenetic inheritance. *Trends Genet*, 20, 320-6.
- HENLEY, S. A. & DICK, F. A. 2012. The retinoblastoma family of proteins and their regulatory functions in the mammalian cell division cycle. *Cell Div*, 7, 10.
- HERMAN, J. G., MERLO, A., MAO, L., LAPIDUS, R. G., ISSA, J. P., DAVIDSON, N. E., SIDRANSKY, D. & BAYLIN, S. B. 1995. Inactivation of the CDKN2/p16/MTS1 gene is frequently associated with aberrant DNA methylation in all common human cancers. *Cancer Res*, 55, 4525-30.
- HERNANDEZ, L. G., VAN STEEG, H., LUIJTEN, M. & VAN BENTHEM, J. 2009. Mechanisms of non-genotoxic carcinogens and importance of a weight of evidence approach. *Mutat Res*. Netherlands.
- HIRAKAWA, T., NEMOTO, N., YAMADA, M. A. & TAKAYAMA, S. 1979. Metabolism of benzo[A]pyrene and the related enzyme activities in hamster embryo cells. *Chem Biol Interact*, 25, 189-95.
- HOLLSTEIN, M., SIDRANSKY, D., VOGELSTEIN, B. & HARRIS, C. C. 1991. p53 mutations in human cancers. *Science*, 253, 49-53.
- HONDA, R., TANAKA, H. & YASUDA, H. 1997. Oncoprotein MDM2 is a ubiquitin ligase E3 for tumor suppressor p53. *FEBS Lett*, 420, 25-7.
- HONOKI, K., TSUJIUCHI, T., MORI, T., YOSHITANI, K., TSUTSUMI, M., TAKAKURA, Y. & MII, Y. 2004. Expression of the p16INK4a gene and methylation pattern of CpG sites in the promoter region in rat tumor cell lines. *Mol Carcinog*, 39, 10-4.
- ISFORT, R. J., KERCKAERT, G. A., CODY, D. B., CARTER, J., DRISCOLL, K. E. & LEBOEUF, R. A. 1996a. Isolation and biological characterization of morphological transformation-sensitive Syrian hamster embryo cells. *Carcinogenesis*, 17, 997-1005.
- ISFORT, R. J., KERCKAERT, G. A. & LEBOEUF, R. A. 1996b. Comparison of the standard and reduced pH Syrian hamster embryo (SHE) cell in vitro transformation assays in predicting the carcinogenic potential of chemicals. *Mutat Res*. Netherlands.
- ISFORT, R. J. & LEBOEUF, R. A. 1996. Application of in vitro cell transformation assays to predict the carcinogenic potential of chemicals. *Mutat Res*, 365, 161-73.
- ITAHANA, K., ZOU, Y., ITAHANA, Y., MARTINEZ, J. L., BEAUSEJOUR, C., JACOBS, J. J., VAN LOHUIZEN, M., BAND, V., CAMPISI, J. & DIMRI, G. P. 2003. Control of the replicative life span of human fibroblasts by p16 and the polycomb protein Bmi-1. *Mol Cell Biol*, 23, 389-401.

- ITAHANA, Y., NEO, S. H. & ITAHANA, K. 2013. miR-141, a new player, joins the senescence orchestra. *Cell Cycle*, 12, 3586-7.
- JACOBS, J. J. & DE LANGE, T. 2004. Significant role for p16INK4a in p53-independent telomere-directed senescence. *Curr Biol*. England.
- JACOBS, J. J., KIEBOOM, K., MARINO, S., DEPINHO, R. A. & VAN LOHUIZEN, M. 1999. The oncogene and Polycomb-group gene bmi-1 regulates cell proliferation and senescence through the ink4a locus. *Nature*, 397, 164-8.
- JARVIS, I. W., DREIJ, K., MATTSSON, A., JERNSTROM, B. & STENIUS, U. 2014. Interactions between polycyclic aromatic hydrocarbons in complex mixtures and implications for cancer risk assessment. *Toxicology*, 321, 27-39.
- JELTSCH, A. & JURKOWSKA, R. Z. 2014. New concepts in DNA methylation. *Trends Biochem Sci*, 39, 310-318.
- JHA, A. K., NIKBAKHT, M., JAIN, V., CAPALASH, N. & KAUR, J. 2012. p16(INK4a) and p15(INK4b) gene promoter methylation in cervical cancer patients. *Oncol Lett*, 3, 1331-1335.
- JIA, N., LI, Q., TAO, X., WANG, J., HUA, K. & FENG, W. 2014. Enhancer of zeste homolog 2 is involved in the proliferation of endometrial carcinoma. *Oncol Lett*, 8, 2049-2054.
- JONES, P. A. & BAYLIN, S. B. 2002. The fundamental role of epigenetic events in cancer. *Nat Rev Genet*, 3, 415-28.
- JUTTERMANN, R., LI, E. & JAENISCH, R. 1994. Toxicity of 5-aza-2'-deoxycytidine to mammalian cells is mediated primarily by covalent trapping of DNA methyltransferase rather than DNA demethylation. *Proc Natl Acad Sci U S A*, 91, 11797-801.
- KAMIJO, T., BODNER, S., VAN DE KAMP, E., RANDLE, D. H. & SHERR, C. J. 1999. Tumor spectrum in ARF-deficient mice. *Cancer Res*, 59, 2217-22.
- KAMIJO, T., ZINDY, F., ROUSSEL, M. F., QUELLE, D. E., DOWNING, J. R., ASHMUN, R. A., GROSVELD, G. & SHERR, C. J. 1997. Tumor suppression at the mouse INK4a locus mediated by the alternative reading frame product p19ARF. *Cell*, 91, 649-59.
- KANDOTH, C., MCLELLAN, M. D., VANDIN, F., YE, K., NIU, B., LU, C., XIE, M., ZHANG, Q., MCMICHAEL, J. F., WYCZALKOWSKI, M. A., LEISERSON, M. D., MILLER, C. A., WELCH, J. S., WALTER, M. J., WENDL, M. C., LEY, T. J., WILSON, R. K., RAPHAEL, B. J. & DING, L. 2013. Mutational landscape and significance across 12 major cancer types. *Nature*, 502, 333-9.
- KENZELMANN BROZ, D. & ATTARDI, L. D. 2010. In vivo analysis of p53 tumor suppressor function using genetically engineered mouse models. *Carcinogenesis*, 31, 1311-8.
- KERCKAERT, G. A., BRAUNINGER, R., LEOEUF, R. A. & ISFORT, R. J. 1996a. Use of the Syrian hamster embryo cell transformation assay for carcinogenicity prediction of chemicals currently being tested by the National Toxicology Program in rodent bioassays. *Environ Health Perspect*, 104 Suppl 5, 1075-84.
- KERCKAERT, G. A., ISFORT, R. J., CARR, G. J., AARDEMA, M. J. & LEOEUF, R. A. 1996b. A comprehensive protocol for conducting the Syrian hamster embryo cell transformation assay at pH 6.70. *Mutat Res*. Netherlands.
- KERCKAERT, G. A., LEOEUF, R. A. & ISFORT, R. J. 1996c. pH effects on the lifespan and transformation frequency of Syrian hamster embryo (SHE) cells. *Carcinogenesis*, 17, 1819-24.
- KHOURY, M. P. & BOURDON, J. C. 2011. p53 Isoforms: An Intracellular Microprocessor? *Genes Cancer*, 2, 453-65.
- KIM, H. G., KIM, D. J., LI, S., LEE, K. Y., LI, X., BODE, A. M. & DONG, Z. 2012. Polycomb (PcG) proteins, BMI1 and SUZ12, regulate arsenic-induced cell transformation. *J Biol Chem*, 287, 31920-8.
- KIM, S. H., MITCHELL, M., FUJII, H., LLANOS, S. & PETERS, G. 2003. Absence of p16INK4a and truncation of ARF tumor suppressors in chickens. *Proc Natl Acad Sci U S A*, 100, 211-6.
- KIM, W. Y. & SHARPLESS, N. E. 2006. The regulation of INK4/ARF in cancer and aging. *Cell*, 127, 265-75.
- KOHLI, R. M. & ZHANG, Y. 2013. TET enzymes, TDG and the dynamics of DNA demethylation. *Nature*, 502, 472-9.

- KOOISTRA, S. M., NORGAARD, L. C., LEES, M. J., STEINHAEUER, C., JOHANSEN, J. V. & HELIN, K. 2014. A screen identifies the oncogenic micro-RNA miR-378a-5p as a negative regulator of oncogene-induced senescence. *PLoS One*, 9, e91034.
- KRIMPENFORT, P., IJPENBERG, A., SONG, J. Y., VAN DER VALK, M., NAWIJN, M., ZEVENHOVEN, J. & BERNS, A. 2007. p15Ink4b is a critical tumour suppressor in the absence of p16Ink4a. *Nature*, 448, 943-6.
- KRISHNAMURTHY, J., TORRICE, C., RAMSEY, M. R., KOVALEV, G. I., AL-REGAIEY, K., SU, L. & SHARPLESS, N. E. 2004. Ink4a/Arf expression is a biomarker of aging. *J Clin Invest*, 114, 1299-307.
- KRUSE, J. P. & GU, W. 2008. SnapShot: p53 posttranslational modifications. *Cell*, 133, 930-30.e1.
- KUILMAN, T., MICHALOGLOU, C., MOOI, W. J. & PEEPER, D. S. 2010. The essence of senescence. *Genes Dev*. United States.
- KURZ, D. J., DECARY, S., HONG, Y. & ERUSALIMSKY, J. D. 2000. Senescence-associated (beta)-galactosidase reflects an increase in lysosomal mass during replicative ageing of human endothelial cells. *J Cell Sci*, 113 (Pt 20), 3613-22.
- LANDKOCZ, Y., POUPIN, P., ATIENZAR, F. & VASSEUR, P. 2011. Transcriptomic effects of di-(2-ethylhexyl)-phthalate in Syrian hamster embryo cells: an important role of early cytoskeleton disturbances in carcinogenesis? *BMC Genomics*, 12, 524.
- LARKIN, M. A., BLACKSHIELDS, G., BROWN, N. P., CHENNA, R., MCGETTIGAN, P. A., MCWILLIAM, H., VALENTIN, F., WALLACE, I. M., WILM, A., LOPEZ, R., THOMPSON, J. D., GIBSON, T. J. & HIGGINS, D. G. 2007. Clustal W and Clustal X version 2.0. *Bioinformatics*, 23, 2947-8.
- LARSSON, L. G. 2011. Oncogene- and tumor suppressor gene-mediated suppression of cellular senescence. *Semin Cancer Biol*, 21, 367-76.
- LEBOEUF, R. A. & KERCKAERT, G. A. 1987. Enhanced morphological transformation of early passage Syrian hamster embryo cells cultured in medium with a reduced bicarbonate concentration and pH. *Carcinogenesis*, 8, 689-97.
- LEBOEUF, R. A., KERCKAERT, G. A., AARDEMA, M. J. & GIBSON, D. P. 1990. Multistage neoplastic transformation of Syrian hamster embryo cells cultured at pH 6.70. *Cancer Res*, 50, 3722-9.
- LEBOEUF, R. A., KERCKAERT, G. A., AARDEMA, M. J., GIBSON, D. P., BRAUNINGER, R. & ISFORT, R. J. 1996. The pH 6.7 Syrian hamster embryo cell transformation assay for assessing the carcinogenic potential of chemicals. *Mutat Res*. Netherlands.
- LEBOEUF, R. A., KERCKAERT, K. A., AARDEMA, M. J. & ISFORT, R. J. 1999. Use of Syrian hamster embryo and BALB/c 3T3 cell transformation for assessing the carcinogenic potential of chemicals. *IARC Sci Publ*, 409-25.
- LEE, T. Y., CHANG, W. C., HSU, J. B., CHANG, T. H. & SHIEN, D. M. 2012. GPMiner: an integrated system for mining combinatorial cis-regulatory elements in mammalian gene group. *BMC Genomics*, 13 Suppl 1, S3.
- LEROY, B., FOURNIER, J. L., ISHIOKA, C., MONTI, P., INGA, A., FRONZA, G. & SOUSSI, T. 2013. The TP53 website: an integrative resource centre for the TP53 mutation database and TP53 mutant analysis. *Nucleic Acids Res*, 41, D962-9.
- LI, H., COLLADO, M., VILLASANTE, A., STRATI, K., ORTEGA, S., CANAMERO, M., BLASCO, M. A. & SERRANO, M. 2009. The Ink4/Arf locus is a barrier for iPS cell reprogramming. *Nature*, 460, 1136-9.
- LI, J., KNOBLOCH, T. J., POI, M. J., ZHANG, Z., DAVIS, A. T., MUSCARELLA, P. & WEGHORST, C. M. 2014. Genetic alterations of RD(INK4/ARF) enhancer in human cancer cells. *Mol Carcinog*, 53, 211-8.
- LI, J., POI, M. J. & TSAI, M. D. 2011. Regulatory mechanisms of tumor suppressor P16(INK4A) and their relevance to cancer. *Biochemistry*, 50, 5566-82.
- LI, J., WARNER, B., CASTO, B. C., KNOBLOCH, T. J. & WEGHORST, C. M. 2008. Tumor suppressor p16(INK4A)/Cdkn2a alterations in 7, 12-dimethylbenz(a)anthracene (DMBA)-induced hamster cheek pouch tumors. *Mol Carcinog*, 47, 733-8.

- LI, J., WEGHORST, C. M., TSUTSUMI, M., POI, M. J., KNOBLOCH, T. J., CASTO, B. C., MELVIN, W. S., TSAI, M. D. & MUSCARELLA, P. 2004. Frequent p16INK4A/CDKN2A alterations in chemically induced Syrian golden hamster pancreatic tumors. *Carcinogenesis*, 25, 263-8.
- LI, L. C. & DAHIYA, R. 2002. MethPrimer: designing primers for methylation PCRs. *Bioinformatics*, 18, 1427-31.
- LI, M., HE, Y., DUBOIS, W., WU, X., SHI, J. & HUANG, J. 2012. Distinct regulatory mechanisms and functions for p53-activated and p53-repressed DNA damage response genes in embryonic stem cells. *Mol Cell*, 46, 30-42.
- LIU, J., XIE, Y. S., WANG, F. L., ZHANG, L. J., ZHANG, Y. & LUO, H. S. 2013. Cytotoxicity of 5-Aza-2'-deoxycytidine against gastric cancer involves DNA damage in an ATM-P53 dependent signaling pathway and demethylation of P16(INK4A). *Biomed Pharmacother*, 67, 78-87.
- LOUGHERY, J., COX, M., SMITH, L. M. & MEEK, D. W. 2014. Critical role for p53-serine 15 phosphorylation in stimulating transactivation at p53-responsive promoters. *Nucleic Acids Res*, 42, 7666-80.
- MAIRE, M. A., PANT, K., PHRAKONKHAM, P., POTH, A., SCHWIND, K. R., RAST, C., BRUCE, S. W., SLY, J. E., BOHNENBERGER, S., KUNKELMANN, T., SCHULZ, M. & VASSEUR, P. 2012a. Recommended protocol for the Syrian hamster embryo (SHE) cell transformation assay. *Mutat Res*, 744, 76-81.
- MAIRE, M. A., PANT, K., POTH, A., SCHWIND, K. R., RAST, C., BRUCE, S. W., SLY, J. E., KUNZ-BOHNENBERGER, S., KUNKELMANN, T., ENGELHARDT, G., SCHULZ, M. & VASSEUR, P. 2012b. Prevalidation study of the Syrian hamster embryo (SHE) cell transformation assay at pH 7.0 for assessment of carcinogenic potential of chemicals. *Mutat Res*, 744, 64-75.
- MAIRE, M. A., RAST, C., LANDKOCZ, Y. & VASSEUR, P. 2007. 2,4-Dichlorophenoxyacetic acid: effects on Syrian hamster embryo (SHE) cell transformation, c-Myc expression, DNA damage and apoptosis. *Mutat Res*, 631, 124-36.
- MAIRE, M. A., RAST, C., PAGNOUT, C. & VASSEUR, P. 2005a. Changes in expression of bcl-2 and bax in Syrian hamster embryo (SHE) cells exposed to ZnCl₂. *Arch Toxicol*, 79, 90-101.
- MAIRE, M. A., RAST, C. & VASSEUR, P. 2005b. Di-(2-ethylhexyl)phthalate (DEHP) increases Bcl-2/Bax ratio and modifies c-myc expression in Syrian hamster embryo (SHE) cells. *Toxicol Lett*, 158, 237-45.
- MAIRE, M. A., RAST, C. & VASSEUR, P. 2012c. Photo catalogue for the classification of cell colonies in the Syrian hamster embryo (SHE) cell transformation assay at pH 7.0. *Mutat Res*, 744, 97-110.
- MANFREDI, J. J. 2010. The Mdm2-p53 relationship evolves: Mdm2 swings both ways as an oncogene and a tumor suppressor. *Genes Dev*, 24, 1580-9.
- MARKOVITS, P., PAPADOPOULOU, D., HUBERT-HABART, M., MANN, S. K., LABREQUE, A. & SABHARWAL, P. S. 1975. Establishment of normal diploid and malignant heteroploid cell lines from non-treated and benzo(a)pyrene treated hamster embryo cell cultures. *Experientia*, 31, 1215-8.
- MAROUCO, D., GARABADGIU, A. V., MELINO, G. & BARLEV, N. A. 2013. Lysine-specific modifications of p53: a matter of life and death? *Oncotarget*, 4, 1556-71.
- MARTIN, N., POPOV, N., AGUILO, F., O'LOGHLEN, A., RAGUZ, S., SNIJDERS, A. P., DHARMALINGAM, G., LI, S., THYMIAKOU, E., CARROLL, T., ZEISIG, B. B., SO, C. W., PETERS, G., EPISKOPOU, V., WALSH, M. J. & GIL, J. 2013. Interplay between Homeobox proteins and Polycomb repressive complexes in p16INK(4)a regulation. *Embo j*, 32, 982-95.
- MARTINS, C. P., BROWN-SWIGART, L. & EVAN, G. I. 2006. Modeling the therapeutic efficacy of p53 restoration in tumors. *Cell*, 127, 1323-34.
- MASCOLO, M. G., PERDICHIZZI, S., ROTONDO, F., MORANDI, E., GUERRINI, A., SILINGARDI, P., VACCARI, M., GRILLI, S. & COLACCI, A. 2010. BALB/c 3T3 cell transformation assay for the prediction of carcinogenic potential of chemicals and environmental mixtures. *Toxicol In Vitro*, 24, 1292-300.

- MAUTHE, R. J., GIBSON, D. P., BUNCH, R. T. & CUSTER, L. 2001. The syrian hamster embryo (SHE) cell transformation assay: review of the methods and results. *Toxicol Pathol*, 29 Suppl, 138-46.
- MCKENZIE, H. A., FUNG, C., BECKER, T. M., IRVINE, M., MANN, G. J., KEFFORD, R. F. & RIZOS, H. 2010. Predicting functional significance of cancer-associated p16(INK4a) mutations in CDKN2A. *Hum Mutat*, 31, 692-701.
- MELLERT, H., SYKES, S. M., MURPHY, M. E. & MCMAHON, S. B. 2007. The ARF/oncogene pathway activates p53 acetylation within the DNA binding domain. *Cell Cycle*, 6, 1304-6.
- MENG, S., LUO, M., SUN, H., YU, X., SHEN, M., ZHANG, Q., ZHOU, R., JU, X., TAO, W., LIU, D., DENG, H. & LU, Z. 2010. Identification and characterization of Bmi-1-responding element within the human p16 promoter. *J Biol Chem*, 285, 33219-29.
- MILLS, A. A. 2010. Throwing the cancer switch: reciprocal roles of polycomb and trithorax proteins. *Nat Rev Cancer*, 10, 669-82.
- MODI, S., HUGHES, M., GARROW, A. & WHITE, A. 2012. The value of in silico chemistry in the safety assessment of chemicals in the consumer goods and pharmaceutical industries. *Drug Discov Today*, 17, 135-42.
- MOMPARLER, R. L. 2005. Epigenetic therapy of cancer with 5-aza-2'-deoxycytidine (decitabine). *Semin Oncol*, 32, 443-51.
- MULLER, P. A. & VOUSDEN, K. H. 2013. p53 mutations in cancer. *Nat Cell Biol*, 15, 2-8.
- MULLER, P. A. & VOUSDEN, K. H. 2014. Mutant p53 in cancer: new functions and therapeutic opportunities. *Cancer Cell*, 25, 304-17.
- MUSCARELLA, P., KNOBLOCH, T. J., ULRICH, A. B., CASTO, B. C., MONIAUX, N., WITTEL, U. A., MELVIN, W. S., POUR, P. M., SONG, H., GOLD, B., BATRA, S. K. & WEGHORST, C. M. 2001. Identification and sequencing of the Syrian Golden hamster (*Mesocricetus auratus*) p16(INK4a) and p15(INK4b) cDNAs and their homozygous gene deletion in cheek pouch and pancreatic tumor cells. *Gene*, 278, 235-43.
- NAG, S., QIN, J., SRIVENUGOPAL, K. S., WANG, M. & ZHANG, R. 2013. The MDM2-p53 pathway revisited. *J Biomed Res*, 27, 254-71.
- NARITA, M., NUNEZ, S., HEARD, E., LIN, A. W., HEARN, S. A., SPECTOR, D. L., HANNON, G. J. & LOWE, S. W. 2003. Rb-mediated heterochromatin formation and silencing of E2F target genes during cellular senescence. *Cell*. United States.
- NEBERT, D. W., DALTON, T. P., OKEY, A. B. & GONZALEZ, F. J. 2004. Role of aryl hydrocarbon receptor-mediated induction of the CYP1 enzymes in environmental toxicity and cancer. *J Biol Chem*. United States.
- NEMOTO, N., HIRAKAWA, T. & TAKAYAMA, S. 1979. Metabolism of benzo[A]pyrene in hamster embryo cells. Effect of the concentration of benzo[A]pyrene on its metabolism. *Chem Biol Interact*, 25, 177-88.
- NEWBOLD, R. F. 1985a. Malignant transformation of mammalian cells in culture: delineation of stages and role of cellular oncogene activation. *IARC Sci Publ*, 67, 31-53.
- NEWBOLD, R. F. 1985b. Multistep malignant transformation of mammalian cells by carcinogens: induction of immortality as a key event. *Carcinog Compr Surv*, 9, 17-28.
- NEWBOLD, R. F. & OVERELL, R. W. 1983. Fibroblast immortality is a prerequisite for transformation by EJ c-Ha-ras oncogene. *Nature*, 304, 648-51.
- NEWBOLD, R. F., OVERELL, R. W. & CONNELL, J. R. 1982. Induction of immortality is an early event in malignant transformation of mammalian cells by carcinogens. *Nature*, 299, 633-5.
- NEWBOLD, R. F., WIGLEY, C. B., THOMPSON, M. H. & BROOKES, P. 1977. Cell-mediated mutagenesis in cultured Chinese hamster cells by carcinogenic polycyclic hydrocarbons: nature and extent of the associated hydrocarbon-DNA reaction. *Mutat Res*, 43, 101-16.
- OECD 2007. Detailed review paper on cell transformation assays for detection of chemical carcinogens. Paris: OECD Environment, Health and Safety Publications.
- OGRUNC, M. & FAGAGNA, F. 2011. Never-ageing cellular senescence. *Eur J Cancer*. England: 2011 Elsevier Ltd.

- OKANO, M., BELL, D. W., HABER, D. A. & LI, E. 1999. DNA methyltransferases Dnmt3a and Dnmt3b are essential for de novo methylation and mammalian development. *Cell*, 99, 247-57.
- OREFFO, V. I., LIN, H. W., PADMANABHAN, R. & WITSCHI, H. 1993. K-ras and p53 point mutations in 4-(methylnitrosamino)-1-(3-pyridyl)-1-butanone-induced hamster lung tumors. *Carcinogenesis*, 14, 451-5.
- OVERHOFF, M. G., GARBE, J. C., KOH, J., STAMPFER, M. R., BEACH, D. H. & BISHOP, C. L. 2014. Cellular senescence mediated by p16INK4A-coupled miRNA pathways. *Nucleic Acids Res*, 42, 1606-18.
- PALII, S. S., VAN EMBURGH, B. O., SANKPAL, U. T., BROWN, K. D. & ROBERTSON, K. D. 2008. DNA methylation inhibitor 5-Aza-2'-deoxycytidine induces reversible genome-wide DNA damage that is distinctly influenced by DNA methyltransferases 1 and 3B. *Mol Cell Biol*, 28, 752-71.
- PANT, K., BRUCE, S. W., SLY, J. E., KUNKELMANN, T., KUNZ-BOHNENBERGER, S., POTH, A., ENGELHARDT, G., SCHULZ, M. & SCHWIND, K. R. 2012. Prevalidation study of the Syrian hamster embryo (SHE) cell transformation assay at pH 6.7 for assessment of carcinogenic potential of chemicals. *Mutat Res*, 744, 54-63.
- PANT, K., SLY, J. E., BRUCE, S. W., LEUNG, C. & SAN, R. H. 2008. Syrian hamster embryo (SHE) cell transformation assay with conditioned media (without X-ray irradiated feeder layer) using 2,4-diaminotoluene, 2,6-diaminotoluene and chloral hydrate. *Mutat Res*. Netherlands.
- PANT, K., SLY, J. E., BRUCE, S. W., SCOTT, A. D., CARMICHAEL, P. L. & SAN, R. H. 2010. Syrian Hamster Embryo (SHE) cell transformation assay with and without X-ray irradiation of feeder cells using Di(2-ethylhexyl)phthalate (DEHP) and N-nitroso-N-methylnitroguanidine (MNNG). *Mutat Res*, 698, 6-10.
- PARKINSON, E. K. 2010. Senescence as a modulator of oral squamous cell carcinoma development. *Oral Oncol*. England: 2010 Elsevier Ltd.
- PARRINELLO, S., SAMPER, E., KRTOLICA, A., GOLDSTEIN, J., MELOV, S. & CAMPISI, J. 2003. Oxygen sensitivity severely limits the replicative lifespan of murine fibroblasts. *Nat Cell Biol*, 5, 741-7.
- PAULSON, T. G., GALIPEAU, P. C., XU, L., KISSEL, H. D., LI, X., BLOUNT, P. L., SANCHEZ, C. A., ODZE, R. D. & REID, B. J. 2008. p16 mutation spectrum in the premalignant condition Barrett's esophagus. *PLoS One*, 3, e3809.
- PETERS, G. 2008. An INKlination for epigenetic control of senescence. *Nat Struct Mol Biol*. United States.
- PIENTA, R. J., POILEY, J. A. & LEBHERZ, W. B., 3RD 1977. Morphological transformation of early passage golden Syrian hamster embryo cells derived from cryopreserved primary cultures as a reliable in vitro bioassay for identifying diverse carcinogens. *Int J Cancer*, 19, 642-55.
- POPOV, N. & GIL, J. 2010. Epigenetic regulation of the INK4b-ARF-INK4a locus: in sickness and in health. *Epigenetics*, 5, 685-90.
- PROWSE, K. R. & GREIDER, C. W. 1995. Developmental and tissue-specific regulation of mouse telomerase and telomere length. *Proc Natl Acad Sci U S A*, 92, 4818-22.
- QIAN, Y. & CHEN, X. 2013. Senescence regulation by the p53 protein family. *Methods Mol Biol*, 965, 37-61.
- RAYBURN, E., ZHANG, R., HE, J. & WANG, H. 2005. MDM2 and human malignancies: expression, clinical pathology, prognostic markers, and implications for chemotherapy. *Curr Cancer Drug Targets*, 5, 27-41.
- REYNGOLD, M., TURCAN, S., GIRI, D., KANNAN, K., WALSH, L. A., VIALE, A., DROBNJAK, M., VAHDAT, L. T., LEE, W. & CHAN, T. A. 2014. Remodeling of the methylation landscape in breast cancer metastasis. *PLoS One*, 9, e103896.
- RHEE, I., BACHMAN, K. E., PARK, B. H., JAIR, K. W., YEN, R. W., SCHUEBEL, K. E., CUI, H., FEINBERG, A. P., LENGAUER, C., KINZLER, K. W., BAYLIN, S. B. & VOGELSTEIN, B. 2002. DNMT1 and DNMT3b cooperate to silence genes in human cancer cells. *Nature*, 416, 552-6.
- RIDDER, G. M., STUARD, S. B., KERCKAERT, G. A., CODY, D. B., LEBOEUF, R. A. & ISFORT, R. J. 1997. Computerized image analysis of morphologically transformed and nontransformed Syrian

- hamster embryo (SHE) cell colonies: application to objective SHE cell transformation assay scoring. *Carcinogenesis*, 18, 1965-72.
- ROBERTSON, K. D. & JONES, P. A. 1998. The human ARF cell cycle regulatory gene promoter is a CpG island which can be silenced by DNA methylation and down-regulated by wild-type p53. *Mol Cell Biol*, 18, 6457-73.
- ROMAGOSA, C., SIMONETTI, S., LOPEZ-VICENTE, L., MAZO, A., LLEONART, M. E., CASTELLVI, J. & RAMON Y CAJAL, S. 2011. p16(Ink4a) overexpression in cancer: a tumor suppressor gene associated with senescence and high-grade tumors. *Oncogene*. England.
- RUFINI, A., TUCCI, P., CELARDO, I. & MELINO, G. 2013. Senescence and aging: the critical roles of p53. *Oncogene*, 32, 5129-43.
- RUSSO, I., SILVER, A. R., CUTHBERT, A. P., GRIFFIN, D. K., TROTT, D. A. & NEWBOLD, R. F. 1998. A telomere-independent senescence mechanism is the sole barrier to Syrian hamster cell immortalization. *Oncogene*, 17, 3417-26.
- SAITO, S., YAMAGUCHI, H., HIGASHIMOTO, Y., CHAO, C., XU, Y., FORNACE, A. J., JR., APPELLA, E. & ANDERSON, C. W. 2003. Phosphorylation site interdependence of human p53 post-translational modifications in response to stress. *J Biol Chem*, 278, 37536-44.
- SASAKI, K., BOHNENBERGER, S., HAYASHI, K., KUNKELMANN, T., MURAMATSU, D., PHRAKONKHAM, P., POTH, A., SAKAI, A., SALOVAARA, S., TANAKA, N., THOMAS, B. C. & UMEDA, M. 2012. Recommended protocol for the BALB/c 3T3 cell transformation assay. *Mutat Res*, 744, 30-5.
- SCHECHTMAN, L. M. 2012. Rodent cell transformation assays-a brief historical perspective. *Mutat Res*, 744, 3-7.
- SCHLUTER, C., DUCHROW, M., WOHLBERG, C., BECKER, M. H., KEY, G., FLAD, H. D. & GERDES, J. 1993. The cell proliferation-associated antigen of antibody Ki-67: a very large, ubiquitous nuclear protein with numerous repeated elements, representing a new kind of cell cycle-maintaining proteins. *J Cell Biol*, 123, 513-22.
- SCOUMANNE, A. & CHEN, X. 2008. Protein methylation: a new mechanism of p53 tumor suppressor regulation. *Histol Histopathol*, 23, 1143-9.
- SEALEY, D. C., ZHENG, L., TABOSKI, M. A., CRUICKSHANK, J., IKURA, M. & HARRINGTON, L. A. 2010. The N-terminus of hTERT contains a DNA-binding domain and is required for telomerase activity and cellular immortalization. *Nucleic Acids Res*, 38, 2019-35.
- SELKIRK, J. K., CROY, R. G., WIEBEL, F. J. & GELBOIN, H. V. 1976. Differences in benzo(a)pyrene metabolism between rodent liver microsomes and embryonic cells. *Cancer Res*, 36, 4476-9.
- SELUANOV, A., CHEN, Z., HINE, C., SASAHARA, T. H., RIBEIRO, A. A., CATANIA, K. C., PRESGRAVES, D. C. & GORBUNOVA, V. 2007. Telomerase activity coevolves with body mass not lifespan. *Aging Cell*, 6, 45-52.
- SERRANO, M., LIN, A. W., MCCURRACH, M. E., BEACH, D. & LOWE, S. W. 1997. Oncogenic ras provokes premature cell senescence associated with accumulation of p53 and p16INK4a. *Cell*. United States.
- SHARMA, S., KELLY, T. K. & JONES, P. A. 2010. Epigenetics in cancer. *Carcinogenesis*, 31, 27-36.
- SHARPLESS, N. E., BARDEESY, N., LEE, K. H., CARRASCO, D., CASTRILLON, D. H., AGUIRRE, A. J., WU, E. A., HORNER, J. W. & DEPINHO, R. A. 2001. Loss of p16Ink4a with retention of p19Arf predisposes mice to tumorigenesis. *Nature*, 413, 86-91.
- SHARPLESS, N. E. & DEPINHO, R. A. 1999. The INK4A/ARF locus and its two gene products. *Curr Opin Genet Dev*, 9, 22-30.
- SHARPLESS, N. E. & DEPINHO, R. A. 2004. Telomeres, stem cells, senescence, and cancer. *J Clin Invest*, 113, 160-8.
- SHARPLESS, N. E., RAMSEY, M. R., BALASUBRAMANIAN, P., CASTRILLON, D. H. & DEPINHO, R. A. 2004. The differential impact of p16(INK4a) or p19(ARF) deficiency on cell growth and tumorigenesis. *Oncogene*, 23, 379-85.
- SHERR, C. J. 2006. Divorcing ARF and p53: an unsettled case. *Nat Rev Cancer*, 6, 663-73.

- SHERR, C. J. & DEPINHO, R. A. 2000. Cellular senescence: mitotic clock or culture shock? *Cell*, 102, 407-10.
- SIMBOECK, E., RIBEIRO, J. D., TEICHMANN, S. & DI CROCE, L. 2011. Epigenetics and senescence: learning from the INK4-ARF locus. *Biochem Pharmacol*, 82, 1361-70.
- SMOGORZEWSKA, A. & DE LANGE, T. 2002. Different telomere damage signaling pathways in human and mouse cells. *EMBO J*, 21, 4338-48.
- STAMPFER, M. R., GARBE, J., NIJJAR, T., WIGINGTON, D., SWISSHELM, K. & YASWEN, P. 2003. Loss of p53 function accelerates acquisition of telomerase activity in indefinite lifespan human mammary epithelial cell lines. *Oncogene*, 22, 5238-51.
- STAMPFER, M. R. & YASWEN, P. 2003. Human epithelial cell immortalization as a step in carcinogenesis. *Cancer Lett*, 194, 199-208.
- STEWART, J. A., CHAIKEN, M. F., WANG, F. & PRICE, C. M. 2012. Maintaining the end: roles of telomere proteins in end-protection, telomere replication and length regulation. *Mutat Res*, 730, 12-9.
- STRANO, S., FONTEMAGGI, G., COSTANZO, A., RIZZO, M. G., MONTI, O., BACCARINI, A., DEL SAL, G., LEVRERO, M., SACCHI, A., OREN, M. & BLANDINO, G. 2002. Physical interaction with human tumor-derived p53 mutants inhibits p63 activities. *J Biol Chem*, 277, 18817-26.
- STRESEMANN, C. & LYKO, F. 2008. Modes of action of the DNA methyltransferase inhibitors azacytidine and decitabine. *Int J Cancer*, 123, 8-13.
- SU, X., CHAKRAVARTI, D., CHO, M. S., LIU, L., GI, Y. J., LIN, Y. L., LEUNG, M. L., EL-NAGGAR, A., CREIGHTON, C. J., SURAOOKAR, M. B., WISTUBA, I. & FLORES, E. R. 2010. TAp63 suppresses metastasis through coordinate regulation of Dicer and miRNAs. *Nature*, 467, 986-90.
- SUPEK, F., MINANA, B., VALCARCEL, J., GABALDON, T. & LEHNER, B. 2014. Synonymous mutations frequently act as driver mutations in human cancers. *Cell*, 156, 1324-35.
- SURGET, S., KHOURY, M. P. & BOURDON, J. C. 2013. Uncovering the role of p53 splice variants in human malignancy: a clinical perspective. *Onco Targets Ther*.
- SZKLARCZYK, R., HERINGA, J., POND, S. K. & NEKRUTENKO, A. 2007. Rapid asymmetric evolution of a dual-coding tumor suppressor INK4a/ARF locus contradicts its function. *Proc Natl Acad Sci U S A*, 104, 12807-12.
- SZTALMACHOVA, M., HLAVNA, M., GUMULEC, J., HOLUBOVA, M., BABULA, P., BALVAN, J., SOCHOR, J., TANHAUSEROVA, V., RAUDENSKA, M., KRIZKOVA, S., ADAM, V., ECKSCHLAGER, T., KIZEK, R. & MASARIK, M. 2012. Effect of zinc(II) ions on the expression of pro- and anti-apoptotic factors in high-grade prostate carcinoma cells. *Oncol Rep*, 28, 806-14.
- TAKEUCHI, S., TAKAHASHI, A., MOTOI, N., YOSHIMOTO, S., TAJIMA, T., YAMAKOSHI, K., HIRAO, A., YANAGI, S., FUKAMI, K., ISHIKAWA, Y., SONE, S., HARA, E. & OHTANI, N. 2010. Intrinsic cooperation between p16INK4a and p21Waf1/Cip1 in the onset of cellular senescence and tumor suppression in vivo. *Cancer Res*, 70, 9381-90.
- TALLURI, S. & DICK, F. A. 2012. Regulation of transcription and chromatin structure by pRB: here, there and everywhere. *Cell Cycle*, 11, 3189-98.
- TANAKA, N., BOHNENBERGER, S., KUNKELMANN, T., MUNARO, B., PONTI, J., POTH, A., SABBIONI, E., SAKAI, A., SALOVAARA, S., SASAKI, K., THOMAS, B. C. & UMEDA, M. 2012. Prevalidation study of the BALB/c 3T3 cell transformation assay for assessment of carcinogenic potential of chemicals. *Mutat Res*, 744, 20-9.
- TANG, Y., ZHAO, W., CHEN, Y., ZHAO, Y. & GU, W. 2008. Acetylation is indispensable for p53 activation. *Cell*, 133, 612-26.
- TOUSSAINT, O., MEDRANO, E. E. & VON ZGLINICKI, T. 2000. Cellular and molecular mechanisms of stress-induced premature senescence (SIPS) of human diploid fibroblasts and melanocytes. *Exp Gerontol*, 35, 927-45.
- TOYOOKA, S., TSUDA, T. & GAZDAR, A. F. 2003. The TP53 gene, tobacco exposure, and lung cancer. *Hum Mutat*, 21, 229-39.

- TROTT, D. A., CUTHBERT, A. P., OVERELL, R. W., RUSSO, I. & NEWBOLD, R. F. 1995. Mechanisms involved in the immortalization of mammalian cells by ionizing radiation and chemical carcinogens. *Carcinogenesis*, 16, 193-204.
- TRUONG-TRAN, A. Q., CARTER, J., RUFFIN, R. E. & ZALEWSKI, P. D. 2001. The role of zinc in caspase activation and apoptotic cell death. *Biometals*, 14, 315-30.
- VAN DER RIET, P., NAWROZ, H., HRUBAN, R. H., CORIO, R., TOKINO, K., KOCH, W. & SIDRANSKY, D. 1994. Frequent loss of chromosome 9p21-22 early in head and neck cancer progression. *Cancer Res*, 54, 1156-8.
- VANDESOMPELE, J., DE PRETER, K., PATTYN, F., POPPE, B., VAN ROY, N., DE PAEPE, A. & SPELEMAN, F. 2002. Accurate normalization of real-time quantitative RT-PCR data by geometric averaging of multiple internal control genes. *Genome Biol*, 3, RESEARCH0034.
- VANPARYS, P., CORVI, R., AARDEMA, M., GRIBALDO, L., HAYASHI, M., HOFFMANN, S. & SCHECHTMAN, L. 2011. ECVAM prevalidation of three cell transformation assays. *ALTEX*, 28, 56-9.
- VANPARYS, P., CORVI, R., AARDEMA, M. J., GRIBALDO, L., HAYASHI, M., HOFFMANN, S. & SCHECHTMAN, L. 2012. Application of in vitro cell transformation assays in regulatory toxicology for pharmaceuticals, chemicals, food products and cosmetics. *Mutat Res*, 744, 111-6.
- VARIER, R. A. & TIMMERS, H. T. 2011. Histone lysine methylation and demethylation pathways in cancer. *Biochim Biophys Acta*, 1815, 75-89.
- VASSEUR, P. & LASNE, C. 2012. OECD Detailed Review Paper (DRP) number 31 on "Cell Transformation Assays for Detection of Chemical Carcinogens": main results and conclusions. *Mutat Res*, 744, 8-11.
- VELICHUTINA, I., SHAKNOVICH, R., GENG, H., JOHNSON, N. A., GASCOYNE, R. D., MELNICK, A. M. & ELEMENTO, O. 2010. EZH2-mediated epigenetic silencing in germinal center B cells contributes to proliferation and lymphomagenesis. *Blood*. United States.
- VOGELSTEIN, B., PAPADOPOULOS, N., VELCULESCU, V. E., ZHOU, S., DIAZ, L. A., JR. & KINZLER, K. W. 2013. Cancer genome landscapes. *Science*, 339, 1546-58.
- VOUSDEN, K. H. & LU, X. 2002. Live or let die: the cell's response to p53. *Nat Rev Cancer*, 2, 594-604.
- WALSH, M. J., BRUCE, S. W., PANT, K., CARMICHAEL, P. L., SCOTT, A. D. & MARTIN, F. L. 2009. Discrimination of a transformation phenotype in Syrian golden hamster embryo (SHE) cells using ATR-FTIR spectroscopy. *Toxicology*. Ireland.
- WANG, B., LI, D. & KOVALCHUK, O. 2013. p53 Ser15 phosphorylation and histone modifications contribute to IR-induced miR-34a transcription in mammary epithelial cells. *Cell Cycle*, 12, 2073-83.
- WANG, L., TANG, L., XIE, R., NIE, W., CHEN, L. & GUAN, X. 2012. p16 promoter hypermethylation is associated with increased breast cancer risk. *Mol Med Rep*, 6, 904-8.
- WATANABE, M. & SUZUKI, K. 1991. Expression dynamics of transforming phenotypes in X-irradiated Syrian golden hamster embryo cells. *Mutat Res*. Netherlands.
- WATERHOUSE, A. M., PROCTER, J. B., MARTIN, D. M., CLAMP, M. & BARTON, G. J. 2009. Jalview Version 2--a multiple sequence alignment editor and analysis workbench. *Bioinformatics*, 25, 1189-91.
- WATERS, M. D., JACKSON, M. & LEA, I. 2010. Characterizing and predicting carcinogenicity and mode of action using conventional and toxicogenomics methods. *Mutat Res*. Netherlands: 2010 Elsevier B.V.
- WEBER, J. D., JEFFERS, J. R., REHG, J. E., RANDLE, D. H., LOZANO, G., ROUSSEL, M. F., SHERR, C. J. & ZAMBETTI, G. P. 2000. p53-independent functions of the p19(ARF) tumor suppressor. *Genes Dev*, 14, 2358-65.
- WEMMERT, S., BETTSCHIEDER, M., ALT, S., KETTER, R., KAMMERS, K., FEIDEN, W., STEUDEL, W. I., RAHNENFUHRER, J. & URBSCHAT, S. 2009. p15 promoter methylation - a novel prognostic marker in glioblastoma patients. *Int J Oncol*, 34, 1743-8.

- WILLIAMSON, M. P., ELDER, P. A., SHAW, M. E., DEVLIN, J. & KNOWLES, M. A. 1995. p16 (CDKN2) is a major deletion target at 9p21 in bladder cancer. *Hum Mol Genet*, 4, 1569-77.
- WU, X., JIA, S., ZHANG, X., SI, X., TANG, W. & LUO, Y. 2012. Two mechanisms underlying the loss of p16(Ink4a) function are associated with distinct tumorigenic consequences for WS MEFs escaping from senescence. *Mech Ageing Dev*, 133, 549-55.
- XIONG, J. & EPSTEIN, R. J. 2009. Growth inhibition of human cancer cells by 5-aza-2'-deoxycytidine does not correlate with its effects on INK4a/ARF expression or initial promoter methylation status. *Mol Cancer Ther*, 8, 779-85.
- XUE, W., ZENDER, L., MIETHING, C., DICKINS, R. A., HERNANDO, E., KRIZHANOVSKY, V., CORDON-CARDO, C. & LOWE, S. W. 2007. Senescence and tumour clearance is triggered by p53 restoration in murine liver carcinomas. *Nature*, 445, 656-60.
- YACHDAV, G., KLOPPMANN, E., KAJAN, L., HECHT, M., GOLDBERG, T., HAMP, T., HONIGSCHMID, P., SCHAFFERHANS, A., ROOS, M., BERNHOFER, M., RICHTER, L., ASHKENAZY, H., PUNTA, M., SCHLESSINGER, A., BROMBERG, Y., SCHNEIDER, R., VRIEND, G., SANDER, C., BEN-TAL, N. & ROST, B. 2014. PredictProtein--an open resource for online prediction of protein structural and functional features. *Nucleic Acids Res*, 42, W337-43.
- YASAEI, H., GILHAM, E., PICKLES, J. C., ROBERTS, T. P., O'DONOVAN, M. & NEWBOLD, R. F. 2013. Carcinogen-specific mutational and epigenetic alterations in INK4A, INK4B and p53 tumour-suppressor genes drive induced senescence bypass in normal diploid mammalian cells. *Oncogene*, 32, 171-9.
- ZERDOUMI, Y., AURY-LANDAS, J., BONAITI-PELLIE, C., DERAMBURE, C., SESBOUE, R., RENAUX-PETEL, M., FREBOURG, T., BOUGEARD, G. & FLAMAN, J. M. 2013. Drastic effect of germline TP53 missense mutations in Li-Fraumeni patients. *Hum Mutat*, 34, 453-61.
- ZHAO, Z., PAN, X., LIU, L. & LIU, N. 2014. Telomere length maintenance, shortening, and lengthening. *J Cell Physiol*, 229, 1323-9.
- ZHU, J., WOODS, D., MCMAHON, M. & BISHOP, J. M. 1998. Senescence of human fibroblasts induced by oncogenic Raf. *Genes Dev*, 12, 2997-3007.
- ZINDY, F., WILLIAMS, R. T., BAUDINO, T. A., REHG, J. E., SKAPEK, S. X., CLEVELAND, J. L., ROUSSEL, M. F. & SHERR, C. J. 2003. Arf tumor suppressor promoter monitors latent oncogenic signals in vivo. *Proc Natl Acad Sci U S A*, 100, 15930-5.